

DISCOVERY, OPTIMIZATION, AND VALIDATION EFFORTS TOWARDS POSITIVE
ALLOSTERIC MODULATORS OF THE GLUCAGON-LIKE PEPTIDE 1 RECEPTOR AND
DISCOVERY OF A NOVEL SERIES OF GLUCAGON-LIKE PEPTIDE 1 RECEPTOR
NONCOMPETITIVE ANTAGONISTS. PROGRESS TOWARD THE TOTAL SYNTHESIS OF
MELEARORIDE A

By

Kellie D. Nance

Dissertation

Submitted to the Faculty of the
Graduate School of Vanderbilt University
in partial fulfillment of the requirements
for the degree of

DOCTOR of PHILOSOPHY

In

Chemistry

August 31, 2017

Nashville, Tennessee

Approved:

Craig W. Lindsley, Ph.D.

Kevin D. Niswender, M.D., Ph.D.

Gary A. Sulikowski, Ph.D.

Steven D. Townsend, Ph.D.

To my parents, for always expecting great things of me
and
to Andrew, for companionship and love, even when I was unlovable

ACKNOWLEDGEMENTS

The following work was generously supported by financial assistance from the Vanderbilt University Department of Chemistry, the Vanderbilt Institute for Chemical Biology, and the National Institutes of Health.

I would like to acknowledge my mentors, coworkers, and family for support during the years spent on the journey this document encapsulates. First, I would like to say thank you to my advisor, Dr. Craig Lindsley. Before joining the lab in the capacity of Graduate Student, Craig helped and guided me as a research assistant, freshly minted from my undergraduate studies, and helped me to learn the fundamentals of working as a medicinal chemist. As my graduate mentor, Craig was ever optimistic, and encouraging through the good results and the bad. I believe his positive attitude and advice will follow me through the rest my career.

I would also like to acknowledge my committee members. To Dr. Kevin Niswender, who's ever-present interest in the clinical treatment of diabetes provided the foundations of my projects, and without whom those projects would not exist. To Dr. Gary Sulikowski, who instructed me in organic synthesis and offered up many instances of help and advice in and out of the lab. To Dr. Steven Townsend, for always having an encouraging word and being interested in the nonconventional path my thesis took.

I would also like to acknowledge Dr. P. Jefferey Conn and Dr. Colleen Niswender for allowing me to use their resources and instruments to perform

pharmacological assays for my project. I appreciate their willingness to offer support and advice, and making me feel welcome in lab. I would also like to thank Dr. Hyekyung Plumley, for her inexhaustible knowledge of molecular biology and cell line development techniques. Her mentorship in these disciplines were crucial to troubleshooting efforts at a time when my main project went awry.

I would like to acknowledge my collaborators in the pharmacokinetics group of the VCNDD, Dr. Scott Daniels, Dr. Chuck Locuson and Dr. Annie Blobaum, who have been fundamental in furthering these projects and were always available when I had questions. I would also like to thank all the past and present members of the VCNDD, and members of the campus-based Lindsley lab especially. They were always available whether I needed help, a companion in celebration, or a shoulder to cry on. Without these people, I would not be where I am today, and I am afraid I will be spoiled from their constant support in my future workplaces.

I would like to thank my parents, for always supporting me and understanding my lack of communication when times were hard. Though they did not always understand what I was doing, they always had faith I would accomplish whatever my heart desired. And finally, to friends old and new, and to my loving boyfriend, who helped to give my life meaning even when things looked bleak. I thank you all for everything.

TABLE OF CONTENTS

	Page
DEDICATION	ii
ACKNOWLEDGEMENTS.....	iii
LIST OF TABLES	viii
LIST OF FIGURES.....	ix
LIST OF SCHEMES.....	xi
LIST OF ABBREVIATIONS.....	xii
Chapter	
1. Discovery, Optimization, and Validation efforts towards Positive Allosteric Modulators of the Glucagon-like Peptide 1 Receptor	1
Background and introduction.....	1
Glucagon-like peptide 1	1
Glucagon-like peptide 1 receptor	2
Peripheral and central effects of GLP-1	4
The incretin effect and type 2 diabetes	6
GLP-1 mimetics as T2D therapeutics.....	7
Orthosteric versus allosteric regulation of GPCRs.....	12
Allosteric modulation of GLP-1R.....	14
Conclusion.....	16
Materials and Methods.....	18
General synthetic methods and instrumentation	18
Iterative parallel synthesis.....	19
Cell Culture	20
Mutagenesis.....	22
Calcium mobilization assay	22
Kinetic cAMP accumulation assay	24
β -Arrestin Recruitment and GPCR Internalization Assays.....	26
Genomic DNA isolation and polymerase chain reaction (PCR).....	27
Total RNA isolation, reverse transcription and polymerase chain reaction (RT- PCR).....	28

ERK1/2 Phosphorylation.....	28
Static Islet Experiments.....	30
Ancillary/off-target screening assays.....	30
Plasma protein and brain homogenate binding.....	31
Hepatic microsomal intrinsic clearance.....	32
LC/MS/MS Bioanalysis of Samples.....	33
Cytochrome P450 Cocktail Inhibition Assay in Human Liver	
Microsomes.....	34
<i>In vivo</i> DMPK experimental.....	35
Behavioral pharmacology general methods.....	36
Catalepsy.....	37
Spontaneous Locomotor Activity.....	37
Animal care and use.....	37
Development of the first CNS-penetrant GLP-1R Positive allosteric	
modulator VU0453379.....	39
Prior discovery of GLP-1R PAMs through high-throughput screening.....	39
Optimization of hit VU0110945 to obtain lead GLP-1R PAM	
VU0453379.....	41
<i>In vitro</i> molecular pharmacological characterization of VU0453379.....	53
<i>In vitro</i> & <i>in vivo</i> DMPK characterization of GLP-1 PAM VU0453379.....	58
Ancillary pharmacology of VU0453379.....	61
Behavioral pharmacology studies with VU0453379.....	63
Continued optimization of GLP-1R PAM VU0453379.....	66
Explorations into the replacement of aminopyrrolidine ring.....	66
Explorations into core scaffold modifications.....	74
Validation and troubleshooting efforts of GLP-1R PAMs	
Development of in-house hGLP-1R cell lines.....	90
Evaluation of GLP-1R PAM VU0453379 in new cell lines.....	93
Effect of hGLP-1R SNP sequence on VU0453379 activity.....	96
Elucidation of commercial cell line background species and GLP-1R	
species and sequence.....	199
Determination of VU0453379 activity at rGLP-1R.....	103
Evaluation of VU0453379 ability to potentiate ERK1/2	
phosphorylation.....	104
Assessment of VU0453379 in GLP-1 (-/-) knockout mouse	
islets.....	107
Summary and future directions.....	108
Experimental methods.....	111
2. Discovery of a Novel Series of Glucagon-like Peptide 1 Receptor Noncompetitive	
Antagonists.....	143
Introduction.....	143
GLP-1 antagonism.....	143

GLP-1 antagonists and congenital hyperinsulinemia	145
GLP-1 and chronic stress	147
Small molecule GLP-1 antagonists.....	148
Materials and methods	151
General methods	151
<i>In vivo</i> glucose tolerance methods	151
Discovery of VU0650991, a potent CNS-penetrant, orally bioavailable GLP-1R small molecule antagonists.....	153
Discovery and optimization of GLP-1R agonists VU0138721	153
Synthesis and evaluation of GLP-1 agonists	162
Reclassification of GLP-1R agonists as antagonists	164
<i>In vitro</i> characterization of GLP-1R antagonists.....	167
<i>In vitro</i> & <i>in vivo</i> DMPK characterization of GLP-1R antagonists	169
Ancillary pharmacology of GLP-1R antagonist VU0650991	171
Effect of VU0650991 on oral glucose tolerance.....	173
Summary and future directions.....	175
Experimental methods	176
3. Progress toward the total synthesis of Melearoride A.....	183
Introduction	183
Terrestrial and marine natural product discovery and medicinal uses.....	183
Natural products from marine <i>Penicillium</i> sp.....	185
Total syntheses of PF1163B.....	187
Progress in the synthesis of Melearoride A	192
Retrosynthetic analysis of Melearoride A.....	192
First attempt at the synthesis of Melearoride A	193
Progress toward the second attempt as synthesis of Melearoride A.....	195
Summary and future directions.....	199
Experimental methods	200
Appendix.....	207
A. NMR spectra relevant to chapter 1	207
B. NMR spectra relevant to chapter 2	260
C. NMR spectra relevant to chapter 3.....	273
REFERENCES.....	288

LIST OF TABLES

Chapter 1

Table	Page
1.1 Structures and activities of VU0110945 analogs.....	43
1.2 Structures and activities of VU0449776 analogs.....	45
1.3 DMPK profile of VU0453379.....	59
1.4 Ancillary pharmacology of VU0453379	62
1.5 Structures and activities of aminomethyl pyrrolidine replacements	67
1.6 Structures and activities of 1,4-diamine analogs	73
1.7 Structures and activities of scaffold replacements	78
1.8 Structures and activities of <i>N</i> -cyclopentyl replacements	83
1.9 DMPK profiles of active <i>N</i> -cyclopentyl analogs	88

Chapter 2

Table	Page
2.1 Structures and activities of VU0138721 analogs in calcium assay	154
2.2 Structures and activities of VU0138721 analogs in cAMP assay.....	165
2.3 DMPK profiles of VU0650991 and VU0650973.....	170
2.4 Ancillary pharmacology of VU0650991	171

Chapter 3

Table	Page
3.1 Conditions for troubleshooting RCM of 3.36.....	195

LIST OF FIGURES

Chapter 1

Figure	Page
1.1	Proglucagon and composite hormones.....2
1.2	Primary signaling pathway of GLP-1R.....4
1.3	Structures of FDA-approved GLP-1 receptor agonists9
1.4	Structures of FDA-approved DPP-4 inhibitors..... 11
1.5	Allosteric ternary complex model 14
1.6	Structures of reported GLP-1R PAMs 16
1.7	Example data for determining profile of PAMs..... 25
1.8	Structures of GLP-1 PAMs from HTS campaign 40
1.9	Strategy for optimization of VU0110945 41
1.10	Selectivity and fold-shift analysis of VU0453379 53
1.11	Investigation of probe dependence of VU0453379..... 55
1.12	β -Arrestin recruitment and receptor internalization of VU0453379 56
1.13	Insulin secretion from pancreatic islets by VU0453379 57
1.14	Metabolite identification of VU0453379 61
1.15	Effect of VU0453379 on haloperidol-induced catalepsy in rat 64
1.16	Effect of VY0453379 on spontaneous locomotion in rat..... 65
1.17	Mechanism of T-Rex™ inducible expression system 91
1.18	Comparison of cell background in calcium assay..... 92
1.19	Fold-shift of VU0453379 in hGLP-1R T-Rex™293 calcium cell line 94
1.20	Fold-shift of VU0453379 in hGLP-1R 293T calcium and cAMP cell lines..... 95
1.21	SNP-variants of human <i>GLP1R</i> gene 96
1.22	Snake plot of hGLP-1R SNPs..... 97
1.23	Fold-shift of VU0453379 with SNP variants in calcium cell lines 98
1.24	Intron-exon map of human and rat <i>GLP1R</i> 100
1.25	Gel electrophoresis of intron-exon PCR products..... 102
1.26	Fold-shift of VU0453379 with rGLP-1R in calcium cell line 104
1.27	ERK1/2 phosphorylation assay with VU0453379..... 106
1.28	Insulin secretion from <i>GLP1R</i> (-/-) islets by VU0453379 107

Chapter 2

Figure	Page
2.1	Structures of GLP-1R peptide antagonists..... 144
2.2	Structures of non-peptide GLP-1R antagonists..... 149
2.3	Structure, activity and DMPK profile of VU0138721..... 153

2.4	CRCs of VU0138721 and analogs in calcium assay	161
2.5	Effect on insulin secretion by VU0138721 and analogs	163
2.6	CRCs of VU0650991 and VU0650973 in cAMP assay	166
2.7	Fold-shift analysis of VU0650991 and VU0650973 in cAMP assay	167
2.8	Effect of EX-4 stimulated insulin secretion by antagonists	168
2.9	Effect of VU0650991 on <i>in vivo</i> oral glucose tolerance	174

Chapter 3

Figure		Page
3.1	Structures, indications, and origins of medicinal natural products	184
3.2	Structures of macrolides from <i>Penicillium meleagrinum</i> var. <i>viridiflavum</i>	186

LIST OF SCHEMES

Chapter 1

Scheme	Page
1.1 Synthesis of VU011945 and analogs	42
1.2 Microwave-assisted synthesis of VU0449776 analogs	44
1.3 Synthesis of aminomethylpyrrolidine replacements	66
1.4 Synthesis of isoquinolone scaffold analog	75
1.5 Synthesis of quinoline scaffold analog.....	76
1.6 Synthesis of pyrrolidine modification to quinoline scaffold	76
1.7 Synthesis of biarylaminopyridone scaffold analog.....	76
1.8 Library synthesis of scaffold analogs to install southern ring	77
1.9 Synthesis of β -carboline scaffold and <i>N</i> -cyclopentyl replacements.....	82

Chapter 2

Scheme	Page
2.1 Synthesis of VU0650991 and VU0650973	162

Chapter 3

Scheme	Page
3.1 First total synthesis of PF1163B	188
3.2 Second total synthesis of PF1163B	190
3.3 First retrosynthetic analysis of Melearoride A.....	193
3.4 Synthetic route to Melearoride A with failure of RCM.....	194
3.5 Second synthetic analysis of Melearoride A	196
3.6 Progress in the second pass synthesis of Melearoride A.....	197
3.7 Proposed completion of Melearoride A synthesis	198

LIST OF ABBREVIATIONS

7TM	Seven-transmembrane domain
°C	Degrees Celsius
μW	Microwave radiation
AC	Adenylyl cyclase
ACN	Acetonitrile
AD	Alzheimer's disease
ANOVA	Analysis of Variance
ATCM	Allosteric ternary complex model
BBB	Blood-brain barrier
BHB	Brain-homogenate binding
cAMP	Cyclic adenosine monophosphate
CL _{Hep}	Hepatic clearance
CL _{Int}	Intrinsic clearance
CNS	Central nervous system
CRC	Concentration-response curve
CV	Cardiovascular
DCM	Dichloromethane
DIEA	<i>N,N</i> -diisopropylethylamine
DMEM	Dulbecco's modified Eagle's medium
DMF	Dimethylformamide
DMPK	Drug metabolism and pharmacokinetics
DMSO	Dimethylsulfoxide
DPP-4	Dipeptidyl peptidase IV
EC ₂₀	Concentration required for 20% of maximal receptor activation
EC ₈₀	Concentration required for 80% of maximal receptor activation
ERK1/2	Extracellular signal-regulated kinase 1 and 2
ESI	Electrospray ionization
EtOAc	Ethyl Acetate

EX-4	Exendin-4
FDA	United States Food and Drug Administration
FDSS	Functional Drug Screening System 7000
F_u	Fraction unbound
$F_{u,b}$	Fraction unbound in brain
$F_{u,p}$	Fraction unbound in plasma
G_α	G alpha subunit
$G_{\beta\gamma}$	G beta-gamma complex
GDP	Guanosine Diphosphate
GI	Gastrointestinal
GIP	Gastric inhibitory polypeptide
GLP-1	Glucagon-like peptide 1
GLP-2	Glucagon-like peptide 2
GLP-1R	Glucagon-like peptide 1 receptor
GPCR	G-protein coupled receptor
GRK	G protein-coupled receptor kinase
G_s	Gs alpha subunit
GTP	Guanosine triphosphate
HATU	1-[Bis(dimethylamino)methylene]-1H-1,2,3-triazolo[4,5-b]pyridinium 3-oxid hexafluorophosphate
HEK	Human embryonic kidney cell line 293
HEPES	2-[4-(2-hydroxyethyl)piperazin-1-yl]ethanesulfonic acid
HPLC	High-performance liquid chromatography
HRMS	High resolution mass spectrometry
HTS	High-throughput screening
IC50	Concentration required for 50% inhibition of maximal receptor response
IP	Intraperitoneal
IV	Intravenous
KA/KB	Equilibrium dissociation constant
Ki	Equilibrium dissociation constant from competition binding

Kp	Brain:plasma partition coefficient
Kp,uu	Unbound Brain: plasma partition coefficient
LC/MS	Liquid Chromatography/mass spectrometry
NAL	Neutral allosteric ligand
NAM	Negative allosteric modulator
NMR	Nuclear magnetic resonance
PAM	Positive allosteric modulator
PBL	Plasma: brain level
PBS	Phosphate buffered saline
pEC ₅₀	Negative logarithm of the concentration needed to activate 50% of signaling
PD	Parkinson's disease
PDX-1	Insulin promotor factor 1
pIC ₅₀	Negative logarithm of the concentration needed to inhibit 50% of signaling
PKA	Protein kinase A
PLC	Phospholipase C
PPB	Plasma-protein binding
PPG	Preproglucagon
RA	Receptor agonist
RCF	Relative centrifugal force
SAR	Structure-activity relationship
SEM	Standard error of the mean
SNP	Single nucleotide polymorphism
t _{1/2}	Half-life
T2D	Type-2 diabetes mellitus
TEA	Triethylamine
THF	Tetrahydrofuran
TLC	Thin-layer chromatography
TOF	Time of flight
VANTAGE	Vanderbilt Technologies for Advanced Genomics

VCNDD

Vanderbilt Center for Neuroscience Drug Discovery

VUID

Vanderbilt University identification number

CHAPTER 1

DISCOVERY, OPTIMIZATION, AND VALIDATION EFFORTS TOWARDS POSITIVE ALLOSTERIC MODULATORS OF THE GLUCAGON-LIKE PEPTIDE 1 RECEPTOR

Introduction

Glucagon-like peptide 1

Glucagon-like peptide 1 (GLP-1) is a 30 amino acid incretin gut hormone secreted by the enteroendocrine L cells of the gastrointestinal tract^[1], as well as the nucleus of the solitary tract^[2], upon ingestion of a meal. In these tissues, the proglucagon (PPG) gene is expressed and undergoes posttranslational tissue-dependent processing to derive several hormone peptides, including GLP-1^[3]. In the pancreas, the primary cleavage products are glucagon and the major proglucagon fragment (MPGF)^[4]. In the GI tract and brain, the primary cleavage products are glicentin, GLP-1, GLP-2, oxyntomodulin, and IP-2^[5] (**Figure 1.1**). Along with gastric inhibitory polypeptide (GIP), GLP-1 comprises a class of metabolic peptides called the incretins which act to decrease blood sugar levels in a glucose-dependent manner by potentiating insulin biosynthesis and secretion from pancreatic beta cells of the islets of Langerhans^[6], and limiting the postprandial glucose excursions by inhibiting the release of glucagon from the pancreatic alpha cells^[7]; this action is referred to as the incretin effect.^[8] Other effects of GLP-1 include increased beta cell proliferation and anti-apoptosis^[9], decreased gastric emptying^[10], increased sense of satiety^[11], and decreased food intake^[12]. The initial product of proglucagon cleavage, GLP-1 (1-37)

is quickly amidated and proteolytically cleaved into its two primarily active forms, GLP-1 (7-36) amide and GLP-1 (7-37), the former of which makes up 80% of the active circulating peptide.^[13] Active GLP-1 peptides are rapidly metabolized and inactivated by the enzyme dipeptidyl peptidase IV (DPP-4), which cleaves the first two amino acids His-Ala, giving rise to GLP-1 (9-36) amide^[14]. The half-life of active GLP-1 peptide due to this process is merely 1-4 minutes.^[15]

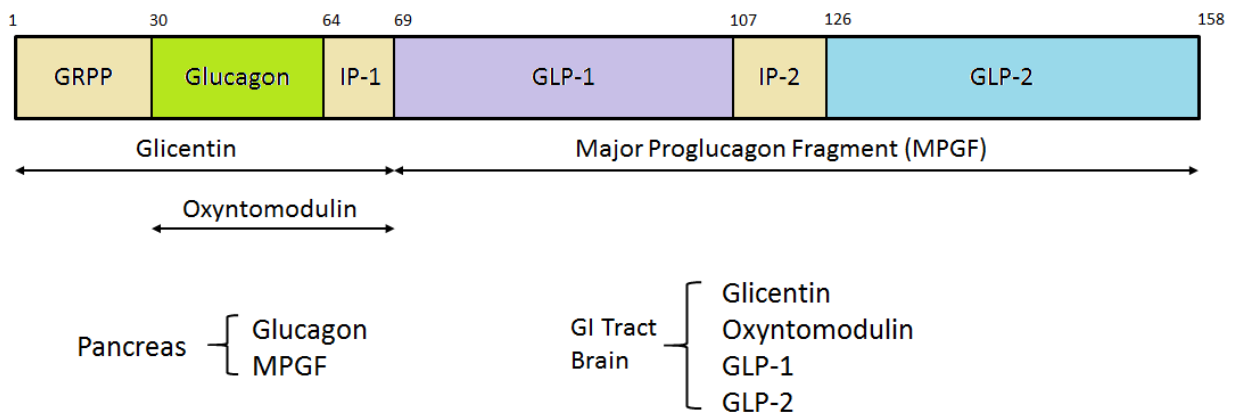


Figure 1.1: Representation of proglucagon and its composite hormone peptides.

Glucagon-like peptide 1 receptor

The glucagon-like peptide 1 receptor (GLP-1R) is a member of the family B G-protein coupled receptors (GPCR)^[16]. This family is distinguished by a long *N*-terminal hormone binding domain and is also known as the secretin family^[17]. GLP-1R is expressed in the pancreatic islets^[18], brain^[19], kidneys^[20], cardiovascular system^[21], and GI tract^[22]. GLP-1R is primary coupled to the heterotrimeric guanine nucleotide binding protein (G-protein) G_s ^[23], however, the potential for signaling

through other G-proteins has been reported^[24, 25] (**Figure 1.2**). Upon activation by its extracellular ligand, G_s coupled receptors adopt a conformation that is transduced to the intracellular G-protein. This conformational shift encourages exchange of GDP for GTP in the complex and the alpha subunit (G α) is released from the beta-gamma (G $\beta\gamma$) subunits. G α_s release into the cytosol promotes the derivation of cyclic AMP from ATP by activation of the enzyme adenylyl cyclase^[26]. Increased cAMP production in this way triggers the camp-dependent signaling cascade, which includes activation of protein kinase A (PKA) and early stage ERK1/2 phosphorylation^[27], and in the case of peripherally expressed GLP-1R, further downstream phosphorylation events that lead to the upregulation of insulin promotor factor 1 (PDX-1), increased transcription of preproinsulin messenger RNA, and exocytosis of insulin granules^[28].

After activation, GLP-1R undergoes rapid desensitization and receptor internalization via phosphorylation of the intracellular C-terminus by the G protein coupled receptor kinases (GRKs) and recruitment of β -arrestins^[29]. Arrestin binding blocks further recruitment of G-proteins and prepares the receptor for internalization into the cell, preventing additional activation^[30]. Though it has been stated throughout the literature that β -arrestin 1 is responsible for GLP-1R desensitization and internalization post activation^[31], it has recently been discovered that GLP-1R mediated β -arrestin 1 signaling stimulates late-stage ERK1/2 phosphorylation events and promotes the anti-apoptotic and proliferative effects GLP-1 has upon pancreatic beta cells^[32].

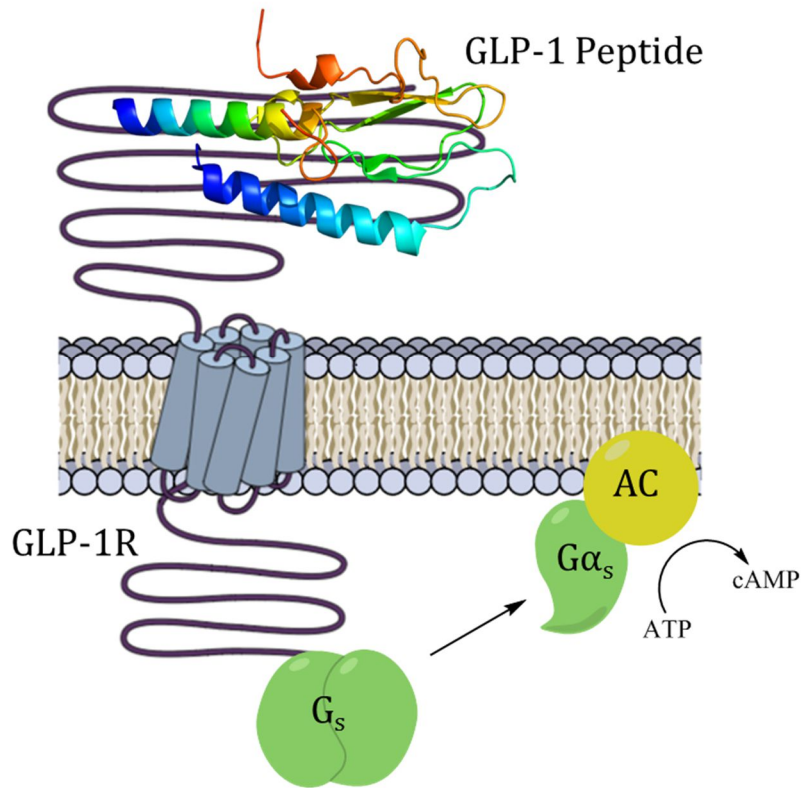


Figure 1.2: Illustrated model of GLP-1R depicting the general structure and the major signaling pathways mediated by G_{α_s} upon activation by GLP-1 peptide

Peripheral and central effect of GLP-1

In addition to its action as an insulin secretagogue, GLP-1 has been shown to act outside of the incretin axis^[33]. In the GI tract, GLP-1 is a strong regulator of gastrointestinal motility, secretion of lipoproteins in the intestines, and gastric emptying^[34]. In the cardiovascular (CV) system, GLP-1 stimulates glucose utilization and increases cardiac function, imparts cardio- and vasoprotection, and has anti-hypertensive properties^[35]. GLP-1 has also been shown to reduce inflammation in the CV system as well as in immune cells^[36]. In the kidneys, GLP-1 increases natriuresis,

a potential explanation for observed anti-hypertensive properties^[37]. Rodent studies have shown GLP-1 therapies to be renoprotective and reduce renal inflammation upon acute kidney injury^[38].

Perhaps the most studied but least understood action of GLP-1 is the role it plays in central regulation of metabolism and food intake. GLP-1R expression has been localized throughout the central nervous system, particularly the hypothalamus and hindbrain^[39]. Central GLP-1 is synthesized in the preproglucagon (PPG) neurons of the lower brain stem, and released through PPG axons to other regions of the CNS expressing GLP-1R, including the forebrain^[40]. Though Pan and coworkers have shown GLP-1 can cross the blood brain barrier (BBB)^[41], to this date it is still controversial whether this permeant GLP-1 has physiological relevance due to rapid degradation^[42]. To this date, little is known of the mechanisms by which central and peripheral GLP-1 production are linked, though it has been suggested by Burcelin and coworkers that glucose-dependent GLP-1 action on the portal vein induces vagus nerve firing, resulting in enteric glucose sensing and CNS-regulation of glucose homeostasis^[43].

Utilizing high dose GLP-1 central administration strategies, many physiological effects of GLP-1R activation in the CNS have been reported. These include decreased food intake^[44], decreased body weight^[45], increased sense of satiety^[46], decreased neuroinflammation^[47], control of energy homeostasis^[48], neuroprotection^[49], and improvements in cognition^[50]. The latter two of these effects suggest there is a role for central GLP-1 dysregulation in the development of

Parkinson's disease (PD), Alzheimer's disease (AD), and other neurodegenerative diseases^[51]. Though the specific mechanisms action between GLP-1 and neuroprotection have thus far remained elusive, the subject has garnered extraordinary interest and debate from basic science as well as clinically.

The incretin effect and type 2 diabetes

The term incretin effect refers to the fact that glucose administered orally produces a greater insulin response than that of glucose administered through isoglycemic intravenous administration^[52]. This effect was originally attributed to hypothetical factors produced in the gut upon nutrient uptake, factors which were later discovered to be the incretin hormones GLP-1 and GIP^[53]. It has been reported that up to two thirds of post-prandial insulin secreted is due to the insulinotropic actions of these two peptides^[54]. Nauck and coworkers first demonstrated in 1986 that the incretin effect is diminished in patients with type 2 diabetes (T2D), and this effect was independent of GIP plasma levels^[55]. This study predates the classification of GLP-1 as an incretin hormone and GLP-1 levels were not measured. However, it was later reported by Holst and coworkers that this incretin defect may be attributed to decreased GLP-1 secretion, as they demonstrated that intact plasma levels of GLP-1 after meal consumption were greatly reduced in subjects with T2D while GIP plasma levels remained unchanged^[56]. Consequent investigations by this group led to the discovery that reduced GLP-1 secretion is not causal of T2D, but is rather an acquired defect of the diabetic state, for the findings that a decrease in GLP-1 half-life in T2D patients is not to blame for reduced plasma levels^[57]. These studies quickly

precipitated an interest in GLP-1 as a T2D therapeutic clinically and in the pharmaceutical industry. While continuous infusion of GLP-1 was efficacious at reducing plasma glucose levels and beta-cell mass clinically^[58], once- or twice-daily injection of GLP-1 as a means to overcome low plasma levels was swiftly invalidated as a therapeutic strategy due to rapid metabolism of exogenous GLP-1 by DPP-4 into the inactivated peptide GLP-1 (9-36) amide, similarly to that of endogenous GLP-1^[59]. Since this time, several peptide mimetics have been developed and gained FDA approval for the treatment of T2D.

GLP-1 mimetics as T2D therapeutics

After GLP-1 administration was eliminated at a T2D therapy, work began on the development of DPP-4 resistant GLP-1 analogues and mimetics. The first of these discovered, exendin-4, was isolated from the venom of the Gila monster in 1992 by John Eng^[60]. The venom of this lizard possessed insulin secretagogue activity^[61]; the bioactive compounds responsible for these effects were of great interest. Once isolated, it was discovered exendin-4 possesses 50% sequence homology to GLP-1, and the peptide binds and activates the human GLP-1R more potently than endogenous GLP-1^[62]. This increased potency is due to DPP-4 resistance, with exendin-4 possessing a glycine rather than alanine at position 2, precluding it from being a DPP-4 substrate^[63]. The synthetic form of this peptide, called exenatide, has proven efficacious clinically in the improvement of beta cell function in T2D patients and was approved by the FDA in 2005 under the trade name Byetta® for twice-a-day injection^[64]. An extended release form of the peptide with the trade name Bydureon®

was approved in 2012 for once-weekly administration^[65]. While primarily developed for the treatment of T2D, exendin-4 has also shown clinically relevant improvements in the treatment of motor and cognitive impairments of PD^[66] and protection of neuronal damage in early stage AD^[67].

Another strategy employed to imbue DPP-4 resistance has been reducing plasma concentrations available for inactivation by increasing plasma protein binding. This method, first developed by Novo Nordisk, resulted in the development of liraglutide, a long acting GLP-1 agonist bearing 97% sequence homology to the GLP-1 (7-37) peptide^[68]. The addition of a palmitic fatty acid chain to Glu26 resulted in increased albumin binding, reducing free peptide available for metabolism and an increased half-life of 13 hours. After showing efficacy at both glucose regulation and weight loss in clinical trials, liraglutide, marketed under the trade name Victoza® was approved by the FDA for the treatment of T2D in 2010^[69], and later approved for the treatment of adults with obesity in 2014^[70]. Both indications require once-per-day injection of the peptide.

Since the initial development of these peptide mimetics, several other strategies have been employed to balance efficacy and pharmacokinetics of these peptide mimetics (**Figure 1.3**). Lixisenatide, first developed by Zealand Pharma and subsequently licensed and marketed by Sanofi, is a modification to exendin-4 in which the terminal proline is removed and replaced with six lysine residues^[71]. Albiglutide, marketed by GlaxoSmithKline, incorporates the alanine to glycine substitution which confers DPP-4 resistance seen in exendin-4, as well as a

dimerization strategy where two peptides are fused to human albumin protein. This complex retain efficacy at GLP-1R and has a biological half-life of 4-7 days, allowing for weekly or biweekly administration^[72]. The final GLP-1 agonist currently approved for T2D, dulaglutide, was developed by Eli Lilly. This peptide combines DPP-4 resistant modifications to the GLP-1 (7-37) peptide with covalent linkage to an Fc antibody fragment, which both protect the peptide from metabolism and combine to provide a half-life of 90 hours, suitable for once weekly administration^[73]. While these are the only GLP-1 peptide mimetics currently approved by the FDA, new modifications and strategies to improve the pharmacokinetic profile of these peptides are regularly published in the literature^[74-77].

While there has been great success employing GLP-1 agonists clinically, the side effects associated with these therapies cannot be overlooked. The most common of the side effects are GI issues including diarrhea, nausea, vomiting, indigestion,

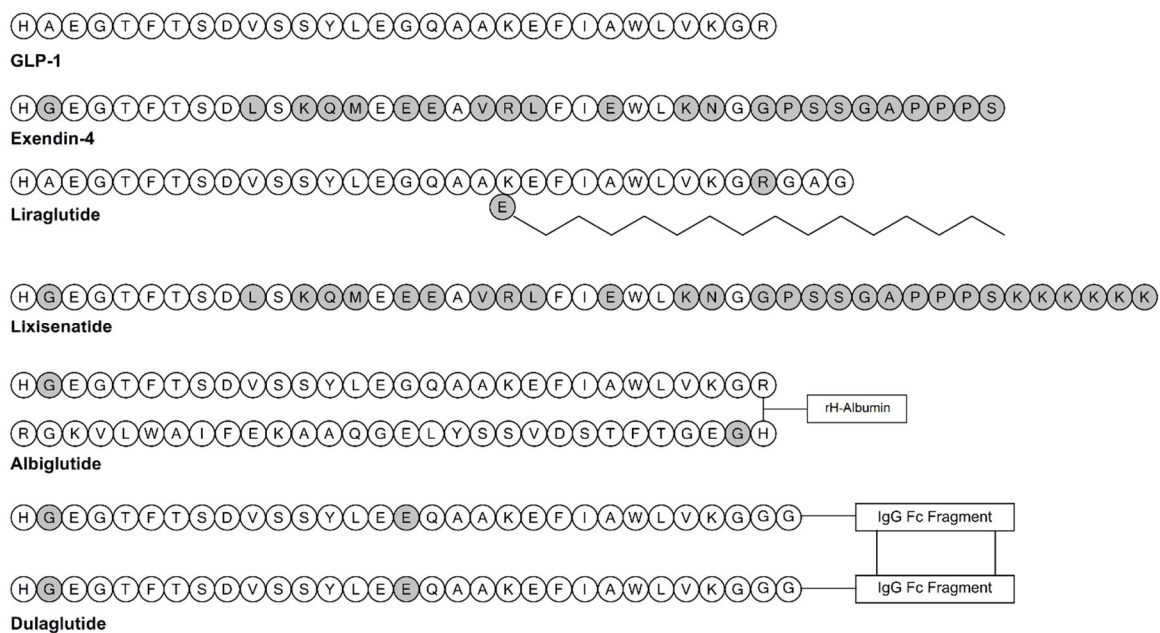


Figure 1.3: Primary structures of FDA-approved GLP-1 RAs, and structure modifications from native peptide GLP-1 (gray).

constipation, and loss of appetite^[78]. These issues are often times mild and tolerable, but escalate with dose and some patients are symptomatic to the point patient non-compliance and halting of treatment^[79]. Furthermore, FDA labels for all GLP-1 agonists warn of a potential for immunogenicity and developing antibodies for the peptides, rendering them ineffective^[80]. Worse even than these, is the potential for GLP-1 agonists to induce acute pancreatitis. Singh and coworkers demonstrated that the risk for pancreatitis is doubled for subjects undergoing GLP-1 based T2D therapies, and even more so for obese patients prone to pancreatitis due to other risk factors, such as gallstones and hypertriglyceridemia^[81]. However, Butler and coworkers found that the potential for pancreatitis may have other explanations, including the increased risk for pancreatitis associated with development of T2D, and that the risks are outweighed by the benefits with monitoring of adverse reactions^[82]. The link between GLP-1 therapies and pancreatitis and pancreatic cancer is still an ongoing source of debate and study.

In an effort to avoid side effects associated with these biologic therapies, as well as any patient non-compliance which often accompanies regular subcutaneous injections, some attention has been directed at developing small molecule, orally bioavailable inhibitors of the DPP-4 enzyme in an attempt to increase endogenous levels of GLP-1 (**Figure 1.4**). The first of these therapies, Januvia® (sitagliptin), was developed by Merck and approved for T2D treatment in 2006^[83]. All DPP-4 inhibitors, comprising the gliptin class, work by competitively inhibiting the active site of DPP-4, resulting in higher circulating concentrations of both incretin hormones. This strategy also effects the circulating levels of other DPP-4 substrates^[84]. At this time,

there are 5 members of the gliptin class approved for T2D, with the addition of vildagliptin (Novartis)^[85], saxagliptin (Bristol-Myers-Squibb)^[86], linagliptin (Boehringer-Ingelheim)^[87], and alogliptin (Takeda)^[88]. This class of drugs avoid most of the worst side effect of peptide-based GLP-1 therapies, but clinical incidence of nausea, cold-like symptoms, and severe joint pain were reported above that of placebo^[89], and post marketing incidence of hypersensitivity and renal failure, as well as pancreatitis have been reported^[90]; however, a causal link between these more severe adverse effects and gliptins has not been confirmed. Furthermore, whilst these drugs are efficacious at increasing the peripheral effects of GLP-1R activation, there is little to no evidence that they are useful for CNS indications, such as weight loss, reduced food intake, slowing of gastric emptying, and neuroprotection^[91]. Due to these drawbacks, increased efforts have been aimed at targeting GLP-1R function and signaling through diverse modes of action.

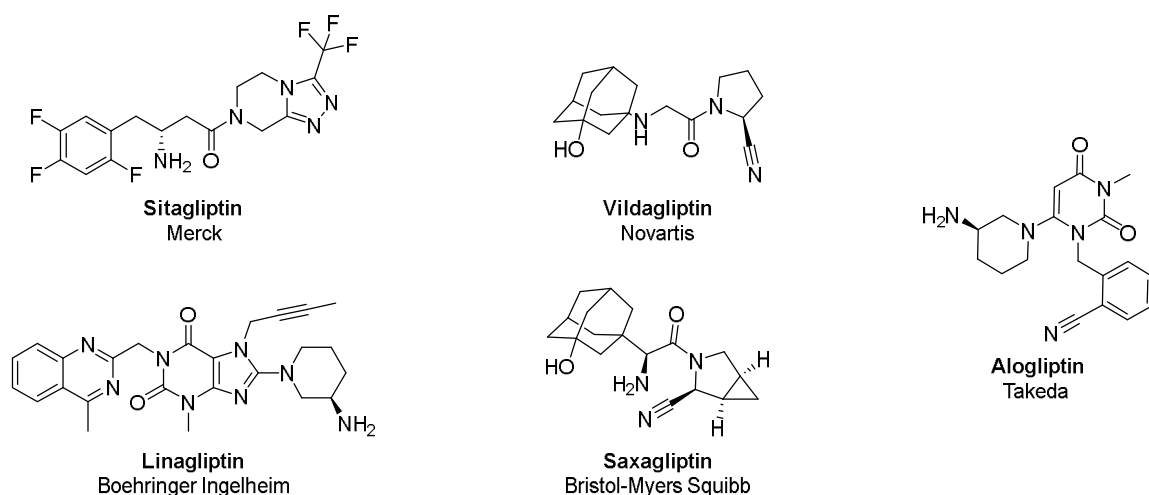


Figure 1.4: Structures of FDA-approved DPP-4 inhibitors for the treatment of T2D

Orthosteric versus allosteric regulation of GPCRs

Traditional methods of regulating the signaling of receptors, including GPCRs and ion channels, involve targeting the same location on the protein that is occupied by the endogenous ligand, deemed the orthosteric site. These strategies seek to find a molecule that can bind to a receptor and either activate it, in the case of agonists, or compete with endogenous ligand binding and antagonize signaling of the receptor^[92]. Molecules that act in this way are normally discovered using classical techniques, such as radioligand binding^[93]. Often, these compounds act as light switches and are only able to turn on receptor signaling or turn it off. While useful for many indications, this strategy can also lead to increased side effects clinically, particularly where the therapeutic window for receptor activation is small^[94]. An example of this is the discovery of xanomeline, an orthosteric agonist of the muscarinic acetyl choline receptors (mAChRs)^[95]. While this compound showed efficacy in many preclinical models of schizophrenia and impaired cognition^[96], it often caused adverse cholinergic side effects often associated with high levels of muscarinic receptor activation^[97]. This effect can also be seen with the GLP-1R receptor agonist class of drugs. While endogenous GLP-1 is released in a controlled fashion after meal consumption, exogenous receptor agonists constantly circulate through the system, and can lead to more constant GLP-1R activation than is likely with the endogenous system. This has been hypothesized as the source of adverse effects such as nausea and pancreatitis^[98].

In addition to these orthosteric binding sites, GPCRs are known to possess allosteric sites that are often topologically and functionally distinct and are less conserved across receptor families^[99]. These sites can be targeted with small molecules to stabilize advantageous conformations of the receptor^[100]. Allosteric ligands may modulate receptor signaling either in the presence of the orthosteric ligand or alone, and often stabilize either active (positive) and inactive (negative) conformations of the receptor, though some allosteric ligands are known to bind but exert no change on receptor signaling (neutral)^[101]. In the case of activating allosteric ligands dependent on orthosteric ligand, known as positive allosteric modulators (PAMs), molecule binding often affects the sensitivity and the efficacy of the orthosteric ligand. Pure PAMs, with no allosteric agonist qualities, do not show an observable receptor effect on their own, but only when orthosteric agonist is present^[102]. The response from allosteric modulators are divided into three vectors: affinity modulation, efficacy modulation, and allosteric agonism. Allosteric modulators can exist anywhere along the activation spectrum, and produce a multitude of modes of action that provide spatial and temporal control over nuanced system activation^[103]. This may be mathematically modeled using the allosteric ternary complex model (ATCM) (**Figure 1.5**)^[104].

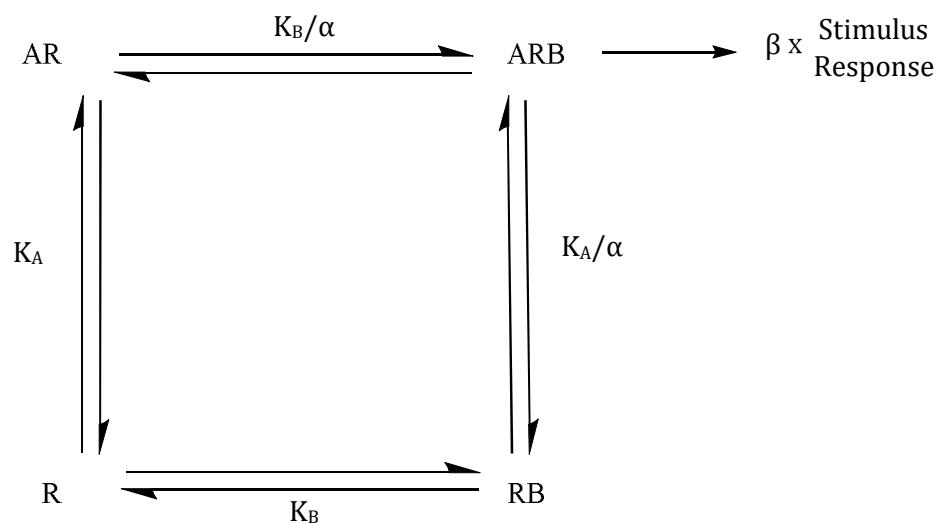


Figure 1.5: The allosteric ternary complex model (ATCM). K_A and K_B are dissociation constants describing the interaction between the orthosteric ligand (A) and the allosteric ligand (B) with the receptor (R). Cooperativity factor α describes the magnitude and direction of one ligand's effect on the binding affinity of the second ligand. Efficacy modulation factor β describes the magnitude and direction of the one ligand's effect on the second ligand's efficacy

Allosteric modulation of GLP-1R

Though the idea of allosteric protein regulation by small molecules was proposed in the 1950's^[105], allosteric modulation as a viable therapeutic mode of action was first validated upon the clinical success of the benzodiazepines from 1960 on^[106]. These compounds are allosteric ligands that potentiate the effect of the neurotransmitter GABA at the ionotropic GABA_A receptor and are much preferred over direct GABA_A agonists, which are potentially deadly^[107].

Increased interest in allostery with regards to GPCRs has been precipitated by the optimization of known high-throughput screening methods and functional assays

for the identification of molecules that engage the target irrespective of site binding^[108]. These assays rely more on functional output than target engagement and seek to look at receptor response as a whole through diverse signaling pathways. This innovation has become paramount to the identification of PAMs, a class of compounds difficult to detect through conventional screening^[109]. Rather than conventional HTS assays, which look for compound-mediated activation or antagonism of agonist-mediated signaling, these assays utilize submaximal concentrations of orthosteric ligands to find compounds that can potentiate the efficacy of a set ligand concentration. These techniques are especially useful in the search for small molecule ligands of receptors that have no published crystal structure, such as GLP-1R. Utilizing HTS methods optimized for allosteric modulators, groups in both industry and academia have had some success in discovering small molecule ligands of GLP-1R, though many suffer from low potencies, lack validating *in vivo* data, are electrophilic, or possess poor pharmacokinetic profiles (**Figure 1.6**)^[110]. Compound 2, developed by Novo-Nordisk, has both agonist and PAM qualities^[111]. The compound produces GLP-1-mediated insulin secretion from wild-type mouse islets alone, but does not bind to the orthosteric site of GLP-1R. It does, however, modulate the affinity of GLP-1 for the receptor, giving it the status of ago-PAM. BETP, another electrophilic GLP-1 ago-PAM, is known to covalently modify cysteines 347 and 438 in GLP-1R, and while it has been shown to potentiate GLP-1R-dependent intracellular calcium mobilization, it does not potentiate cAMP accumulation in response to GLP-1 (7-36) amide in recombinant cell lines, and instead potentiates the effect of oxyntomodulin at GLP-1R.^[112] Quercetin, plant polyphenol from the flavonoid group,

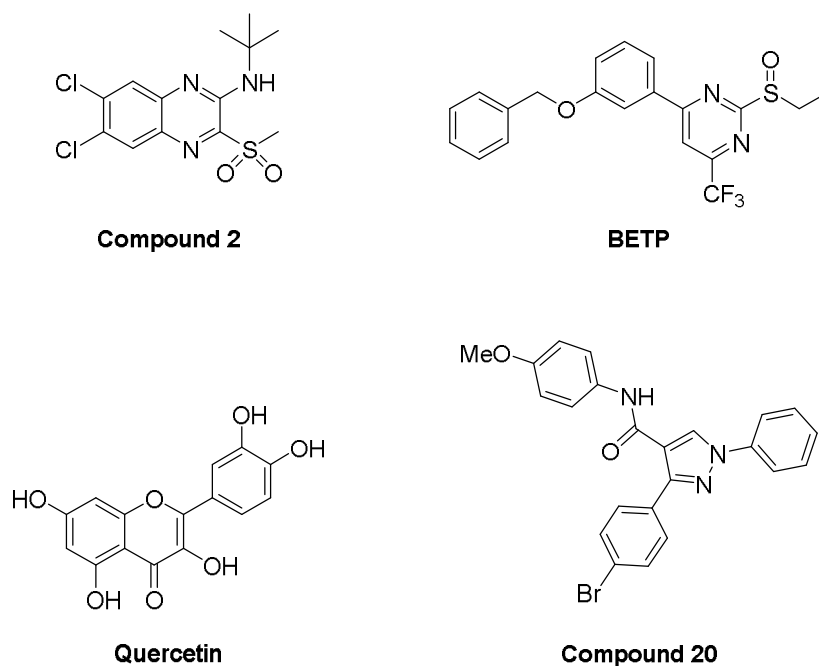


Figure 1.6: Structures of reported GLP-1R PAMs

similarly only modulates GLP-1R–dependent intracellular calcium mobilization^[113], and is also known to augment many other physiological pathways^[114]. Finally, compound 20 does not show functional activity at this receptor, but it is observed to potentiate cAMP accumulation at endogenously-expressed GLP-1R in mouse TC6 cells^[115]. While these compounds have shed some light on the possible validity of targeting GLP-1R with an allosteric approach, there are still many questions left unanswered and none operate as tool molecules.

Conclusion

Overall, a GLP-1 PAM with good pharmacological, physicochemical, and pharmacokinetic properties has remained elusive. Targeting GLP-1R through this mode of action, while a worthy endeavor to overcome liabilities of GLP-1 RAs, is an arduous task due to the pleiotropic and orthosterically promiscuous nature of the

receptor. However, a novel and selective GLP-1 PAM that could serve as an *in vivo* tool molecule would revolutionize the study of GLP-1R, and shed light on the therapeutic relevance of modulating GLP-1R activity. The following sections of this chapter describe our efforts in the optimization and characterization of a novel, CNS-penetrant series of GLP-1R PAMs with the goal of providing new chemical tools for the study of GLP1-R in the CNS and periphery.

Materials and Methods

General synthetic methods and instrumentation

All reactions were carried out employing standard chemical techniques under inert atmosphere. Solvents used for extraction, washing, and chromatography were HPLC grade. Unless otherwise noted, all reagents were purchased from Sigma-Aldrich Chemical Co. and were used without further purification. Analytical thin layer chromatography was performed on 250 μm silica gel plates from Sorbent Technologies. Analytical HPLC was performed on an Agilent 1200 LCMS with UV detection at 215 nm and 254 nm along with ELSD detection and electrospray ionization, with all final compounds showing > 95% purity and a parent mass ion consistent with the desired structure. All NMR spectra were recorded on a 400 MHz Brüker AV-400 instrument. ^1H chemical shifts are reported as δ values in ppm relative to the residual solvent peak (MeOD = 3.31, CDCl_3 = 7.26, DMSO). Data are reported as follows: chemical shift, multiplicity (br = broad, s = singlet, d = doublet, t = triplet, q = quartet, quint = quintet, m = multiplet), coupling constant (Hz), and integration. ^{13}C chemical shifts are reported as δ values in ppm relative to the residual solvent peak (MeOD = 49.0, CDCl_3 = 77.16). Low resolution mass spectra were obtained on an Agilent 1200 LCMS with electrospray ionization. High resolution mass spectra were recorded on a Waters QToF-API-US plus Acquity system with electrospray ionization. Automated flash column chromatography was performed on a Teledyne ISCO Combiflash Rf system. Preparative purification of library compounds was performed

on a Gilson chromatograph using a Luna 5u C18 (2) 100A AXIA column (30 x 50 mm) using a water/acetonitrile gradient. Optical rotations were acquired on a Jasco P-2000 polarimeter at 23 °C and 589 nm. The specific rotations were calculated according to the equation where l is path length in decimeters and c is the concentration in g/100 mL: $[\alpha]_D^{23} = \frac{100\alpha}{l \times c}$

Iterative parallel synthesis

Medicinal chemistry efforts were carried out using an iterative, parallel synthesis paradigm. This strategy was implemented in order to optimize compound potency, efficacy, and pharmacokinetic properties over repeated cycles of synthesis and pharmacological analysis. At the start of hit-to-lead optimization efforts, the hit compound, resultant of a high-throughput screening campaign, was retrosynthetically divided into synthetically accessible segments most amenable to library synthesis. After this, new compounds were synthesized starting with the smallest, most convenient modifications first, then proceeding to larger modifications, and finally core scaffold modifications aimed at determining the minimum pharmacophore. Libraries containing 5-50 members were generated, focusing on the installation of targeted modifications at one of the previously identified regions. Following purification, final compounds were diluted to a 10 μ M storage concentration with Dimethylsulfoxide (DMSO) in 2D-barcoded vials. Individual compounds were then assigned 7-digit VU numbers for identification, which were cross-referenced with the notebook number of synthesis and chemical

structure during registration into the Dotmatics™ database maintained by the Vanderbilt Center for Neuroscience Drug Discovery (VCNDD).

These final compounds were then analyzed in one or more molecular pharmacology assays described later in this section, in order to determine a structure-activity relationship (SAR) between chemical modifications and activity of the compounds at hGLP-1R. Compounds with advantageous potency or efficacy when compared to other synthesized analogues or the original hit compounds were then subjected to *in vitro* pharmacokinetic analysis using the pharmacokinetic analysis and metabolite identification protocols described later in this section. These data were then utilized to inform the design of new chemical modifications to further improve the given parameters. In this way, many compound modifications may be studied in parallel. This process was continued until an analogue of the original hit compounds was generated that fulfilled the goal of optimization.

Cell Culture

Human GLP-1R Chem-9 cells were obtained by clonal selection of the calcium-optimized ChemiSCREEN™ human recombinant GLP-1 receptor cell line that also overexpress a proprietary promiscuous G-protein (Millipore #HTS163C; Millipore, Billerica, MA, USA). Cell cultures were maintained in Dulbecco's Modified Eagles Medium (DMEM) with 10% fetal bovine serum (FBS), 4.0 mM L-glutamine, 1X non-essential amino acids (NEAAs), 100 U/mL penicillin, 100 µg/mL streptomycin, and 10.0 mM hydroxyethyl piperazineethanesulfonic acid (HEPES), and they were retained under selection using 500 µg/mL geneticin and 500 µg/mL hygromycin B.

Human Glucagon receptor (hGCGR) Chem-1 cells were obtained by clonal selection the calcium-optimized ChemiSCREEN™ human recombinant glucagon receptor cell line (Millipore #HTS112C). Cells were maintained in DMEM with 10% FBS, 1X NEAAs, 100 U/mL penicillin, 100 µg/mL streptomycin, and 10.0 mM HEPES, and were retained under selection using 250 µg/mL geneticin.

Rat INS-1 cells stably co-transfected with a pIRESpuro3 vector (Clontech #631619; Clontech, Mountain View, CA) containing human GLP-1R cDNA (OriGene #TC124060; OriGene, Rockville, MD) and with a plasmid encoding a cAMP-sensitive luciferase (p-GLOsensor-20F™, Promega #E1171; Promega, Madison, WI). Clones were selected based on functional expression and response to GLP-1 peptide using the GloSensor cAMP reagent (Promega #E1290). Cells were maintained in RPMI-1640 with 10% FBS, 1.0 mM sodium pyruvate, 100 U/mL penicillin, 100 µg/mL streptomycin, 50.0 µM beta-mercaptoethanol, and 10.0 mM HEPES.

TREx293 human embryonic kidney cells (Invitrogen) were used for troubleshooting efforts and underwent transient expression of hGLP-1R and either cAMP or calcium reporter. These cells were grown in high-glucose DMEM with 10% tetracycline-tested fetal bovine serum (tet-FBS), 4.0 mM GlutaMAX, 1X NEAAs, 1X sodium pyruvate, 10.0 mM HEPES, and 1X antibiotic/antimitotic (AA). Prior to transfection, cells were seeded in 10 cm tissue culture dishes at a confluence of about 30% and grown 24 hours at 37 °C and 5% CO₂. These cells were co-transfected with a plasmid encoding a human GLP-1 receptor cDNA construct (pcDNA5/TO vector, Invitrogen) and a plasmid either encoding an engineered cAMP-sensitive luciferase

(pGloSensor™-22F plasmid, Promega #E2301) or promiscuous G-protein mGα15 (pCMV6-Entry vector, Origene) using the FuGene 6 transfection protocol (Promega). After 24 hours of transfection, cells were used for the either calcium mobilization assay or cAMP accumulation assay.

All cells were maintained at 37 °C in the presence of 5% CO₂, and all cell culture reagents were purchased from Invitrogen Corp. (Carlsbad, CA) unless otherwise noted.

Mutagenesis

Mutations were introduced into the wild-type human GLP-1R gene by using site-directed mutagenesis (Quikchange II; Agilent Technologies, Santa Clara, CA) and were verified through Sanger sequencing (Genewiz, Boston MA). Wild-type and mutant hGLP-1R receptor constructs were transfected into HEK TReX293 cells by using Fugene6 (Promega, Madison, WI) as the transfection reagent. Cells transfected this way were used transiently for assays.

Calcium mobilization assay

Human GLP-1R Chem-9 cells, hGCGR Chem-1 cells, or hGLP-1R mGα15 TReX293 cells were plated at a concentration of 15,000 cells/20μL/well in black-walled, clear-bottomed, 384 well plates (Greiner Bio-One, Monroe, North Carolina), with TReX293 cells also requiring poly-D-lysine coating, in DMEM containing 10% FBS, 20 mM HEPES, 100 U/mL penicillin/streptomycin, and 1X NEAA). These cells were grown overnight at 37 °C in the presence of 5% CO₂. During the day of assay, medium was removed with an ELx405CW cell washer (Bio-Tek, Winooski, VT) and

replaced with 40 μ L of 2 μ M Fluo-4, AM (Invitrogen, Carlsbad, CA) prepared as a 2.3 mM stock in DMSO and mixed in a 1:1 ratio with 10% (w/v) pluronic acid F-127 and diluted in Assay Buffer (Hank's balanced salt solution, 20 mM HEPES, 350mg/liter NaHCO_3 and 2.5 mM Probenecid (Sigma-Aldrich, St. Louis, MO) using a Multidrop Combi (Thermofisher Scientific, Waltham, MA) and cells were incubated with this dye solution for 50 minutes at 37 $^{\circ}$ C and 5% CO_2 . Dye was then removed and replaced with 20 μ L of Assay Buffer. Test compounds were transferred to daughter plates using an ECHO acoustic plate reformatter (Labcyte, Sunnyvale, CA) and then diluted into Assay Buffer. Ca^{2+} flux was measured using the Functional Drug Screening System 7000 (FDSS, Hamamatsu, Japan). Baseline readings were taken (10 images at 1 Hz, excitation, 470 \pm 20 nm, emission, 540 \pm 30 nm) and continued every second for the entirety of the assay. Next, 20 μ L/well test compounds at a 2X concentration were added using the FDSS's integrated liquid handler. Cells were incubated with compounds for approximately 2.5 min and then an EC20 concentration of GLP-1 or Glucagon as a solution in Peptide Diluent (Hank's balanced salt solution, 20 mM HEPES, and 350mg/liter NaHCO_3 , and 0.1% bovine serum albumin (BSA)) was applied. For concentration-response curve experiments, compounds were serially diluted 1:3 into 10-point concentration response curves and were transferred to daughter plates using the ECHO. Test compounds were again applied and followed by EC20 concentrations of GLP-1 or Glucagon. For fold shift experiments, compounds were added at 2X their final concentration and then increasing concentrations of GLP-1 were added in the presence of vehicle or the appropriate concentration of test compound. Data were obtained as maximum-minimum fluorescent ratios and then

normalized to percentage of maximum GLP-1 response. Calculation of compound EC50 was performed using the curve-fitting software of GraphPad Prism (version 5.01). GLP-1fold shift was calculated as a ratio of GLP-1 EC50 in the presence of vehicle to the GLP-1 EC50 in the presence of test compound. Data shown represent mean values obtained from at least three independent determinations performed in triplicate or greater (error bars represent \pm SEM) unless otherwise specified. Together, the CRC and fold-shift data were used to determine the potency and mechanism of action for each compound at hGLP-1R or selectivity against hGCGR (**Figure 1.7**).

Kinetic cAMP accumulation assay

hGLP-1R INS-1 cells or transiently-transfected hGLP-1R pGLO TReX293 cells were plated in 20 μ L at a density of 15,000 total cells per well in a 384-well, clear-bottom, black, poly-D-lysine coated plates (#354663; Corning, Corning, NY) in plating medium (growth medium without selection antibiotics) and were incubated overnight at 37 °C and 5% CO₂. Prior to assaying, medium was removed using the flick-and-slam method and cell plates were then loaded with GloSensor™ cAMP Reagent (Promega) resuspended in HEPES buffer at a concentration of 2% (v/v) in CO₂-independent medium (Invitrogen). Plates were then incubated at 37 °C and 5% CO₂ for 90 minutes before being transferred quickly to an FDSS7000 set to 37 °C for

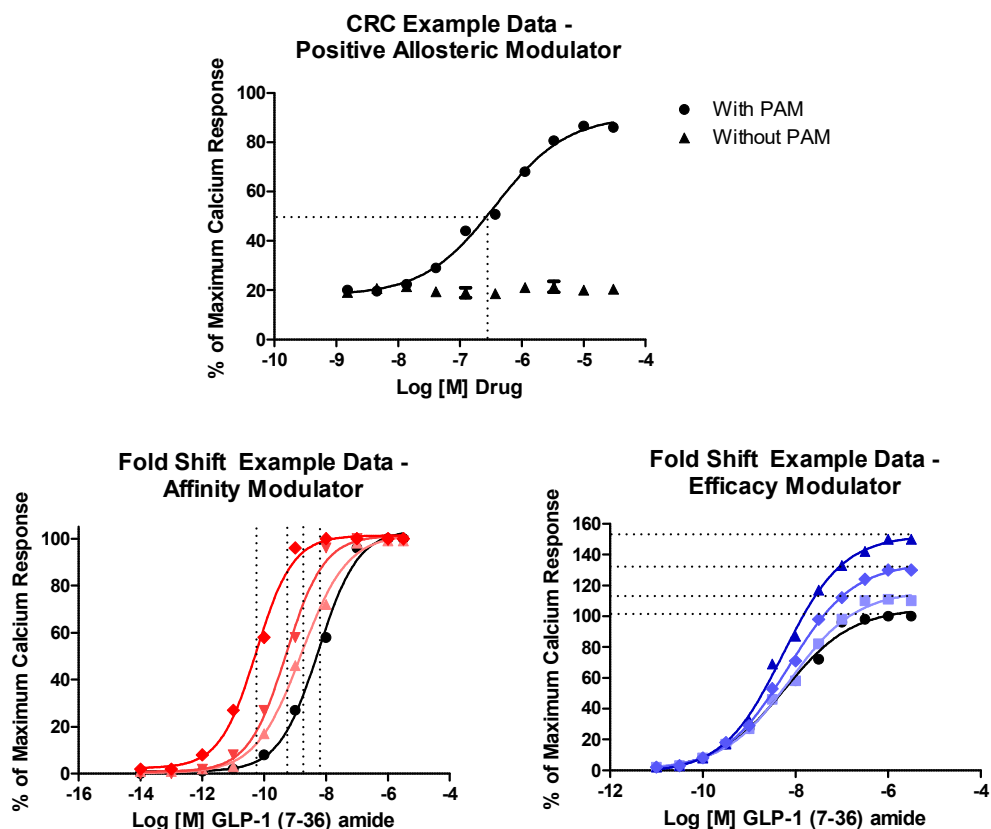


Figure 1.7: Example data for CRC and fold shift experiments using positive allosteric modulators. Potency for a PAM can be determined by increasing the compound's concentration in the presence of a fixed concentration of an agonist (in this case, GLP-1). The concentration of PAM that potentiates an EC_{20} concentration of GLP-1 to 50% of the maximal cellular response will define that compound's EC_{50} . In the CRC example above, the PAM potentiates a GLP-1 EC_{20} with a potency of 370 nM. The shape of this curve will not distinguish between PAMs that increase the affinity and/or efficacy of the orthosteric agonist in a CRC assay. However, a foldshift assay can distinguish between these two types of PAMs, and any variation between. In this assay, the response to a range of agonist concentrations (in this case, GLP-1) is measured in the presence of several different fixed concentrations of a PAM. Increasing concentrations of an affinity PAM (red) will proportionally increase the apparent potency of the agonist. In contrast, increasing concentrations of an efficacy PAM (blue) will proportionally increase the maximal response of the agonist.

kinetic luminescence reading. Baseline readings were taken (160 images at 1 image/3 seconds) and continued every 3 seconds for the entirety of the assay. Next, 20 μ L/well test compounds at a 2X concentration were added using the FDSS's integrated liquid

handler. Cells were incubated with compounds for approximately 5 minutes and then an EC20 concentration of GLP-1 as a solution in Peptide Diluent was applied. For concentration-response curve experiments, compounds were serially diluted 1:3 into 10-point concentration response curves and were transferred to daughter plates using the ECHO and diluted in CO₂-independent medium to a 2X concentration. For fold shift experiments, compounds were added at 2X their final concentration and then increasing concentrations of GLP-1 were added in the presence of vehicle or the appropriate concentration of test compound. Data were obtained as max-min luminescence ratios and then normalized to percentage of maximal GLP-1 (7-36) amide response. Single point values represent mean values obtained from at least three independent determinations performed in triplicate or greater (error bars represent +/- SEM) unless otherwise specified.

β-Arrestin Recruitment and GPCR Internalization Assays

The recruitment of β-arrestin was measured using PathHunter™ Express hGLP-1R CHO cells (DiscoverX; Fremont, CA) and the internalization of GLP-1R was measured using PathHunter™ Express hGLP-1R U2OS cells (DiscoverX; Fremont, CA). For each assay, single use cell vials were reconstituted in 12 mL of CP reagent and plated at 20 μL per well in 384-well plates (Greiner Bio-one, Austria). The following day, cells were treated with 2.5 μL of compound and incubated at 37 °C for 15-30 minutes, followed by treatment with 2.5 μL of 10⁻¹⁰ to 10⁻⁶ M liraglutide (Novo Nordisk, Denmark) and incubated at 37 °C for 90-180 minutes. All Incubation times used were according to manufacturer's specific instructions. Substrate was added to

each well and after a 60-minute room temperature incubation, luminescence values were obtained using a Perkin Elmer Enspire (Perkin Elmer, Foster City, CA).

Genomic DNA isolation and polymerase chain reaction (PCR)

hGLP-1R Chem9 cells were seeded in 10 cm cell culture dishes one day before the experiment. On the second day, cells were harvested and total DNA was extracted using an DNeasy Blood and Tissue kit (Qiagen, Valencia, CA). Total DNA was quantified by spectrophotometer reading at 260 nm and 280 nm and 500 ng of this genomic DNA sample was used to perform polymerase chain reaction (PCR) using *Pfu*Turbo DNA polymerase (Agilent, Santa Clara, CA) and the provided protocol. The primers were designed to amplify human and rat GLP-1R at complementary sequences of the intron-exon bounds of exon 10 and 11 in order to provide differentiation between genomic and over-expressed DNA for subsequent sequencing.

GLP-1R 976 Forward: CGGGTCATCTGCATCGTG

GLP-1R 1120 Reverse: GCTCGTCCATCACAAAGGC

The amplification protocol for GLP-1R was 95 °C for 2 min, 30 cycles of 95 °C for 30 s, 55 °C for 30 s, and 72 °C for 1 min. The final extension step was at 72 °C for 10 min. The PCR products were then electrophoresed on a 1.5% agarose gel containing ethidium bromide in parallel with 1 Kb Plus DNA Ladder (Invitrogen).

Total RNA isolation, reverse transcription and polymerase chain reaction (RT-PCR)

hGLP-1R Chem9 cells were seeded in 10 cm cell culture dishes one day before the experiment. On the second day, cells were harvested and total mRNA was extracted using an RNeasy Mini Kit (Qiagen, Valencia, CA). Total RNA was quantified by spectrophotometer reading at 260 nm and 280 nm and 5 ug was reversely transcribed into cDNA using SuperScript II™ Reverse Transcriptase (Invitrogen, Carlsbad, CA) according to the manufacturer's protocol. One tenth of each yielded cDNA sample was used to perform polymerase chain reaction (PCR). The primers were designed to amplify full sequence of human and rat GLP-1R. An internal primer at position 478 was also designed to in the case that the G-C abundant ATG primers failed.

hGLP-1R ATG Forward: ATGGCCGGCGCCCCCG

hGLP-1R TGA Reverse: TCAGCTGCAGGAGGCCTG

hGLP-1R 478 Forward: GTTATCGCCTCTGCGATCC

The amplification protocol for hGLP-1R was 95 °C for 2 min, 30 cycles of 95 °C for 30 s, 55 °C for 30 s, and 72 °C for 1.5 min. The final extension step was at 72 °C for 10 min. The PCR products were then electrophoresed on a 1.5% agarose gel containing ethidium bromide in parallel with 1 Kb Plus DNA Ladder (Invitrogen).

ERK1/2 Phosphorylation

Receptor-mediated ERK1/2 phosphorylation was determined by quantitative western blot analysis with fluorescent antibodies. Transiently-expressing hGLP-1R

TREx293 cell populations were homogenized and seeded into poly-d-lysine-coated, clear, 6-well plates at a density of 1,000,000 cells/well, in assay medium 24 h before assays. The medium was aspirated, cells were washed once with serum-free medium (DMEM supplemented with 20 mM HEPES), and then cells were serum-starved for a minimum of 1 hour before assay. At room temperature, cells were pretreated with PAM or vehicle for 5 minutes, then GLP-1 or vehicle for 10 minutes. Assays were terminated through the aspiration of ligand-containing medium and the addition of 1 mL of lysis buffer (50 mM Tris HCl, pH 7.4, 50 mM NaCl, 5 mM EDTA, 2 mM NaF, 1 mM Na₃VO₄, 1 mM PMSF, 1X Complete protease inhibitor cocktail, 1X phosphatase inhibitor cocktails 2 and 3) per well. Cell lysates were incubated on ice for 20-30 min. The supernatant was separated from cell debris by centrifugation at 16,000×g for 10 min at 4°C. Protein concentrations in cell lysates were quantified by Pierce BCA Protein Assay (Pierce Biotechnology, Waltham, MA) and aliquots of lysate were prepared in protein loading buffer, containing 10% β-mercaptoethanol and 1X Protein Sample Loading Buffer (LI-COR Biosciences, Lincoln, NE). Samples were loaded on 10% Mini-Protean TGX Precast SDS-polyacrylamide gel (Bio-Rad) for electrophoresis and transferred to Protran Nitrocellulose Membrane (Whatman, Maidstone, United Kingdom). After transfer, membranes were blocked in Odyssey® Blocking Buffer (LI-COR) at room temperature for 1 h. Primary antibodies p44/42 MAPK (Erk1/2) rabbit (Cell Signaling, Danvers, MA, cat # 9102) and Phospho-p44/42 MAPK (Erk1/2) (Thr202/Tyr204) (E10) Mouse mAb were diluted in blocking solution and incubated with the membranes at 4°C overnight. Membranes were then washed with TBST and incubated with IRDye® 800CW Goat anti-Rabbit IgG (H + L)

(LI-COR, cat. # 926-32211) and IRDye® 680LT Goat anti-Mouse IgG (H + L) (LI-COR, cat. # 926-68020) at room temperature for 1 h. Membranes were washed again with TBST and visualized with a fluorescent imaging assay using the Odyssey Imaging System (LI-COR) to detect immunoreactive proteins. Data are normalized to non-phosphorylated ERK of vehicle control.

Static Islet Experiments

Murine islets were isolated from 9- to 10-week-old C57BL/6 J male mice as previously described by dissection of the splenic portion of the pancreas followed by digestion with collagenase P (Roche Molecular Biochemicals). Groups of two pancreases were digested in 2 mg of collagenase/pancreas in Hanks buffered saline for 6–9 min at 37 °C using a wrist-action shaker. Purified islets were cultured overnight at 37 °C in RPMI-1640 with 5.6 mM glucose. After overnight culture, glucose-stimulated insulin secretion (GSIS) of islets was assessed using a static incubation protocol. Static incubation studies were performed in 12-well plates for 60 minutes at 37°C and 5% CO₂ in RPMI-1640 containing 5.6 mM or 16.7 mM glucose in the presence of 10 nM exendin-4 alone or with 30 • M compound. Islets were matched for size and number. Insulin concentration was determined by radioimmunoassay (Millipore, St. Charles, MO, USA). Insulin secretion was normalized to islet equivalents (IEQ), representing islet volume.

Ancillary/off-target screening assays

Prior to conducting in vivo experiments, compounds were submitted to Eurofins Panlabs Lead profiling screening panel of 68 GPCRs, ion channels, enzymes,

transporters, and nuclear hormone receptors. Test compounds (10 μ M) were evaluated in competition binding assays using standard orthosteric radioligands for each target (n = 2). Results were calculated as % inhibition of radioligand binding, with >50% inhibition representing significant activity at a given target

Plasma protein and brain homogenate binding

The protein binding of each compound was determined in plasma via equilibrium dialysis employing RED Plates (ThermoFisher Scientific, Rochester, NY). Plasma was added to the 96 well plate containing test compound and mixed thoroughly for a final compound concentration of 5 μ M. Subsequently, an aliquot of the plasma-compound mixture was transferred to the *cis* chamber (red) of the RED plate, with a phosphate buffer (25 mM, pH 7.4) in the *trans* chamber. The RED plate was sealed and incubated for 4 hours at 37° C with shaking. At completion, aliquots from each chamber were diluted 1:1 with either plasma (*cis*) or buffer (*trans*) and transferred to a new 96 well plate, at which time ice-cold acetonitrile containing internal standard (50 ng/mL carbamazepine) (2 volumes) was added to extract the matrices. The plate was centrifuged (3000 RFC, 10 min) and supernatants transferred and diluted 1:1 (supernatant: water) into a new 96 well plate, which was then sealed in preparation for LC/MS/MS analysis. Each compound was assayed in triplicate within the same 96-well plate. Fraction unbound was determined using the following equation:

$$F_u = \frac{Conc_{buffer}}{Conc_{plasma}}$$

A similar approach was used to determine the degree of brain homogenate binding, which employed the same methodology and procedure with the following modifications: 1) a final compound concentration of 1 μM was used, 2) naïve rat brains were homogenized in DPBS (1:3 composition of brain:DPBS, w/w) using a Mini-Bead Beater machine in order to obtain brain homogenate, which was then utilized in the same manner as plasma in the previously described plasma protein binding assay. Fraction unbound was determined using the following equation:

$$\text{Diluted: } f_{u,d} = \frac{\text{Conc}_{\text{buffer}}}{\text{Conc}_{\text{plasma}}}$$

$$\text{Undiluted: } f_u = \frac{1/D}{\left\{ \left(\frac{1}{f_{u,d}} \right) - 1 \right\} + 1/D}$$

where D = dilution factor

Hepatic microsomal intrinsic clearance

Human or rat hepatic microsomes (0.5 mg/mL) and 1 μM test compound were incubated in 100 mM potassium phosphate pH 7.4 buffer with 3 mM MgCl_2 at 37 °C with constant shaking. After a 5 min preincubation, the reaction was initiated by addition of NADPH (1 mM). At selected time intervals (0, 3, 7, 15, 25, and 45 min), aliquots were taken and subsequently placed into a 96-well plate containing cold acetonitrile with internal standard (50 ng/mL carbamazepine). Plates were then centrifuged at 3000 rcf (4° C) for 10 min, and the supernatant was transferred to a separate 96-well plate and diluted 1:1 with water for LC/MS/MS analysis. The in vitro half-life ($T_{1/2}$, min, Eq. 1), intrinsic clearance (CL_{int} , mL/min/kg, Eq. 2) and

subsequent predicted hepatic clearance (CL_{hep} , mL/min/kg, Eq. 3) was determined employing the following equations:

$$T_{1/2} = \frac{\ln(2)}{k}$$

where k represents the slope from linear regression analysis of the natural log percent remaining of test compound as a function of incubation time

$$CL_{int} = \frac{0.693}{in\ vitro\ T_{1/2}} \times \frac{mL\ incubation}{mg\ microsomes} \times \frac{45\ mg\ microsomes}{gram\ liver} \times \frac{20^a\ gram\ liver}{kg\ body\ wt}$$

^ascale-up factors: of 20 (human) or 45 (rat)

$$CL_{hep} = \frac{Q_h \cdot CL_{int}}{Q_h + CL_{int}}$$

where Q_h (hepatic blood flow, mL/min/kg) is 21 (human) or 70 (rat).

LC/MS/MS Bioanalysis of Samples

Samples were analyzed on a Thermo Electron TSQ Quantum Ultra triple quad mass spectrometer (San Jose, CA) via electrospray ionization (ESI) with two Thermo Electron Accella pumps (San Jose, CA), and a Leap Technologies CTC PAL autosampler (Carrboro, NC). Analytes were separated by gradient elution on a dual column system with two Thermo Hypersil Gold (2.1 x 30 mm, 1.9 μ m) columns (San Jose, CA) thermostated at 40°C. HPLC mobile phase A was 0.1% formic acid in water and mobile phase B was 0.1% formic acid in acetonitrile. The gradient started at 10% B after a 0.2 min hold and was linearly increased to 95% B over 0.8 min; hold at 95% B for 0.2 min; returned to 10% B in 0.1 min. The total run time was 1.3 min and the HPLC flow rate was 0.8 mL/min. While pump 1 ran the gradient method, pump 2

equilibrated the alternate column isocratically at 10% B. Compound optimization, data collection and processing was performed using Thermo Electron's QuickQuan software (v2.3) and Xcalibur (v2.0.7 SP1).

Cytochrome P450 Cocktail Inhibition Assay in Human Liver Microsomes:

A cocktail of substrates for cytochrome P450 enzymes (1A2: Phenacetin, 10 μ M; 2C9: Diclofenac, 5 μ M; 2D6: Dextromethorphan, 5 μ M; 3A4: Midazolam, 2 μ M) were mixed for cocktail analysis. The positive control for pan-P450 inhibition (miconazole) was included alongside test compound in analysis. A reaction mixture of 100 mM potassium phosphate (KPi), pH 7.4, 0.1 mg/mL human liver microsomes (HLM) and Substrate Mix is prepared and aliquoted into a 96-deepwell block. Test compound and positive control (in duplicate) were then added such that the final concentration of test compound ranged from 0.1 – 30 μ M. The plate was vortexed briefly and then pre-incubated at 37 °C while shaking for 15 minutes. The reaction was initiated with the addition of NADPH (1 mM final concentration). The incubation continued for 8 min and the reaction quenched by 2x volume of cold acetonitrile containing internal standard (50 nM carbamazepine). The plate was centrifuged for 10 minutes (4000 rcf, 4 °C) and the resulting supernatant diluted 1:1 with water for LC/MS/MS analysis. A 12-point standard curve of substrate metabolites over the range of 0.98 nM to 2000 nM.

Samples were analyzed via electrospray ionization (ESI) on an AB Sciex API-4000 (Foster City, CA) triple-quadrupole instrument that was coupled with Shimadzu LC-10AD pumps (Columbia, MD) and a Leap Technologies CTC PAL auto-sampler

(Carrboro, NC). Analytes were separated by gradient elution using a Fortis C18 3.0 x 50 mm, 3 μ m column (Fortis Technologies Ltd, Cheshire, UK) thermostated at 40 °C. HPLC mobile phase A was 0.1% formic acid in water (pH unadjusted), mobile phase B was 0.1% formic acid in acetonitrile (pH unadjusted). The gradient started at 10% B after a 0.2 min hold and was linearly increased to 90% B over 1.2 min; held at 90% B for 0.1 min and returned to 10% B in 0.1 min followed by a re-equilibration (0.9 min). The total run time was 2.5 min and the HPLC flow rate was 0.5 mL/min. The source temperature was set at 500 °C and mass spectral analyses were performed using multiple reaction monitoring (MRM), with transitions specific for each compound utilizing a Turbo-Ionspray® source in positive ionization mode (5.0 kV spray voltage).

The IC₅₀ values for each compound were obtained for the individual CYP enzymes by quantitating the inhibition of metabolite formation for each probe substrate. A 0 μ M compound condition (or control) was set to 100% enzymatic activity and the effect of increasing test compound concentrations on enzymatic activity could then be calculated from the % of control activity. Curves were fitted using XLfit 5.2.2 (four-parameter logistic model, equation 201) to determine the concentration that produces half-maximal inhibition (IC₅₀).

In vivo DMPK experimental

Discrete IV PK experiments were carried out at the Vanderbilt Center for Neuroscience Drug Discovery in male rats (n=2) at a dose of 1.0 mg/kg in 10% EtOH, 50% PEG 400, 40% saline. Each compound formulation was administered IV via the

jugular vein to dual-cannulated (carotid artery and jugular vein) adult male Sprague-Dawley rats, each weighing between 250 and 350 g (Harlan, Indianapolis, IN). Whole blood collections via the carotid artery were performed at 0.033, 0.117, 0.25, 0.5, 1, 2, 4, 7, and 24 hours post dose and plasma samples prepared for bioanalysis. Discrete oral (PO) PK experiments in rats (n=2) were carried out analogously using a 3 mg/kg dose in a Tween 80 and 0.5% methyl cellulose (MC) based vehicle administered by oral gavage. Whole blood collections via the carotid artery were performed at 0.25, 0.5, 1, 2, 4, 7, and 24 hours post dose. Single time point (1 hr) samples of plasma and brain were collected after oral dosing of each compound at 3 mg/kg in order to assess brain distribution (brain:plasma partition coefficient, K_p). *In vivo* samples were analyzed via LC/MS/MS utilizing electrospray ionization (ESI) and MRM transition(s) specific to the analyte.

Behavioral pharmacology general methods

Male Sprague-Dawley rats weighing between 275 and 300 grams (Harlan Laboratories, Inc Indianapolis, IN) were used for the behavioral studies and were housed maintained under a 12-h light/dark cycle (lights on at 6 AM, lights off at 6 PM) with free access to food and water. The experimental protocols, which were performed during the light cycle, were approved by the Institutional Animal Care and Use Committee of Vanderbilt University and conformed to the guidelines established by the National Research Council Guide for the Care and Use of Laboratory Animals.

Catalepsy

Rats were administered haloperidol (1.5mg/kg, i.p., dissolved in 8.5% lactic acid) 60 minutes prior to vehicle (10% Tween 80), compound, (10 and 30mg/k, i.p.) or Neurocrine A2A antagonist (56.6mg/kg, i.p.). After an additional 30 minutes' pretreatment interval, all rats were assessed in the catalepsy model. Catalepsy was measured by placing the forepaws of each rat gently onto a horizontal bar placed 6 cm from the testing surface and with the body positioned at an angle of $\sim 45^\circ$ to the testing surface. The latency in seconds required for the rat to remove one or both forepaws from the bar was measured with a testing cutoff of 30 seconds.

Spontaneous Locomotor Activity

Locomotor activity studies were conducted by using a SmartFrame Open Field System (Kinder Scientific, San Diego, CA) equipped with 16×16 infrared photobeams located 1 in above the floor of the chamber. Rats were pretreated with vehicle or test compound (10–30 mg/kg i.p.) for 30 min and then placed in the open-field chambers for a 60-min test session. Ambulation was measured as the total number of photobeam breaks per 30-min interval and recorded with a Pentium I computer equipped with Motor Monitor System software (Kinder Scientific). Data were analyzed by one-way ANOVA followed by Dunnett's test using JMP version 11 statistical software (SAS Institute, Cary, NC).

Animal care and use

All animal study procedures were approved by the Institutional Animal Care and Use Committee and were conducted in accordance with the National Institutes of

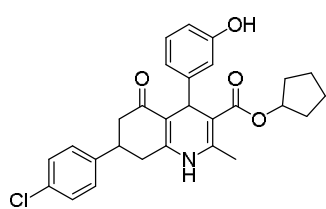
Health regulations of animal care covered in Principles of Laboratory Animal Care
(National Institutes of Health).

Development of the first CNS-penetrant GLP-1R Positive allosteric modulator

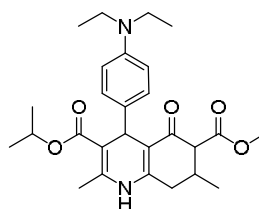
Prior discovery of GLP-1R PAMs through high-throughput screening^[116]

To this date, very few non-peptidic ligands for GLP-1R have been reported, and even fewer of those presented have been allosteric modulators. At the outset of this project, our laboratory was most interested in the discovery of positive allosteric modulators for GLP-1R due to the benefits of this mode of action imparts, mentioned previously in this chapter. Utilizing commercially available cell lines, our laboratory pioneered a novel mixed-cell, high-throughput intracellular calcium mobilization screen looking for agonists, modulators, and antagonists of GLP-1R with selectivity against GCGR. First pass screening of the 172,000 Vanderbilt Institute for Chemical Biology (VICB) compound collection was performed with co-plated GLP-1R- and GCGR-expressing cells. Cells were treated with a triple-add format: 1) compound addition, 2) EC₅₀ concentration of GLP-1, and 3) EC₅₀ concentration of glucagon. With the addition of positive controls (EC_{MAX} of both GLP-1 and glucagon) and negative controls (vehicle), this assay format revealed three windows of compound action: receptor agonists, GLP-1 potentiators and antagonists, and GCGR potentiators and antagonists, respectively. This HTS campaign yielded 98 hit compounds, which were subjected to subsequent confirmation and selectivity assays, including the native pathway of cAMP accumulation, activity in CHO-K1 cells, and activity in the related melanocortin 4 receptor (MC4R). After these hit compounds were fully characterized and divided into activity categories, only six compounds were GLP-1R selective with

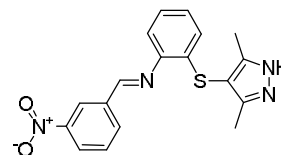
activity in both calcium mobilization and cAMP accumulation. (**Figure 1.8**) Four of these compounds had reliable calcium mobilization potencies below 10 μM . These compounds were subjected to tier 1 DMPK assay, consisting of predicted hepatic clearance assays and plasma protein binding assays. While all four compounds suffered from high clearance at the rate of hepatic blood-flow, one compound, VU0110945 (**1.6**), had a much higher fraction unbound (F_u) when compared with the others, at over 10%. As **1.6** possessed the highest potency of the 6 hits, and did not suffer from high plasma protein binding, it was chosen as the putative PAM lead compound.



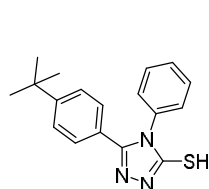
VU0056556 (1.1)
Potentiator
 hGLP-1R EC_{50} : 5.6 μM
 human CL_{hep} (mL/min/kg): 20.7
 rat CL_{hep} (mL/min/kg): 68.3
 human PPB (F_u): 0.005
 rat PPB (F_u): 0.006



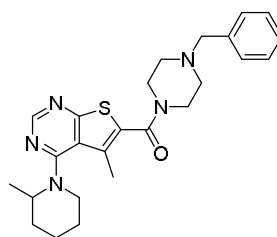
VU0074057 (1.2)
Potentiator
 hGLP-1R EC_{50} : >10 μM
 DMPK not determined
 due to high potency



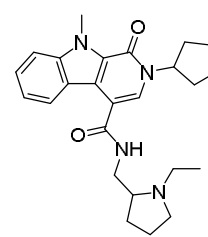
VU0021375 (1.3)
Potentiator
 hGLP-1R EC_{50} : >10 μM
 DMPK not determined
 due to high potency



VU0055252 (1.4)
Potentiator
 hGLP-1R EC_{50} : 4.7 μM
 human CL_{hep} (mL/min/kg): 18.1
 rat CL_{hep} (mL/min/kg): 67.9
 human PPB (F_u): 0.006
 rat PPB (F_u): 0.001



VU0094076 (1.5)
Potentiator
 hGLP-1R EC_{50} : >10 μM
 DMPK not determined
 due to high potency



VU0110945 (1.6)
Ago-Potentiator
 hGLP-1R EC_{50} : 4.1 μM
 human CL_{hep} (mL/min/kg): 19.9
 rat CL_{hep} (mL/min/kg): 68.8
 human PPB (F_u): 0.115
 rat PPB (F_u): 0.160

Figure 1.8: Structures, activities and DMPK data of hGLP-1R-selective PAMs discovered during HTS campaign. These data were used to prioritize and choose hits for further SAR studies.

Optimization of hit VU0110945 to obtain lead GLP-1R PAM VU0453379

Of the PAMs identified in the HTS campaign, we decided to focus on **1.6**, which possessed the highest potency and best pharmacokinetic and physiochemical properties of the identified hits. The unique racemic 1-oxo-2,9-dihydro-1*H*-pyrido[3,4-*b*]indole-4-amide scaffold also piqued our interests, as this scaffold had not been reported in the literature as a chemotype known to bind with GPCRs. In order to rationally alter the lead compound structure, we divided the structure into regions of interest that would give us the most information in the structure-activity relationship (**Figure 1.9**) We engaged a strategy whereby we would make the smallest modifications first, such as synthesizing enantiopure analogs of **1.6** and replacing the *N*-alkyl pyrrolidine chain, then work our way up to larger, scaffold based modifications. We started by synthesizing the enantiopure analogs of **1.6**

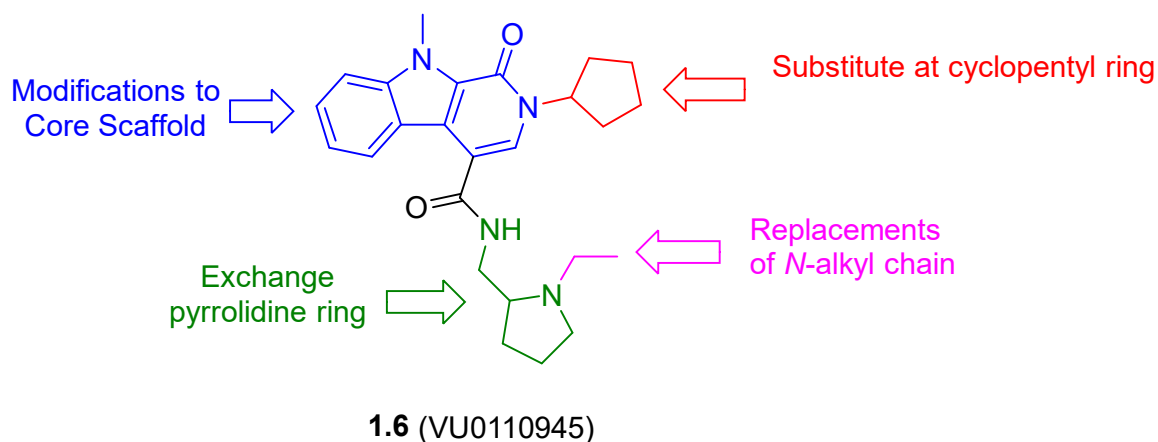
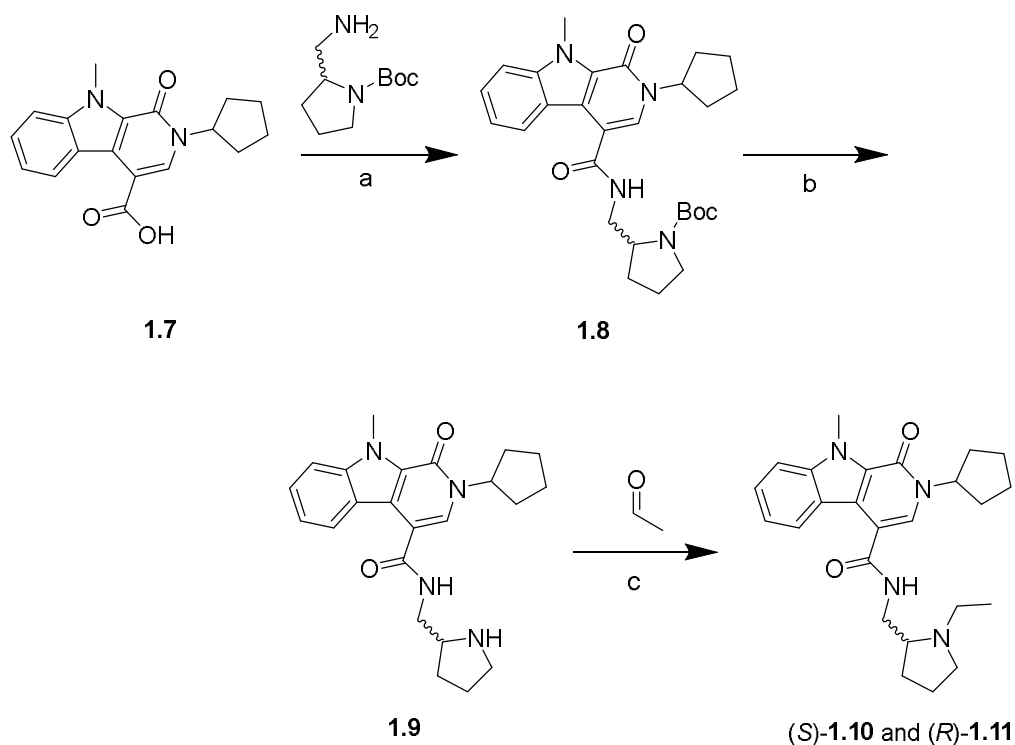


Figure 1.9: Library optimization strategy for VU0110945 to evaluate the structure-activity relationship and increase PAM potency and efficacy

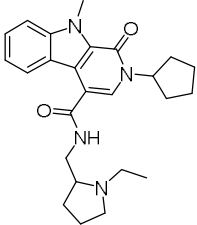
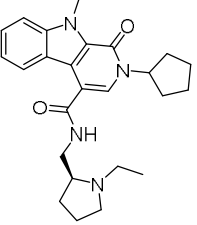
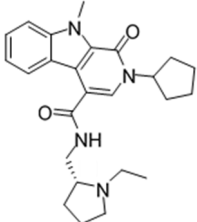


Scheme 1.1: Route to resynthesis of VU0110945 and enantiopure analogs. Reagents and conditions: (a) HATU, DIEA, DMF, (S)- or (R)-tert-butyl-2-(aminomethyl)pyrrolidine-1-carboxylate, 82–85%; (b) 4 M HCl in dioxane, DCM, 99%; (c) acetaldehyde, NaBH(OAc)₃, DCM, 81–83%.

following **Scheme 1.1**. Commercially available acid **1.7** was coupled to either (S)- or (R)-tert-butyl-2-(aminomethyl)pyrrolidine-1-carboxylate to provide **1.8**. Deprotection of the Boc moiety under acidic conditions delivered **1.9**, which underwent a subsequent reductive amination reaction with acetaldehyde to give **1.10** and **1.11** in 62–68% overall yield for the three-step sequence. These compounds, along with **1.6**, were next screened in CRC-format with the aforementioned calcium mobilization assay in the presence of an EC₂₀ concentration of GLP-1 using the

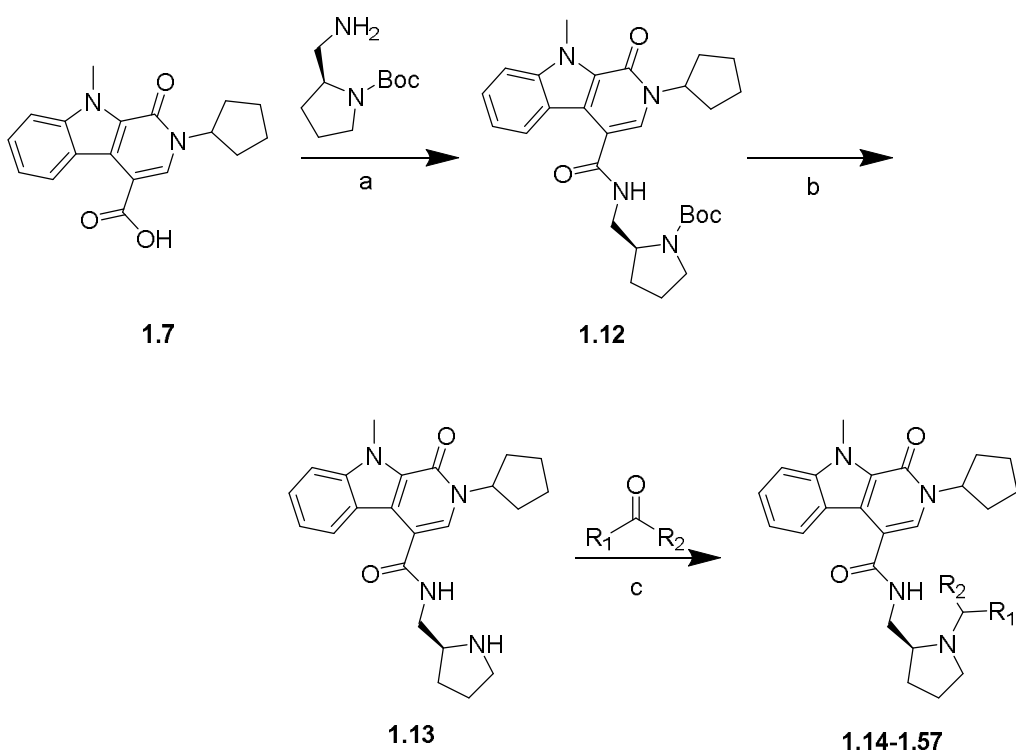
commercial hGLP-1R Chem-9 cell line used in the HTS screen. The results of this screen are shown in **Table 1.1**.

Table 1.1: Structures for VU0110945 and enantio-pure analogs **1.10** and **1.11** with associated potency and efficacy activity data from 10-point CRC-format screen at hGLP-1R. Ca²⁺ mobilization responses for each compound are reported as a percentage of the maximum GLP-1 response. VU number denotes the compound identifier assigned by Vanderbilt University. Data represent the mean of at least 3 replicate experiments with similar results.

Structure	Compound Number	VOID	hGLP-1R EC ₅₀ (μM)	hGLP-1R %GLP-1 _{MAX}
	1.6	VU0110945	4.1	58.9
	1.10	VU0449776	2.4	53.4
	1.11	VU6005188	>30	42.2

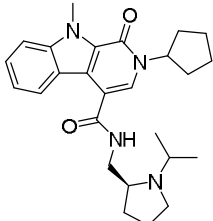
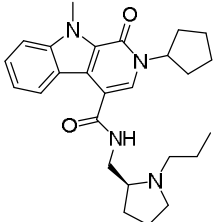
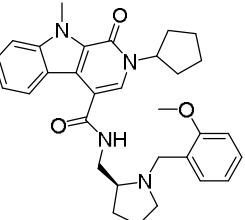
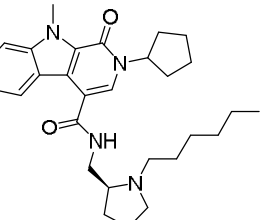
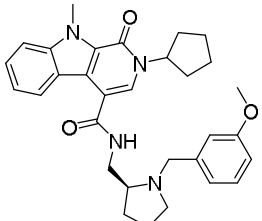
Through this experiment, we determined the (*S*)-enantiomer of the aminopyrrolidine ring of **1.6**, **1.11** (VU0449776) held all the activity, and were happy to observe a modest 2-fold increase in potency. We decided to use this enantiomer for all further SAR studies of this scaffold. Next, we began to modify the *N*-alkyl chain of the southern pyrrolidine ring. Utilizing a similar route to that of **1.6**, we chose the

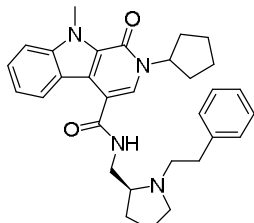
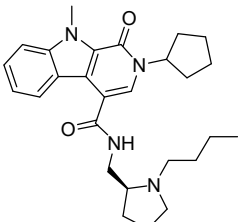
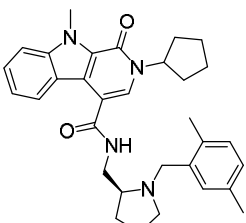
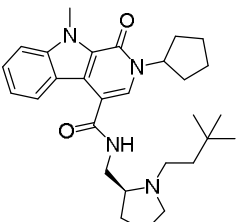
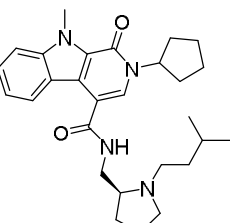
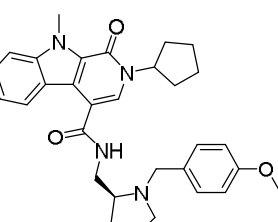
final step as the point of variation. We incorporated various alkyl, benzyl, and heterocyclic groups with the corresponding aldehydes and ketones using a microwave-assisted reductive amination procedure, providing compound **1.14-1.57** in 22-94% yield (**Scheme 1.2**). These library analogs were then assayed in CRC format against the hGLP-1R Chem-9 cell line using the calcium mobilization assay. The results of this screen are shown in **Table 1.2**.

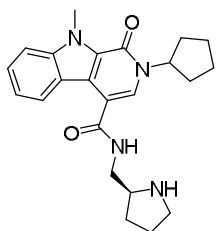
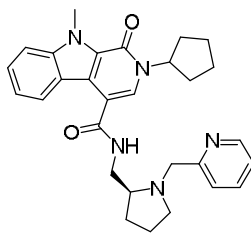
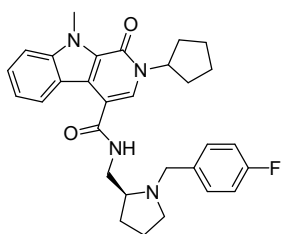
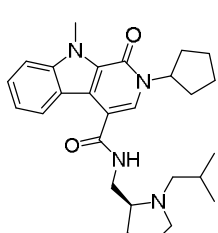
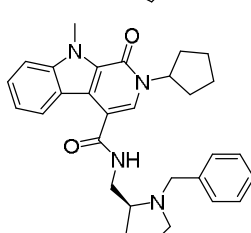
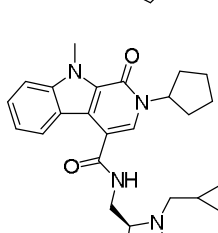
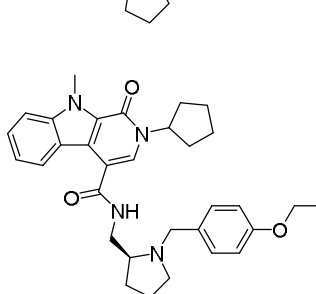


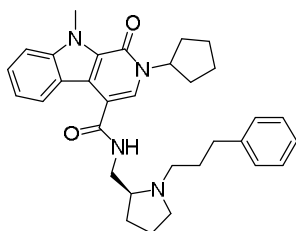
Scheme 1.2: Microwave-assisted library synthesis of analogs **1.14-1.57** varying *N*-alkyl substituent of aminopyrrolidine ring. Reagents and conditions: (a) HATU, DIEA, DMF, (*S*)-tert-butyl-2-(aminomethyl)pyrrolidine-1 carboxylate, 84%; (b) 4 M HCl in dioxane, DCM, 99%; (c) carbonyl compound, HOAc, MP-CNBH₃, DCM, μ W, 10 min., 100 °C, 56–82%. Synthesis performed in combination with P. Gentry

Table 1.2: Structures for N-substituted VU0449776 analogs **1.14-1.57** and associated potency and efficacy activity data from 10-point CRC-format screen at hGLP-1R. Ca²⁺ mobilization responses for each compound are reported as a percentage of the maximum GLP-1 response. VU number denotes the compound identifier assigned by Vanderbilt University. Data represent the mean of at least 3 replicate experiments with similar results.

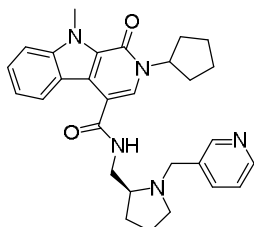
Structure	Compound Number	VOID	hGLP-1R EC ₅₀ (μM)	hGLP-1R %GLP-1MAX
	1.14	VU0453379	1.3	59.2
	1.15	VU0453332	6.5	48.4
	1.16	VU0453240	>10	68.3
	1.17	VU0453334	>10	55.7
	1.18	VU0453223	>10	44.1

	1.19	VU0453385	>10	68.5
	1.20	VU0453249	>10	47
	1.21	VU0453251	>10	32
	1.22	VU0453261	>10	40
	1.23	VU0453282	>10	50
	1.24	VU0453296	>10	46

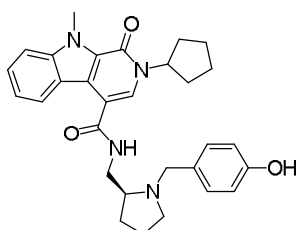
	1.25	VU0453297	>10	41
	1.26	VU0453299	>10	44
	1.27	VU0453306	>10	34
	1.28	VU0453323	>10	52
	1.29	VU0453329	>10	40
	1.30	VU0453335	>10	45
	1.31	VU0453337	>10	30



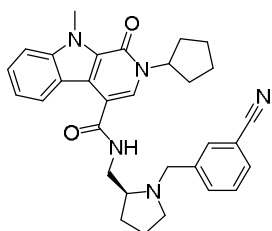
1.32 VU0453344 >10 59



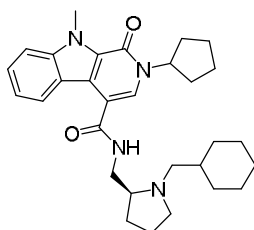
1.33 VU0453349 >10 49



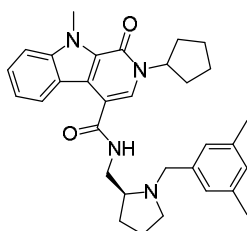
1.34 VU0453358 >10 53



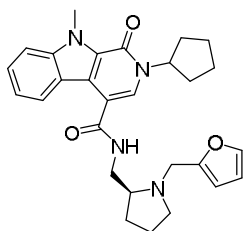
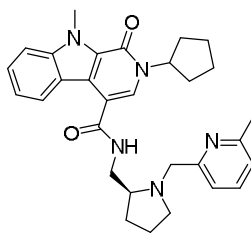
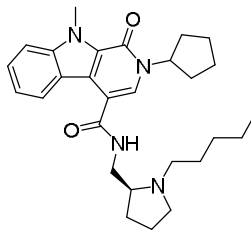
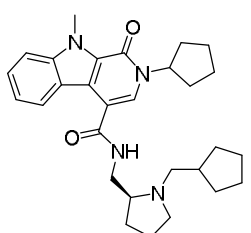
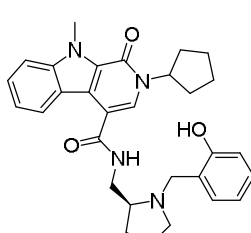
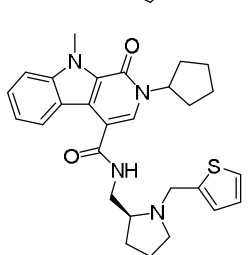
1.35 VU0453359 >10 32

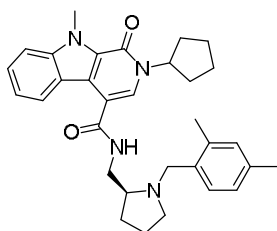


1.36 VU0453364 >10 38



1.37 VU0453369 >10 30

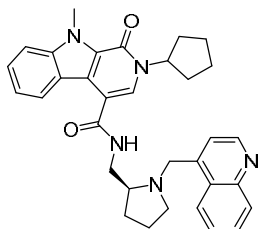
	1.38	VU0453371	>10	43
	1.39	VU0453377	>10	39
	1.40	VU0453382	>10	84
	1.41	VU0453383	>10	61
	1.42	VU0453234	Inactive	
	1.43	VU0453244	Inactive	



1.44

VU0453250

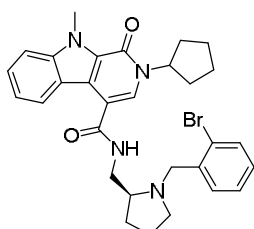
Inactive



1.45

VU0453257

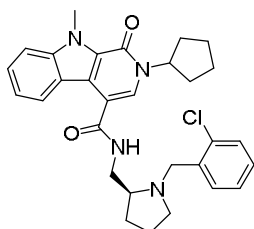
Inactive



1.46

VU0453295

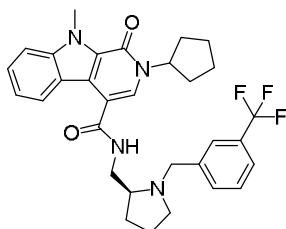
Inactive



1.47

VU0453298

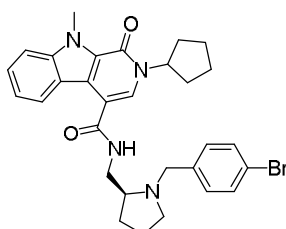
Inactive



1.48

VU0453301

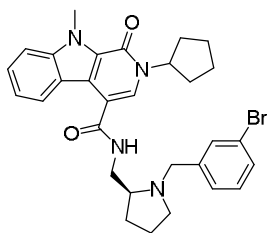
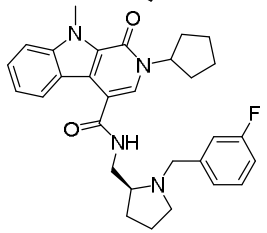
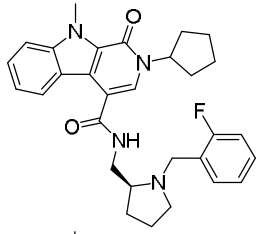
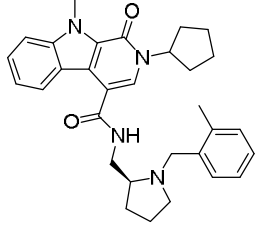
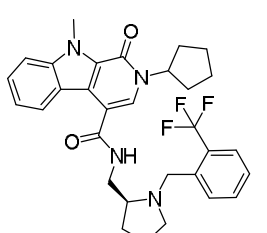
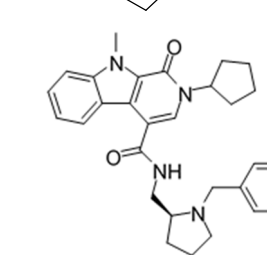
Inactive

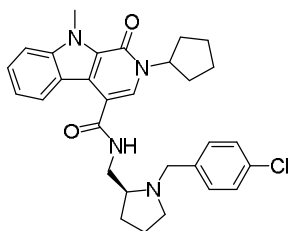


1.49

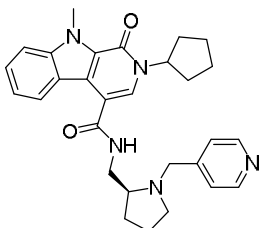
VU0453307

Inactive

	1.50	VU0453324	Inactive
	1.51	VU0453325	Inactive
	1.52	VU0453331	Inactive
	1.53	VU0453333	Inactive
	1.54	VU0453350	Inactive
	1.55	VU0453351	Inactive



1.56 VU0453365 Inactive



1.57 VU0453370 Inactive

Most of the analogs assayed demonstrated little or no ability to potentiate the EC₂₀ of GLP-1. Out of the 43 novel analogs tested, only two showed measurable potency above 10 μM. These two compounds **1.14** (VU0453379) and **1.15** (VU0453332) possessed short alkyl chains similar to the *N*-ethyl chain of **1.6**. While all analogs with alkyl substitutions showed some amount of activity, including carbocycles and branched chains, the SAR of the benzyl and heterocyclic analogs was not clear. Most of these analogs with activity required an electron-rich ring, but this was not a rule. It became clear we may experience steep SAR with this compound series. However, we were happy to find the exchange of ethyl for isopropyl of 1.14 provided a 2-fold boost in potency, and we were approaching a sub-micromolar GLP-1R PAM. In light of this, we began to further characterize the compound as our new lead, with the hopes we would discover properties that would improve our SAR strategy.

In vitro molecular pharmacological characterization of VU0453379

After the discovery of improved GLP-1R PAM 1.14, we sought to obtain a more in-depth pharmacological profile for this compound. First, we assayed the compound against the closely related hGCGR to determine whether the compound possessed the same selectivity as its parent 1.6. To our delight, 1.14 was inactive against hGCGR, much like 1.6, and we gained more confidence that the β -carboline scaffold was a generally selective chemotype (**Figure 1.10**). Further investigation into the potency

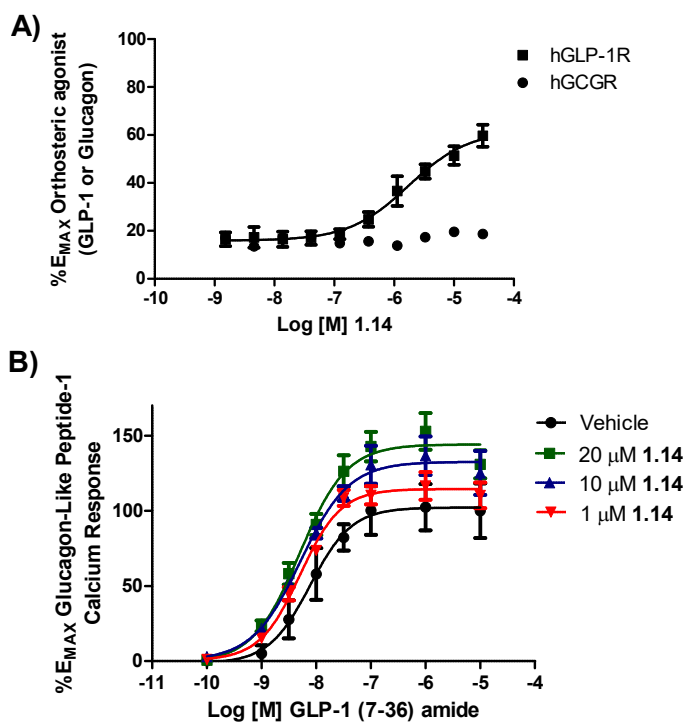


Figure 1.10: (A) Selectivity of hGLP-1R PAM VU0453379 (1.14). Calcium mobilization assays with hGLP-1R and hGCGR cells were used to obtain CRCs of compound 1.14 in the presence of a EC₂₀ concentration of GLP-1 (EC₅₀ values: hGLP-1R EC₅₀ = 1.7 μ M, hGCGR EC₅₀ = inactive). (B) GLP-1 CRC progressive fold-shifts of compound 1.14 at hGLP-1R. Calcium mobilization assays with hGLP-1R cells obtain GLP-1 CRCs in the presence of vehicle or 20 μ M, 10 μ M, and 1 μ M compound 1.14 (EC₅₀ values: hGLP-1R EC₅₀ of GLP-1 + vehicle = 7.7 nM, hGLP-1R EC₅₀ of GLP-1 + 20 μ M 1.14 = 4.9 nM, hGLP-1R fold-shift at 20 μ M = 1.6; 40% increase in GLP-1_{MAX} at 20 μ M concentration. Data represent the mean \pm S.E.M. of at least 3 independent experiments with similar results

and efficacy of the compound was carried out using a progressive fold-shift analysis. The results of this showed an insignificant 1.6-fold increase in the GLP-1 EC₅₀, but a much more dramatic increase in overall peptide efficacy at the receptor, an increase of 40% at the top concentration (**Figure 1.10**). These results suggested that compound 1.14 acts as a β -PAM, however this shift in efficacy could be misrepresented due to the inherent agonism often seen with this compound and others of the same series.

After further investigating the effects of **1.14** on hGLP-1R with respect to intracellular calcium flux, we looked toward identifying activity in more native systems, such as cAMP accumulation, β -arrestin recruitment, and receptor internalization. As calcium mobilization is not the native signaling pathway of GLP-1R, and the cell lines used to effect this response are engineered and over-expressing, we sought to alleviate any concerns on the ability of these compounds to act in native tissues. We first turned to cAMP accumulation as the secondary confirmatory assay. Unfortunately, due to instrument and cell-line issues, we were unable to gather this data for compound **1.14**. We were, however able to use this assay at a later date, and the troubleshooting, optimization, and results of those experiments will be discussed later in this chapter.

Next, we sought to discover any probe dependence associated with **1.14**. As GLP-1R has been reported to have 7 endogenous ligands, and there is an ever-growing list of FDA-approved GLP-1R RAs, we hoped our PAMs could potentiate the effects of these ligands regardless of their origin. This idea stemmed from the idea that PAMs could be used to lessen the dose and thus the negative effects of these RAs.

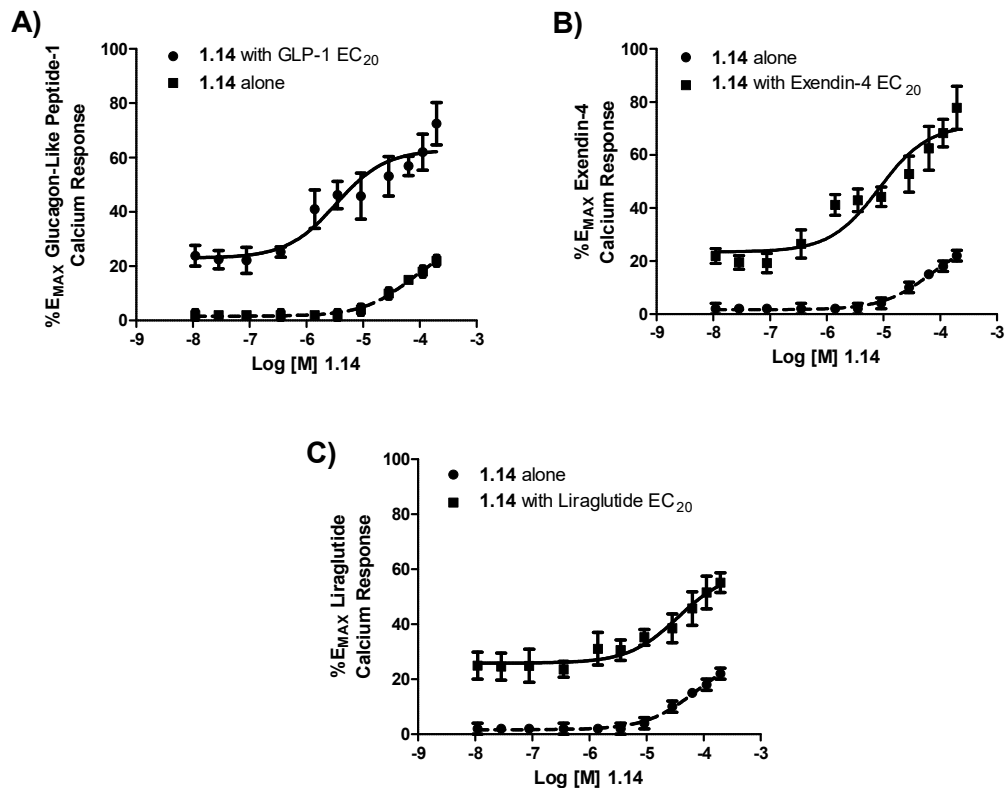


Figure 1.11: Molecular pharmacology of **1.14**. **(A)** CRC of **1.14** in the presence and absence of an EC₂₀ of GLP-1 ($EC_{50} = 1.8 \mu\text{M}$, $pEC_{50} = 5.74 \pm 0.2$, $59.2 \pm 2\%$ GLP-1 max). **(B)** CRC of **1.14** in the presence and absence of an EC₂₀ of exendin-4 ($EC_{50} = 8.4 \mu\text{M}$, $pEC_{50} = 5.07 \pm 0.3$, $1.5 \pm 5\%$ 1 max). **(C)** CRC of **1.14** in the presence and absence of an EC₂₀ of liraglutide ($EC_{50} = 30 \mu\text{M}$, $pEC_{50} = 4.5 \pm 0.2$, $59.2 \pm 1\%$ 1 max). Data represent the mean \pm S.E.M. of at least 3 independent experiments with similar results

First, we chose to examine the potential of 1.14 to potentiate the two primary GLP-1R RAs, exendin-4 and liraglutide. We screened our PAM in CRC format utilizing our standard calcium assay with and EC₂₀ of these two ligands as well as GLP-1 for comparison (**Figure 1.11**) To our delight, we found that 1.14 potentiated the effects of exendin-4- and liraglutide-mediated receptor activation to a similar degree of that of the native GLP-1 peptide. These data gave us hope that we may use out PAMs to investigate the effects of GLP-1R RA potentiation *in vivo*. After determining the degree of probe dependence associated with **1.14**, we desired more information on the effect

1.14 had on signaling pathways other than the primary pathway of G_s -induced cyclic AMP production. The first of these was β -arrestin recruitment to the receptor. β -arrestin signaling at GLP-1R, described earlier in this chapter, mediates a handful of the known anti-diabetic effects seen with receptor activation. As allosteric modulators often stabilize select conformations leading to signal bias, we sought to determine whether our PAMs shunted receptor activation down one signaling pathway over another. Similarly, we were also interested in the ability of **1.14** to induce a higher rate of receptor internalization above that of orthosteric agonists. For these experiments, liraglutide was used as the orthosteric ligand due to ease of formulation, and as we just discovered the ability of **1.14** to potentiate this ligand (Figure 1.12).

To our surprise, **1.14** had little to no effect on the recruitment of β -arrestin to the receptor at any concentration, but had a marked effect on receptor

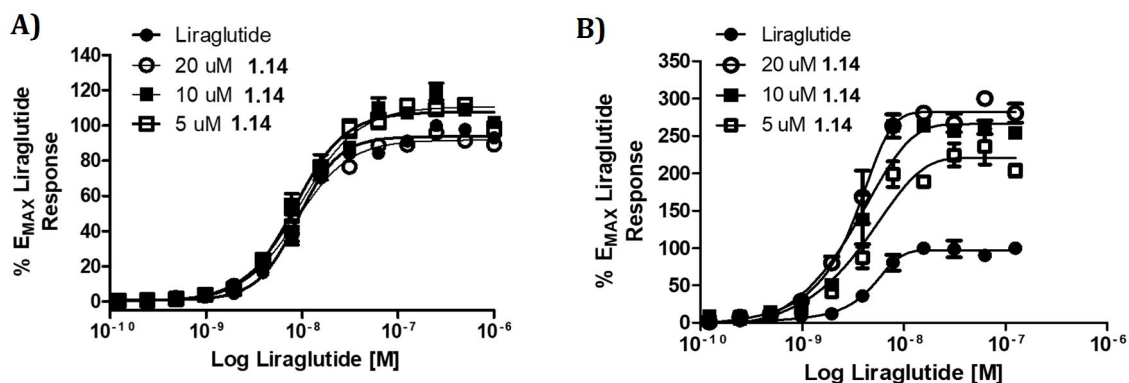


Figure 1.12: β -Arrestin recruitment and receptor internalization molecular pharmacology of **1.14**. Fold shift experiment of liraglutide in the presence of 5, 10, and 20 μ M **1.14** on the recruitment of β -arrestin (A) and GLP-1 receptor internalization (B) using the PathHunter Express DiscoverX assay platform. Efficacy of receptor internalization was increased by 2.26-fold at 20 μ M, while there was little to no effect on β -arrestin recruitment. Data are normalized to the maximal response of liraglutide alone and fit to a four-parameter logistic equation with variable slope. Values are expressed as mean \pm SEM, $n = 3$. These experiments were performed in conjunction with Dr. Lindsey Morris.

internalization. Thought the total fold-shift at the 20 μM was only 2.26-fold, we observed an over 150% increase in the maximum efficacy seen with liraglutide alone. With these data, we could to put together a more complete pharmacological profile of **1.14**.

Up to this point, all our *in vitro* pharmacology assays and discoveries were performed in engineered cell lines. While these data may provide insight into the decoupled actions of PAMs, we lastly sought to determine whether **1.14** could effect a response in native tissues. To this end, we employed a static islet incubation assay, where primary pancreatic islets are harvested from wild-type mice and treated with compound. After treatment, cell medium is removed and tested for hormone levels, namely how much insulin is produced by these cells post-treatment (**Figure 1.13**). In

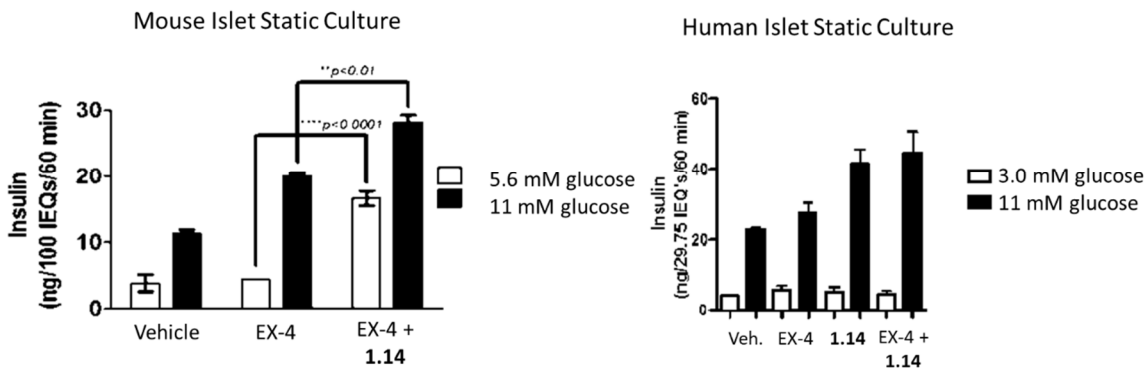


Figure 1.13: Measurement of the effect of 30 μM **1.14** on potentiation of glucose-stimulated insulin secretion in primary mouse islets and primary human islets in the presence of 10 nM exendin-4. (A) Islets were isolated from C57BL/6 male mice, size-matched into wells of a 12-well plate, and treated with vehicle, exendin-4, or exendin-4 + **1.14** at both low (5.6 mM) and high (11 mM) glucose for 60 min. $n = 3$. Data are represented as mean insulin response \pm SEM per 100 islet equivalents and analyzed using 2-way ANOVA followed by Sidak's multiple comparisons test. $**p < 0.01$, $****p < 0.0001$. (B) Islets were isolated from male human donor, size-matched into wells of a 12-well plate, and treated with vehicle, exendin-4, **1.14** alone, or exendin-4 + **1.14** at both low (3.0 mM) and high (11 mM) glucose for 60 min. $n = 3$. Data are represented as mean insulin response \pm SEM per 100 islet equivalents. Experiments performed by the Islet Core at Vanderbilt University Medical Center.

addition to mouse islets, were fortunately able to also test **1.14** with human islets. We were elated to find that not only does **1.14** show efficacy in hGLP-1R cell lines, but also in primary tissues. While there was some effect at potentiating EX-4-induced insulin secretion, it was clear the variable agonist effect often observed in primary calcium assays with **1.14** were physiologically relevant, leading to a robust effect on insulin secretion alone, as well. Overall, from these studies, we determined some key properties of **1.14** as a GLP-1R PAM, and also showed efficacy in primary tissues. With this knowledge in hand, we began to evaluate the DMPK profile of **1.14** to assess its potential as an *in vivo* tool.

In vitro & in vivo DMPK characterization of GLP-1 PAM VU0453379

Now that we possessed a GLP-1 PAM with modest potency and activity in primary tissues, we sought to determine the *in vitro* DMPK profile of compound **1.14** (VU0453379) in order to evaluate its potential to serve as a future *in vivo* tool compound with which to study its potential therapeutic effect with regards to T2D. The compound was assayed in several *in vitro* DMPK assays (**Table 1.3**), including plasma protein binding, rat and human microsomal stability, and a CYP450 inhibition panel. These studies revealed **1.14** to have a somewhat favorable DMPK profile with high free-fraction and low CYP450 inhibition. However, we found that like its parental compound **1.6** (VU0110945), **1.14** suffered from high clearance, at the rate of hepatic blood flow. We then turned to *in vivo* DMPK studies (**Table 1.3**), including distribution in rat, to determine the extent to which **1.14** may be useful as a tool compound. We were pleased to find that though this compound possessed liabilities,

Table 1.3: Full *in vitro* and *in vivo* DMPK profile of compound **1.14** (VU0453379) in Sprague–Dawley rat and human. Liver microsomal clearance was predicted using the well-stirred model with 20 and 45 g liver per kg body weight and 21 and 70 mL/kg hepatic blood flow for human and rat, respectively

Parameter	VU0453379
MW	434.28
TPSA	59.7
cLogP	3.51
P450 inhibition	IC₅₀ (μM)
P450 (1A2, 2C9, 3A4, 2D6)	>30, >30, 3.89, 10.1
<i>In Vitro</i> PK	
Rat CL _{HEP} (mL/min/kg)	69.9
Rat CL _{HEP} (mL/min/kg)	19.9
Rat PPB (f _u)	0.158
Human PPB (f _u)	0.146
Rat BHB	0.015
<i>In Vivo</i> Rat PK (IP, 10 mg/kg, 0.5 h)	
Plasma (nM)	181
Brain (nM)	481
Brain:Plasma (K _p)	2.7
<i>In Vivo</i> Rat PK (IV, 1mg/kg, PO, 1 mg/mL)	
Cl _{obs} (mL/min/kg)	72
t _{1/2} (min)	58
V _{ss} (L/kg)	4.0
%F	<0.01

it was highly brain penetrant, with a K_p of 2.7, making compound **1.14** the first known CNS-penetrant GLP-1R PAM. The observed clearance confirmed our *in vitro* results of high clearance, but when coupled with the high volume of distribution of 4 L/kg, we

achieved a half-life of just under an hour, an amount of time feasible for *in vivo* studies. Unfortunately, the oral bioavailability of **1.14** was very poor, at below 1%. This would require compound to be dosed either intraperitoneally or intravenously. We determined this profile to be less than ideal, but still workable for proof-of-concept studies; improvements to the compound would still need to be made to improve both clearance and potency. However, we were able to collect *in vivo* data for **1.14** in a model for Parkinson's disease, the haloperidol-induced catalepsy model. This experiment will be discussed later in this chapter. As the most prominent liability observed from DMPK studies was high clearance, we subjected compound **1.14** to metabolism identification studies looking for any soft spots in the structure that could be modified to improve this metric (**Figure 1.14**). The results of this study showed species-differential metabolism. The primary metabolite observed with rat liver microsomes was oxidation of the cyclopentyl ring attached to the β -carbolinone scaffold (**1.58**). Further oxidation of this compound lead to the secondary metabolite **1.60**. Human metabolism followed the path of oxidative *N*-dealkylation of the

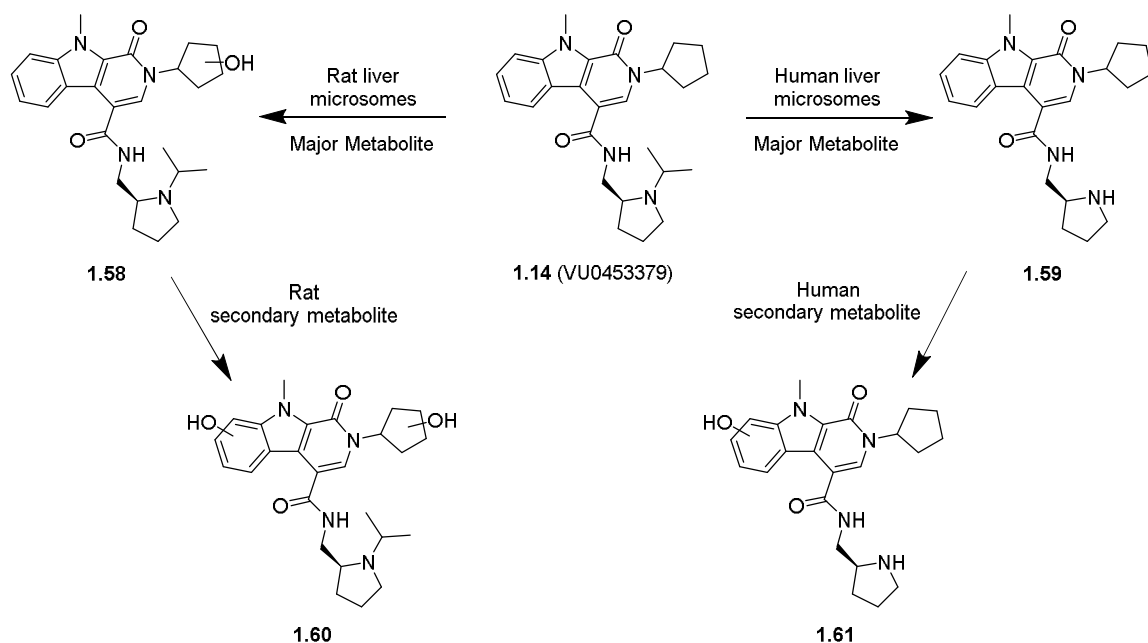


Figure 1.14: Results of metabolite identification following incubation of **1.14** with human and rat hepatic microsomes and NADPH. The rat primary metabolite identified, **1.58**, is the product of cyclopentyl hydroxylation. The human primary metabolite identified, **1.59**, is the product of oxidative *N*-dealkylation. Studies performed by R. Morrison

southern pyrrolidine ring (**1.59**), with further scaffold oxidation providing secondary metabolite **1.61**. These data provided valuable information as to where we should direct our SAR studies with regards to mitigating clearance.

Ancillary pharmacology of VU0453379

After determining both the pharmacological and pharmacokinetic profile of compound **1.14** (VU0453379), but before continuing on into *in vivo* studies, we sought to determine what, if any, wider ancillary pharmacology **1.14** may possess, in the hopes that we may learn of any off-target effects. In order to do this, we employed a commercial radioligand competition binding screen of 68 GPCRs, ion channels, and transporters (**Table 1.4**).

Table 1.4: Ancillary/off-target competition binding screen results for compound **1.14** (VU0453379). Compound **1.14** was dosed at 10 μ M for single point competition binding assays. Targets displaying significant binding ($\geq 50\%$ at 10 μ M) are outlined. Data represent the mean of 2 independent experiments with similar results. Studies performed by Eurofins Panlabs, Inc.

Target/Protein	Species	% Inhibition
Adenosine A ₁	Human	-1
Adenosine A _{2A}	Human	6
Adenosine A ₃	Human	14
Adrenergic α_{1A}	Rat	16
Adrenergic α_{1B}	Rat	-10
Adrenergic α_{1D}	Human	9
Adrenergic α_{2A}	Human	37
Adrenergic β_1	Human	24
Adrenergic β_2	Human	-8
Androgen (Testosterone) AR	Rat	11
Bradykinin B ₁	Human	12
Bradykinin B ₂	Human	11
Calcium Channel L-Type, Benzothiazepine	Rat	41
Calcium Channel L-Type, Dihydropyridine	Rat	22
Calcium Channel N-Type	Rat	2
Cannabinoid CB ₁	Human	48
Dopamine D ₁	Human	5
Dopamine D _{2S}	Human	8
Dopamine D ₃	Human	26
Dopamine D _{4.2}	Human	-2
Endothelin ET _A	Human	11
Endothelin ET _B	Human	3
Epidermal Growth Factor (EGF)	Human	11
Estrogen ER α	Human	15
GABA _A , Flunitrazepam, Central	Rat	12
GABA _A , Muscimol, Central	Rat	-1
GABA _{B1A}	Human	-2
Glucocorticoid	Human	1
Glutamate, Kainate	Rat	-6
Glutamate, NMDA, Agonism	Rat	1
Glutamate, NMDA, Glycine	Rat	-2
Glutamate, NMDA, Phencyclidine	Rat	18
Histamine H ₁	Human	22
Histamine H ₂	Human	25
Histamine H ₃	Human	26
Imidazoline I ₂ , Central	Rat	15
Interleukin IL-1	Mouse	-1
Leukotriene, Cysteinyl CysLT ₁	Human	22
Melatonin MT ₁	Human	37
Muscarinic M ₁	Human	-1
Muscarinic M ₂	Human	1

Muscarinic M ₃	Human	12
Neuropeptide Y Y ₁	Human	5
Neuropeptide Y Y ₂	Human	3
Nicotinic Acetylcholine	Human	8
Nicotinic Acetylcholine α 1, Bungarotoxin	Human	1
Opiate δ ₁ (OP1, DOP)	Human	6
Opiate κ (OP2, KOP)	Human	5
Opiate μ (OP3, MOP)	Human	5
Phorbol Ester	Mouse	2
Platelet Activating Factor (PAF)	Human	7
Potassium Channel [K _{ATP}]	Human	5
Potassium Channel hERG	Human	39
Prostanoid EP ₄	Human	30
Purinergic P2X	Rabbit	28
Purinergic P2Y	Rat	4
Rolipram	Rat	4
Serotonin (5-HT _{1A})	Human	3
Serotonin (5-HT _{2B})	Human	41
Serotonin (5-HT ₃)	Human	-4
Sigma σ ₁	Human	47
Sodium Channel, Site 2	Rat	49
Tachykinin NK ₁	Human	23
Thyroid Hormone	Rat	7
Transporter, Dopamine (DAT)	Human	42
Transporter, GABA	Rat	-2
Transporter, Norepinephrine (NET)	Human	28
Transporter, Serotonin (SERT)	Human	22

Agreeably, compound **1.14** demonstrated no significant binding (>50%) at any of the 68 tested targets. With these data, we were more confident to begin *in vivo* proof-of-concept studies.

Behavioral pharmacology studies with VU0453379

With the knowledge that we had developed the first selective, CNS-penetrant GLP-1R PAM, compound **1.14**, we began to explore its behavioral pharmacology profile. At this time, little was known of the relationship between GLP-1R tone in the CNS and neurodegenerative diseases such as Parkinson's disease, Alzheimer's

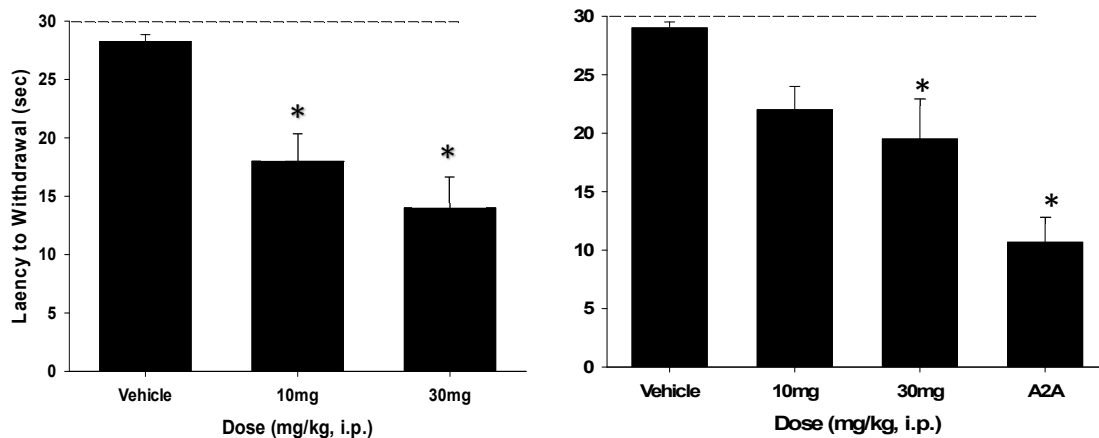


Figure 1.15: Compound **1.14** produces a dose-dependent reversal of haloperidol induced catalepsy in rats. (A) **1.14** at doses of 10 and 30 mg/kg ip (10% Tween 80) significantly reverse a 0.75 mg/kg ip dose of haloperidol. (B) (**1.14**) at doses of 30 mg/kg ip significantly reverse a 1.5 mg/kg ip dose of haloperidol and the clinically validated A2A antagonist preladenant is shown for comparison. Catalepsy was measured as the latency to withdraw the forepaws from a horizontal bar with a cutoff of 30 s. Vertical bars represent the means \pm SEM of 10–12 rats/treatment group. * $p < 0.0001$ vs vehicle by Dunnett's test. Experiments were performed by the Jones lab of the VCND.

disease, and Huntington's disease, however, correlations were arising suggesting decreased GLP-1R activity in these regions may be pathogenic. We decided to examine the effects of **1.14** in a well validated model of Parkinson's disease: haloperidol induced catalepsy (HIC). Haloperidol, a first-generation antipsychotic medication used to treat schizophrenia, is known to produce parkinsonian symptoms such as catalepsy (rigidity), bradykinesia (slowness of movement), and tremor. In the HIC model, haloperidol is used to induce a parkinsonian state, and test compounds are evaluated on their ability to reverse this state. The clinically validated A2A antagonist preladenant is used as a positive control and benchmark for the assay. Interestingly, neither GLP-1 agonists, such as exendin-4 or liraglutide, or GLP-1R PAMs had been evaluated in this preclinical model of the motor symptoms of PD. We tested both 10 and 30 mg/kg doses, administered ip, for their ability to reverse the

catalepsy induced by two doses of haloperidol, a screening dose of 0.75 mg/kg, and a more robust challenge at 1.5 mg/kg (**Figure 1.15**). Excitingly, at the lower challenge of 0.75 mg/kg haloperidol, statistically significant reversal in catalepsy was noted at both the 10 mg/kg (36.3% reversal) and 30 mg/kg (50.4% reversal) doses. For the 1.5 mg/kg dose of haloperidol, the same trend is noted, but significance is only achieved at the 30 mg/kg dose (36.6% reversal); data for the preladenant is shown for comparison (62% reversal). To further eliminate non-mechanism based efficacy in this model, we performed a spontaneous locomotor activity assay and noted no effect on locomotion or sedative effects (**Figure 1.16**). With these data, we determined **1.14** is the first example of GLP-1R activation displaying efficacy in a haloperidol-induced catalepsy model.

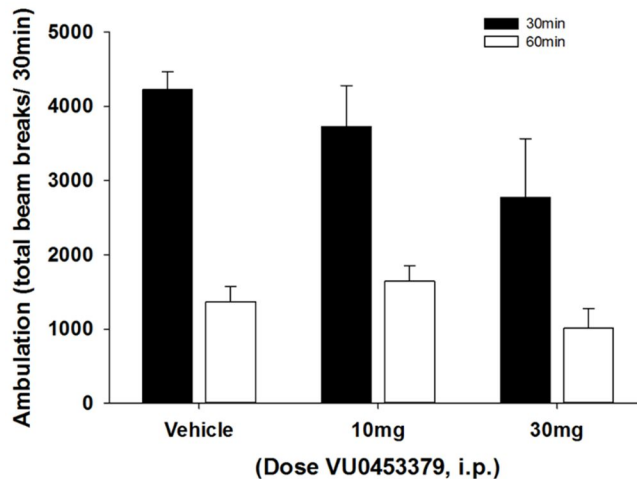
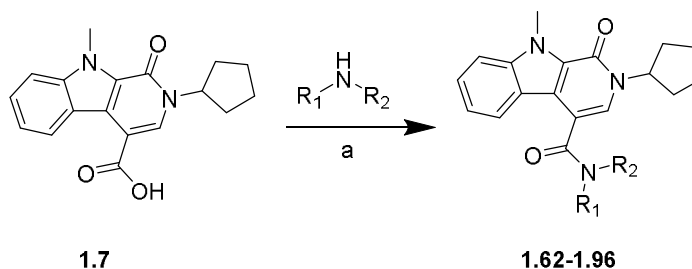


Figure 1.16: Effect of **1.14**, VU0453379, on spontaneous locomotor activity in male Sprague Dawley rats. No sedation was observed, supporting the efficacy noted in the HIC assay. Vehicles was 10% Tween 80.

Continued optimization of GLP-1R PAM VU0453379

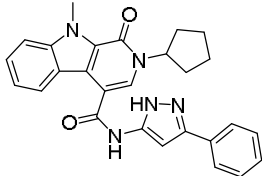
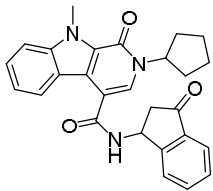
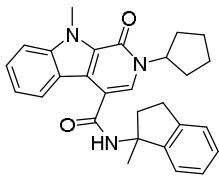
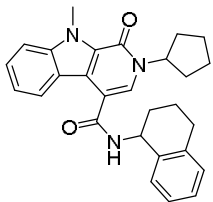
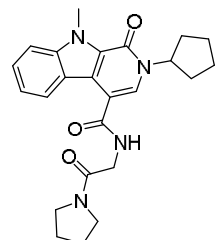
Explorations into the replacement of aminopyrrolidine ring

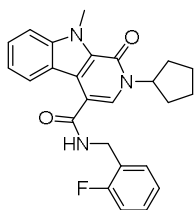
While we were elated to discover the first CNS-penetrant and efficacious GLP-1R PAM, compound **1.14** (VU0453379), we knew much more of the structure could be modified to effect improvements in the pharmacological and DMPK profiles with regards to potency, efficacy, and metabolism. As our first investigation into the SAR provided limited, but still useful results, we were optimistic that our future endeavors would succeed in achieving our goals. We first began to work out way up the structure, with the goal of replacing the aminopyrrolidine moiety responsible for much of the metabolism observed with human liver microsomes. Using a one-step amide coupling with our commercially available acid and commercially available amines (**Scheme 1.3**), we sought to cover a large portion of chemical space, including small aliphatic rings and chains, heterocycles, and aryl rings with an without alkyl linkers. (**Table 1.5**). All compounds synthesized were then tested in our primary calcium screening assay against hGLP-1R Chem-9 cells.



Scheme 1.3: Amide coupling sequence for the synthesis of analogues exploring potential replacements for the aminopyrrolidine ring of VU0453379 (**1.14**). Reagents and conditions: (a) HATU, DIEA, DMF, 3-13 hrs, 23-96% yield.

Table 1.5: Structures of compounds from library prepared as in **Scheme 1.3** and associated potency and efficacy activity data from 10-point CRC-format screen at hGLP-1R. Calcium mobilization responses for each compound are reported as a percentage of the maximum GLP-1 response. VU number denotes the compound identifier assigned by Vanderbilt University. Data represent the mean of at least 3 replicate experiments with similar results

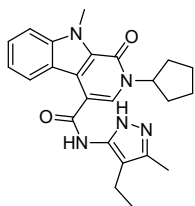
Structure	Compound Number	VUID	hGLP-1R EC50 (μ M)	hGLP-1R %GLP-1MAX
	1.62	VU6012906		Inactive
	1.63	VU6012907		Inactive
	1.64	VU6012908		Inactive
	1.65	VU6012909		Inactive
	1.66	VU6012910		Inactive



1.67

VU6012911

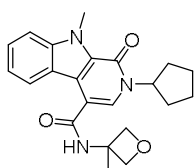
Inactive



1.68

VU6012912

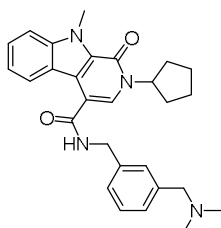
Inactive



1.69

VU6012913

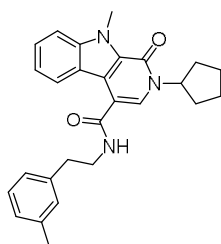
Inactive



1.70

VU6012914

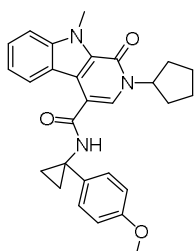
Inactive



1.71

VU6012915

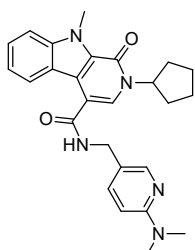
Inactive



1.72

VU6012916

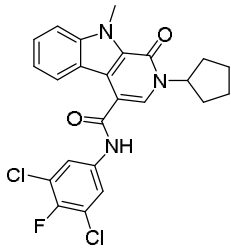
Inactive



1.73

VU6012917

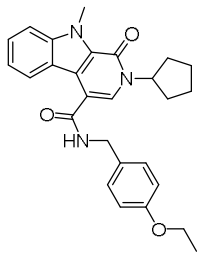
Inactive



1.74

VU6012919

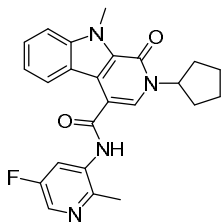
Inactive



1.75

VU6012918

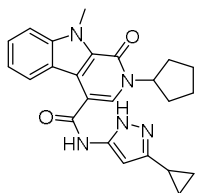
Inactive



1.76

V7U6012920

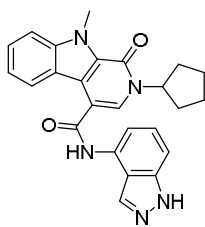
Inactive



1.77

VU6012921

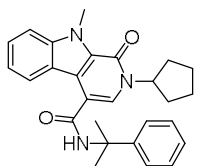
Inactive



1.78

VU6012922

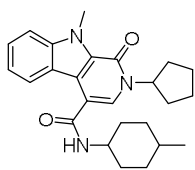
Inactive



1.79

VU6012923

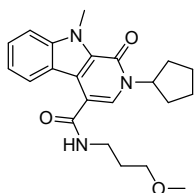
Inactive



1.80

VU6012924

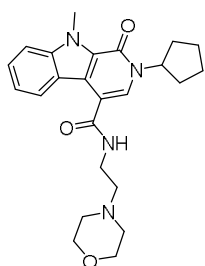
Inactive



1.81

VU6012925

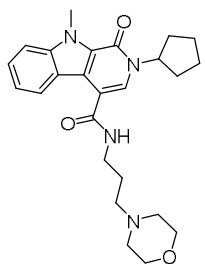
Inactive



1.82

VU0077523

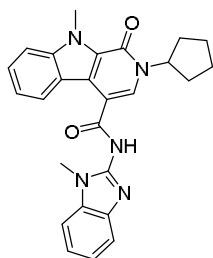
Inactive



1.83

VU0144196

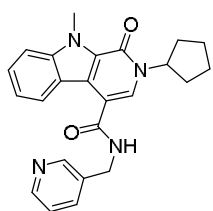
Inactive



1.84

VU0449647

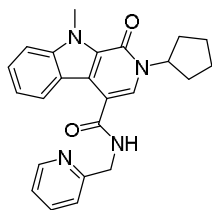
Inactive



1.85

VU0449777

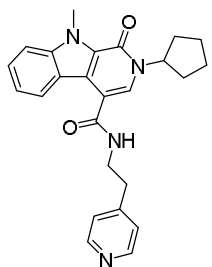
Inactive



1.86

VU0449778

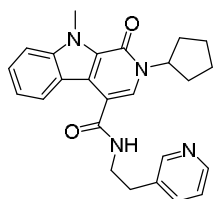
Inactive



1.87

VU0449779

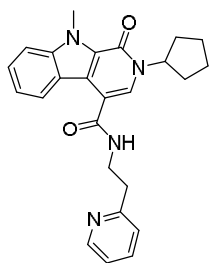
Inactive



1.88

VU0449780

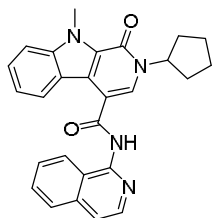
Inactive



1.89

VU0449781

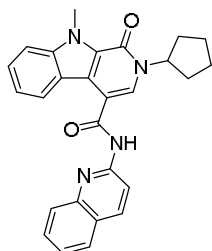
Inactive



1.90

VU0449782

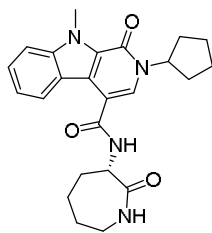
Inactive



1.91

VU0449783

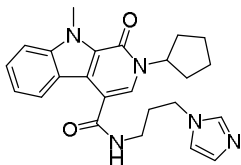
Inactive



1.92

VU0449784

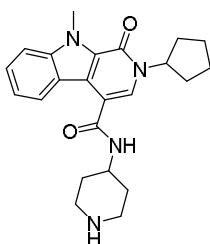
Inactive



1.93

VU0449785

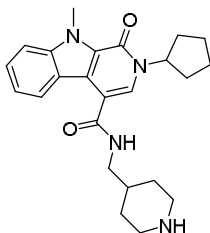
Inactive



1.94

VU0450252

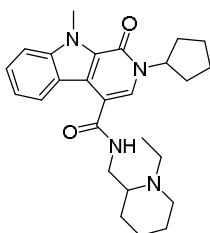
Inactive



1.95

VU0450253

Inactive



1.96

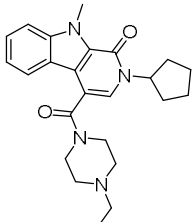
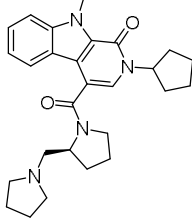
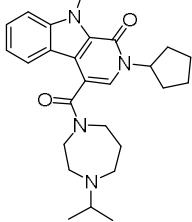
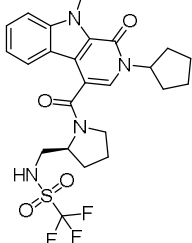
VU0453275

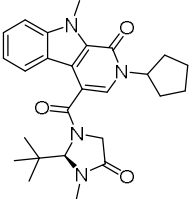
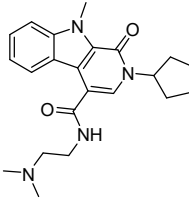
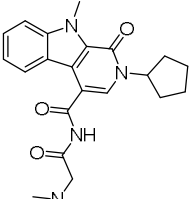
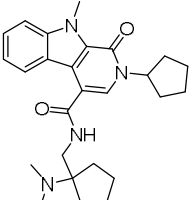
Inactive

To our surprise, and subsequent disappointment, none of the substitutions incorporated provided any activity in potentiating a GLP-1 EC₂₀ in the calcium flux assay. It became clear to us that the SAR of this compound was particularly steep. We subsequently invoked a strategy by which to mimic the 1,4-diamine moiety seen with

the aminomethylpyrrolidine ring, conjecturing that the hydrogen bond acceptors of this ring must be have a pivotal role in protein interaction. Using a synthetic route much like **Scheme 1.3**, several analogues were synthesized incorporating pieces that would mimic the aminomethylpyrrolidine ring more closely (**Table 1.6**).

Table 1.6: Structures of compounds from library prepared as in **Scheme 1.3** and associated potency and efficacy activity data from 10-point CRC-format screen at hGLP-1R. Calcium mobilization responses for each compound are reported as a percentage of the maximum GLP-1 response. VU number denotes the compound identifier assigned by Vanderbilt University. Data represent the mean of at least 3 replicate experiments with similar results

Structure	Compound Number	VUID	hGLP-1R EC50 (μM)	hGLP-1R %GLP-1MAX
	1.97	VU6012926		Inactive
	1.98	VU6012927		Inactive
	1.99	VU6012928		Inactive
	1.100	VU6012929		Inactive

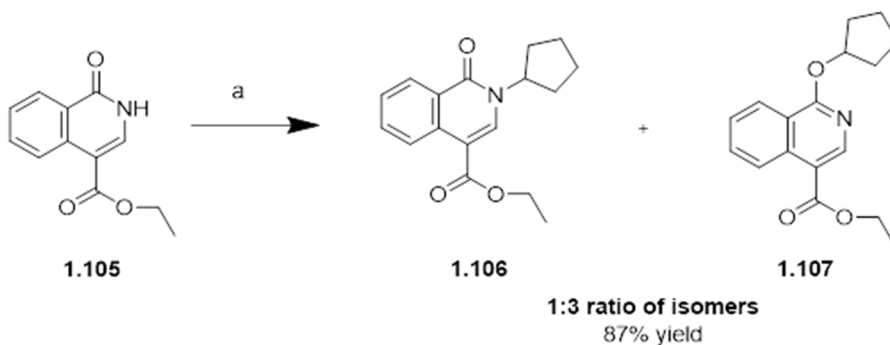
	1.101	VU6012930	Inactive
	1.102	VU6012931	Inactive
	1.103	VU6012932	Inactive
	1.104	VU6012933	Inactive

As with all other attempts to modify the aminopyrrolidine ring of VU0453379 (**1.14**), these substitutions were also completely devoid of activity. At this point, we ceased modifications to the southern portion of **1.14** and began to direct our attention toward the core β -carbolinone scaffold.

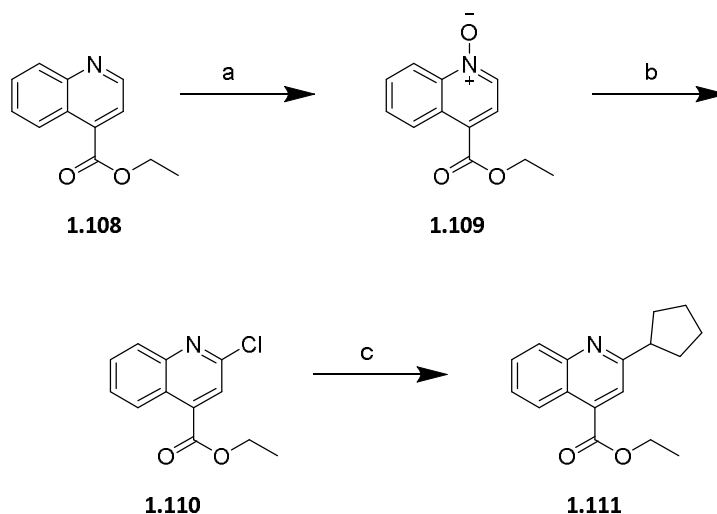
Explorations into core scaffold modifications

While there were a few commercially available compounds with modifications to the cyclopentyl ring of the scaffold, many more than were available would need to be made. We set about developing a synthetic route to arrive at these analogues,

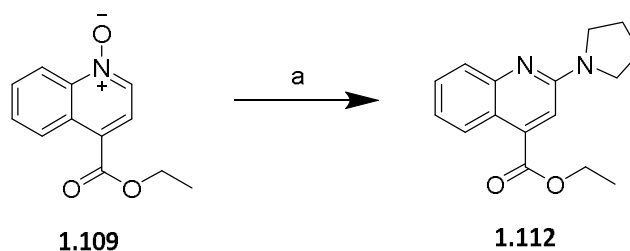
which will be discussed later in this section. In the meantime, we were curious if any minimization to the core scaffold would be tolerated. We envisioned substituting the tricyclic ring system with smaller rings, such as quinolones, isoquinolines, and isoquinolones, while also cleaving the β -carbolinone scaffold into a biarylaminopyridone to achieve more flexibility, and hopefully, more protein interactions. While some of these scaffolds were commercially available, the more directly analogous systems needed to be synthesized. First, we synthesized ethyl 2-cyclopentyl-1-oxo-1,2-dihydroisoquinoline-4-carboxylate (**1.106**) utilizing the method of **Scheme 1.4**. Using standard alkylation procedures on commercially available isoquinolone **1.105**, we were able to arrive at **1.106** in one step, albeit with low regioselectivity over the *O*-alkylation product. Still, enough of the desired alkylation product was isolated to push forward toward library synthesis in order to interrogate the SAR of the desired compounds. We then began developing a method to arrive at structurally similar quinolones, incorporating the same cyclopentyl moiety seen with **1.14** (**Scheme 1.5**). Starting with commercially available ethyl quinoline-4-carboxylate (**1.108**), we performed a 2-step N-oxide halogenation procedure to



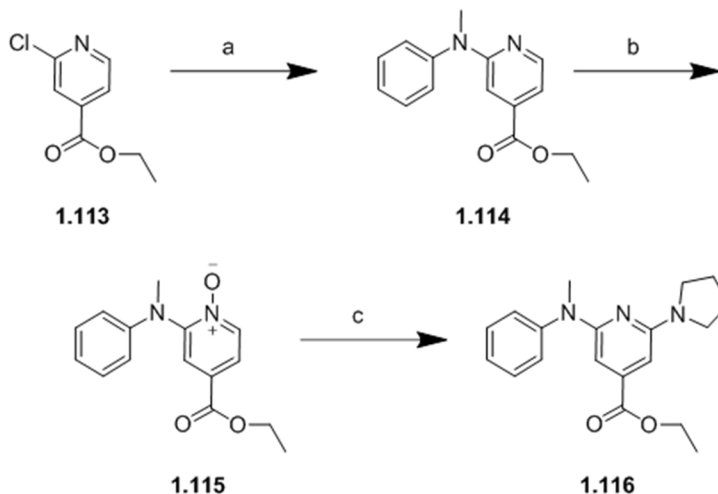
Scheme 1.4: Synthesis of isoquinolone scaffold analog. Reagents and conditions: (a) cyclopentyl iodide, Cs_2CO_3 , DMF, 100 °C, 24 hrs., 29% yield of desired isomer



Scheme 1.5: Synthesis of quinoline scaffold analog **1.111**. Reagents and conditions: (a) mCPBA, DCM, 71%; (b) TCICA, DCM, 48%; (c) cyclopentylzinc bromide, Pd(PtBu)₂, THF, 65%.

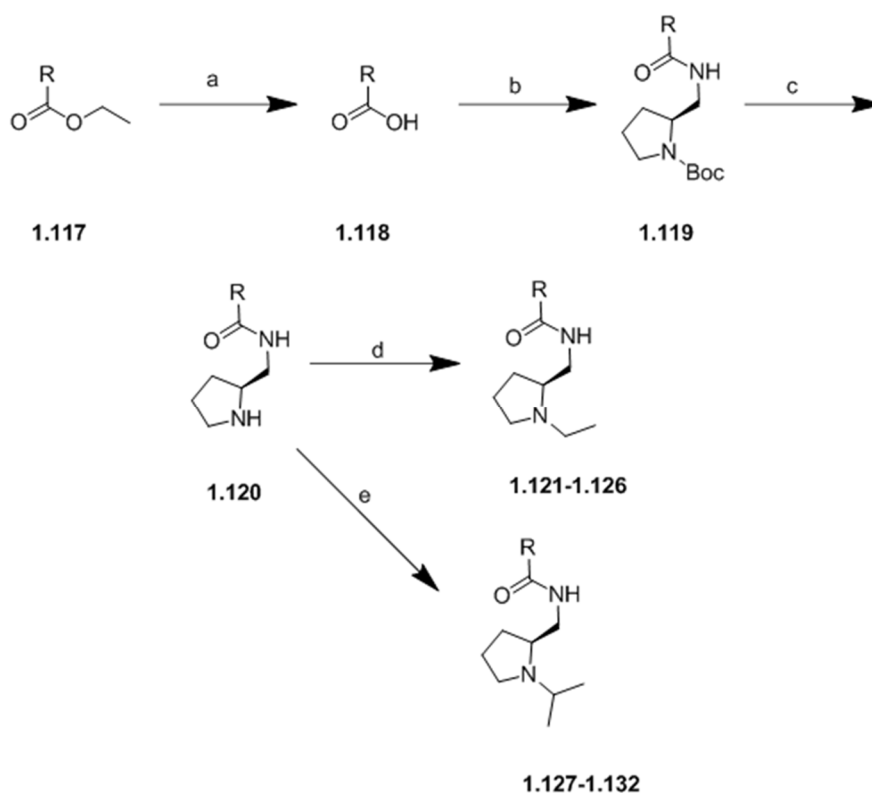


Scheme 1.6: Synthesis of pyrrolidine modification to provide quinoline scaffold analog **1.112**. Reagents and conditions: (a) pyrrolidine, PyBrOP, DIEA, DCM, 23%.



Scheme 1.7: Synthesis of biarylaminopyridone scaffold **1.116**. Reagents and conditions: (a) *N*-methylaniline, Pd(OAc)₂, dppf, CsCO₃, toluene, 37%; (b) mCPBA, DCM, 74%; (c) pyrrolidine, PyBrOP, DIEA, DCM, 19%.

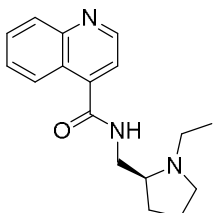
arrive at the desired ethyl 2-chloroquinoline-4-carboxylate (**1.110**). This material was then cyclopentylquinoline-4-carboxylate (**1.111**). At this point, we were also interested in subjected cyclopentylquinoline-4-carboxylate (**1.111**). At this point, we were also interested utilizing Negishi cross-coupling conditions to arrive at ethyl 2-(pyrrolidin-1-yl)quinoline-4-carboxylate (**1.112**), incorporating a second hydrogen bond acceptor, again with the anticipation of achieving more protein interactions. We envisioned substituting the cyclopentyl ring with pyrrolidine to this end, and achieved this with the PyBrOP-mediated *N*-oxide amination of **1.108** (Scheme 1.6). Finally, we developed a synthetic route to arrive at a modified biarylaminopyridone

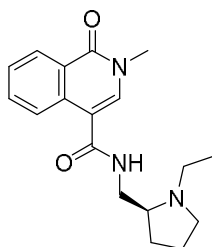


Scheme 1.8: Library synthesis of scaffold modifications to final compounds **1.127-1.132**. Reagents and conditions: (a) 1 M LiOH_(aq), THF, 95-99%; (b) HATU, DIEA, DMF, (*S*)-tert-butyl-2-(aminomethyl)pyrrolidine-1 carboxylate, 79-86%; (c) 4 M HCl in dioxane, DCM, 95-99%; (d,e) acetaldehyde or acetone, HOAc, MP-CN₃BH₃, DCM, μ W 100 °C, 10 min., 57-91%.

scaffold we proposed would provide more flexibility to the rigid β -carbolinone scaffold of **1.14** (**Scheme 1.7**). Buchwald-Hartwig amination of commercially available methyl 2-chloroisonicotinate with *N*-methylaniline provided compound **1.114**, which was then subjected to *N*-oxide amination to provide compound **1.116**. With these esters in hand, we then began the process of saponification and uniting these acids **1.117** with the (*S*)-(1-pyrrolidin-2-yl)methanamine piece we had discovered was crucial to compound activity (**Scheme 1.8**). We also synthesized the *N*-ethyl analogs of these compounds as this substitution was present with the parent compound **1.6** (VU0110945). These analogs were screened in CRC format in our primary calcium mobilization assay to determine ability to potentiate GLP-1 EC₂₀, the results of which comprise **Table 1.7**. To our continued dismay, all of these scaffold modifications were devoid of activity at hGLP-1R in the calcium flux assay. We, at that juncture, decided to take a more rational, directed approach to our next round of SAR development.

Table 1.7: Structures compounds from library prepared as in **Scheme 1.8** and associated potency and efficacy activity data from 10-point CRC-format screen at hGLP-1R. Calcium mobilization responses for each compound are reported as a percentage of the maximum GLP-1 response. VU number denotes the compound identifier assigned by Vanderbilt University. Data represent the mean of at least 3 replicate experiments with similar results

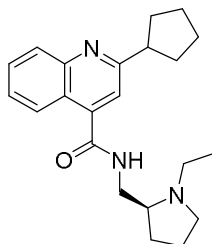
Structure	Compound Number	VUID	hGLP-1R EC50 (μ M)	hGLP-1R %GLP-1 _{MAX}
	1.121	VU6014477	Inactive	



1.122

VU6014476

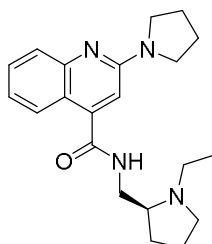
Inactive



1.123

VU6014475

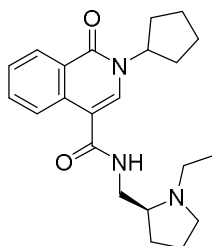
Inactive



1.124

VU6014474

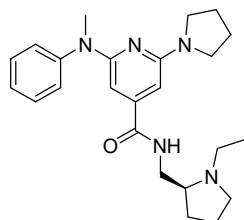
Inactive



1.125

VU6014473

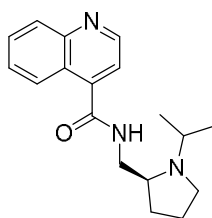
Inactive



1.126

VU6012896

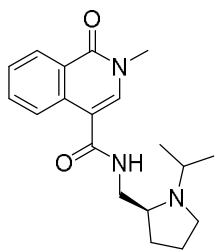
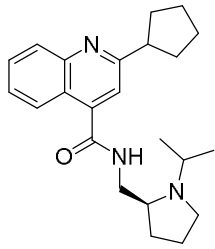
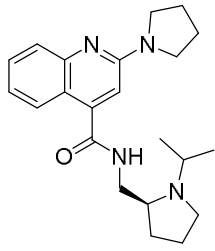
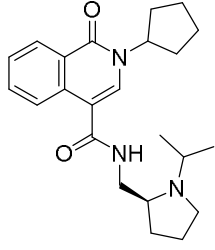
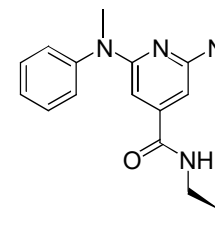
Inactive



1.127

VU6014472

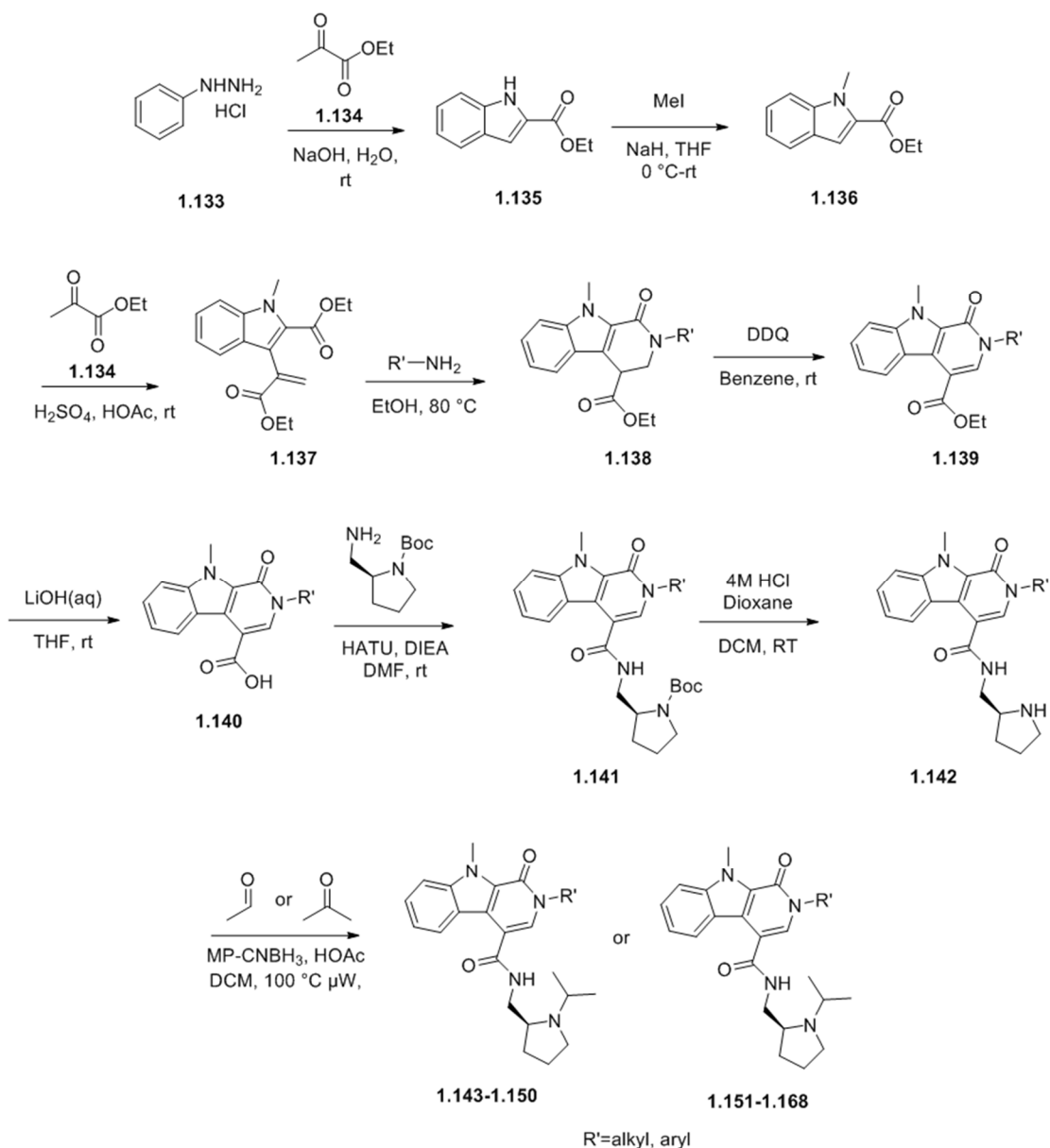
Inactive

	1.128	VU6014471	Inactive
	1.129	VU6014470	Inactive
	1.130	VU6014469	Inactive
	1.131	VU6014468	Inactive
	1.132	VU6012897	Inactive

Having had no success at developing active compounds incorporating broad modifications to the chemical structure of VU0453379 (**1.14**), we decided to employ a more directed strategy at our next modification site; the *N*-cyclopentyl ring attached to the β -carbolinone scaffold. As this ring was found to be a hot spot for rat

metabolism, we hoped to at least mitigate first-pass metabolism and improve the molecule as a tool compound for proof-of-concept studies, even if we were not able to effect a large increase potency due to the nature of this steep SAR. To do this, we developed a synthetic route to arrive at scaffolds with these desired modifications. This route would also provide a method to interrogate changes to the western ring of the scaffold in the future (**Scheme 1.9**). Starting with commercially available phenyl hydrazine **1.133**, base-catalyzed Fisher indole synthesis with ethyl pyruvate **1.134** provides indole **1.135** in excellent yield. Standard methylation procedure of the indole nitrogen gives compound **1.136**. Acid catalyzed nucleophilic addition and subsequent condensation of another equivalent of ethyl pyruvate to the α -ester indole provides **1.137**, and subsequent cyclization of primary alkyl and aryl amines affords compounds **1.138**. Dehydrogenation of the 3,4-dihydro- β -carbolinones with DDQ affords product aromatized β -carbolinones **1.139**, which are then subjected to basic saponification to provide carboxylic acids **1.140**. It was at this point we merged with this library the four commercially available carboxylic acid analogs of the VU0453379 (**1.14**) scaffold. Molecules synthesized with the commercial acids as opposed to in house synthesized acids are indicated in **Table 1.8**, along with SAR results. HATU-mediated amide coupling to commercially available (S)-aminomethyl-N-Boc-pyrrolidine and, acidic removal of the Boc group afford compounds **1.141** and **1.142** respectively. Finally, microwave-assisted reductive amination with acetaldehyde or acetone to arrive at final products **1.143-1.150** and **1.151-1.168**. In the case that there was only enough material to employ one analog at the ultimate step, synthesis of the *N*-isopropyl analog with acetone was preferred due to the

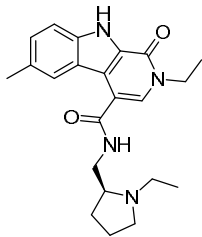
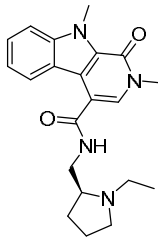
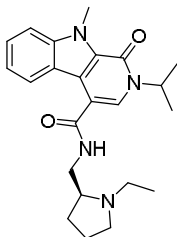
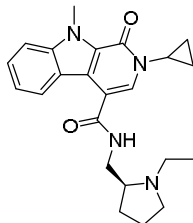
increased activity of this piece over that of the *N*-ethyl analog. Compounds synthesized in this way were again subjected to our primary calcium mobilization assay in CRC form to provide a potency in potentiating the GLP-1 EC₂₀ and the results

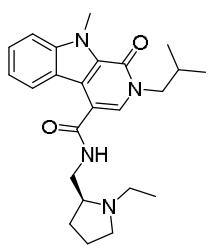
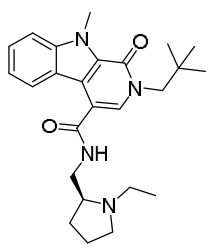
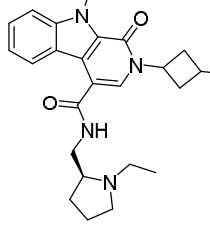
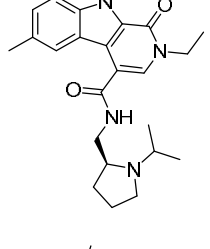
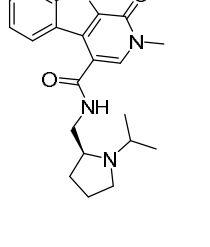
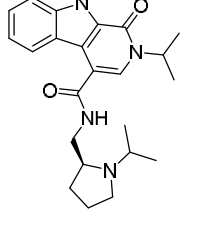


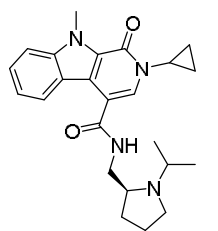
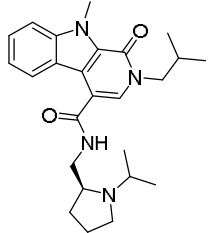
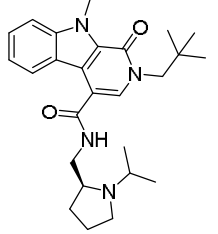
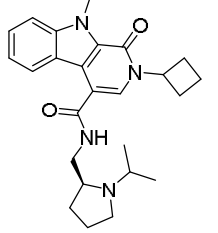
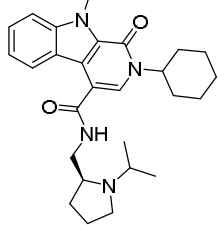
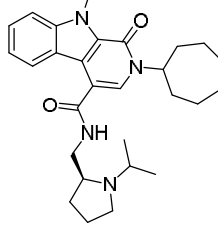
Scheme 1.9: Synthetic route to arrive at β -carboline scaffold and produce modifications to *N*-cyclopentyl moiety

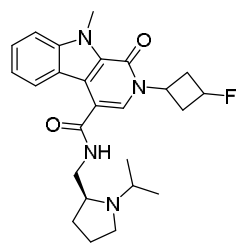
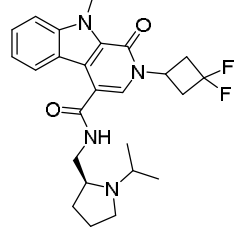
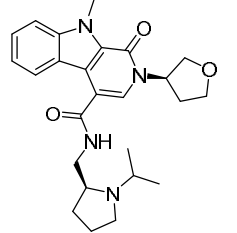
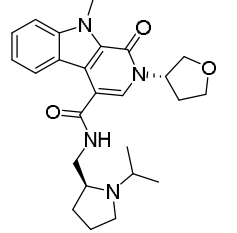
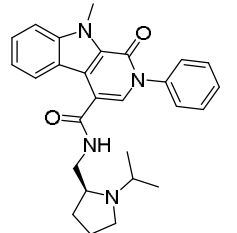
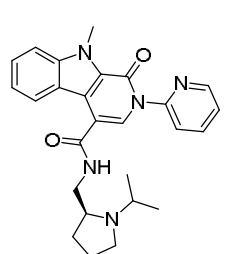
of this screen comprise **Table 1.8**. To our delight, a handful of these analogs provided potency and efficacy on par with that of compound **1.14**.

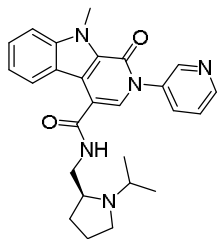
Table 1.8: Structures compounds from library prepared as in **Scheme 1.9** and associated potency and efficacy activity data from 10-point CRC-format screen at hGLP-1R. Calcium mobilization responses for each compound are reported as a percentage of the maximum GLP-1 response. VU number denotes the compound identifier assigned by Vanderbilt University. Data represent the mean of at least 3 replicate experiments with similar results.

Structure	Commercial acid?	Compound Number	VUID	hGLP-1R EC50 (μM)	hGLP-1R %GLP-1 _{MAX}
	Yes	1.143	VU6005488	Inactive	
	Yes	1.144	VU6014467	Inactive	
	Yes	1.146	VU6014466	>10	42.6
	Yes	1.147	VU6014465	>10	39.1

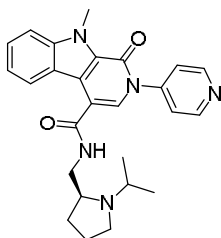
	No	1.148	VU0449356		Inactive
	No	1.149	VU6014464		Inactive
	No	1.150	VU6005189	>10	42.3
	Yes	1.151	VU6005491		Inactive
	Yes	1.152	VU6005492		Inactive
	Yes	1.154	VU6005493	5.1	48.4

	Yes	1.155	VU6005494	3.3	45.2
	No	1.156	VU6014463		Inactive
	No	1.157	VU6014462		Inactive
	No	1.158	VU6005525	1.0	52.3
	No	1.159	VU6005526	3.9	57.2
	No	1.160	VU6005527	>10	57.3

	No	1.161	VU6005185	2.7	46.3
	No	1.162	VU6005184		Inactive
	No	1.163	VU6005462	3.1	44.5
	No	1.164	VU6005463	>10	42.1
	No	1.165	VU6014458		Inactive
	No	1.166	VU6014461		Inactive



No **1.167** VU6014460 Inactive



No **1.168** VU6014459 Inactive

While all aryl substitutions were inactive, small modifications to the parent cyclopentyl moiety were tolerated and provided a fairly logical SAR profile. While small alkyl modifications such as methyl and ethyl were not tolerated, isopropyl (**1.154**, GLP-1R EC₅₀ = 5.1 μM, GLP-1R%_{MAX} = 48.4) and cyclopropyl (**1.155**, GLP-1R EC₅₀ = 3.3 μM, GLP-1R%_{MAX} = 45.2) analogs had measurable potencies below 10 μM and were progressively more potent with increased size. The compound of most interest from this library, cyclobutyl (**1.158**, GLP-1R EC₅₀ = 1.0 μM, GLP-1R%_{MAX} = 52.3), was slightly more potent than compound **1.14** (VU0453379). Potencies then began to decrease with the addition of larger carbocycles such as cyclohexyl (**1.159**, GLP-1R EC₅₀ = 3.9 μM, GLP-1R%_{MAX} = 57.2) and cycloheptyl (1.160, GLP-1R EC₅₀ = >10 μM, GLP-1R%_{MAX} = 57.3), and heavily branched alkyl chains such as neopentyl and isobutyl were devoid of activity. While we were encouraged by these results, we were most interested in the activity of the tetrahydrofuran and fluorinated cyclobutyl analogs due to our hypothesis that these compounds, if active, would block some of

the metabolism contributing to the high clearance observed with compound **1.14**. Both diastereomers of the tetrahydrofuran moiety were active, and we were happy to see a preference for the (*R*)-tetrahydrofuran-3-amine (**1.163**, GLP-1R EC₅₀ = 3.1 μM, GLP-1R%_{MAX} = 44.5) over the (*S*)-enantiomer at this position (**1.164**, GLP-1R EC₅₀ = >10 μM, GLP-1R%_{MAX} = 42.1). Additionally, while the monofluorocyclobutane substitution was active (**1.161**, GLP-1R EC₅₀ = 2.7 μM, GLP-1R%_{MAX} = 46.3), the difluoro counterpart to it was not, lending more evidence to our supposition of a small binding area precluding the binding of larger rings.

With these data in hand, we subjected all compounds that were active below 5 μM potency in the calcium flux assay to tier 1 DMPK assays to determine clearance and brain penetrance (**Table 1.9**). While we were finally able to synthesize active

Table 1.9: Full in vitro and in vivo DMPK profile of compound active compounds in Sprague–Dawley rat and human. Liver microsomal clearance was predicted using the well-stirred model with 20 and 45 g liver per kg body weight and 21 and 70 mL/kg hepatic blood flow for human and rat, respectively.

Parameter	1.154	1.155	1.158	1.159	1.161	1.163
MW	408.55	406.53	420.56	448.61	438.55	436.56
TPSA	55.89	55.89	55.89	55.89	55.89	65.12
cLogP	3.78	3.52	3.85	4.97	3.54	2.76
<i>In Vitro</i> PK						
Rat CL _{HEP}	64.1	65.3	68.0	67.2	63.8	68.4
Rat CL _{HEP}	20	19.0	18.9	19.2	17.4	18.2
Rat PPB (f _u)	0.163	0.253	0.204	0.105	0.242	0.477
Human PPB (f _u)	0.116	0.173	0.144	0.074	0.175	0.284
<i>In Vivo</i> Rat PK (IV, 0.2 mg/kg, 0.25 h)						
Plasma (ng/mL)	ND	4.91	5.09	4.50	6.58	4.28
Brain (ng/mL)	ND	BLQ	BLQ	BLQ	BLQ	BLQ
Brain:Plasma (K _p)	N/A	N/A	N/A	N/A	N/A	N/A

analogs of **1.14**, none the modifications incorporated improved metabolism. Furthermore, these modifications disallowed brain penetration at the dose tested. 0.2 mg/kg IV. At this point, we paused SAR studies with the intention of performing metabolism identification and softspot analysis of **1.161** and **1.163** to understand if we were detecting metabolism at the same location on the molecule, or if through blocking one metabolic hot spot, we were shunting metabolism down and equally liable pathway. SAR on this molecule has since been halted indefinitely due to issues that arose during cell-line development and optimization. The experiments and results that led to the hiatus and ultimate disruption of this project are discussed in the next section of this chapter.

Validation and troubleshooting efforts of GLP-1R PAMs

Development of in-house hGLP-1R cell lines

Concurrently with the efforts to improve the pharmacological and pharmacokinetic profiles of our GLP-1 PAMs, we were interested in developing new cell lines to evaluate these compounds. The cell line used for our HTS campaign, and subsequent optimization efforts was a commercial cell line was the Chemiscreen™ Human recombinant Glucagon-like peptide receptor calcium-optimized stable cell line purchased from Millipore. This cell line was subsequently sub-cloned to arrive at a clone with improved fluorescent signal over the original. Issues arose with these cells as they were made of a proprietary cell background and were co-expressed with an unknown sequence of hGLP-1R with an unknown expression system and a proprietary promiscuous G-protein to allow the normally G_s-coupling of GLP-1R to be transduced through the G_q- pathway; this G-protein provided intracellular calcium mobilization upon activation, a signaling pathway particularly convenient for modern pharmacological assay techniques. We desired a new cell-line with a known background, expression system, and signaling system that would allow us more control and knowledge while developing new assays and developing a more in-depth pharmacological profile of our compounds. Furthermore, as our PAMs regularly showed agonist-PAM activity, we desired a cell line with inducible and regulatable

hGLP-1R expression, as the agonist activity of this class of compounds may often be an artifact of high receptor reserve and can thus be modulated in contemporaneously with receptor expression levels.

We chose the T-Rex™ inducible protein expression system due to our lab's previous success with this system. The T-Rex™ system utilizes the *E. coli* Tn10-encoded tetracycline (Tet) resistance operon to regulate expression of a desired protein. Cell lines used with this system express a Tet repressor, which when combined with an inducible expression plasmid possessing tetracycline operator 2 (TetO2) sites after a strong promoter, such as human cytomegalovirus (CMV), allow for the induction of protein expression upon the addition of tetracycline to the cell medium (**Figure 1.17**).

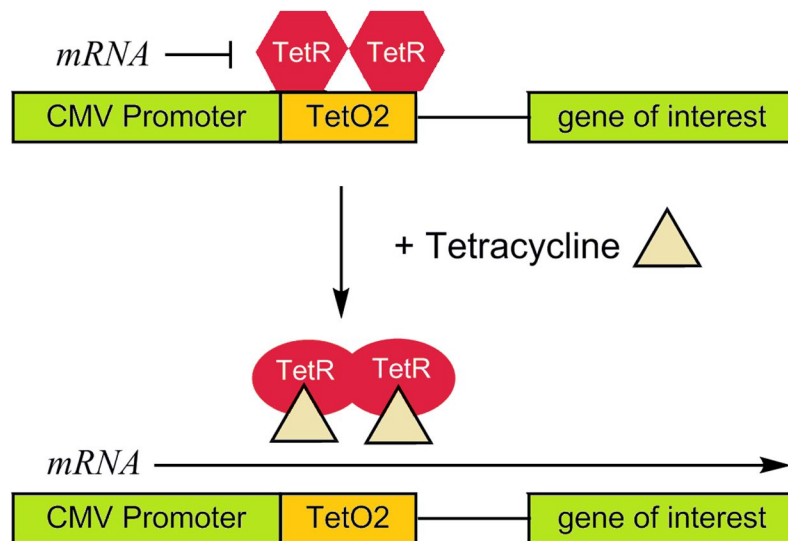


Figure 1.17: Tetracycline inducible expression system used in T-Rex™ cell line

In addition to choosing an expression vector, we also needed to choose a desirable cell background and G-protein that would provide calcium flux when stimulated. We selected Chinese Hamster Ovary (CHO) as the background due to their hardy, strongly adherent nature and fast doubling time of 16-18 hours, and decided upon mouse $G\alpha_{15}$, a promiscuous G-protein known to couple a wide variety of receptors to the PLC pathway.

To develop these cell lines, we first cloned the commercially available hGLP-1R cDNA into the pcDNA5™/TO tetracycline regulated expression vector using standard cloning and plasmid preparation techniques. With plasmid in hand, we transiently co-transfected T-REX CHO cells stably expressing the TetR with hGLP-1R and m $G\alpha_{15}$ and assayed them for GLP-1-induced calcium flux. Unfortunately, this cell line combination provided very little fluorescence output, and the experiment was repeated with T-Rex™ 293 Human Embryonic Kidney cells (**Figure 1.18**). We were happy to see a considerable increase in relative fluorescence after migrating to HEK 293 as

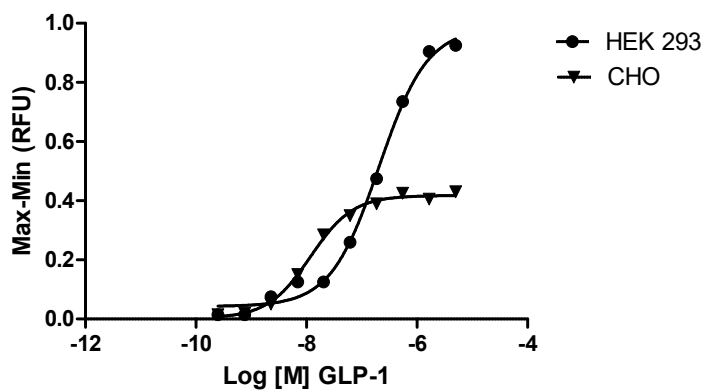


Figure 1.18: Comparison of relative fluorescence produced through calcium flux with T-Rex™ 293 HEK and T-Rex™ CHO cells

the cell background, and continued with this cell type for the remainder of the validation and troubleshooting efforts.

Evaluation of GLP-1R PAM VU0453379 in new cell lines

Once we had established our constructed expression system provided GLP-1 mediated calcium flux with good signal-to-background ratio, we sought to examine the efficacy of our lead GLP-1R PAM VU0453379 (**1.14**) in this cell line to compare to the previous commercial cell line. This was the key inflection point of the project, where we halted all SAR efforts and focused our attention solely on target engagement and compound validation studies. We examined our PAM in a fold-shift assay due to unreliable nature of the EC₂₀ GLP-1 concentration after transient transfection. At our top PAM concentration of 30 μ M, we observed no potentiation of GLP-1 at any concentration. This data was most troubling to us, and we immediately began searching for a rational explanation. One hypothesis for this effect was the idea that our PAMs stabilize a conformation of the receptor that preclude binding of the promiscuous G-protein, preventing the receptor from signaling through G_q and producing no calcium flux. We sought to evaluate our compounds in a cAMP accumulation assay which would utilize the native signaling pathway. We desired a cAMP assay using a kinetic cAMP sensor that would allow for live-cell, real-time analysis. Most cAMP accumulation assays rely on end-point cell lysis and bead-based technologies to quantify signaling, which instills difficulties when parsing the difference between agonists and allosteric

modulators as both would increase total cAMP accumulation from that of the endogenous ligand. To that end, we chose the GloSensor™ cAMP assay which employs a genetically encoded biosensor variant with cAMP binding domains fused to mutant forms of *Photinus pyralis* luciferase. Upon binding to cAMP, conformational changes occur that promote high quantities of chemiluminescence. This assay is suitable for stable or transiently transfected cells, which allowed for us to test compounds without developing a stable cell line. Upon choosing this assay, we transiently co-transfected the previously used T-REx™ 293 cell line with hGLP-1R and the pGloSensor™-22F cAMP Plasmid and assayed our PAM in fold-shift format using the provided protocol. We were pleased to see a nearly 50-fold increase in luminescence from baseline, providing a large signal-to-background, but unfortunately the PAM failed again to produce any potentiation GLP-1-induced cAMP accumulation (Figure 1.19). We were deeply saddened by this result, and it became was

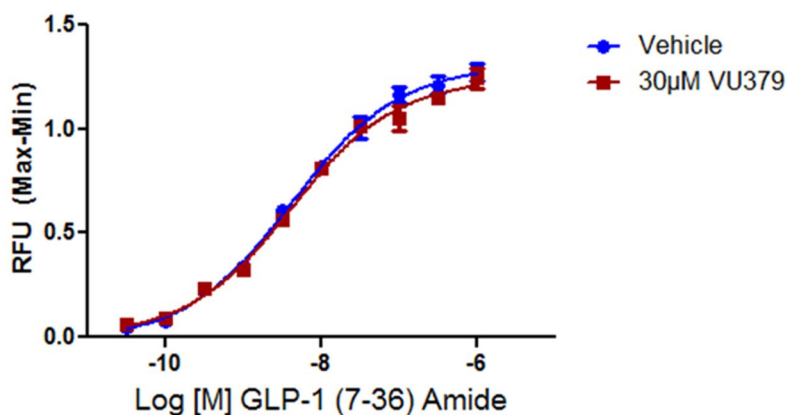


Figure 1.19: Fold-shift analysis of GLP-1 CRC in the presence and absence of 30 μ M concentration of VU0453379 (1.14). Calcium mobilization assay performed in hGLP-1R mG α 15 T-Rex™ 293 transient cell line. No potentiation of GLP-1 observed at any concentration. Data represent the mean \pm S.E.M

clear we would need to delve deeper into the reasoning for why our compounds were no longer active.

To determine whether this was an issue isolated to our cell lines, or a larger issue, we were generously gifted a stable hGLP-1R HEK 293T cell line from the Powers lab at the Vanderbilt University Medical Center. We then followed the same protocols described previously to transiently transfect this cell line with the pGloSensor™-22F plasmid to provide a readout of cAMP accumulation. Fold shift analysis of this cell line in the presence of several

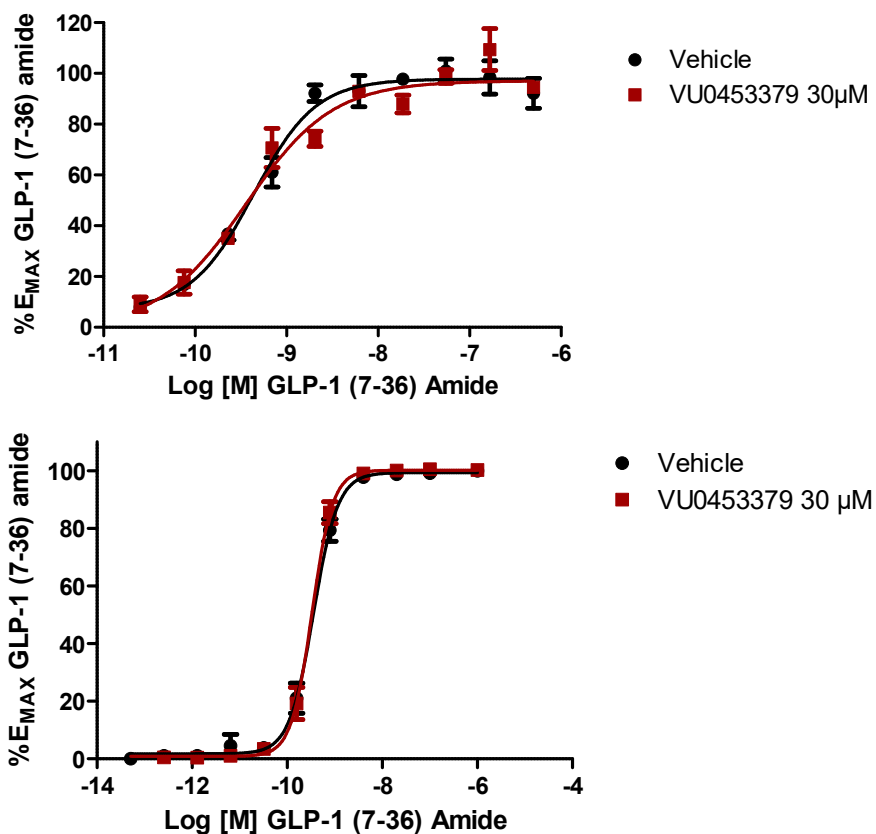


Figure 1.20: Fold-shift analysis of GLP-1 CRC in the presence and absence of 30 μM concentration of VU0453379 (1.14). Top panel: Calcium mobilization assay performed in hGLP-1R 293T cell line transiently transfected with mG α 15 for calcium flux. Data represent the mean \pm S.E.M. Bottom panel: cAMP accumulation assay performed in hGLP-1R 293T cell line transiently transfected with pGLO-22F™ cAMP reporter. Data represent the mean \pm S.E.M

concentrations of our PAM and GLP-1 showed the inactivity issue we had observed in our cell lines was not an isolated event and was persistent (**Figure 1.20**). We then shifted away from these analyses and began searching for mechanisms that would disrupt PAM signaling, resulting in our compounds appearing inactive with these new cell lines.

Effect of hGLP-1R SNP sequence on GLP-1R PAM activity

Since the advent of this project, the hGLP-1R protein sequence (accession number NP_002053) derived from epidemiological studies has been updated three times on the protein database of the National Center for Biotechnology Information (NCBI). Each of these updates included modifications to the primary protein structure due to single nucleotide changes of the mRNA sequence (accession number NM_002062), and thus the cDNA derivation of this. These alterations, called single nucleotide polymorphisms (SNPs), are variation in a single nucleotide that occur at a specific position in the genome, where each variation is present to some appreciable degree within a population. SNPs are of particular interest when employing allosteric modes of GPCR target engagement due to pursuing often-unknown allosteric binding sites. SNPs that cause amino acid modifications in

Variant ID	Base Change	Amino Acid Change	Population genetics	Consequence
rs1042044	A780C	L260F	A: 42% C: 58%	Missense
rs1126745	A947G	A316G	Unknown	Missense

Figure 1.21: SNP variant data compiled from the Single Nucleotide Polymorphism database of the NCBI

allosteric binding sites can disrupt molecule binding and thus efficacy. After discovering these SNPs hGLP-1R, we were curious which if these variants would affect binding of our GLP-1R PAMs. As we had sequenced the cDNA incorporated in the hGLP-1R-containing pcDNA5™/TO plasmid during preparation, a sequence which aligned with the sequence provided on data sheets from the commercial supplier of that cDNA, we knew the cDNA used for our experiments in which VU0453379 (1.14) was inactive matched that of version 3. Through this we confirmed the receptor used in these experiments had AAs L260 and A316. We then sought to construct a plasmid incorporating the sequence of version 2, with AAs F260 and G316 to investigate whether these AA modifications would provide efficacy for our PAM. We also chose to construct crossover sequences that would have AAs F260/G316, and L260/A316.

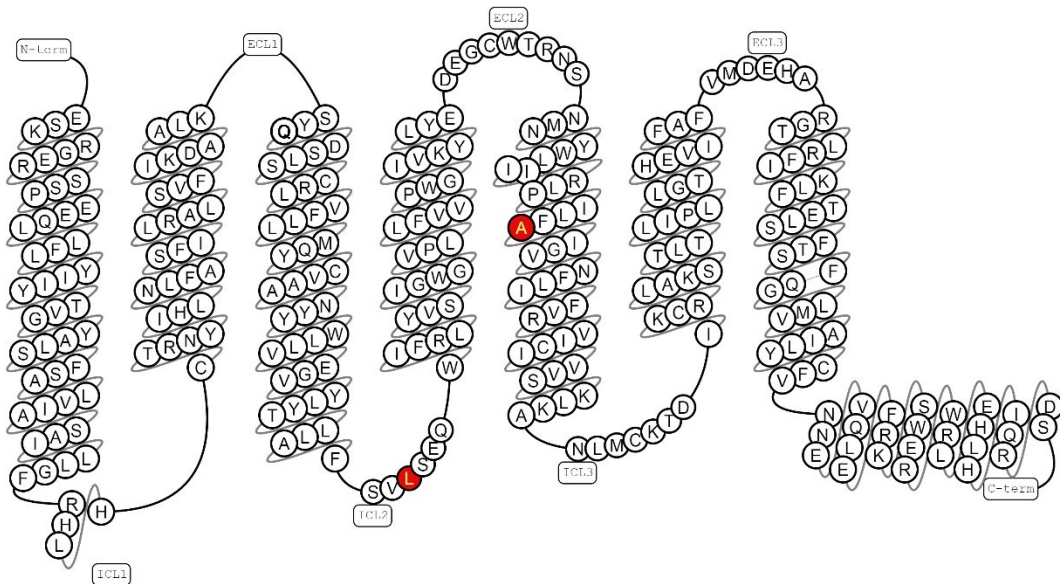


Figure 1.22: Snake plot of the hGLP-1R secondary structure denoting intracellular, transmembrane, and extracellular regions. Residues affect by SNP variants of interest are highlighted in red.

To arrive the desired SNP variants, we carried out site-directed mutagenesis of our hGLP-1R plasmid, incorporating base modifications that would provide the desired amino acid variants. After plasmid preparation and purification, we transiently transfected our newly constructed hGLP-1R mutant, along with mGα16 for calcium flux readout, into the T-REx™ 293 cell line and performed a fold-shift analysis of before, looking for PAM potentiation at any of the SNP variants (**Figure 1.23**). Unfortunately, compound **1.14** showed no efficacy in potentiating the GLP-1 CRC at any concentration in any of the SNP variants constructed. As this effort was

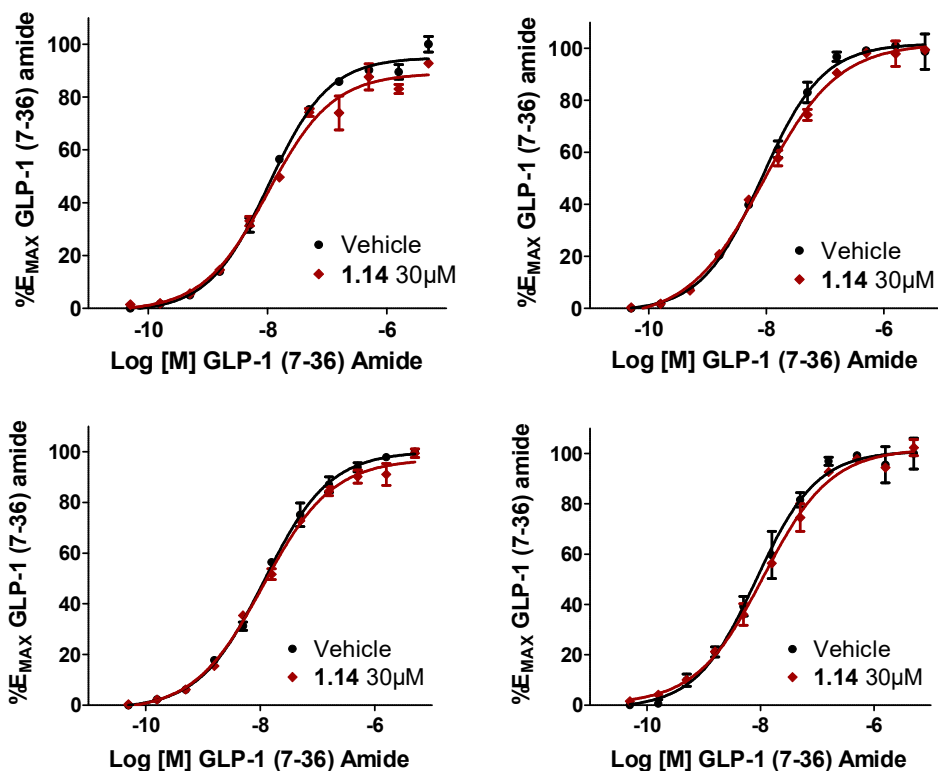


Figure 1.23: Fold-shift analysis of GLP-1 CRC with 30 μM PAM compound **1.14**. PAM shows no potentiation of GLP-1 at any SNP variants tested, F260/G316 (top left), F260/A316 (right), L260/A316 (bottom left), and L260/G316. Calcium mobilization assay performed in hGLP-1R mGα15 T-Rex™ 293 transient cell line. Data represent the mean ± S.E.M

ultimately fruitless in providing reasoning for our dilemma, we set to work devising a new hypothesis.

Elucidation of commercial cell line background species and GLP-1R species and sequence

As our previous efforts at understanding the mechanism behind our sudden loss in activity had failed, we began to search deeper for answers. Our focus fell to the commercial cell line used for the HTS campaign and subsequent lead optimization efforts. This cell line, the hGLP-1R Chem-9 cell line, was a veritable black box to us, and we sought to elucidate some of the properties of this cell line that may be producing activity where our in-house cell line could not.

Initially, we desired knowledge of the species of this cell-line, information we were not given at the time of purchase. If the cell background was human, we could be encouraged that the cell backgrounds was playing a small, if any, role in our present difficulties. However, if the cell line were of another species, we imagined a scenario where we had developed compounds that were only active at GLP-1R in that species, and not actually active at the human homolog. We devised a method to decipher this using PCR and subsequent Sanger sequencing. We chose rat as the first

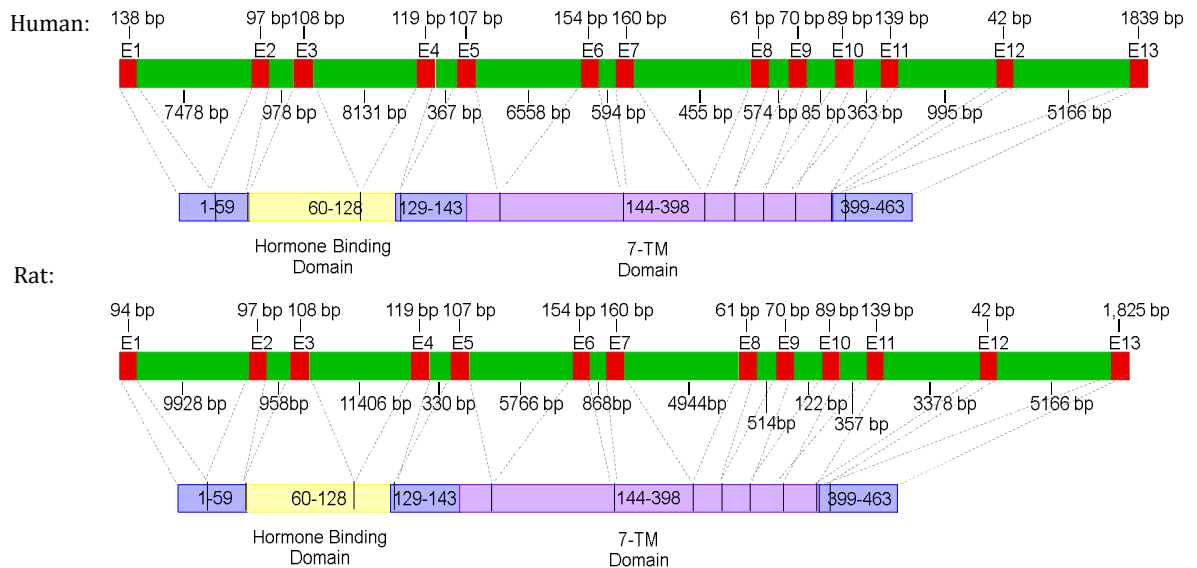


Figure 1.24: Intron-Exon map of human and rat *GLP1R* to find optimal sequence for PCR analysis

species to examine in this study. First, we aligned the human and rat genomic *GLP-1R* sequences, and searched for an exon/intron bound with identical sequences that would produce one size of amplicon for genomic DNA and differently-sized amplicon for incorporated cDNA, such as you would observe in an exogenously over-expressing cell line (**Figure 1.24**). As cDNA does not include introns, this change in DNA length allowed for differentiation between these two types of *GLP-1R* DNA. After a section of DNA was chosen with these characteristics, we designed primers to bind to these sequences. The primers designed would provide three possible outcomes depending on the results of the PCR experiment: a single 144 base-pair amplicon of only over-expressed *GLP-1R*, signifying the background was a species other than rat or human; a single 501/507 base-pair amplicon, signifying only genomic *GLP-1R* and no over-expressed receptor of either human or rat species; or a 144 base-pair and 507/501 base-pair double amplicon, signifying the presence of over-expressed and

endogenous GLP-1R of either rat or human species. After extracting genomic DNA from the hGLP-1R Chem-9 cell line to use as our template, we engaged a standard PCR protocol with PfuTurbo DNA polymerase, optimizing the protocol for the particular polymerase and primers used. After this protocol terminated, we visualized the amplicons by running the reactions on a 1.5% agarose gel with ethidium bromide (**Figure 1.25**). We were elated to find a double amplicon of the expected sizes after this experiment, demonstrating we has successfully retrieved both endogenous and exogenous GLP-1R DNA from the commercial cell line. After band extraction, we sent the DNA for sequencing using the same primers as for PCR. Once received, both sequences were blasted against the NCBI database to determine which DNA sequences our PCR products matched and to what degree. What we discovered after this analysis was that the overexpressed GLP-1R was human, which we were anticipating. We also discovered the species of the genomic DNA, and thus the species of the cell line, was indeed rat.

Considering the commercial cell line was sub-cloned after purchase with no understanding of how this cloning may have affected gene expression, and also considering we still did not know the tissue type of this cell line or whether it expressed endogenous rGLP-1R, we were then curious if sub-cloning has somehow altered the cell line in such a way that the endogenous rGLP-1R was more highly expressed than the introduced exogenous hGLP-1R. To this end, we set about devising a method with which we could satisfy this curiosity. We began by extracting total RNA from the hGLP-1R Chem-9 cell line, and performing RT-PCR first-strand synthesis to synthesize cDNA copies of the present RNA strands using . SuperScript

II™ Reverse Transcriptase. Next, we designed full-length open reading frame (ORF) primers for human and rat GLP-1R from ATG to TGA codons. We also designed internal primers, as the ATG sites for both species were GC-heavy and we were concerned the primers would self-bind and we would get no amplification. We designed the internal primers for the hGLP-1R sequence such that it was upstream of the known SNP sites and if present would provide the SNP identity of this cell line. After receiving the primers, we performed a standard PCR protocol, optimizing for the properties of the individual primers. Products of these reactions were ran on a 1.5% agarose gel with DNA ladder to visualize (**Figure 1.25**). While we were able to amplify DNA from the hGLP-1R primers, we did not observe bands with either the ATG-TGA or internal-TGA rat primers.. After sequencing, the hGLP-1R amplified

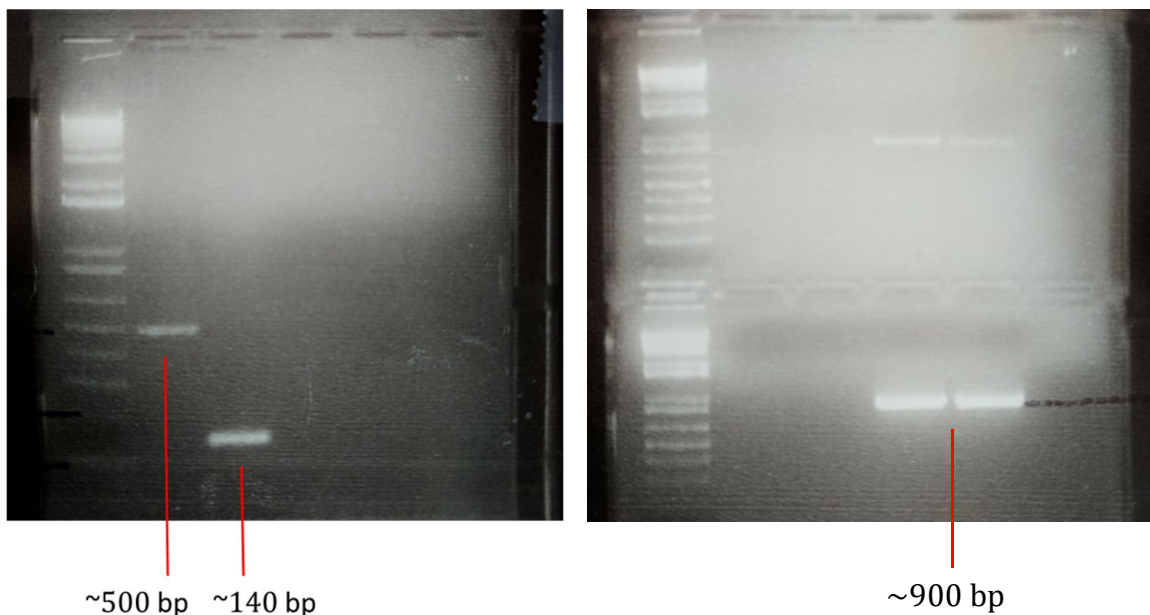


Figure 1.25: DNA gel visualizations from PCR experiments. (Left panel): PCR products from experiments providing double amplicon corresponding to endogenous and exogenous GLP-1R DNA. (Right panel): PCR product of from hGLP-1R internal-TGA primers at ~900 bp. No rGLP-1R amplicon was observed.

matched that of the sequence version 2, having amino acid identities of F260 and G316, further filling in the gaps in our knowledge about that cell line.

Determination of VU0453379 activity at rGLP-1R

As the traditional aphorism goes, “absence of evidence is not evidence of absence.” In that same vein, we could not prove the absence of rGLP1-R expression in the commercial hGLP-1R Chem-9 cell line, just that we were unable to find evidence with our protocol and conditions. We decided to examine activity of our compounds with rGLP-1R directly by incorporating this receptor homolog into our in-house cell line, as that would determine if species-differential activity was causing our issues.

In order to do this, commercially available rGLP-1R cDNA was cloned into the pcDNA5™/TO vector and transiently co-transfected this plasmid alongside the mGα15 plasmid, to provide calcium flux, into the T-REx™ 293 cell line. We then examined whether VU0453379 (**1.14**) could potentiate GLP-1 in a cell line expressing the rGLP-1R. We tested **1.14** at a concentration of 30 μM in the presence of a CRC of GLP-1 in our typical fold-shift assay (**Figure 1.26**). Unfortunately, compound **1.14** showed no efficacy in potentiating the GLP-1 CRC at any concentration in rGLP-1R. Though we knew it was a long shot, we were disappointed that yet again we were unable to unravel the mystery that plagued our project. At this point, we abandoned methods that involved direct measurement of GLP-1 potentiation, and instead elected to investigate whether **1.14** could potentiate a process downstream of GLP-1R activation—ERK1/2 phosphorylation.

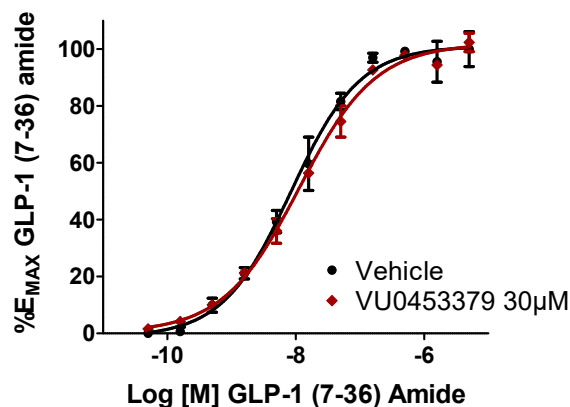


Figure 1.26: Fold-shift analysis of GLP-1 CRC in the presence and absence of 30 μ M concentration of VU0453379 (**1.14**). Calcium mobilization assay performed in rGLP-1R mG α 15 T-Rex™ 293 transient cell line. No potentiation of GLP-1 observed at any concentration. Data represent the mean \pm S.E.M

Evaluation of VU0453379-facilitated potentiation of ERK1/2 phosphorylation

All previous attempts to understand why our GLP-1 PAM, VU0453379 (**1.14**) is active in one cell line, but not others, were executed by measuring direct GLP-1R activation using either the promiscuous mG α 15 protein to illicit a calcium flux, or a cAMP reporter to measure total cAMP accumulation. As the calcium flux reporter system was the one aspect of the original hGLP-1R Chem-9 cell line of which we could garner no more information, we began to speculate that we would perhaps see a PAM response when probing a downstream signaling partner of GLP-1R. This technique is often employed when compiling full PAM activity profiles, and we knew GLP-1 mediated ERK1/2 phosphorylation, described in the introduction of this chapter, would be an adequate interaction to test our hypothesis.

In this assay, ERK1/2 phosphorylation was quantified by western blot analysis using fluorescently labeled secondary antibodies that provided visualization for

normal ERK1/2 (green) and phosphor-ERK1/2 (red). Cells were plated and serum starved, then pretreated with PAM and GLP-1. After treatment with test compounds, cells were lysed and total protein was extracted and quantified by BCA analysis to ensure consistent gel loading. After quantification, protein samples were loaded onto SDS-PAGE gels for electrophoresis, then transferred to nitrocellulose membranes and incubated in the presence of first primary, then secondary antibodies. Membranes were then subjected to fluorescent imaging, and quantified using imaging software, normalizing to total ERK1/2 of the vehicle treatments. The full methods and procedure for this assay is found in the Materials and Methods section of this chapter.

Initial optimization efforts of this assay lead to the discovery that 10-minute GLP-1 treatment provided the highest level of ERK1/2 phosphorylation. Shorter and longer treatments led to smaller amounts of phospho-ERK1/2, as the process is reversible and phosphor-ERK is dephosphorylated over time. We incorporated this small optimization into an ERK1/2 PAM assay seeking evidence of downstream potentiation of GLP-1-mediated phosphorylation. Cells were pretreated with GLP-1 PAM VU0453379 (**1.14**) for 5 minutes, when treated with a submaximal GLP-1 concentration to provide a potentiation window. Vehicle control, as well as a maximal GLP-1 concentrated were also incorporated to set normalization bounds. After protein harvesting, western blotting, and analyzing the fluorescently labeled blot, we were disheartened find **1.14** produced no potentiation of GLP-1-mediated ERK1/2 phosphorylation (**Figure 1.27**). Other GLP-1 PAMs in the literature have shown efficacy in this type of assay, and we were truly confounded at why our compound was not showing efficacy in any GLP-1 assay outside of the initial cell-line. At this

result, we had run out of explanations for our confounding lack of efficacy, and began to believe perhaps our supposed GLP-1 PAM was not. We then formulated a plan for a final experiment, one much more definitive than assays reliant on exogenous reporter systems and engineered cell lines—static islet studies with GLP-1-knockout mice.

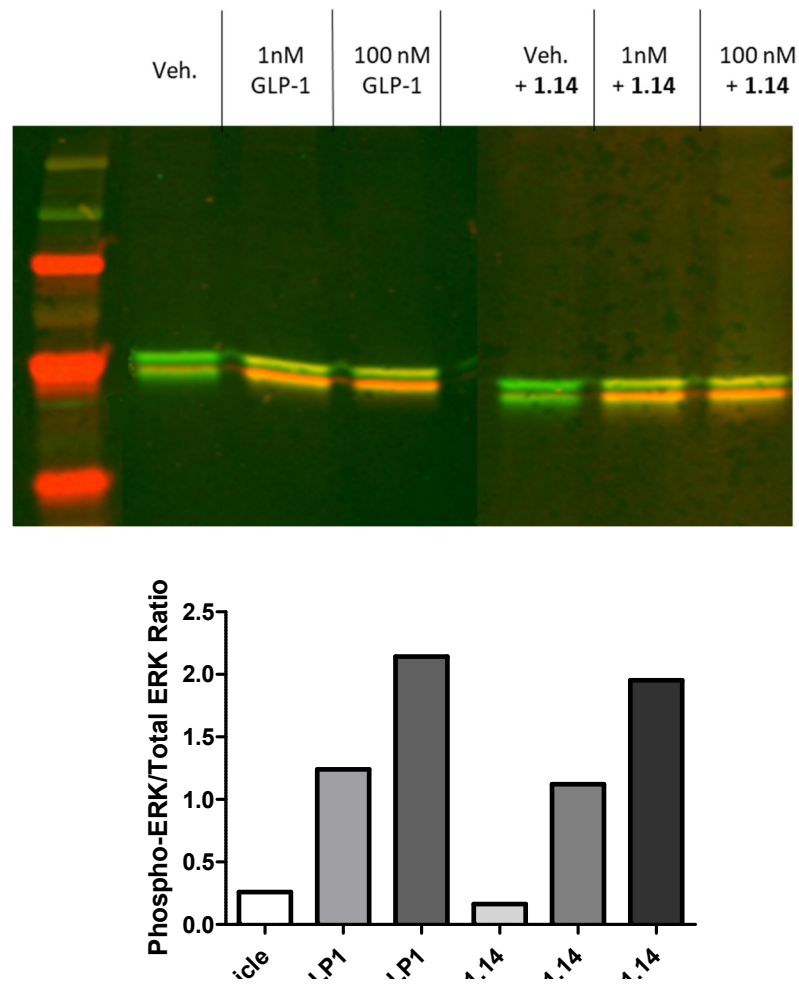


Figure 1.27: ERK1/2 phosphorylation assay. (Top panel): Fluorescent western blot analysis of experiment conditions. Assay performed in hGLP-1R T-Rex™-293 transiently expressing cell line. (Bottom panel): Quantification of ERK1/2 western blot analysis. Fluorescent data normalized to total ERK1/2 of vehicle control. No potentiation of GLP-1-mediated ERK1/2 phosphorylation observed with 30 μ M concentration of PAM VU0453379 (1.14)

Assessment of VU0453379 in GLP-1 (-/-) knockout mouse islets

The final step in our efforts to revive confidence in our GLP-1 PAM VU0453379 (**1.14**) was also the most definitive. We sought to evaluate whether the insulintropic activity of **1.14** observed with wild-type mouse islets was still present in islets of *Glp1r*(-/-) knockout mice, or if it was indeed GLP-1R-mediated. To this end, *Glp1r*(-/-) knockout mice were purchased and the primary pancreatic islets were harvested from treated with compound in the presence of EX-4. Wild-type islets were procured and tested alongside the *Glp1r*(-/-) islets for direct comparison. (**Figure 1.28**) While we were interested to observe EX-4 activity in the knockout-islets, were disheartened to find activity of **1.14** to induce insulin secretion in the absence of GLP-1R, particularly when amount of insulin was normalized to %content/min. It is known

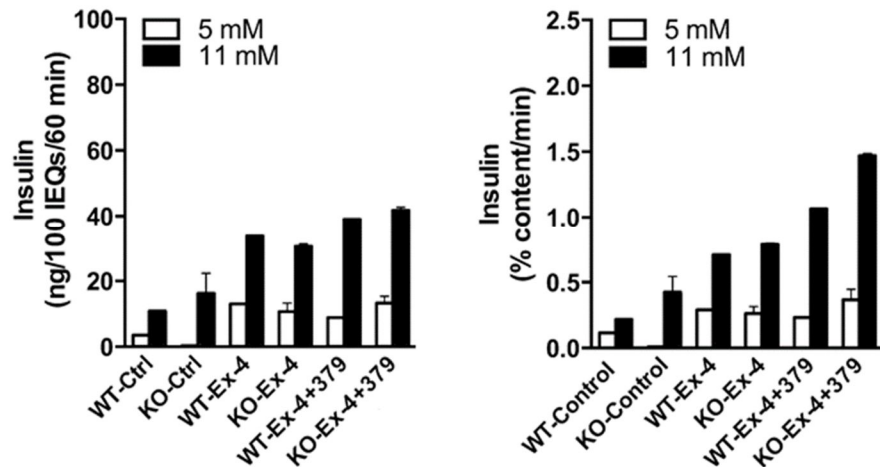


Figure 1.28: Measurement of the effect of 30 μ M **1.14** on potentiation of glucose-stimulated insulin secretion in WT and *GLP1r*(-/-) mouse islets in the presence of 10 nM exendin-4. Islets were isolated, size-matched into wells of a 12-well plate, and treated with vehicle, exendin-4, or exendin-4 + **1.14** at both low (5 mM) and high (11 mM) glucose for 60 min. n = 3. Data are represented as mean insulin response \pm SEM per 100 islet equivalents and analyzed using 2-way ANOVA followed by Sidak's multiple comparisons test. Experiments performed by the Islet Core at Vanderbilt University Medical Center.

that *GLP1R*(-/-) mice present with an upregulation of GIP synthesis and secretion, and we hypothesized that a compensatory mechanism may be interfering with insulin levels. However, it is clear there is an effect by **1.14** in the absence of GLP-1R.

Summary and Future directions

In summary, we endeavored to discover and optimize a CNS-penetrant GLP-1 PAM. Through an HTS campaign and subsequent iterative parallel synthesis, we discovered VU0453379 (**1.14**). Pharmacological studies showed **1.14** to be a GLP-1R ago-PAM with an EC₅₀ of 1.3 μM. Compound **1.14** showed no probe dependence with other GLP-1R orthosteric agonists, and showed efficacy in primary tissues. Furthermore, **1.14** showed efficacy at reversing haloperidol-induced catalepsy in rats, an effect not caused by sedation. We then strove to improve the properties of **1.14** using SAR studies, but ran into trouble with compound efficacy when employing cell lines other than what was used for the initial discovery. After SAR studies were halted, we searched for an explanation for our sudden loss in efficacy. We uncovered SNP sequences and incorporated them into our cell line, but were unable to recapitulate prior results. We probed the former cell line, searching for the missing piece of compound efficacy, but to no avail. We looked at effects on downstream signaling and were met with further inactivity. Compound **1.14** appeared active in *Glp1r*(-/-), and troubleshooting efforts were halted. It is possible compound **1.14** is a false positive from the HTS campaign, as the parental Chem-9 commercial cell line was not purchased and employed in the validation process, in favor of the more ubiquitous CHO K1 cell line. Without this direct cell-line comparison, it is difficult to

know whether the effects of **1.14** are truly GLP-1R-mediated, though it is still possible that the proprietary G-protein used in this cell line provides a signal-biased pathway for our compounds to activate, an effect we have been unable to reproduce without access to said promiscuous G-protein. We hope to employ more target engagement studies in the future.

To further investigate off-target effects, compound **1.14** was sent to Eurofins Panlabs, Inc. to be screened on a broad panel of family B GPCRs, as well as orphan GPCRs, but showed little activity at any of these targets, including GLP-1R. One piece of information we desperately wanted has been uncovered, however. With the acquisition of Milipore by Eurofins Panlabs, Inc, the Chem-9 cell line has been reported as a rat hematopoietic cell line. This validated our data that the cell line is of rat origin, and gave us a better clue to understanding what endogenous systems in this cell line may have produced GLP-1R-like effects. One receptor we became interested in was the bile acid membrane receptor TGR5. This receptor was not included in either broad panel but is an available target for assay at, Eurofins Panlabs, Inc.. We sent **1.14** for a discrete assay against this target, and were surprised to find **1.14** displayed 45% inhibition of TGR5-mediated cAMP accumulation. We are still unsure how this result relates to insulin secretion observed with **1.14**, but research into this is ongoing.

Finally, as we still believe GLP-1R to be a valuable target, and allosteric modulation to be a particularly useful way to target this receptor, we are developing stable, in-house GLP-1R cell lines for use in a new HTS campaign in the future. We

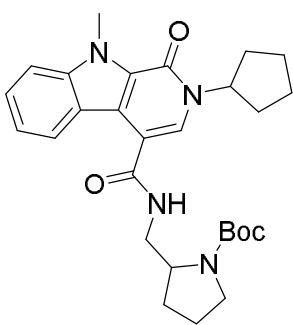
continue to believe GLP-1R PAMs, while elusive, could provide ground-breaking information with regards to GLP-1R physiology, how we may better target this receptor for the treatment of T2D, and elucidating the relationship between GLP-1R and neurodegenerative diseases.

Experimental methods

General synthetic methods and instrumentation

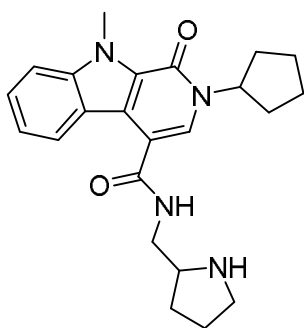
All reactions were carried out employing standard chemical techniques under inert atmosphere. Solvents used for extraction, washing, and chromatography were HPLC grade. Unless otherwise noted, all reagents were purchased from Sigma-Aldrich Chemical Co. and were used without further purification. Analytical thin layer chromatography was performed on 250 μm silica gel plates from Sorbent Technologies. Analytical HPLC was performed on an Agilent 1200 LCMS with UV detection at 215 nm and 254 nm along with ELSD detection and electrospray ionization, with all final compounds showing > 95% purity and a parent mass ion consistent with the desired structure. All NMR spectra were recorded on a 400 MHz Brucker AV-400 instrument or a 600 MHz Bruker AV-600 instrument. ^1H chemical shifts are reported as δ values in ppm relative to the residual solvent peak (MeOD = 3.31, CDCl_3 = 7.26, DMSO). Data are reported as follows: chemical shift, multiplicity (br = broad, s = singlet, d = doublet, t = triplet, q = quartet, quint = quintet, m = multiplet), coupling constant (Hz), and integration. ^{13}C chemical shifts are reported as δ values in ppm relative to the residual solvent peak (MeOD = 49.0, CDCl_3 = 77.16). Low resolution mass spectra were obtained on an Agilent 1200 LCMS with electrospray ionization. High resolution mass spectra were recorded on a Waters QToF-API-US plus Acquity system with electrospray ionization. Automated flash column chromatography was performed on a Teledyne ISCO Combiflash Rf system.

Preparative purification of library compounds was performed on a Gilson chromatograph using a Luna 5u C18 (2) 100A AXIA column (30 x 50 mm) using a water/acetonitrile gradient. Optical rotations of final compounds were acquired on a Jasco P-2000 polarimeter at 23 °C and 589 nm. The specific rotations were calculated according to the equation where l is path length in decimeters and c is the concentration in g/100 mL: $[\alpha]_D^{23} = \frac{100\alpha}{l \times c}$



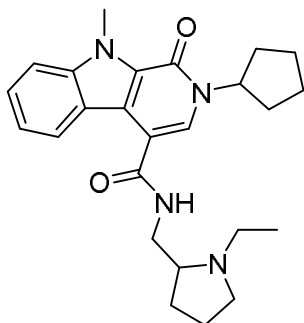
Tert-butyl (R,S)-2-((2-cyclopentyl-9-methyl-1-oxo-2,9-dihydro-1H-pyrido[3,4-b]indole-4-carboxamido)methyl)pyrrolidine-1-carboxylate (1.8a). To a vial was added 2-cyclopentyl-9-methyl-1-oxo-2,9-dihydro-1H-pyrido[3,4-b]indole-4-carboxylic acid (**1.7**) (100 mg, 0.32 mmol; ChemDiv), 1-[Bis(dimethylamino)methylene]-1H-1,2,3-triazolo[4,5-b]pyridinium 3-oxid hexafluorophosphate (HATU) (135 mg, 0.35 mmol; Oakwood Products, Inc.; Lot No.: E03J), and N,N-diisopropylethylamine (DIEA) (168 μ L, 0.97 mmol), which was then dissolved in N,N-Dimethylformamide (DMF) (2 mL). This mixture was stirred 30 minutes at room temperature to allow activation of the acid before adding 2-aminomethyl-1-Boc-pyrrolidine (68 mg, 0.34 mmol). The resultant mixture was stirred an additional 15 hours at room temperature. Upon completion by LC/MS, the

reaction mixture was dissolved in 1:1 water/DCM (10 mL), and extracted with DCM (10 mL). The combined organic layers were washed once with a 5% LiCl solution (15 mL), passed through a phase separator to dry, and concentrated *in vacuo*. The brown residue was then purified by automated flash chromatography using 40-70% ethyl acetate in hexanes to elute. Desired product was afforded in 89% yield. ¹H NMR (400 MHz, CDCl₃) δ ppm): 8.46 (s, 1H), 7.99 (s, 1H), 7.47- 7.41 (m, 2H), 7.23-7.19 (m, 1H), 5.51-5.47 (m, 1H), 4.34 (s, 3H), 4.15-4.07 (m, 1H), 3.82-3.77 (m, 3H), 3.47-3.34 (m, 3H) 2.25-2.16 (m, 2H), 2.12-2.05 (m, 1H), 1.98-1.74 (m, 10H), 1.36 (s, 9H); ¹³C NMR (100.6 MHz, CDCl₃) δ (ppm): 166.93, 156.73, 141.51, 127.01, 126.79, 125.05, 120.76, 120.31, 113.50 109.73, 80.23, 57.09, 55.71, 47.53, 32.52, 32.48, 31.46, 30.13, 28.38, 24.49, 24.10; HRMS (TOF, ES+) calc'd for C₂₈H₃₇N₄O₄ (M+1), 493.2809; found 493.2810.



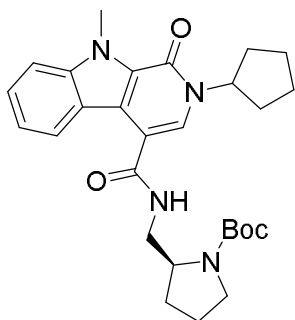
(*R,S*)-2-cyclopentyl-9-methyl-1-oxo-*N*-(pyrrolidin-2-ylmethyl)-2,9-dihydro-1*H*-pyrido[3,4-*b*]indole-4-carboxamide (1.9a). To a round-bottom flask was added at room temperature **1.8a** (140 mg, 0.28 mmol) dissolved in DCM (8 mL). 4M HCl in dioxane (4 mL) was added to this solution while stirring, and the resultant solution was stirred 10 hours at room temperature. At this point a light brown precipitate had formed, and reaction completion was confirmed via LC/MS. Solvent

was removed in vacuo to afford the desired product in quantitative yield as the HCl salt with no purification.



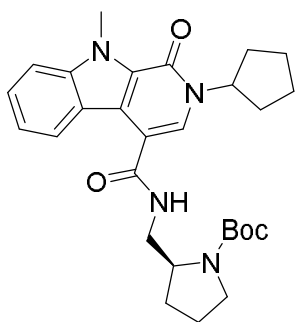
(*R,S*)-2-cyclopentyl-*N*-((1-ethylpyrrolidin-2-yl)methyl)-9-methyl-1-oxo-2,9-dihydro-1*H*-pyrido[3,4-*b*]indole-4-carboxamide (1.6). To a round-bottom flask was added at room temperature **1.9a** (100 mg, 0.26 mmol) dissolved in DCM (2 mL) and dry acetaldehyde (100 μ L). The resultant mixture was stirred at room temperature for 5 minutes before adding sodium triacetoxyborohydride (83 mg, 0.39 mmol), at which point the mixture was stirred an additional 4 hours. Upon completion by LC/MS, the reaction was quenched with sodium bicarbonate (10 mL), and extracted with DCM. The combined organic layers were dried by passage through a phase separator and concentrated in vacuo. The orange residue was taken up in dimethyl sulfoxide (DMSO) and purified via reverse-phase preparative HPLC using acetonitrile in water with 0.5% NH_4OH added to elute. Pure fractions were pooled and concentrated to dryness in vacuo to afford desired product as a foamy yellow solid in 74% yield. ^1H NMR (400 MHz, CDCl_3) δ (ppm): 8.35 (d, J = 8 Hz, 1H), 7.54-7.44 (m, 3H), 7.29-7.21 (m, 1H), 6.92 (br, 1H), 5.51-5.47 (m, 1H), 4.34 (s, 3H), 3.86-3.80 (m, 1H), 3.47-3.42 (m, 1H), 3.20-3.16 (m, 1H) 2.79 (br, 1H), 2.33-2.19 (m, 4H), 2.02-1.87 (m, 3H), 1.82-1.69 (m, 7H) 1.09 (t, J = 7.2, 3H); ^{13}C NMR (100.6 MHz, CDCl_3) δ

(ppm): 167.25, 156.63, 141.41, 126.91, 126.84, 125.30, 124.31, 120.39, 120.16, 113.38, 109.97, 62.85, 55.78, 53.54, 48.43, 40.99, 32.62, 32.59, 31.44, 28.33, 24.66, 22.95, 13.81; HRMS (TOF, ES+) calc'd for C₂₅H₃₃N₄O₂ (M+1), 421.2598; found 421.2596.

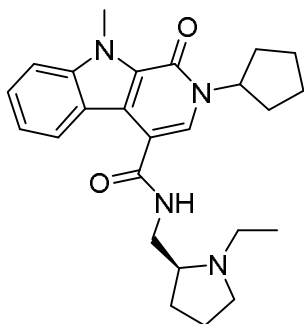


Tert-butyl (S)-2-((2-cyclopentyl-9-methyl-1-oxo-2,9-dihydro-1H-pyrido[3,4-b]indole-4-carboxamido)methyl)pyrrolidine-1-carboxylate (1.12). To a vial was added **1.7** (300 mg, 0.97 mmol; ChemDiv), HATU (404 mg, 1.06 mmol), and DIEA (505 μ L, 2.90 mmol), which was then dissolved in DMF (3 mL). This mixture was stirred 30 minutes at room temperature to allow activation of the acid before adding (S)-2-aminomethyl-1-Boc-pyrrolidine (203 mg, 1.02 mmol). The resultant mixture was then stirred an additional 15 hours at room temperature. Upon completion by LC/MS, the reaction mixture was dissolved in 1:1 water/DCM (15 mL), and extracted with DCM (15 mL). The combined organic layers were washed once with a 5% LiCl solution (20 mL), passed through a phase separator, and concentrated in vacuo. The brown residue was then purified by automated flash chromatography using 40-70% ethyl acetate in hexanes to elute. Desired product was afforded in 82% yield. ¹H NMR (400 MHz, CDCl₃) δ ppm): 8.46 (s, 1H), 7.99 (s, 1H), 7.49- 7.41 (m, 2H), 7.23-7.19 (m, 1H), 5.51-5.47 (m, 1H), 4.34 (s, 3H), 4.13-4.07 (m, 1H), 3.81-3.78 (m, 3H), 3.47-3.34

(m, 3H) 2.25-2.16 (m, 2H), 2.12-2.05 (m, 1H), 1.98-1.74 (m, 10H), 1.37 (s, 9H); ¹³C NMR (100.6 MHz, CDCl₃) δ (ppm): 166.94, 156.74, 141.52, 127.02, 126.80, 125.07, 120.76, 120.33, 113.51, 109.75, 80.24, 57.10, 55.72, 47.53, 32.53, 32.49, 31.46, 30.13, 28.39, 24.49, 24.07; HRMS (TOF, ES+) calc'd for C₂₈H₃₇N₄O₄ (M+1), 493.2809; found 493.2811.

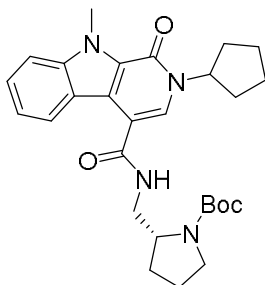


(S)-2-cyclopentyl-9-methyl-1-oxo-N-(pyrrolidin-2-ylmethyl)-2,9-dihydro-1H-pyrido[3,4-*b*]indolecarboxamide (1.13). To a round-bottom flask was added at room temperature **1.12** (390 mg, 0.80 mmol) dissolved in DCM (10 mL). 4M HCl in dioxane (5 mL) was added to this solution while stirring, and the resultant solution was stirred 10 hours at room temperature. At this point a light brown precipitate had formed, and reaction completion was confirmed via LC/MS. Solvent was removed in vacuo to afford the desired product in quantitative yield as the HCl salt.



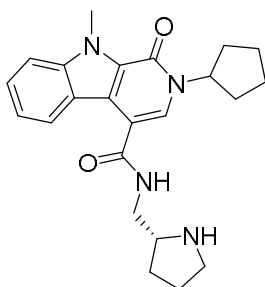
(S)-2-cyclopentyl-N-((1-ethylpyrrolidin-2-yl)methyl)-9-methyl-1-oxo-2,9-dihydro-1H-pyrido[3,4- b]indole-4-carboxamide (1.10). To a round-bottom flask was added at room temperature **1.9b** (100 mg, 0.26 mmol) dissolved in DCM (2 mL) and dry acetaldehyde (100 μ L). The resultant mixture was stirred at room temperature for 5 minutes before adding sodium triacetoxyborohydride (222 mg, 0.39 mmol), at which point the mixture was stirred an additional 4 hours. Upon completion by LC/MS, the reaction was quenched with sodium bicarbonate (10 mL), and extracted with DCM. The combined organic layers were dried by passage through a phase separator and concentrated in vacuo. The orange residue was taken up in dimethyl sulfoxide and purified via reverse-phase preparative HPLC using acetonitrile in water with 0.5% NH₄OH added to elute. Pure fractions were pooled and concentrated to dryness in vacuo to afford desired product as a foamy yellow solid in 76% yield. Specific rotation $[\alpha]_{D}^{20} = -29.178^{\circ}$ ($c = 1.0$, MeOH); ¹H NMR (400 MHz, CDCl₃) δ (ppm): 8.34 (d, $J = 8$ Hz, 1H), 7.54-7.43 (m, 3H), 7.28-7.21 (m, 1H), 6.90 (br, 1H), 5.51-5.47 (m, 1H), 4.33 (s, 3H), 3.85-3.79 (m, 1H), 3.46-3.41 (m, 1H), 3.19-3.15 (m, 1H), 2.92-2.88 (m, 1H), 2.79 (br, 1H), 2.32-2.21 (m, 4H), 2.02-1.86 (m, 3H), 1.82- 1.68 (m, 7H) 1.08 (t, $J = 7.2$, 3H); ¹³C NMR (100.6 MHz, CDCl₃) δ (ppm) 167.25, 156.63, 141.42, 126.91, 126.85, 125.3, 124.32, 120.40, 120.16, 113.39, 109.98, 62.84,

55.78, 53.54, 48.42, 41.00, 32.63, 32.60, 31.45, 28.34, 24.66, 22.96, 13.83; HRMS (TOF, ES+) calc'd for C₂₅H₃₃N₄O₂ (M+1), 421.2598; found 421.2597.

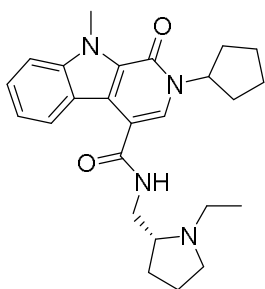


Tert-butyl (R)-2-((2-cyclopentyl-9-methyl-1-oxo-2,9-dihydro-1H-pyrido[3,4-b]indole-4-carboxamido)methyl)pyrrolidine-1-carboxylate (1.8c). To a vial was added **1.6** (100 mg, 0.32 mmol; ChemDiv), HATU (135 mg, 0.35 mmol; Oakwood Products, Inc.; Lot No.: E03J), and DIEA (168 μ L, 0.97 mmol), which was then dissolved in DMF (2 mL). This mixture was stirred 30 minutes at room temperature to allow activation of the acid before adding (*R*)-2-aminomethyl-1-Bocpyrrolidine (68 mg, 0.34 mmol). The resultant mixture was stirred an additional 15 hours at room temperature. Upon completion by LC/MS, the reaction mixture was dissolved in 1:1 water/DCM (10 mL), and extracted with DCM (10 mL). The combined organic layers were washed once with a 5% LiCl solution (15 mL), passed through a phase separator, and concentrated in vacuo. The brown residue was then purified by automated flash chromatography using 40-70% ethyl acetate in hexanes to elute. Desired product was afforded in 85% yield. ¹H NMR (400 MHz, CDCl₃) δ (ppm): 8.46 (s, 1H), 7.99 (s, 1H), 7.49- 7.41 (m, 2H), 7.23-7.19 (m, 1H), 5.51-5.47 (m, 1H), 4.34 (s, 3H), 4.13-4.07 (m, 1H), 3.81-3.78 (m, 3H), 3.47-3.34 (m, 3H) 2.25-2.16 (m, 2H), 2.12-2.05 (m, 1H), 1.98-1.74 (m, 10H), 1.37 (s, 9H); ¹³C NMR (100.6 MHz, CDCl₃) δ (ppm): 166.93, 156.74,

141.51, 127.01, 126.79, 125.06, 120.76, 120.32, 113.51, 109.74, 80.23, 57.10, 55.71, 47.54, 32.52, 32.48, 31.46, 30.13, 28.39, 24.49, 24.09; HRMS (TOF, ES+) calc'd for $C_{28}H_{37}N_4O_4$ (M+1), 493.2809; found 493.2807.

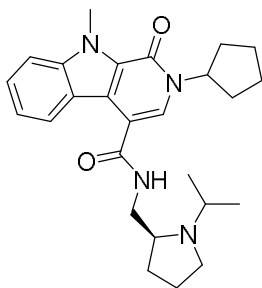


(R)-2-cyclopentyl-9-methyl-1-oxo-N-(pyrrolidin-2-ylmethyl)-2,9-dihydro-1H-pyrido[3,4-*b*]indole-4-carboxamide (1.9c). To a round-bottom flask was added at room temperature **1.8c** (130 mg, 0.26 mmol) dissolved in DCM (8 mL). 4M HCl in dioxane (4 mL) was added to this solution while stirring, and the resultant solution was stirred 10 hours at room temperature. At this point a light brown precipitate had formed, and reaction completion was confirmed via LC/MS. Solvent was removed in vacuo to afford the desired product in quantitative yield as the HCl salt.



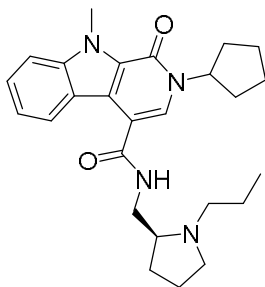
(R)-2-cyclopentyl-N-((1-ethylpyrrolidin-2-yl)methyl)-9-methyl-1-oxo-2,9-dihydro-1H-pyrido[3,4-*b*]indole-4-carboxamide (1.11). To a round-bottom flask was added at room temperature **1.9c** (100 mg, 0.26 mmol) dissolved in DCM (2 mL)

and dry acetaldehyde (100 μ L). The resultant mixture was stirred at room temperature for 5 minutes before adding sodium triacetoxyborohydride (83 mg, 0.39 mmol), at which point the mixture was stirred an additional 4 hours. Upon completion by LC/MS, the reaction was quenched with sodium bicarbonate (10 mL), and extracted with DCM. The combined organic layers were dried by passage through a phase separator and concentrated in vacuo. The orange residue was taken up in dimethyl sulfoxide and purified via reverse-phase preparative HPLC using acetonitrile in water with 0.5% NH_4OH added to elute. Pure fractions were pooled and concentrated to dryness in vacuo to afford desired product as a foamy yellow solid in 81% yield. Specific rotation $[\alpha]_D^{20} = +28.77^\circ$ ($c = 1.0$, MeOH); ^1H NMR (400 MHz, CDCl_3) δ (ppm): 8.33 (d, $J = 8$ Hz, 1H), 7.52-7.43 (m, 3H), 7.24-7.20 (m, 1H), 6.89 (br, 1H), 5.50-5.46 (m, 1H), 4.32 (s, 3H), 3.83-3.79 (m, 1H), 3.43-3.39 (m, 1H), 3.15-3.13 (m, 1H), 2.92-2.87 (m, 1H), 2.76 (br, 1H), 2.31-2.19 (m, 4H), 2.98-1.91 (m, 3H), 1.82-1.69 (m, 7H) 1.07 (t, $J = 7.2$, 3H); ^{13}C NMR (100.6 MHz, CDCl_3) δ (ppm) 167.22, 156.58, 141.37, 126.85, 126.81, 125.22, 124.26, 120.37, 120.12, 113.39, 109.94, 62.72, 55.75, 53.51, 48.33, 41.03, 32.60, 32.57, 31.40, 28.33, 24.63, 22.91, 13.87; HRMS (TOF, ES+) calc'd for $\text{C}_{25}\text{H}_{33}\text{N}_4\text{O}_2$ ($\text{M}+1$), 421.2598; found 421.2599.



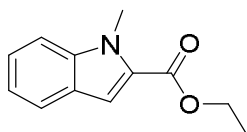
(S)-2-cyclopentyl-N-((1-isopropylpyrrolidin-2-yl)methyl)-9-methyl-1-oxo-2,9-dihydro-1H-pyrido[3,4-b]indole-4-carboxamide (1.14). To a round-bottom flask was added at room temperature **1.13** (200 mg, 0.51 mmol) dissolved in DCM (4 mL) and dry acetone (100 μ L). The resultant mixture was stirred at room temperature for 5 minutes before adding sodium triacetoxyborohydride (150 mg, 0.71 mmol), at which point the mixture was stirred an additional 4 hours. Upon completion by LC/MS, the reaction was quenched with sodium bicarbonate (5 mL), and extracted with DCM. The combined organic layers were dried by passage through a phase separator and concentrated in vacuo. The orange residue was taken up in dimethyl sulfoxide and purified via reverse phase preparative HPLC using acetonitrile in water with 0.5% NH_4OH added to elute. Pure fractions were pooled and concentrated to dryness in vacuo to afford desired product as a foamy yellow solid in 73% yield. Specific rotation $[\alpha]_D^{20} = -20.6^\circ$ ($c = 1.0$, MeOH); ^1H NMR (400 MHz, CDCl_3) δ (ppm): 8.32 (d, $J = 8.2$ Hz, 1H), 7.49-7.45 (m, 2H), 7.39-7.37 (m, 1H), 7.24-7.20 (m, 1H), 7.08 (m, 1H), 5.47-5.43 (m, 1H), 4.24 (s, 3H), 3.74-3.68 (m, 1H), 3.38-3.32 (m, 1H), 3.12-3.07 (m, 1H), 3.02-2.95 (m, 1H), 2.94-2.89 (m, 1H), 2.57-2.51 (m, 1H), 2.25-2.22 (m, 2H), 1.96-1.81 (m, 3H) 1.81-1.67 (m, 7H), 1.12 (d, $J = 6.6$ Hz, 3H), 1.02 (d, $J = 6.4$ Hz, 3H); ^{13}C NMR (100.6 MHz, CDCl_3) δ (ppm): 166.93, 156.23, 141.05, 126.54, 126.47,

124.77, 124.06, 120.09, 119.92, 113.34, 109.64, 58.17, 55.52, 49.70, 47.36, 42.47, 32.35, 32.32, 31.05, S13 29.06, 24.41, 23.48, 22.23, 16.24; HRMS (TOF, ES+) calc'd for $C_{26}H_{35}N_4O_2$ (M+1), 435.5915; found 435.5917.

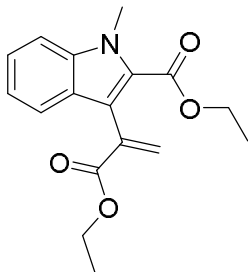


(S)-2-cyclopentyl-9-methyl-1-oxo-N-((1-propylpyrrolidin-2-yl)methyl)-2,9-dihydro-1H-pyrido[3,4-b]indole-4-carboxamide (1.15). To a microwave vial with stir bar was added at room temperature **1.13** (25 mg, 0.51 mmol) dissolved in DCM (1 mL), propionaldehyde (50 μ L), HOAc, (50 μ L), and MP-Cyanoborohydride (2.53 mmol/g, Biotage Inc.). The resultant mixture was stirred under microwave irradiation at 100 °C for 10 minutes, at which point reaction completion was verified by LC/MS. Upon completion, the reaction was quenched with sodium bicarbonate (5 mL), and extracted with DCM. The combined organic layers were dried by passage through a phase separator and concentrated *in vacuo*. The orange residue was taken up in DMSO and purified via reverse phase preparative HPLC using acetonitrile in water with 0.5% NH_4OH added to elute. Pure fractions were pooled and concentrated to dryness *in vacuo* to afford desired product as a foamy yellow solid in 67% yield. 1H NMR (400 MHz, $CDCl_3$) δ (ppm): 8.36 (d, $J = 8.1$ Hz, 1H), 7.55-7.47 (m, 3H), 7.27-7.23 (m, 1H), 6.66 (br, 1H), 5.57-5.49 (m, 1H), 4.38 (s, 3H), 3.89-3.83 (m, 1H), 3.43-3.39 (m, 1H), 3.16-3.12 (m, 1H), 2.74-2.68 (m, 2H), 2.28-2.15 (m, 4H), 2.03 (m, 3H), 1.82-

1.63 (m, 7H), 1.57-1.38 (m, 2H), 0.86 (t, $J = 7.5$ Hz, 3H); ^{13}C NMR (100.6 MHz, CDCl_3) δ (ppm): 167.0, 156.5, 141.3, 126.7, 124.8, 124.2, 120.3, 120.2, 120.0, 113.5, 109.8, 62.5, 56.1, 55.5, 53.7, 40.5, 32.5, 32.5, 31.3, 28.1, 24.5, 22.8, 22.0, 11.9; LRMS (ES+) found for $\text{C}_{26}\text{H}_{34}\text{N}_4\text{O}_2$ ($M+1$) = 435.2

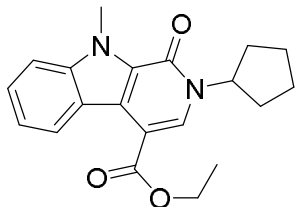


Ethyl 1-methyl-1H-indole-2-carboxylate (1.136). To a round-bottom flash with a stir bar was added ethyl 1H-indole-2-carboxylate (**1.135**) (1 g, 5.29 mmol, Chem-Impex) and THF (27 mL). This solution was cooled to 0 °C before adding NaH as a 60% suspension in mineral oil (423 mg, 10.58 mmol). This mixture was stirred 2 hours before adding methyl iodide (658 μL , 10.58 mmol), warming to room temperature, and stirring for 12 hours. Upon completion by LC/MS, the reaction was quenched with ethanol (10 mL) and concentrated *in vacuo*. Residue was taken up in DCM (200 mL) and washed with 1 N HCl (50 mL) and brine (50 mL). The organic layer was then dried over sodium sulfate, filtered, concentrated, and adsorbed to silica gel for purification by flash chromatography using 100% DCM to elute. Pure fractions were pooled and concentrated to afford product in 89% yield as a light yellow solid (955 mg). ^1H NMR (400 MHz, $(\text{CD})_3\text{SO}$) δ (ppm): 7.68 (d, $J = 8.0$ Hz, 1H), 7.56 (d, $J = 8.4$ Hz, 1H), 7.34 (t, $J = 7.63$ Hz, 1H), 7.26 (s, 1H), 7.13 (t, $J = 7.3$ Hz, 1H), 4.32 (q, $J = 7.1$ Hz, 2H), 4.01 (s, 3H), 1.34 (t, $J = 7.08$, 3H); ^{13}C NMR (100.6 MHz, $(\text{CD})_3\text{SO}$) δ (ppm): 161.29, 139.20, 127.56, 125.25, 124.80, 122.20, 120.41, 110.79, 109.49, 31.42, 14.11.

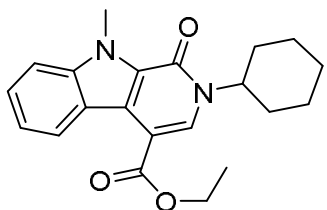


Ethyl 3-(3-ethoxy-3-oxoprop-1-en-2-yl)-1-methyl-1H-indole-2-carboxylate

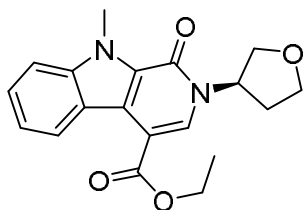
(1.137). To a round-bottom flask with a stir bar was added ethyl 1-methylindole-2-carboxylate (6.0 g, 29.52mmol) and Acetic acid (7.3 mL). This was stirred 5 mins before adding sulfuric acid (0.6 mL, 10.8mmol). This mixture was stirred 3 hours until consumption of starting material by LC/MS. Upon completion, the reaction was diluted with water, made alkaline with conc. NH_4OH until pH 10, and extracted with DCM (50 mL, 3x). The organic layers were dried and concentrated and residue was taken up in minimum amount of toluene and crude product was purified by flash chromatography using 10-60% EtOAc to elute. Pure fractions were pooled and concentrated to afford product in 51% yield as a light yellow solid (4.600 g). ^1H NMR (400 MHz, $(\text{CD})_3\text{SO}$) δ (ppm): 7.60 (dd, $J = 8.3$ Hz, 15.0, 2H), 7.41-7.37 (m, 1H), 7.20-7.16 (m, 1H), 6.50 (d, $J = 1.3$ Hz, 1H), 5.89, (d, $J = 1.3$ Hz, 1H), 4.22 (q, $J = 7.1$ Hz, 2H), 4.12 (q, $J = 7.1$ Hz, 2H), 4.00, (s, 3H), 1.25 (t, $J = 7.1$ Hz, 3H), 1.16 (t, $J = 7.1$ Hz, 3H); ^{13}C NMR (100.6 MHz, $(\text{CD})_3\text{SO}$) δ (ppm): 166.26, 161.33, 137.95, 134.23, 127.07, 125.68, 125.17, 125.14, 121.01, 117.62, 111.02, 60.69, 60.55, 31.73, 13.94, 13.70.



Ethyl 2-cyclopentyl-9-methyl-1-oxo-2,9-dihydro-1H-pyrido[3,4-b]indole-4-carboxylate (1.138a). To a vial with a stir bar was added **1.137** (200 mg 0.66 mmol), cyclopentyl amine (195 μ L, 1.98 mmol) and ethanol (2 mL). This mixture was heated to 80 $^{\circ}$ C for 24 hours, until consumption of starting material was observed by LC/MS. Upon completion, the reaction mixture was concentrated, dissolved in DCM, and passed through a silica gel plug to remove excess amine. The resultant solution was then concentrated and resuspended in benzene (1 mL) before adding 2,3-dichloro-5,6-dicyano-1,4-benzoquinone (300 mg, 1.32 mmol) and stirring 4 hours. Reaction completion was verified by LC/MS. Upon completion, the reaction was quenched with 2 mL of 1N NaOH, extracted 3x with DCM (3 mL), dried, and concentrated *in vacuo*. Residue was dissolved in DCM and adsorbed to silica for purification by flash chromatography with 0-20% EtOAc in hexanes to elute. Pure fractions were pooled and concentrated to afford product in 67% yield as light tan solid (149 mg). ^1H NMR (400 MHz, CDCl_3) δ (ppm): 8.31, (d, J = 8.3 Hz, 1H), 7.49 (s, 1H) 6.95-6.91 (m, 1H), 6.86-6.84 (m, 1H), 6.70-6.66 (m, 1H), 4.93-4.85 (m, 1H), 3.90 (q, J = 7.1 Hz, 2H), 3.76 (s, 3H), 1.73-1.66 (m, 2H), 1.42-1.34 (m, 2H), 1.27-1.18 (m, 4H), 0.89 (t, J = 7.1 Hz, 3H); ^{13}C NMR (100.6 MHz, CDCl_3) δ (ppm): 165.69, 156.86, 141.64, 131.12, 127.04, 126.83, 126.48, 120.99, 120.81, 120.36, 109.71, 107.95, 60.99, 56.35, 32.73, 31.52, 24.61, 14.62.

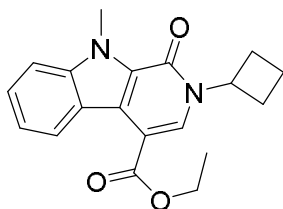


Ethyl 2-cyclohexyl-9-methyl-1-oxo-2,9-dihydro-1H-pyrido[3,4-b]indole-4-carboxylate (1.138b). To a vial with a stir bar was added **1.137** (200 mg 0.66 mmol), cyclopentyl amine (227 μ L, 1.98 mmol) and ethanol (2 mL). This mixture was heated to 80 $^{\circ}$ C for 24 hours, until consumption of starting material was observed by LC/MS. Upon completion, the reaction mixture was concentrated, dissolved in DCM, and passed through a silica gel plug to remove excess amine. The resultant solution was then concentrated and resuspended in benzene (1 mL) before adding 2,3-dichloro-5,6-dicyano-1,4-benzoquinone (300 mg, 1.32 mmol) and stirring 4 hours. Reaction completion was verified by LC/MS. Upon completion, the reaction was quenched with 2 mL of 1N NaOH, extracted 3x with DCM (3 mL), dried, and concentrated *in vacuo*. Residue was dissolved in DCM and adsorbed to silica for purification by flash chromatography with 0-20% EtOAc in hexanes to elute. Pure fractions were pooled and concentrated to afford product in 59% yield as light tan solid (137 mg). ^1H NMR (400 MHz, CDCl_3) δ (ppm): 8.29 (d, J = 8.3 Hz, 1H), 7.46 (s, 1H), 6.93-6.89 (m, 1H), 6.85-6.83 (m, 1H), 6.68-6.64 (m, 1H), 4.45 (tt, J = 3.4, 11.3 Hz, 1H), 3.89 (q, J = 7.1 Hz, 2H), 3.75 (s, 3H), 1.43-1.35 (m, 4H), 1.22-1.17 (m, 2H), 1.10-0.92 (m, 4H), 0.88 (m, J = 7.1 Hz, 3H); ^{13}C NMR (100.6 MHz, CDCl_3) δ (ppm): 165.8, 156.4, 141.7, 130.9, 127.1, 126.9, 126.5, 121.0, 120.8, 120.4, 109.7, 107.8, 61.0, 54.2, 33.1, 31.5, 26.1, 25.6, 14.7.



Ethyl (R)-9-methyl-1-oxo-2-(tetrahydrofuran-3-yl)-2,9-dihydro-1H-pyrido[3,4-b]indole-4-carboxylate (1.138c). To a vial with a stir bar was added **1.137** (200 mg 0.66 mmol), (*R*)-tetrahydrofuran-3-amine (170 mg, 1.98 mmol) and ethanol (2 mL). This mixture was heated to 80 °C for 24 hours, until consumption of starting material was observed by LC/MS. Upon completion, the reaction mixture was concentrated, dissolved in DCM, and passed through a silica gel plug to remove excess amine. The resultant solution was then concentrated and resuspended in benzene (1 mL) before adding 2,3-dichloro-5,6-dicyano-1,4-benzoquinone (300 mg, 1.32 mmol) and stirring 4 hours. Reaction completion was verified by LC/MS. Upon completion, the reaction was quenched with 2 mL of 1N NaOH, extracted 3x with DCM (3 mL), dried, and concentrated *in vacuo*. Residue was dissolved in DCM and adsorbed to silica for purification by flash chromatography with 0-20% EtOAc in hexanes to elute. Pure fractions were pooled and concentrated to afford product in 58% yield as a tan solid (130 mg). ¹H NMR (400 MHz, CDCl₃) δ (ppm): 8.42 (d, *J* = 8.3 Hz, 1H), 7.69 (s, 1H), 7.07-7.02 (m, 1H), 6.96 (d, *J* = 8.4 Hz, 1H), 6.82-6.78 (m, 1H), 5.36-5.31 (m, 1H), 4.00 (q, *J* = 7.1 Hz, 2H), 3.84 (s, 3H), 3.82-3.76 (m, 1H), 3.64 (dd, *J* = 2.1, 10.4 Hz, 1H), 3.56 (dd, *J* = 6.2, 10.5 Hz, 1H), 3.47-3.41 (m, 1H), 2.22-2.13 (m, 1H), 1.68-1.60 (m, 1H), 1.00 (t, *J* = 7.1 Hz, 3H); ¹³C NMR (100.6 MHz, CDCl₃) δ (ppm): 165.46, 156.45, 141.60,

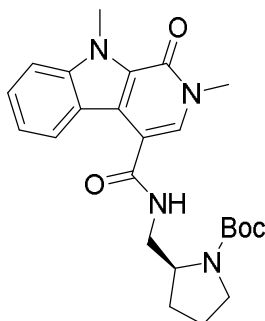
130.79, 127.18, 126.52, 126.38, 121.18, 120.73, 120.48, 109.68, 108.73, 73.22, 67.72, 61.04, 54.84, 33.93, 31.46, 14.56.



Ethyl 2-cyclobutyl-9-methyl-1-oxo-2,9-dihydro-1H-pyrido[3,4-b]indole-4-carboxylate (1.138d). To a vial with a stir bar was added **1.137** (200 mg 0.66 mmol), cyclobutylamine hydrochloride (211 mg, 1.98 mmol) and ethanol (2 mL). This mixture was heated to 80 °C for 24 hours, until consumption of starting material was observed by LC/MS. Upon completion, the reaction mixture was concentrated, dissolved in DCM, and passed through a silica gel plug to remove excess amine. The resultant solution was then concentrated and resuspended in benzene (1 mL) before adding 2,3-dichloro-5,6-dicyano-1,4-benzoquinone (300 mg, 1.32 mmol) and stirring 4 hours. Reaction completion was verified by LC/MS. Upon completion, the reaction was quenched with 2 mL of 1N NaOH, extracted 3x with DCM (3 mL), dried, and concentrated *in vacuo*. Residue was dissolved in DCM and adsorbed to silica for purification by flash chromatography with 0-20% EtOAc in hexanes to elute. Pure fractions were pooled and concentrated to afford product in 71% yield as a tan solid (152 mg). ¹H NMR (400 MHz, CDCl₃) δ (ppm): 8.46 (d, *J* = 8.3 Hz, 1H), 7.67 (s, 1H), 7.09-7.05 (m, 1H), 6.96 (d, *J* = 8.3 Hz, 1H), 6.85-6.81 (m, 1H), 4.86-4.76 (m, 1H), 4.06 (q, *J* = 7.1 Hz, 2H), 3.86 (s, 3H), 2.22-2.14 (m, 2H), 1.99-1.89 (m, 2H), 1.56-1.48 (m, 2H), 1.07 (t, *J* = 7.1 Hz, 3H); ¹³C NMR (100.6 MHz, CDCl₃) δ (ppm): 165.4, 156.3, 141.3,

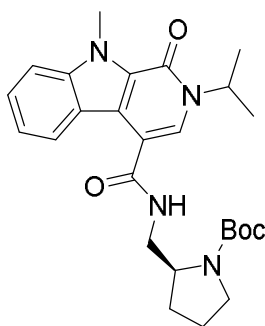
130.7, 126.8, 126.5, 121.0, 120.5, 120.1, 109.4, 107.2, 60.7, 51.4, 31.2, 30.0, 14.9, 14.4.

LRMS (ES+) found for C₁₉H₂₀N₂O (M+1) = 325.2.



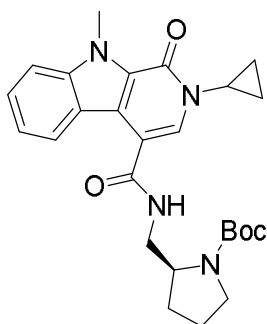
Tert-butyl (S)-2-((2,9-dimethyl-1-oxo-2,9-dihydro-1H-pyrido[3,4-b]indole-4-carboxamido)methyl)pyrrolidine-1-carboxylate (1.141a). To a vial was added 2,9-dimethyl-1-oxo-2,9-dihydro-1H-pyrido[3,4-b]indole-4-carboxylic acid (82 mg, 0.32 mmol; ChemDiv), HATU (135 mg, 0.35 mmol; Oakwood Products, Inc.; Lot No.: E03J), and DIEA (168 μ L, 0.97 mmol), which was then dissolved in DMF (2 mL). This mixture was stirred 30 minutes at room temperature to allow activation of the acid before adding (S)-2-aminomethyl-1-Boc-pyrrolidine (68 mg, 0.34 mmol). The resultant mixture was stirred an additional 15 hours at room temperature. Upon completion by LC/MS, the reaction mixture was dissolved in 1:1 water/DCM (10 mL), and extracted with DCM (10 mL). The combined organic layers were washed once with a 5% LiCl solution (15 mL), passed through a phase separator to dry, and concentrated *in vacuo*. The brown residue was then purified by automated flash chromatography using 40-70% ethyl acetate in hexanes to elute. Desired product was afforded as a light yellow foamy solid (83%, 116 mg). ¹H NMR (400 MHz, CDCl₃) δ ppm): 8.42 (d, *J* = 8.0 Hz, 1H), 7.67 (br, 1H), 7.46-7.42 (m, 2H), 7.36 (d, *J* = 8.2 Hz, 1H),

7.19 (t, $J = 7.5$ Hz, 1H), 4.25 (s, 3H), 4.19-4.10 (m, 1H), 3.64-3.59 (m, 4H), 3.46-3.36 (m, 3H), 2.08-1.86 (m, 3H), 1.78 (br, 1H), 1.40 (s, 9H); ^{13}C NMR (100.6 MHz, CDCl_3) δ (ppm): 166.5, 156.8, 156.5, 141.1, 129.3, 126.8, 126.6, 125.0, 121.3, 120.6, 120.1, 113.0, 109.5, 80.0, 56.3, 47.2, 46.4, 36.7, 31.1, 29.5, 28.3, 23.9; LRMS (ES+) found for $\text{C}_{24}\text{H}_{30}\text{N}_4\text{O}_4$ ($M+1$) = 439.2.



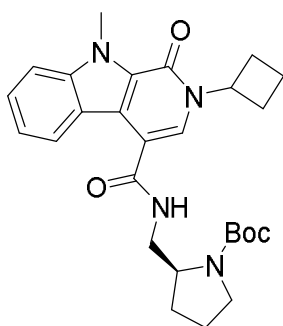
Tert-butyl (S)-2-((2-isopropyl-9-methyl-1-oxo-2,9-dihydro-1H-pyrido[3,4-b]indole-4-carboxamido)methyl)pyrrolidine-1-carboxylate (1.141b). To a vial was added 2-isopropyl-9-methyl-1-oxo-2,9-dihydro-1H-pyrido[3,4-b]indole-4-carboxylic acid (91 mg, 0.32 mmol; ChemDiv), HATU (135 mg, 0.35 mmol; Oakwood Products, Inc.; Lot No.: E03J), and DIEA (168 μL , 0.97 mmol), which was then dissolved in DMF (2 mL). This mixture was stirred 30 minutes at room temperature to allow activation of the acid before adding (S)-2-aminomethyl-1-Boc-pyrrolidine (68 mg, 0.34 mmol). The resultant mixture was stirred an additional 15 hours at room temperature. Upon completion by LC/MS, the reaction mixture was dissolved in 1:1 water/DCM (10 mL), and extracted with DCM (10 mL). The combined organic layers were washed once with a 5% LiCl solution (15 mL), passed through a phase separator to dry, and concentrated *in vacuo*. The brown residue was then purified by automated

flash chromatography using 40-70% ethyl acetate in hexanes to elute. Desired product was afforded as a light yellow foamy solid (78%, 117 mg). ¹H NMR (400 MHz, CDCl₃) δ ppm): 8.49 (d, *J* = 8.1 Hz, 1H), 8.25 (br, 1H), 7.60 (s, 1H), 7.47-7.39 (m, 2H), 7.19 (t, *J* = 8.1 Hz, 1H), 5.53-5.40 (m, 1H), 4.32 (s, 3H), 4.14-4.11 (m, 1H), 3.80-3.77 (m, 1H), 3.45-3.31 (m, 3H), 2.13-2.03 (m, 1H), 1.98-1.80 (m, 2H), 1.80-1.76 (m, 1H), 1.45 (d, *J* = 6.5 Hz, 6H), 1.37 (s, 9H); ¹³C NMR (100.6 MHz, CDCl₃) δ (ppm): 166.8, 157.0, 155.9, 141.3, 126.9, 126.6, 125.3, 124.1, 120.6, 120.1, 113.3, 109.5, 80.1, 56.9, 53.4, 47.4, 46.8, 45.7, 31.3, 29.9, 28.1, 24.0, 22.1, 22.1; LRMS (ES+) found for C₂₆H₃₄N₄O₄ (M+1) = 467.3.



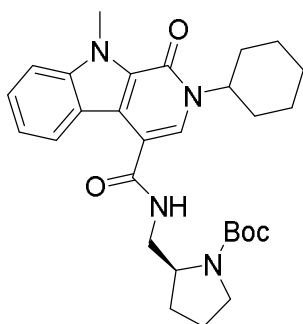
Tert-butyl (S)-2-((2-cyclopropyl-9-methyl-1-oxo-2,9-dihydro-1H-pyrido[3,4-b]indole-4-carboxamido)methyl)pyrrolidine-1-carboxylate (1.141c). To a vial was added 2-cyclopropyl-9-methyl-1-oxo-2,9-dihydro-1H-pyrido[3,4-b]indole-4-carboxylic acid (90 mg, 0.32 mmol; ChemDiv), HATU (135 mg, 0.35 mmol; Oakwood Products, Inc.; Lot No.: E03J), and DIEA (168 μL, 0.97 mmol), which was then dissolved in DMF (2 mL). This mixture was stirred 30 minutes at room temperature to allow activation of the acid before adding (S)-2-aminomethyl-1-Boc-pyrrolidine (68 mg, 0.34 mmol). The resultant mixture was stirred an additional 15 hours at room temperature. Upon completion by LC/MS, the reaction mixture was dissolved in 1:1

water/DCM (10 mL), and extracted with DCM (10 mL). The combined organic layers were washed once with a 5% LiCl solution (15 mL), passed through a phase separator to dry, and concentrated *in vacuo*. The brown residue was then purified by automated flash chromatography using 40-70% ethyl acetate in hexanes to elute. Desired product was afforded as a light yellow foamy solid (84%, 125 mg). ¹H NMR (400 MHz, CDCl₃) δ ppm): 8.45 (d, *J* = 8.1 Hz, 1H), 8.12 (br, 1H), 7.55 (s, 1H) 7.46-7.43 (m, 1H), 7.38 (d, *J* = 8.3 Hz, 1H), 7.19 (t, *J* = 7.5 Hz, 1H), 4.29 (s, 3H), 4.16-4.10 (m, 1H), 3.74-3.67 (m, 1H), 3.43-3.34 (m, 4H), 2.12-2.00 (m, 1H), 2.00-1.81 (m, 2H), 1.81-1.73 (m, 1H), 1.39 (s, 9H); 1.19-0.97 (m, 4H). ¹³C NMR (100.6 MHz, CDCl₃) δ (ppm): 166.6, 157.8, 156.9, 141.3, 128.4, 126.9, 126.6, 125.1, 120.9, 120.6, 120.1, 112.7, 109.5, 80.0, 56.6, 47.3, 45.7, 31.9, 21.2, 29.8, 28.3, 23.9, 7.3, 6.8; LRMS (ES+) found for C₂₆H₃₂N₄O₄ (*M*+1) = 465.2.

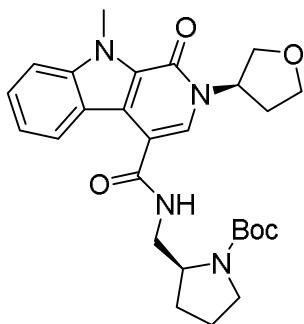


Tert-butyl (S)-2-((2-cyclobutyl-9-methyl-1-oxo-2,9-dihydro-1H-pyrido[3,4-b]indole-4-carboxamido)methyl)pyrrolidine-1-carboxylate (1.141d). To a vial with stirbar was added ethyl 2-cyclobutyl-9-methyl-1-oxo-2,9-dihydro-1H-pyrido[3,4-b]indole-4-carboxylate (103 mg, 0.32 mmol) in a solution of THF (4 mL). To this was added LiOH (23 mg, 960 μL, 0.96 mmol) as a 1 M aqueous solution and the mixture was stirred at 50°C for 24 hours. Reaction completion was verified by

LCMS. Upon completion, mixture concentrated to dryness and suspended in DMF (2 mL) before adding HATU (135 mg, 0.35 mmol; Oakwood Products, Inc.; Lot No.: E03J), and DIEA (168 μ L, 0.97 mmol). This mixture was stirred 30 minutes at room temperature to allow activation of the acid before adding (*S*)-2-aminomethyl-1-Boc-pyrrolidine (68 mg, 0.34 mmol). The resultant mixture was stirred an additional 15 hours at room temperature. Upon completion by LC/MS, the reaction mixture was dissolved in 1:1 water/DCM (10 mL), and extracted with DCM (10 mL). The combined organic layers were washed once with a 5% LiCl solution (15 mL), passed through a phase separator to dry, and concentrated *in vacuo*. The brown residue was then purified by automated flash chromatography using 40-70% ethyl acetate in hexanes to elute. Desired product was afforded as a light yellow foamy solid (84%, 125 mg). ^1H NMR (400 MHz, CDCl_3) δ ppm): 7.89 (d, $J = 7.5$ Hz, 1H), 7.60 (s, 1H), 7.51-7.55 (m, 2H), 7.38 (s, 1H), 7.22 (t, $J = 7.1$ Hz, 1H), 5.33-5.24 (m, 1H), 4.55 (br, 1H), 4.33 (s, 3H), 3.60-3.29 (m, 3H), 2.60-2.51 (m, 2H), 2.38-2.27 (m, 2H), 1.91-1.82 (m, 6H), 1.43 (s, 9H); ^{13}C NMR (100.6 MHz, CDCl_3): 168.5, 156.4, 156.0, 141.1, 126.9, 126.6, 123.5, 121.9, 120.7, 120.1, 119.9, 112.6, 110.1, 19.1, 57.6, 51.0, 49.4, 45.2, 31.3, 30.3, 30.2, 29.1, 28.4, 24.4, 14.9; LRMS (ES+) found for $\text{C}_{27}\text{H}_{34}\text{N}_4\text{O}_4$ (M+1) = 479.3.



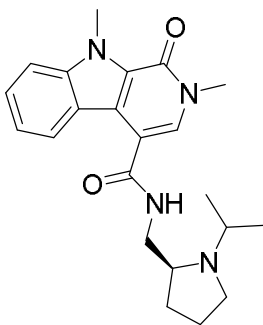
Tert-butyl (S)-2-((2-cyclohexyl-9-methyl-1-oxo-2,9-dihydro-1H-pyrido[3,4-b]indole-4-carboxamido)methyl)pyrrolidine-1-carboxylate (1.141e). To a vial with stirbar was added ethyl 2-cyclohexyl-9-methyl-1-oxo-2,9-dihydro-1H-pyrido[3,4-b]indole-4-carboxylate (113 mg, 0.32 mmol) in a solution of THF (4 mL). To this was added LiOH (23 mg, 960 μ L, 0.96 mmol) as a 1 M aqueous solution and the mixture was stirred at 50°C for 24 hours. Reaction completion was verified by LCMS. Upon completion, mixture concentrated to dryness and suspended in DMF (2 mL) before adding HATU (135 mg, 0.35 mmol; Oakwood Products, Inc.; Lot No.: E03J), and DIEA (168 μ L, 0.97 mmol). This mixture was stirred 30 minutes at room temperature to allow activation of the acid before adding (S)-2-aminomethyl-1-Boc-pyrrolidine (68 mg, 0.34 mmol). The resultant mixture was stirred an additional 15 hours at room temperature. Upon completion by LC/MS, the reaction mixture was dissolved in 1:1 water/DCM (10 mL), and extracted with DCM (10 mL). The combined organic layers were washed once with a 5% LiCl solution (15 mL), passed through a phase separator to dry, and concentrated *in vacuo*. The brown residue was then purified by automated flash chromatography using 40-70% ethyl acetate in hexanes to elute. Desired product was afforded as a light yellow foamy solid (76%, 123 mg). ^1H NMR (400 MHz, CDCl_3) δ ppm): 7.93 (d, $J = 7.9$ Hz, 1H), 7.53-7.47 (m, 2H), 7.31 (s, 1H), 7.24 (t, $J = 7.1$ Hz, 1H), 5.92 (br, 1H), 5.12-5.05 (m, 1H), 4.56 (br, 1H), 4.36 (s, 3H), 3.67-3.36 (m, 3H), 2.19-1.24 (m, 23H); ^{13}C NMR (100.6 MHz, CDCl_3): 168.5, 156.4, 155.6, 141.1, 126.8, 126.7, 123.5, 122.1, 120.6, 120.1, 119.7, 112.6, 110.4, 110.1, 79.1, 57.6, 53.7, 49.5, 45.2, 32.9, 31.3, 29.1, 28.4, 25.9; LRMS (ES+) found for $\text{C}_{29}\text{H}_{38}\text{N}_4\text{O}_4$ (M+1) = 507.3.



Tert-butyl (S)-2-((9-methyl-1-oxo-2-((R)-tetrahydrofuran-3-yl)-2,9-dihydro-1H-pyrido[3,4-b]indole-4-carboxamido)methyl)pyrrolidine-1-carboxylate

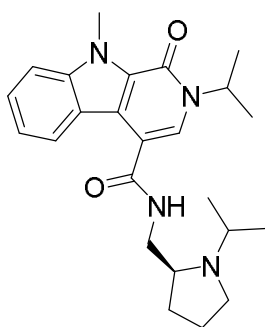
(1.141f). To a vial with stirbar was added ethyl (R)-9-methyl-1-oxo-2-(tetrahydrofuran-3-yl)-2,9-dihydro-1H-pyrido[3,4-b]indole-4-carboxylate (109 mg, 0.32 mmol) in a solution of THF (4 mL). To this was added LiOH (23 mg, 960 μ L, 0.96 mmol) as a 1 M aqueous solution and the mixture was stirred at 50°C for 24 hours. Reaction completion was verified by LCMS. Upon completion, mixture concentrated to dryness and suspended in DMF (2 mL) before adding HATU (135 mg, 0.35 mmol; Oakwood Products, Inc.; Lot No.: E03J), and DIEA (168 μ L, 0.97 mmol). This mixture was stirred 30 minutes at room temperature to allow activation of the acid before adding (S)-2-aminomethyl-1-Boc-pyrrolidine (68 mg, 0.34 mmol). The resultant mixture was stirred an additional 15 hours at room temperature. Upon completion by LC/MS, the reaction mixture was dissolved in 1:1 water/DCM (10 mL), and extracted with DCM (10 mL). The combined organic layers were washed once with a 5% LiCl solution (15 mL), passed through a phase separator to dry, and concentrated *in vacuo*. The brown residue was then purified by automated flash chromatography using 40-70% ethyl acetate in hexanes to elute. Desired product was afforded as a light yellow foamy solid (72%, 114 mg). ¹H NMR (400 MHz, CDCl₃) δ ppm): 7.89 (d, J

= 7.2 Hz, 1H), 7.50-7.43 (m, 2H), 7.37 (s, 1H), 7.20 (t, $J = 7.3$ Hz) 5.90 (br, 1H), 5.85-5.81 (m, 1H), 4.49 (br, 1H), 4.31 (s, 3H), 4.24-4.18 (m, 2H), 4.05-4.03 (m, 1H), 3.98-3.94 (m, 1H), 3.82 (q, $J = 8.3$ Hz, 1H), 3.52-3.35 (m, 4H), 2.65-2.56 (m, 1H), 2.13-2.03 (m, 2H), 1.96 (s, 2H), 1.85-1.79 (m, 2H), 1.78-1.71 (m, 1H), 1.41 (s, 9H); ^{13}C NMR (100.6 MHz, CDCl_3): 167.9, 156.3, 155.8, 141.1, 127.0, 126.3, 123.2, 122.2, 120.8, 120.1, 120.0, 113.7, 110.1, 79.1, 73.2, 67.6, 57.8, 54.2, 49.6, 45.0, 33.8, 31.3, 29.1, 28.3; LRMS (ES+) found for $\text{C}_{27}\text{H}_{34}\text{N}_4\text{O}_5$ ($\text{M}+1$) = 495.2



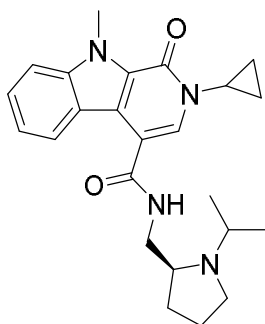
(S)-N-((1-isopropylpyrrolidin-2-yl)methyl)-2,9-dimethyl-1-oxo-2,9-dihydro-1H-pyrido[3,4-b]indole-4-carboxamide (1.152). To a vial with stirbar was added **1.141a** (50 mg, 0.11 mmol) in DCM (4 mL). To this was added hydrochloric acid (41mg, 1.1 mL, 1.14 mmol) as a 1 M solution in dioxane. This was stirred 18 hours and completion was verified by LCMS. Upon completion, mixture was concentrated *in vacuo*, and residue was diluted with DCM (2 mL) before transferring to a microwave vial and adding acetone (50 μL), HOAc, (50 μL), and MP-Cyanoborohydride (50 mg, 2.53 mmol/g, Biotage Inc.). The resultant mixture was stirred under microwave irradiation at 100 $^\circ\text{C}$ for 10 minutes, at which point reaction completion was verified by LC/MS. Upon completion, the reaction was quenched with sodium bicarbonate (5 mL), and extracted with DCM. The combined organic layers were dried by passage

through a phase separator and concentrated *in vacuo*. The orange residue was taken up in DMSO and purified via reverse phase preparative HPLC using acetonitrile in water with 0.5% NH₄OH added to elute. Pure fractions were pooled and concentrated to dryness *in vacuo* to afford desired product as a foamy light-yellow solid (19.7 mg, 47% yield). ¹H NMR (400 MHz, CDCl₃) δ ppm): 8.31 (d, *J* = 8.2, 1H), 7.53-7.43 (m, 3H), 7.26-7.22 (m, 2H), 6.66 (br, 1H), 4.33 (s, 3H), 3.77-3.71 (m, 1H), 3.67 (s, 3H), 3.39-3.33 (m, 1H), 3.08-3.06 (m, 1H), 2.98 (sept, *J* = 6.4 Hz), 2.89-2.85 (m, 1H), 2.55-2.49 (m, 1H), 1.93-1.85 (m, 1H), 1.72-1.60 (m, 4H), 1.07 (d, *J* = 6.6 Hz), 0.99 (d, *J* = 6.4 Hz); ¹³C NMR (100.6 MHz, CDCl₃): 166.6, 156.6, 141.1, 129.6, 126.8, 124.0, 120.7, 120.4, 113.1, 109.9, 57.9, 49.4, 47.1, 42.1, 36.9, 21.3, 29.1, 23.5, 22.3, 15.9; LRMS (ES+) found for C₂₂H₂₈N₄O₂ (M+1) = 381.3



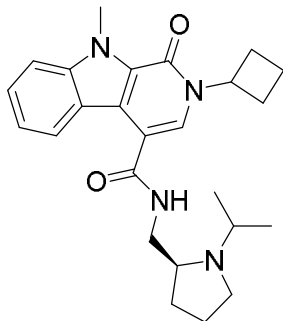
(S)-2-isopropyl-N-((1-isopropylpyrrolidin-2-yl)methyl)-9-methyl-1-oxo-2,9-dihydro-1H-pyrido[3,4-b]indole-4-carboxamide (1.154). To a vial with stirbar was added **1.141b** (51 mg, 0.11 mmol) in DCM (4 mL). To this was added hydrochloric acid (41mg, 1.1 mL, 1.14 mmol) as a 1 M solution in dioxane. This was stirred 18 hours and completion was verified by LCMS. Upon completion, mixture was concentrated *in vacuo*, and residue was diluted with DCM (2 mL) before transferring to a microwave vial and adding acetone (50 μL), HOAc, (50 μL), and MP-

Cyanoborohydride (50 mg, 2.53 mmol/g, Biotage Inc.). The resultant mixture was stirred under microwave irradiation at 100 °C for 10 minutes, at which point reaction completion was verified by LC/MS. Upon completion, the reaction was quenched with sodium bicarbonate (5 mL), and extracted with DCM. The combined organic layers were dried by passage through a phase separator and concentrated *in vacuo*. The yellow residue was taken up in DMSO and purified via reverse phase preparative HPLC using 35-70% acetonitrile in water with 0.5% NH₄OH added to elute. Pure fractions were pooled and concentrated to dryness *in vacuo* to afford desired product as a foamy light-yellow solid (19.7 mg, 38% yield). ¹H NMR (600 MHz, CDCl₃) δ ppm): 8.33 (d, *J* = 8.2 Hz, 1H), 7.52-7.44 (m, 3H), 7.25-7.20 (m, 1H), 6.75 (br, 1H), 5.46 (sept, *J* = 6.8 Hz, 1H), 4.35 (s, 3H), 3.75-3.69 (m, 1H), 3.41-3.35 (m, 1H), 3.12-3.10 (m, 1H), 3.01-2.96 (sept, *J* = 6.6 Hz, 1H), 2.92-2.88 (m, 1H), 2.57-2.51 (m, 1H), 1.94-1.85 (m, 1H), 1.73-1.66 (m, 3H), 1.44 (d, *J* = 6.8 Hz, 6H), 1.09 (d, *J* = 6.6 Hz, 3H), 1.00 (d, *J* = 6.4 Hz, 3H); ¹³C NMR (150.9 MHz, CDCl₃): 167.0, 155.9, 141.3, 126.9, 126.7, 124.1, 124.1, 120.3, 120.2, 120.0, 113.4, 109.8, 58.1, 49.7, 47.2, 45.7, 42.2, 31.3, 29.1, 23.6, 22.3, 22.1, 16.0; LRMS (ES⁺) found for C₂₄H₃₂N₄O₂ (M+1) = 409.3.



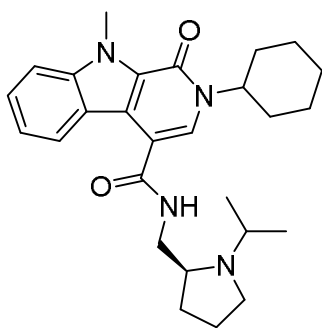
(S)-2-cyclopropyl-N-((1-isopropylpyrrolidin-2-yl)methyl)-9-methyl-1-oxo-2,9-dihydro-1H-pyrido[3,4-*b*]indole-4-carboxamide (1.155). To a vial with stirbar

was added **1.141c** (50 mg, 0.11 mmol) in DCM (4 mL). To this was added hydrochloric acid (41mg, 1.1 mL, 1.14 mmol) as a 1 M solution in dioxane. This was stirred 18 hours and completion was verified by LCMS. Upon completion, mixture was concentrated *in vacuo*, and residue was diluted with DCM (2 mL) before transferring to a microwave vial and adding acetone (50 μ L), HOAc, (50 μ L), and MP-Cyanoborohydride (50 mg, 2.53 mmol/g, Biotage Inc.). The resultant mixture was stirred under microwave irradiation at 100 °C for 10 minutes, at which point reaction completion was verified by LC/MS. Upon completion, the reaction was quenched with sodium bicarbonate (5 mL), and extracted with DCM. The combined organic layers were dried by passage through a phase separator and concentrated *in vacuo*. The yellow residue was taken up in DMSO and purified via reverse phase preparative HPLC using 35-70% acetonitrile in water with 0.5% NH₄OH added to elute. Pure fractions were pooled and concentrated to dryness *in vacuo* to afford desired product as a foamy light-yellow solid (18.3 mg, 41% yield). ¹H NMR (600 MHz, CDCl₃) δ ppm): 8.29 (d, *J* = 8.4 Hz, 1H), 7.50-7.47 (m, 1H), 7.45 (s, 1H), 7.42 (d, *J* = 8.4 Hz, 1H), 7.23-7.21 (m, 1H), 6.74 (br, 1H), 4.30 (s, 3H), 3.74-3.70 (m, 1H), 3.40-3.34 (m, 2H), 3.09-3.08 (m, 1H), 2.98 (sept, *J* = 6.3 Hz, 1H), 2.89-2.87 (m, 1H), 2.55-2.51 (m, 1H), 1.92-1.89 (m, 1H), 1.72-1.64 (m, 3H), 1.19-1.17 (m, 2H), 1.08 (d, *J* = 6.6 Hz, 3H), 0.99 (d, *J* = 6.6 Hz, 3H), 0.98-0.95 (m, 2H); ¹³C NMR (100.6 MHz, CDCl₃): 167.0, 157.8, 141.3, 129.0, 126.9, 126.7, 124.5, 120.4, 120.4, 120.3, 109.8, 77.1 41.7, 32.1, 31.3, 28.9, 23.7, 16.3, 7.1, 7.0; LRMS (ES+) found for C₂₄H₃₀N₄O₂ (M+1) = 407.2



(S)-2-cyclobutyl-N-((1-isopropylpyrrolidin-2-yl)methyl)-9-methyl-1-oxo-2,9-dihydro-1H-pyrido[3,4-b]indole-4-carboxamide (1.158). To a vial with stirbar was added **1.141d** (52 mg, 0.11 mmol) in DCM (4 mL). To this was added hydrochloric acid (41mg, 1.1 mL, 1.14 mmol) as a 1 M solution in dioxane. This was stirred 18 hours and completion was verified by LCMS. Upon completion, mixture was concentrated *in vacuo*, and residue was diluted with DCM (2 mL) before transferring to a microwave vial and adding acetone (50 μ L), HOAc, (50 μ L), and MP-Cyanoborohydride (50 mg, 2.53 mmol/g, Biotage Inc.). The resultant mixture was stirred under microwave irradiation at 100 $^{\circ}$ C for 10 minutes, at which point reaction completion was verified by LC/MS. Upon completion, the reaction was quenched with sodium bicarbonate (5 mL), and extracted with DCM. The combined organic layers were dried by passage through a phase separator and concentrated *in vacuo*. The yellow residue was taken up in DMSO and purified via reverse phase preparative HPLC using 35-70% acetonitrile in water with 0.5% NH_4OH added to elute. Pure fractions were pooled and concentrated to dryness *in vacuo* to afford desired product as a foamy light-yellow solid (19.7 mg, 38% yield). ^1H NMR (400 MHz, CDCl_3) δ ppm): 8.05 (d, J = 7.1 Hz, 1H), 7.52-7.44 (m, 2H), 7.37 (s, 1H), 7.23-7.19 (m, 1H), 5.34-5.25 (m, 1H), 4.51 (br, 1H), 4.33 (s, 3H), 3.32-3.31 (m, 2H), 2.94-2.86 (m, 2H), 2.60-2.51

(m, 3H), 2.37-2.29 (m, 3H), 1.93-1.84 (m, 4H), 1.76-1.66 (m, 2H), 1.17-1.12 (m, 3H), 0.89-0.82 (m, 3H); ^{13}C NMR (100.6 MHz, CDCl_3): 167.6, 156.0, 141.1, 126.8, 126.6, 123.5, 122.4, 120.4, 120.3, 120.2, 110.1, 58.0, 50.9, 50.6, 49.2, 48.9, 31.5, 31.3, 30.2, 22.6, 20.9, 15.2, 14.9, 14.1; LRMS (ES $^+$) found for $\text{C}_{25}\text{H}_{32}\text{N}_4\text{O}_2$ (M+1) = 421.3.



(S)-2-cyclohexyl-N-((1-isopropylpyrrolidin-2-yl)methyl)-9-methyl-1-oxo-2,9-dihydro-1H-pyrido[3,4-b]indole-4-carboxamide (1.159). To a vial with stirbar was added **1.141e** (55 mg, 0.11 mmol) in DCM (4 mL). To this was added hydrochloric acid (41mg, 1.1 mL, 1.14 mmol) as a 1 M solution in dioxane. This was stirred 18 hours and completion was verified by LCMS. Upon completion, mixture was concentrated *in vacuo*, and residue was diluted with DCM (2 mL) before transferring to a microwave vial and adding acetone (50 μL), HOAc, (50 μL), and MP-Cyanoborohydride (50 mg, 2.53 mmol/g, Biotage Inc.). The resultant mixture was stirred under microwave irradiation at 100 $^{\circ}\text{C}$ for 10 minutes, at which point reaction completion was verified by LC/MS. Upon completion, the reaction was quenched with sodium bicarbonate (5 mL), and extracted with DCM. The combined organic layers were dried by passage through a phase separator and concentrated *in vacuo*. The yellow residue was taken up in DMSO and purified via reverse phase preparative HPLC using 35-70% acetonitrile in water with 0.5% NH_4OH added to elute. Pure fractions were pooled

and concentrated to dryness in vacuo to afford desired product as a foamy light-yellow solid (20.1) mg, 41% yield). ¹H NMR (600 MHz, CDCl₃) δ ppm): 8.09 (d, *J* = 7.0 Hz, 1H), 7.54-7.48 (m, 2H), 7.31 (s, 1H), 7.25-7.22 (m, 1H), 5.12-5.07 (m, 1H), 4.55-4.54 (m, 1H), 4.38 (s, 3H), 3.35-3.34 (m, 2H), 2.96-2.87 (m, 2H), 2.02-1.89 (m, 7H), 1.82-1.75 (m, 3H), 1.66-1.51 (m, 6H), 1.15 (br, 6H); ¹³C NMR (100.6 MHz, CDCl₃): 167.6, 155.7, 141.1, 126.8, 126.7, 123.5, 122.5, 120.4, 119.9, 113.2, 110.0, 58.0, 53.6, 50.6, 49.4, 48.9, 33.0, 32.9, 31.3, 29.3, 25.9; LRMS (ES+) found for C₂₇H₃₆N₄O₂ (M+1) = 449.3.

Sections of this chapter have been reprinted with permission from the following:

Discovery of (*S*)-2-Cyclopentyl-*N*-((1-isopropylpyrrolidin-2-yl)-9-methyl-1-oxo-2,9-dihydro-1*H*-pyrrodo[3,4-*b*]indole-4-carboxamide (VU0453379): A novel, CNS penetrant Glucagon-like Peptide 1 receptor (GLP-1R) positive allosteric modulator (PAM). Lindsey C. Morris, Kellie D. Nance, Patrick R. Gentry, Emily L. Days, C. David Weaver, Colleen M. Niswender, Analisa D. Thompson, Carrie K. Jones, Chuck W. Locuson, Ryan D. Morrison, J. Scott Daniels, Kevin D. Niswender, and Craig W. Lindsley. *Journal of Medicinal Chemistry* **2014** 57 (23), 10192-10197. DOI: 10.1021/jm501375c. Copyright © 2014 American Chemical Society

CHAPTER 2

DISCOVERY OF A NOVEL SERIES OF GLUCAGON-LIKE PEPTIDE 1 RECEPTOR NONCOMPETITIVE ANTAGONISTS

Introduction

GLP-1 antagonism

As previously described in the introduction of Chapter 1, the primary interest in therapeutics targeting GLP-1R is via GLP-1 RA activation for the treatment of T2D. While this strategy has been validated and is a current working therapy for this disease, proof-of-concept studies are presently being carried out on the physiological effects of GLP-1 antagonists^[118]. These studies are often performed with one of two peptides: the DPP-4-truncated GLP-1 (9-36) amide^[119] and exendin (9-39) amide^[120]. These peptides have been shown to possess properties one might expect from GLP-1 antagonism^[121]. First believed to be a biologically inert degradation product, GLP-1 (9-36) amide, has been shown to exhibit both antagonist and partial agonist actions at GLP-1R, though with conflicting results^[122]. To this end, it has been difficult to discern what physiological role this peptide may play, and several groups have shown it to have seemingly GLP-1-independent effects^[123-125]. To circumvent some of these difficulties, researchers have employed exendin (9-39) amide, a truncated version of the gila monster-derived secretagogues exendin-3 and EX-4^[126]. In 1993, Widmann and coworkers first demonstrated *in vitro* that exendin (9-39) amide is a competitive antagonist of the primary circulating GLP-1 (7-36) amide peptide at GLP-1R^[127]. In

these experiments, hGLP-1R was cloned from a human pancreatic islet cDNA library, and expressed in Chinese hamster fibroblast (CHL) cells. While both GLP-1 (7-36) amide and EX-4 acted as an agonist of the receptor, inducing cAMP production, exendin-(9-39) antagonized this effect, inhibiting GLP-1-induced cAMP production. In 1998, Katschinski and coworker showed exendin (9-39) amide dose-dependently reduced the insulinotropic action of GLP-1 in healthy human volunteers^[128]. This effect declined with increasing doses of GLP-1 peptide, evidence of a similarly competitive mechanism *in vivo*. Furthermore, exendin (9-39) amide had no effect on plasma levels of insulin in subject with normal glucose levels, but decreased plasma insulin during hyperglycemia, and exendin (9-39) amide did not alter GIP-stimulated insulin secretion, suggesting this hypoinsulinemic action is GLP-1R-mediated. Exendin (9-39) amide has also been shown to block some central effects of GLP-1. Bloom and coworkers, in 1999, demonstrated that intracerebroventricular injection exendin (9-39), blocked the inhibitory effect of GLP-1 on food intake, and while alone had no influence on fast-induced feeding, more than doubled food intake in satiated

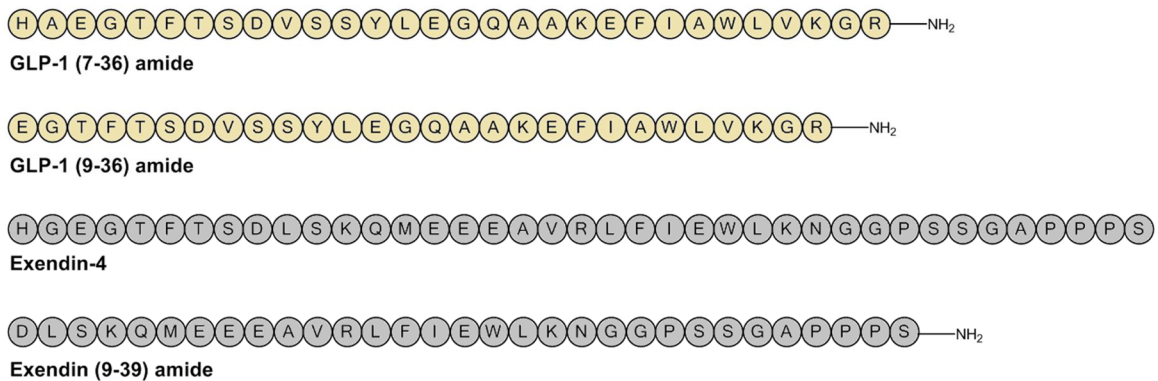


Figure 2.1: Primary structures of known GLP-1 peptide antagonists and their derivative peptide agonists.

rats^[129]. Through these studies, there have been hypothesized several indications for GLP-1 antagonists, examples of which will be discussed in the following sections.

GLP-1 antagonists and congenital hyperinsulinemia

Congenital hyperinsulinemia (CHI) is a condition in which affected individuals have abnormally high basal levels of insulin, potentially causing frequent episodes of hypoglycemia if left untreated^[130]. This disease, often caused by genetic factors, is generally diagnosed in infancy as the first hypoglycemic episode in patients commonly occurs in the first month of life^[131]. Children diagnosed with CHI must be closely monitored and treated as repeated episodes of hypoglycemia increase the risk for serious complications, such as breathing difficulties, seizures, intellectual disability, vision loss, brain damage, and coma^[132]. CHI is a rare disease which affects 1 in 25,000 infants annually, though there are some populations with higher occurrence rates up to 1 in 2,500 children^[133].

The most common genetic causes of CHI are inactivating mutations in ATP-sensitive potassium (K_{ATP}) channels, which are comprised of sulfonylurea (SUR) and inwardly-rectifying potassium channel (Kir) subunits^[134]. In this condition, mutations are often found in the Kir6.2/SUR1 K_{ATP} channel. While acute hypoglycemia may be treated by ingestion of glucose to raise blood levels, most therapeutic efforts toward treating CHI are directed toward preventing these episodes and maintaining normal blood glucose levels^[135]. Strategies employed include K_{ATP} channel openers, such as diazoxide^[136], somatostatin analogs^[137], glucagon infusion^[138], glucocorticoids^[139], and in the case of severe or non-responsive

CHI, partial to full pancreatectomy^[140]. While effective at treating CHI, surgical approaches often carry a high risk the patient developing persistent hypoglycemia or insulin-requiring diabetes. None of the current CHI therapeutics are efficacious without side effects, and to this end the search for new therapies to treat CHI is ongoing.

The use of GLP-1 antagonists has been theorized as a treatment for CHI, but few studies have been carried out, due to the lack of tool molecules. In one pilot study, León and coworkers showed GLP-1 antagonist exendin (9-39) amide suppresses insulin secretion and corrects fasting hypoglycemia in SUR-1(-/-) knockout mice^[141]. Furthermore, this group has also published a proof-of-concept study demonstrating the efficacy of exendin (9-36) amide to increase fasting blood glucose in human subjects with CHI caused by K_{ATP} mutations^[142]. In this study, fasting glucose levels were stabilized and the overall plasma insulin-to-glucose level was increase; however, plasma insulin levels were not significantly lower over the treatment period. The glucose-lowing effect was observed with no effect on circulating proinsulin C-peptide, glucagon, or GLP-1 concentrations. Clinically, these studies have piqued the interest in GLP-1 antagonism as a valid therapeutic for CHI. However, exendin (9-36) amide suffers from the same physiochemical and pharmacokinetic limitations of other GLP-1 peptide drugs^[143]. The development of small molecule GLP-1 antagonists would enable further studies and therapies by improving patient tolerance, ease of administration, and cost of study medications.

GLP-1 and chronic stress

Stress is the collective physiological responses to real or perceived threat to physical or psychological homeostasis^[144]. These responses, primarily acute in nature, allow organisms to manage challenging stimuli and are essential to survival and flourishing; however, chronic stress responses may lead to long-term disorders such as anxiety and depression^[145]. Both acute and chronic stress responses arise from complex neuronal actions in the forebrain, hindbrain, and spinal circuits that activate the sympathetic nervous system (SNS) and hypothalamus-pituitary-adrenal (HPA) axis to produce a “fight-or-flight” response^[146]. These actions produce physiological effects through the release of the catecholaminergic neurotransmitters epinephrine and norepinephrine, as well as adrenocorticotrophic hormone (ACTH) and glucocorticoids, which in concert lead to increased heart rate and blood pressure, increased muscle blood flow, release of corticosteroids, among others^[147]. These effects, in the context of acute response, are generally transient and are vital to the management of stressors. In the context of chronic stress response, however, these effects become detrimental, increasing the risk of hypertension, stress-induced anorexia and weight loss, immunosuppression, and generalized anxiety^[148].

Through tangentially related studies, it has been noted that centrally-administered GLP-1 is anxiogenic and increases cardiovascular responses such as heart beat and blood pressure^[149]. It had been hypothesized that these actions were due to GLP-1-mediated activation of the HPA axis^[150], and in 2016, Trapp and coworkers discussed evidence that GLP-1 is an activator of both the HPA axis and the

SNS, mediating responses to both homeostatic and psychogenic stress^[151]. Furthermore, Seely and coworkers have shown that central administration of exendin (9-39) in rats undergoing acute psychogenic stress results in a decrease in plasma levels of stress-activated hormone ACTH and corticosteroids, along with an anxiolytic effect in behavioral studies^[152]. In another pilot study, Herman and coworkers examined blockade of GLP-1-mediated induction of the HPA axis stress response through receptor knockdown studies. Mice with GLP-1 knockdown on single-minded-1 (*SIM1*) neurons located in the paraventricular nucleus (PVN) of the hypothalamus had a reduced HPA axis response to acute and chronic stress, manifesting in reduced cardiovascular load, and were protected against chronic stress-induced weight-loss and anxiety^[153]. These studies have provided ample evidence that GLP-1 antagonists may be useful in treating chronic stress mechanistically rather than relying on management of symptoms.

Small molecule GLP-1 antagonists

To date, only three non-peptide small molecules have been disclosed as GLP-1R antagonists, each with very little pharmacological data to back up the claims (**Figure 2.2**). The first of these, T-0632 (**2.1**), developed by Beinborn and coworkers at the New England Medical Center, antagonizes GLP-1-induced cAMP production with an IC₅₀ of 21 μM at hGLP-1R, and 353 μM at rGLP-1R and through fold-shift analysis was determined to be a non-competitive antagonist^[154]. Though promising, no *in vitro* effect on insulin secretion, *in vivo* data, nor DMPK data was presented, and it is likely such a low potency molecule would lack the efficacy required to be useful

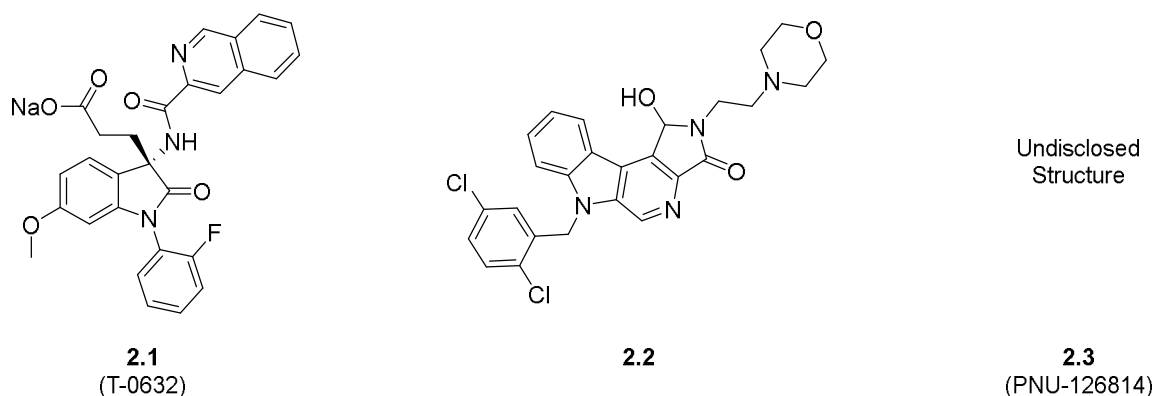


Figure 2.2: Structures of presently disclosed small molecule GLP-1 antagonists.

outside of molecular pharmacology. Furthermore, this compound is not selective for GLP-1R and is a known antagonist of the cholecystinin (CCK) A receptor^[155]. A second antagonist, herein designated compound **2.2**, was disclosed in a patent from Agouron Pharmaceuticals^[156]. In this document, it is claimed **2.2** decreases the binding affinity and activity of GLP-1 at the receptor, as well as antagonizes cAMP production. Though compounds in this patent were alleged to inhibit GLP-1R with an IC_{50} of 100 nm or less, data for individual compounds were not disclosed; furthermore, no *in vivo* or DMPK data were discussed. The final GLP-1 small molecule antagonist, PNU-126814 (**2.3**), was published in an abstract by Gronberg and coworkers with no corresponding structure^[157]. **2.3** is claimed to be a low molecular weight non-peptide competitive antagonist, though no data on potency, efficacy, or pharmacokinetic properties were divulged.

Though there exist small molecule, non-peptidic GLP-1 antagonists, there is much room for improvement. A potent and selective GLP-1 antagonist would be a useful tool molecule for proof of concept studies where peptidic antagonists are currently indicated, mitigating the liabilities of enzymatic degradation, poor

bioavailability and distribution, and patient intolerance. Similarly, a CNS-penetrant GLP-1 antagonist would be paramount to understanding the role GLP-1 signaling plays in the orchestration of the stress response.

Materials and Methods

General methods

Materials and methods for this chapter are the identical to those of Chapter 1 excepting the following.

In vivo glucose tolerance methods

Male Sprague-Dawley rats between 9-10 weeks of age were purchased from Charles River Laboratories (Wilmington, MA). Rats were fed with Formulab Diet 5001 (Purina LabDiet; Purina Mills, Richmond, IN) and were given water ad libitum in an environmentally controlled room with a 12:12-h light-dark cycle. All experiments were conducted in accordance with the Guide for the Care and Use of Laboratory Animals of the United States Department of Agriculture and the National Institutes of Health, and all protocols were approved by the Vanderbilt University Institutional Animal Care and Use Committee.

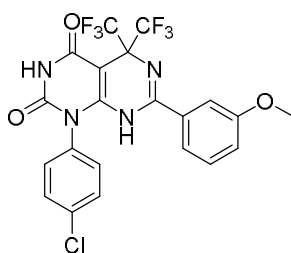
Surgery for implanting the catheter was performed 1 week before the first experiment. Rats were anesthetized with isoflurane. The left common carotid artery was cannulated with a sterile silicone catheter (0.51 mm ID/ 0.94 mm OD). The free end of the catheter was passed subcutaneously to the back of the neck where it was fixed. The catheter was locked with a sterile solution of heparinized glycerol (300 U/ml) and occluded with a metal plug. Studies were performed on 12- to 13-wk-old rats. Rats were fasted from 4:00 P.M. on the evening before the study day. Each oral

glucose tolerance test (OGTT) study consisted of a 30-min equilibration period (8:00 A.M. to 8:30 A.M.). An oral gavage was administered at approximately 8:30 A.M. (-30min) of either Vehicle (0.1% Tween80/0.5% Methocel in Saline) or compound (10 mg/kg @ 1 mg/ml). Thirty minutes after Vehicle/Drug administration an oral load of D50 glucose was administered at 2 g/kg (9:00 A.M.). Samples were taken from the carotid artery at 2, 5, 10, 15, 30, 45, 60, 90, 120, and 150 minutes to measure whole blood glucose via glucometer as well as plasma insulin (measured by the Vanderbilt University Hormone Assay and Analytical Services Core). A measured amount of food was returned to the animals after the 150-minute sample. At 300 minutes, food was remeasured and a final sample was taken for glucose and insulin. The catheter was locked with 300 U/ml heparinized glycerol, occluded with a metal plug, and the animal was returned to normal housing. One week later the study was repeated with the opposite Vehicle/Drug treatment. Surgery and OGTT experiments were conducted by the Vanderbilt University Medical Center Rat Metabolic Physiology Core.

Discovery of VU0650991, a potent CNS-penetrant, orally bioavailable GLP-1R small molecule antagonist^[158]

Discovery and optimization of GLP-1R agonist VU0138721

While our medicinal chemistry and pharmacological efforts resulted in the identification the first known CNS-penetrant, orally bioavailable GLP-1R antagonist, this was not the original goal. Following the HTS campaign detailed in Chapter 1 of this thesis, we identified a GLP-1R small molecule partial agonist, compound **2.4**. This compound possessed an intriguing 1,3-disubstituted-7-aryl-5,5-bis(trifluoromethyl)-5,8-dihydropyrimido[4,5-*d*]pyrimidine-2,4(1*H*,3*H*)-dione core, agonized hGLP-1R with low micromolar potency, and exhibited favorable physicochemical and pharmacokinetic profiles (**Figure 2.3**). As no non-peptidic agonists of GLP-1R had been disclosed at the time, we were inspired to begin



VU0138721 (**2.4**)

hGLP-1R EC₅₀: 6.7 μM

%GLP-1_{MAX}: 15.6%

human CL_{hep} (mL/min/kg): 10.5

rat CL_{hep} (mL/min/kg): 20.8

human PPB (F_w): 0.005

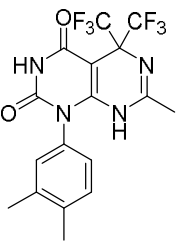
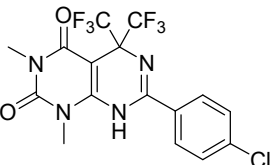
rat PPB (F_w): 0.005

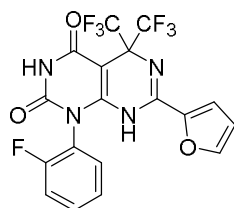
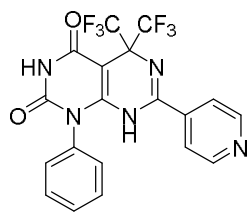
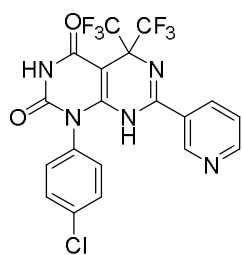
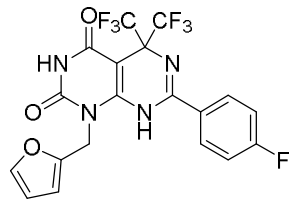
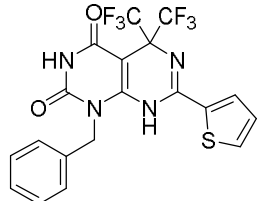
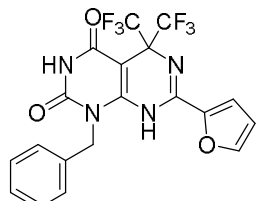
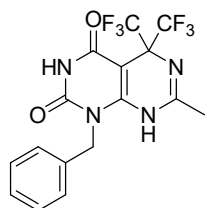
Figure 2.3: Structure, activity and DMPK data of hGLP-1R agonist HTS hit.

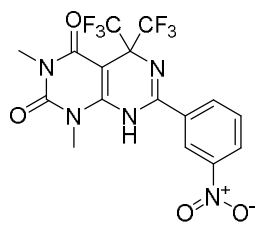
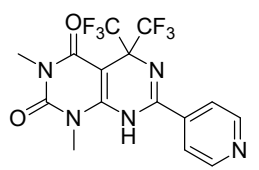
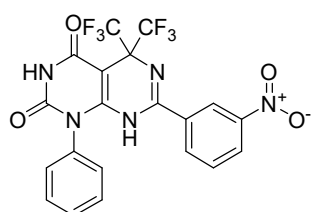
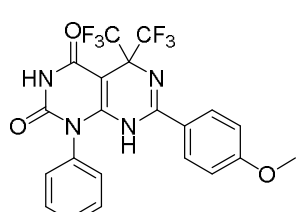
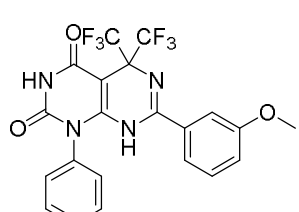
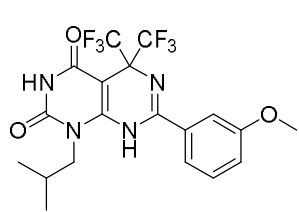
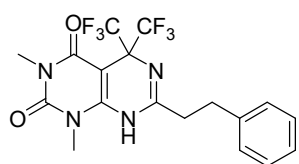
developing **2.4** into a more potent tool molecule to investigate any *in vivo* efficacy the series may possess.

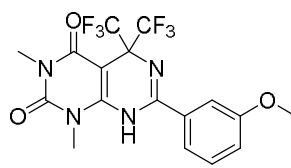
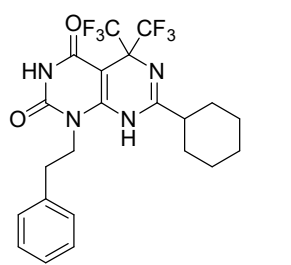
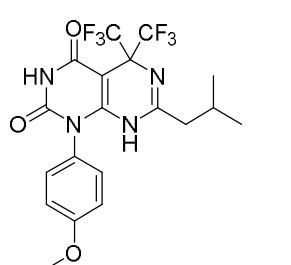
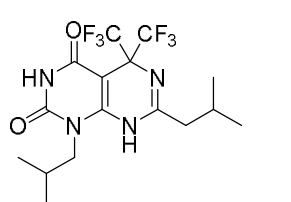
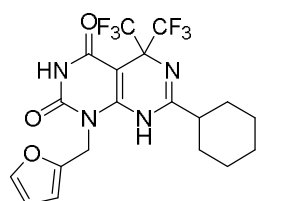
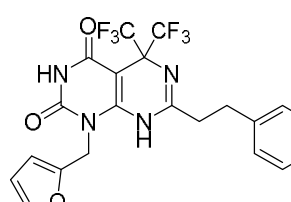
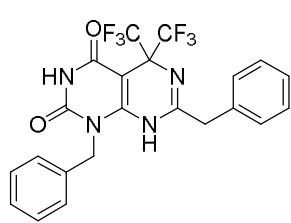
We began our efforts with an SAR by catalogue approach, in which we ordered from ChemBridge Corporation (San Diego, CA), the commercial source of **2.4**, all other compounds which possessed the same core scaffold. This effort resulted in the acquisition of 35 structurally similar compounds. These compounds were subjected to a calcium mobilization assay in CRC format in the presence of an EC₂₀ concentration of GLP-1 using the same commercial hGLP-1R Chem-9 cell from the HTS campaign, including compound **2.4** for reference. This was done to distinguish not only efficacy

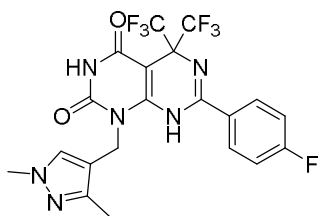
Table 2.1: Structures for **2.4** analogs **2.5-2.39** and associated activation activity data the CRC screen at hGLP-1R by compound alone (agonist mode). Ca²⁺ mobilization responses for each compound are reported as a percentage of the maximum GLP-1 response. VU number denotes the compound identifier assigned by Vanderbilt University. The ChemBridge commercial stock numbers are also provided. Data represent the mean of at least 3 replicate experiments with similar results

Structure	Compound #	VUID	Cat. #	hGLP-1R EC ₅₀ (μM)	hGLP-1R %GLP-1 _{MAX}
	2.5	VU0650990	7904832	Inactive	
	2.6	VU0650991	7905183	0.94	64%

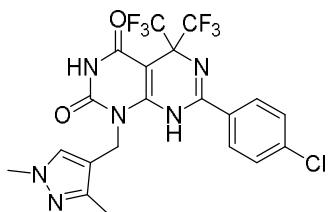
	2.7	VU0650994	7905189	Inactive
	2.8	VU0650995	7905205	Inactive
	2.9	VU0650997	7905206	Inactive
	2.10	VU0650999	7905207	Inactive
	2.11	VU0651000	7905228	Inactive
	2.12	VU0071942	7905245	Inactive
	2.13	VU0105416	7905248	Inactive

	2.14	VU0650973	7905267	0.94	60%
	2.15	VU0135663	7905268		Inactive
	2.16	VU0650974	7905269		Inactive
	2.17	VU0650975	7905270		Inactive
	2.18	VU0650976	7928136		Inactive
	2.19	VU0650977	7932563		Inactive
	2.20	VU0650978	7935347		Inactive

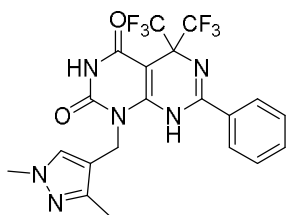
	2.21	VU0650979	7938152	Inactive
	2.22	VU0650980	7938260	Inactive
	2.23	VU0650981	7938944	Inactive
	2.24	VU0650982	7939480	Inactive
	2.25	VU0650983	7939543	Inactive
	2.26	VU0650984	7939958	Inactive
	2.27	VU0105416	7942496	Inactive



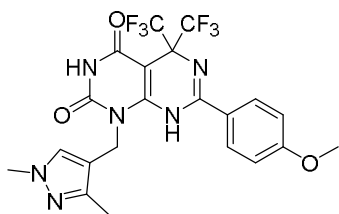
2.28 VU0650985 8909147 Inactive



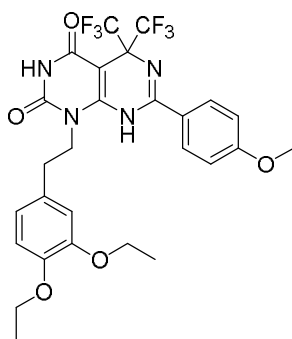
2.29 VU0650986 8909148 Inactive



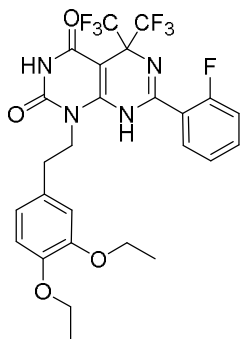
2.30 VU0650987 8909149 Inactive



2.31 VU0650988 8926160 Inactive



2.32 VU0650989 8880117 Inactive

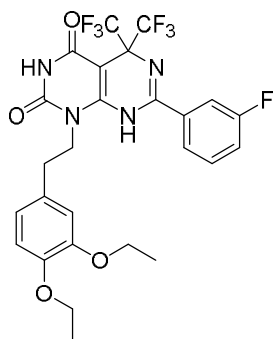


2.33

VU0650992

8880144

Inactive

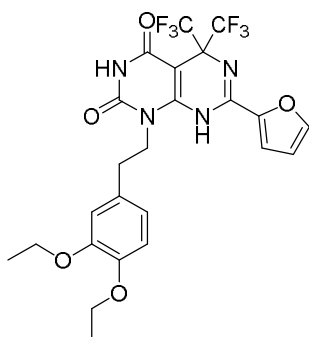


2.34

VU0650993

8880145

Inactive

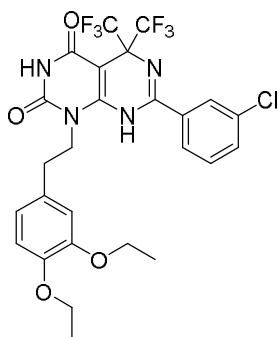


2.35

VU0138317

8880272

Inactive

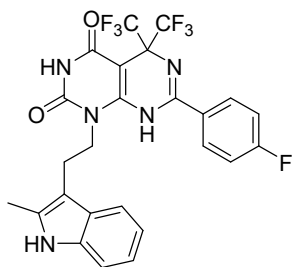


2.36

VU0650996

8880514

Inactive

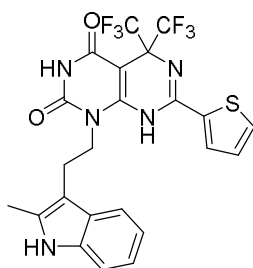


2.37

VU0650998

8880931

Inactive

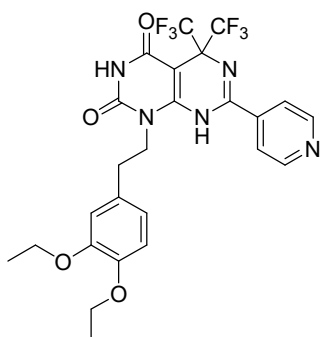


2.38

VU0071871

8881284

Inactive



2.39

VU0105347

8881556

Inactive

at agonizing GLP-1R, but any mode switching that may result in the discovery or potentiators or antagonists (Table 2.1). While most of these analogs failed to produce GLP-1 activation alone at or above 10%, the cutoff for agonist activity, and no mode-switching was observed by any analog, two compounds, **2.6** (VU0650991, $EC_{50} = 936$ nM, $62.4 \pm 2.1\%$ GLP-1 max) and **2.14** (VU0650973, $EC_{50} = 937$ nM, $58.9 \pm 2.3\%$ GLP-1 max) were more potent and efficacious than the parent compound **2.4** (VU0138721, $EC_{50} = 6.3$ μ M, $15.8 \pm 1.1\%$ GLP-1 max) (**Figure 2.4**). Encouraged by the >6-fold increase in potency over the HTS hit, we set out to resynthesize these two analogs to validate the activity and structure of the commercial compounds and evaluate their ability to induce insulin secretion effect in primary tissues through a static islet study.

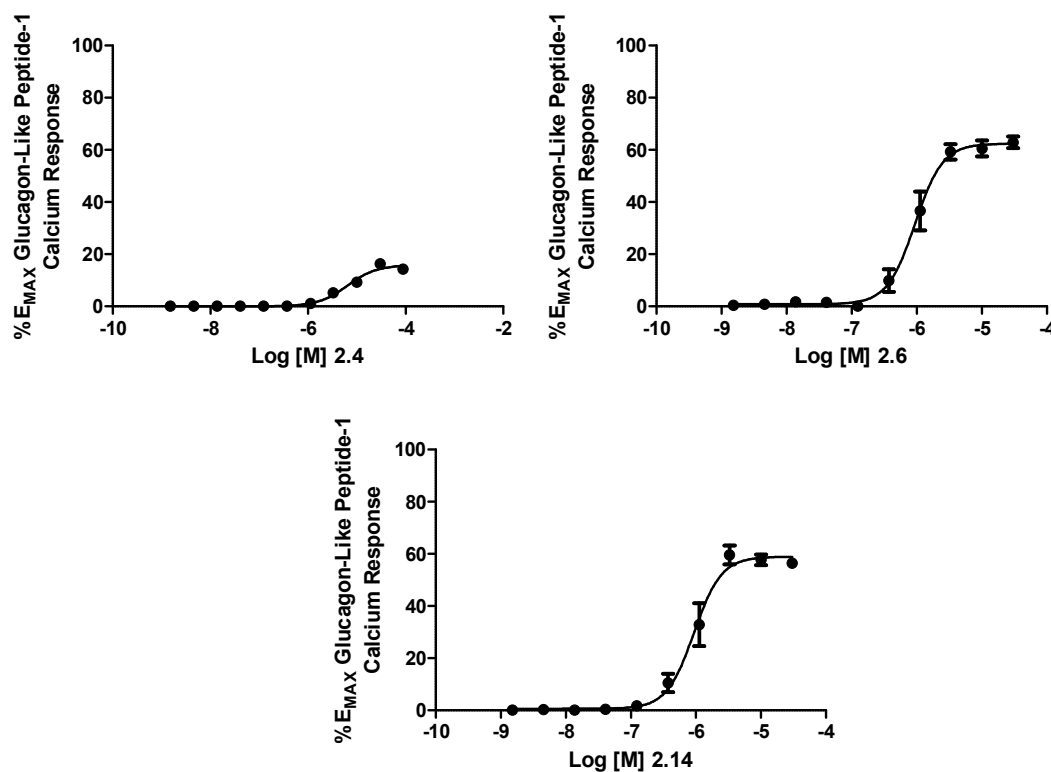
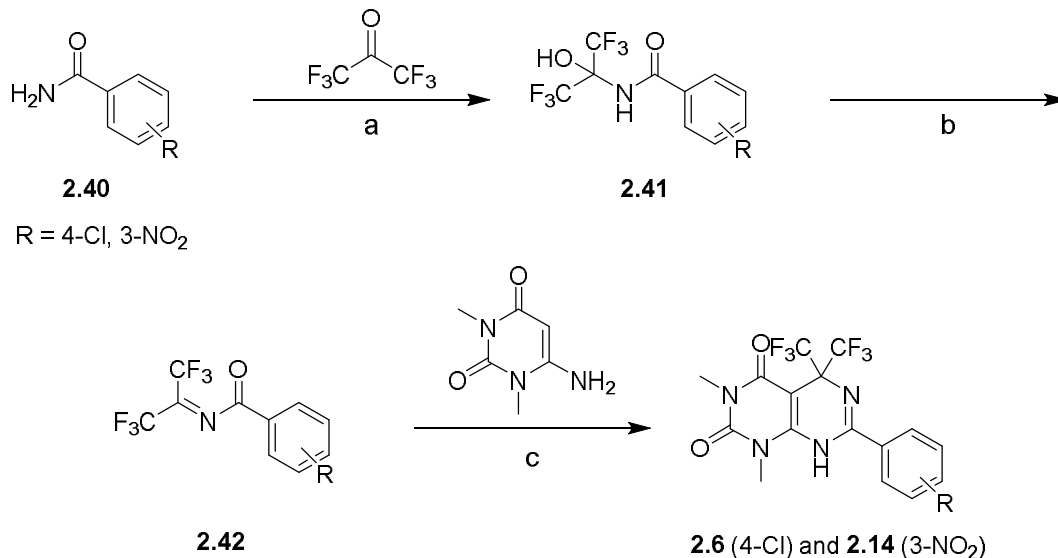


Figure 2.4: Concentration-response curves in agonist mode for HTS hit **2.4** and analogs **2.6** and **2.14** as determined by a calcium mobilization assay at hGLP-1R. Data represented as mean \pm SEM and normalized to EC_{MAX} GLP-1 response.

Synthesis and evaluation of GLP-1R agonists

Considering the promising results of our SAR by catalog screen, we required a synthetic route to the improved VU721 analogs for potency confirmation and to investigate their utility as tool molecules. We developed a 3-step route from commercially available materials that, due to reaction reversibility, must be carried out in a single day (**Scheme 2.1**). Starting with benzamides **2.40**, condensation with hexafluoroacetone under reflux of the gas provided compounds **2.41**, which are then dehydrated to provide imines **2.42**. Cyclization with commercially available uracil derivatives affords compound **2.6** and **2.14** in modest yields (24-32%) across 3 steps, with the primary byproduct being full reversion back to starting material **2.40**. These



Scheme 2.1: Synthetic route to analogs **2.6** and **2.14**. Reagents and conditions: (a) hexafluoroacetone, DCM, 30 °C, 3 hr, 95–98% (crude); (b) (CF₃O)₂O, pyridine, ether, 0 °C, 2 hr, 94–97% (crude); (c) triethylamine, DMF, 80 °C, 5 hr., 24–36%.

newly synthesized compounds were then analyzed in our calcium mobilization assay for potency confirmation, which we were pleased to find were identical to that of the commercial stock. With this corroboration, we set about evaluating these compound in a static islet incubation assay to observe whether they had an effect on glucose-stimulated insulin secretion from primary tissues. Primary pancreatic islets were harvested from wild-type mice and treated with high and low concentration of glucose and 1 μ M concentration of compounds **2.4** (VU721), **2.6** (VU991), or **2.14** (VU973), along with a 10-nM dose of EX-4 as a positive control, or vehicle as a negative control. Post-treatment, cell medium is removed and tested for insulin levels, which are normalized by percent content per hour (**Figure 2.5**). We were quite puzzled to find that all three compounds, which act as agonists in our calcium mobilization assays, failed to increase insulin secretion from the islets, and rather ablated insulin levels below the negative control. At this result, we were perplexed where next to go with this series of compounds, and the project was shelved until we postulated a reasoning for these confounding data.

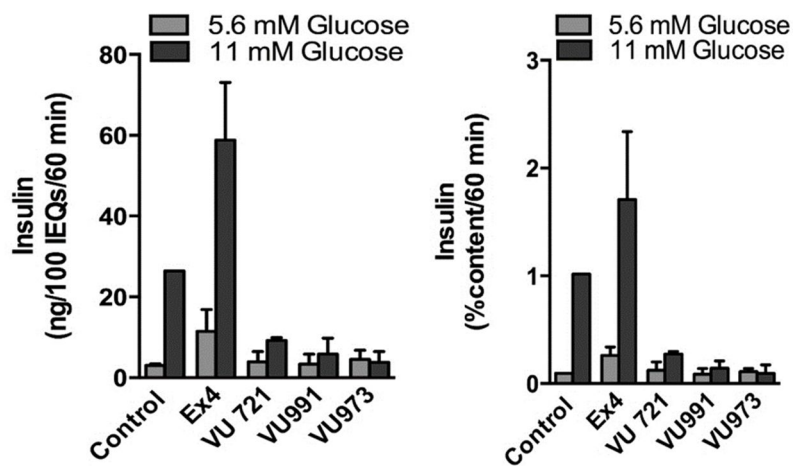
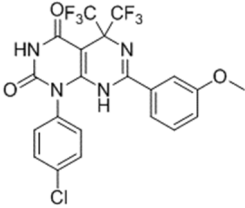
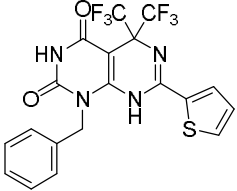
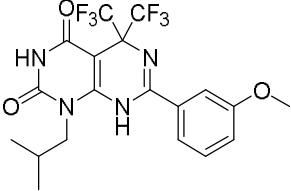
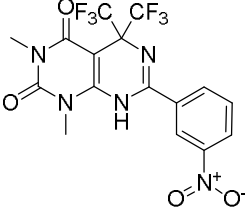
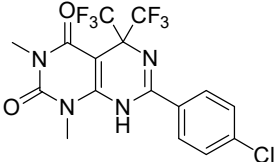


Figure 2.5: Glucose-stimulated insulin secretion in WT primary mouse islets in the presence of 10 nM EX-4 or 1 μ M concentration of VU721 (**2.4**), VU991 (**2.6**), or VU973 (**2.14**) under low and high glucose conditions.

Reclassification of GLP-1R agonists as antagonists

During our investigations into the efficacy issues observed with our GLP-1 PAM series, we sought to examine the effects our GLP-1 agonist series had on GLP-1R-mediated cAMP accumulation. We were perplexed by the dissonance between data from our calcium mobilization assay and static islet insulin secretion assay and desired any data that could explain it. To this end, we subjected all 35 compounds to a cAMP accumulation assay in CRC-format in the presence of an EC₂₀ concentration of GLP-1 using a transiently transfected hGLP-1R pGLO-22F T-REx™ 293 cell line, including compound **2.4** for reference. We were stunned to find that the compounds did not agonize the receptor at all, not potentiated the EC₂₀, but instead antagonized this GLP-1 concentration. While contented to find a pharmacological agreement with our static islet data, we were hesitant to reveal until a full antagonist mode assay was performed. To follow up, we screened the compounds in the same cAMP assay in CRC-format in the presence of an EC₈₀ concentration of GLP-1, looking at the antagonist window to determine potency. We carried this assay out concomitantly with an EC₈₀ concentration of EX-4 to determine if probe dependency was a factor in our assay disagreement. Many compounds remained inactive in this assay, but two **2.18** and **2.19** showed efficacy in this assay where none was observed in the calcium mobilization assay; however, **2.18** was weakly active with a potency higher than that of the parent compound **2.4**, and **2.19** was less potent than either previously highlighted compounds **2.6** and **2.14**. Furthermore, we were elated to find no probe dependence, as all active compounds were comparably potent in antagonizing GLP-1 as EX-4 (**Table 2.2** and **Figure 2.6**).

Table 2.2: Structures for active **2.4** analogs and associated antagonism data at hGLP-1R (antagonist mode). VU number denotes the compound identifier assigned by Vanderbilt University. ^aGLP-1R IC₅₀ and GLP-1_{MIN}(%) in T-REx™293 HEK cell line with GloSensor cAMP assay upon activation with an EC₈₀ of GLP-1 (7-36) amide; ^bGLP-1R IC₅₀ and EX-4_{MIN}(%) in T-REx™293 HEK cell line with GloSensor cAMP assay upon activation with an EC₈₀ of EX-4. Data reported as mean ± SEM of at least 3 replicate experiments with similar results

Structure	Compound #	VUID	hGLP-1 IC ₅₀ (μM) ^{a,b}	Ligand _{MIN} (%) ^{a,b}
	2.4	VU0138721	5.9 ^a	16.8±6.3 ^a
	2.19	VU0651000	1.3 ^a	36.2±1.9 ^a
	2.18	VU0650977	7.2 ^a	22.7±6.2 ^a
	2.16	VU0650973	0.61 ^a	16.4±1.5 ^a
	2.6	VU0650991	0.65 ^a	20.9±1.4 ^a
			0.69 ^b	15.5±1.7 ^a
			0.69 ^b	19.7±2.1 ^a

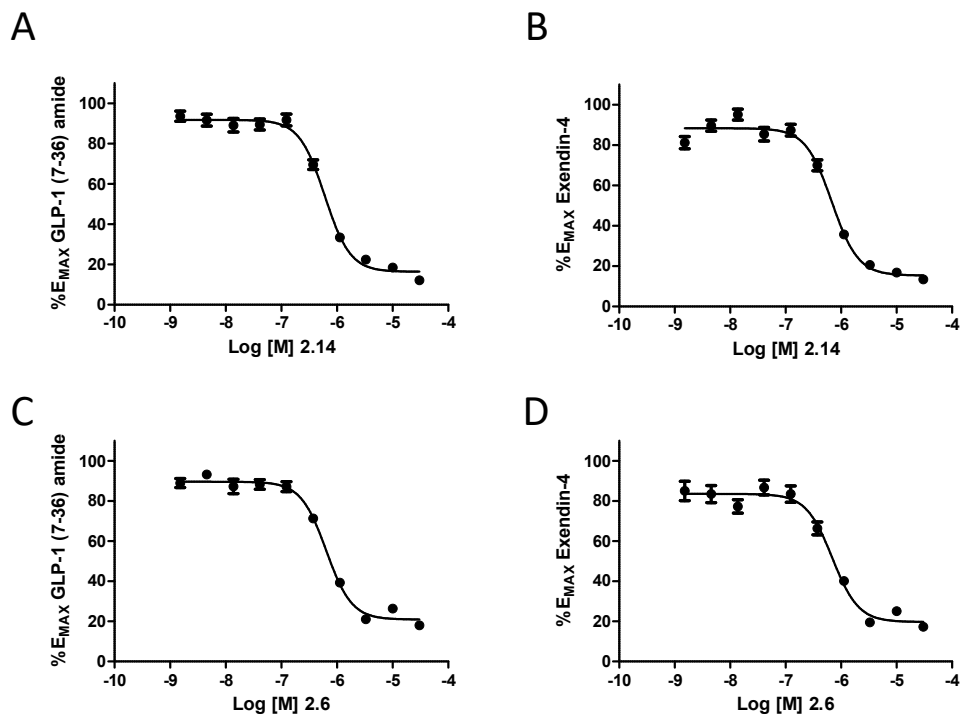


Figure 2.5: Molecular pharmacology of **2.6** and **2.14**. A) CRC for inhibition of GLP-1 (7-36) amide activation of hGLP-1R by **2.14** ($IC_{50} = 0.60 \mu\text{M}$, $16.4 \pm 1.5 \text{ GLP-1}_{\text{MIN}}$); B) CRC for inhibition of EX-4 activation of hGLP-1R by **2.14** ($IC_{50} = 0.69 \mu\text{M}$, EX-4_{MIN}); C) CRC for inhibition of GLP-1 (7-36) amide activation of hGLP-1R by **2.6** ($IC_{50} = 0.6 \mu\text{M}$, $20.9 \pm 1.4 \text{ GLP-1}_{\text{MIN}}$); D) CRC for inhibition of EX-4 activation of hGLP-1R by **2.6** ($IC_{50} = 0.69 \mu\text{M}$, $19.7 \pm 2.1 \text{ EX-4}_{\text{MIN}}$); Data produced from GloSensor cAMP assay in T-REx™293 HEK cells and expressed as mean \pm SEM and normalized to EC_{MAX} agonist response.

With these data in hand, we could reclassify what were previously designated GLP-1R agonist into GLP-1 antagonists. We hypothesize the compounds displayed partial agonism in the hGLP-1R Chem-9 cell line due to high levels of receptor reserve and activation of the proprietary G-protein which provided calcium flux. This receptor expression-mediated partial agonist-antagonist effect has been reported in the literature previously, and the designation of antagonist agreed with the primary tissue data. We proceeded to more thoroughly scrutinize these compounds with regards to mode of inhibition, DMPK profile, and ancillary pharmacology.

In vitro characterization of GLP-1R antagonists

After finding our presumed GLP-1R agonists were actually antagonists, we sought to determine whether these compounds acted as competitive or non-competitive antagonists. While this is normally carried out with radioligand binding studies, we were unable to do this due to being without the necessary lab space and qualifications to use the iodine-125-labeled GLP-1 and EX-4 peptides; thus, we utilized a progressive fold-shift strategy to differentiate between the two modes. Treatment of an agonist CRC with a competitive antagonist results in a rightward shift of agonist potency, while a non-competitive antagonist results in a decrease in agonist efficacy. T-REx™293 cells transiently expressing hGLP-1R and pGLO-22F cAMP sensor were treated with increasing concentrations of antagonist before addition of a GLP-1 CRC (**Figure 2.7**). The observed progressive decrease in GLP-1_{MAX} with increasing compound concentration indicated that both **2.6** and **2.14** act as non-competitive antagonists with GLP-1 at hGLP-1R.

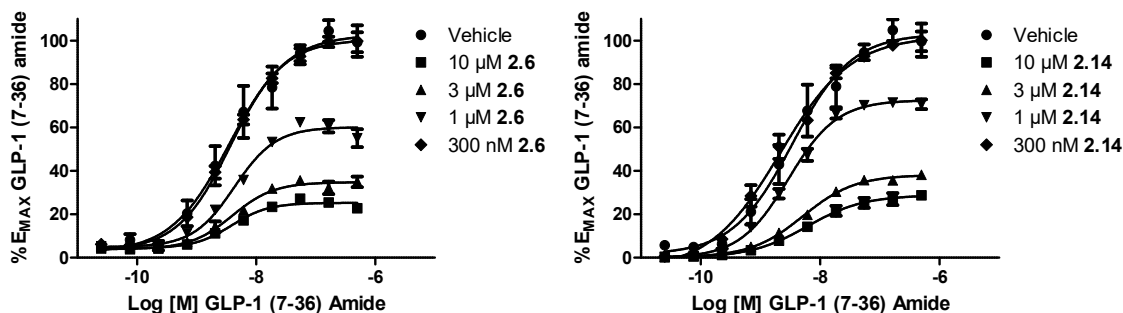


Figure 2.7: Progressive fold-shift studies with **2.6** and **2.14**. Increasing concentrations of compound in the presence of a fixed CRC of GLP-1 (7-36) amide induced a dose-dependent decrease in the GLP-1_{MAX}, consistent with non-competitive inhibition

With this knowledge, we sought to reevaluate these compounds in a static islet incubation assay to determine whether they could inhibit the EX-4 potentiation of glucose-stimulated insulin secretion, as they had only proved efficacious in blocking low and high glucose-stimulated insulin secretion previously. Primary pancreatic islets were harvested from wild-type mice and treated with a 1 μ M concentration of compounds **2.4** or **2.14** along with a 10 nM stimulatory dose of EX-4. We were encouraged to find that, not only could both compounds inhibit glucose-stimulated insulin secretion, but they were also effective at inhibiting EX-4-potentiation of this glucose-stimulated insulin secretion as well (**Figure 2.8**). With our compounds well validated as GLP-1R non-competitive antagonists, we next sought to evaluate the DMPK profiles of **2.6** and **2.14** to assess their potential as *in vivo* tool molecules

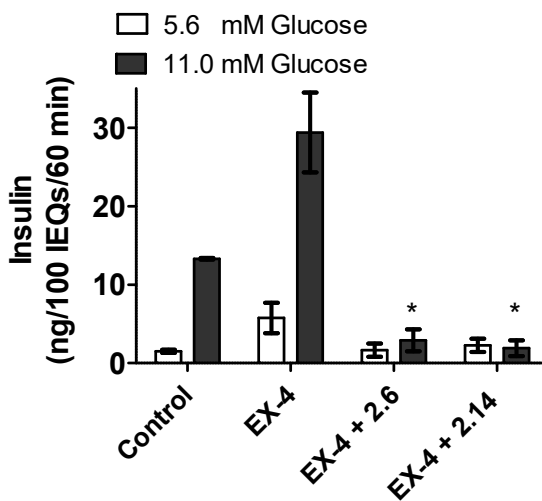


Figure 2.8: Glucose-stimulated insulin secretion in WT primary mouse islets in the presence of 10 nM EX-4 under low and high glucose conditions. Both antagonists, **2.6** and **2.14** (at a concentration of 1 μ M), blocked the potentiation of insulin secretion by EX-4. Significance determined by 2-way ANOVA followed by Sidak's multiple comparison test.

In vitro & in vivo DMPK characterization of GLP-1R antagonists

Possessing GLP-1 well-validated non-competitive antagonists with sub-micromolar potencies and activity in primary tissues, we sought to determine the *in vitro* DMPK profile of compounds **2.6** and **2.14** to evaluate their potential to serve as *in vivo* tool compounds for future proof-of-concept studies. The compounds were assayed in several *in vitro* DMPK assays (**Table 2.3**), including plasma protein binding, rat and human microsomal stability, and a CYP450 inhibition panel. These studies revealed both to have favorable *in vitro* profiles with low predicted hepatic clearance with both human and rat liver microsome, and acceptable levels of CYP450 inhibition for a first-generation tool molecule. However, we found that both were highly protein bound, with free-fractions at or below 1%. We then turned to *in vivo* DMPK studies (**Table 2.3**), including distribution in rat, to see if there was a discernable metric that would cause one compound to be more useful over the other. Most surprisingly, these studies revealed compound **2.6** to be highly CNS penetrant with a plasma:brain K_p of 1.45, making this compound the first known CNS-penetrant GLP-1 small molecule antagonist. Furthermore, **2.6** was found to be highly orally bioavailable, with a %F of 50%. Compound **2.6** also had a much more suitable half-life of 9.8 hours over that of **2.14**, which had a poor half-life of less than an hour. Thus, **2.6** was chosen as the more valuable tool molecule; however, due to the peripheral restriction of **2.14**, it was still a compound of interest to discern differences between central and peripheral GLP-1 antagonism. At this point, prior to any *in vivo* administration, we elected to explore the ancillary pharmacology and off-target binding of tool molecule **2.6**

Table 2.3: Full in vitro and in vivo DMPK profile of compounds **2.14** (VU0650973) and **2.6** (VU0650991) in Sprague–Dawley rat and human. Liver microsomal clearance was predicted using the well-stirred model with 20 and 45 g liver per kg body weight and 21 and 70 mL/kg hepatic blood flow for human and rat, respectively.

Parameter	2.16	2.4
MW	451.29	440.73
TPSA	116.82	65.01
cLogP	3.63	3.63
P450 inhibition (μM)		
P450 (1A2, 2C9, 3A4, 2D6)	25.04, 0.47, >30, 21.20	4.01, 0.41, >30, >30
<i>In vitro</i> PK		
rat CL _{HEP} (mL/min/kg)	35.9	0*
human CL _{HEP} (mL/min/kg)	0*	2.03
rat plasma <i>f</i> _u	.005	.011
human plasma <i>f</i> _u	.005	.007
<i>In vivo</i> rat distribution (PO, 3 mg/kg, 1 h)		
Plasma (ng/mL)	76.7	45.0
Brain (ng/mL)	2.4	65.1
Brain:plasma (<i>K</i> _p)	0.02	1.45
<i>In vivo</i> rat PK (IV, 1 mg/kg; PO, 3 mg/kg)		
CL _p (ml/min/kg)	3.64	4.79
<i>t</i> _{1/2} (min)	42	587
<i>V</i> _{ss} (L/kg)	0.22	3.57
%F	ND	50

Ancillary pharmacology of GLP-1R antagonist VU0650991

After determining both the pharmacological and pharmacokinetic profile of compound **2.6** (VU0650991), but before continuing on into *in vivo* studies, we sought to determine what, if any, wider ancillary pharmacology **2.6** may possess, in the hopes that we may learn of any potential off-target effects. For this, we employed a commercial radioligand competition binding screen of 68 GPCRs, ion channels, and transporters (**Table 2.3**).

Table 2.3: Ancillary/off-target competition binding screen results for compound **2.6** (VU0650991). Compound **2.6** was dosed at 10 μ M for single point competition binding assays. Targets displaying significant binding ($\geq 50\%$ at 10 μ M) are bolded. Data represent the mean of 2 independent experiments with similar results. Studies performed by Eurofins Panlabs, Inc.

Target/Protein	Species	% Inhibition
Adenosine A ₁	Human	13
Adenosine A _{2A}	Human	4
Adenosine A ₃	Human	29
Adrenergic α_{1A}	Rat	-4
Adrenergic α_{1B}	Rat	7
Adrenergic α_{1D}	Human	12
Adrenergic α_{2A}	Human	-2
Adrenergic β_1	Human	-3
Adrenergic β_2	Human	3
Androgen (Testosterone)	Human	2
Bradykinin B ₁	Human	6
Bradykinin B ₂	Human	-2
Calcium Channel L-Type, Benzothiazepine	Rat	21
Calcium Channel L-Type, Dihydropyridine	Rat	-3
Calcium Channel N-Type	Rat	4
Cannabinoid CB ₁	Human	-4
Dopamine D ₁	Human	6
Dopamine D _{2S}	Human	-8
Dopamine D ₃	Human	-6
Dopamine D _{4.2}	Human	3
Endothelin ET _A	Human	-7
Endothelin ET _B	Human	1
Epidermal Growth Factor (EGF)	Human	-5
Estrogen ER α	Human	19

GABA _A , Flunitrazepam, Central	Rat	-5
GABA _A , Muscimol, Central	Rat	1
GABA _{B1A}	Human	-5
Glutamate, Kainate	Rat	4
Glutamate, NMDA, Agonism	Rat	15
Glutamate, NMDA, Glycine	Rat	-13
Glutamate, NMDA, Phencyclidine	Rat	-6
Histamine H ₁	Human	1
Histamine H ₂	Human	-17
Histamine H ₃	Human	-2
Imidazoline I ₂ , Central	Rat	-1
Interleukin IL-1	Mouse	14
Leukotriene, Cysteinyl CysLT ₁	Human	-5
Melatonin MT ₁	Human	12
Muscarinic M ₁	Human	-5
Muscarinic M ₂	Human	3
Muscarinic M ₃	Human	-12
Neuropeptide Y Y ₁	Human	6
Neuropeptide Y Y ₂	Human	-3
Nicotinic Acetylcholine	Human	-23
Nicotinic Acetylcholine α 1, Bungarotoxin	Human	7
Opiate δ ₁ (OP1, DOP)	Human	3
Opiate κ (OP2, KOP)	Human	8
Opiate μ (OP3, MOP)	Human	-2
Phorbol Ester	Mouse	-3
Platelet Activating Factor (PAF)	Human	20
Potassium Channel [K _{ATP}]	Hamster	-4
Potassium Channel hERG	Human	20
Prostanoid EP ₄	Human	4
Purinergic P2X	Rabbit	9
Purinergic P2Y	Rat	1
Rolipram	Rat	-7
Serotonin (5-Hydroxytryptamine) 5-HT _{1A}	Human	-2
Serotonin (5-Hydroxytryptamine) 5-HT _{2B}	Human	19
Serotonin (5-Hydroxytryptamine) 5-HT ₃	Human	3
Sigma σ ₁	Human	4
Sodium Channel, Site 2	Rat	15
Tachykinin NK ₁	Human	14
Thyroid Hormone	Rat	2
Transporter, Dopamine (DAT)	Human	34
Transporter, Dopamine (GABA)	Rat	66
Transporter, Norepinephrine (NET)	Human	20
Transporter, Serotonin (5-Hydroxytryptamine) (SERT)	Human	-3

Gratifyingly, compound **2.6** demonstrated significant binding (>50%) at only one target, the GABA transporter, which was bound at 66%. With these data, we were more confident to begin *in vivo* proof-of concept studies.

Effect of VU0650991 on oral glucose tolerance

With the knowledge that we had developed the first known selective, CNS-penetrant and orally bioavailable GLP-1R small molecule antagonist, compound **2.6**, we sought to determine if the compound had any efficacy *in vivo* at reducing the amount of insulin secreted postprandially. We employed an oral glucose tolerance test for this experiment, a method well established in rodents, as well as humans. In humans, this medical test is most often used to diagnose prediabetes and diabetes, as well as gestational diabetes. Subjects are administered a standard dose of glucose by mouth and blood levels are checked over time to determine how quickly glucose is cleared from the blood stream. For our purposes, fasted male Sprague-Dawley rats were administered a 10 mg/kg dose of compound **2.6** or vehicle via oral gavage 30 minutes prior to a standard glucose challenge of 2 g/kg or vehicle. Blood samples were taken from the carotid artery at 2, 5, 10, 15, 30, 45, 60, 90, 120, and 150 minutes post challenge with whole blood glucose measured by a glucometer and plasma insulin measured by a standard hormone assay. To our delight, **2.6** showed significant efficacy at both increasing blood glucose over the study time, as well as decreasing the overall insulin secreted (Figure **2.9**).

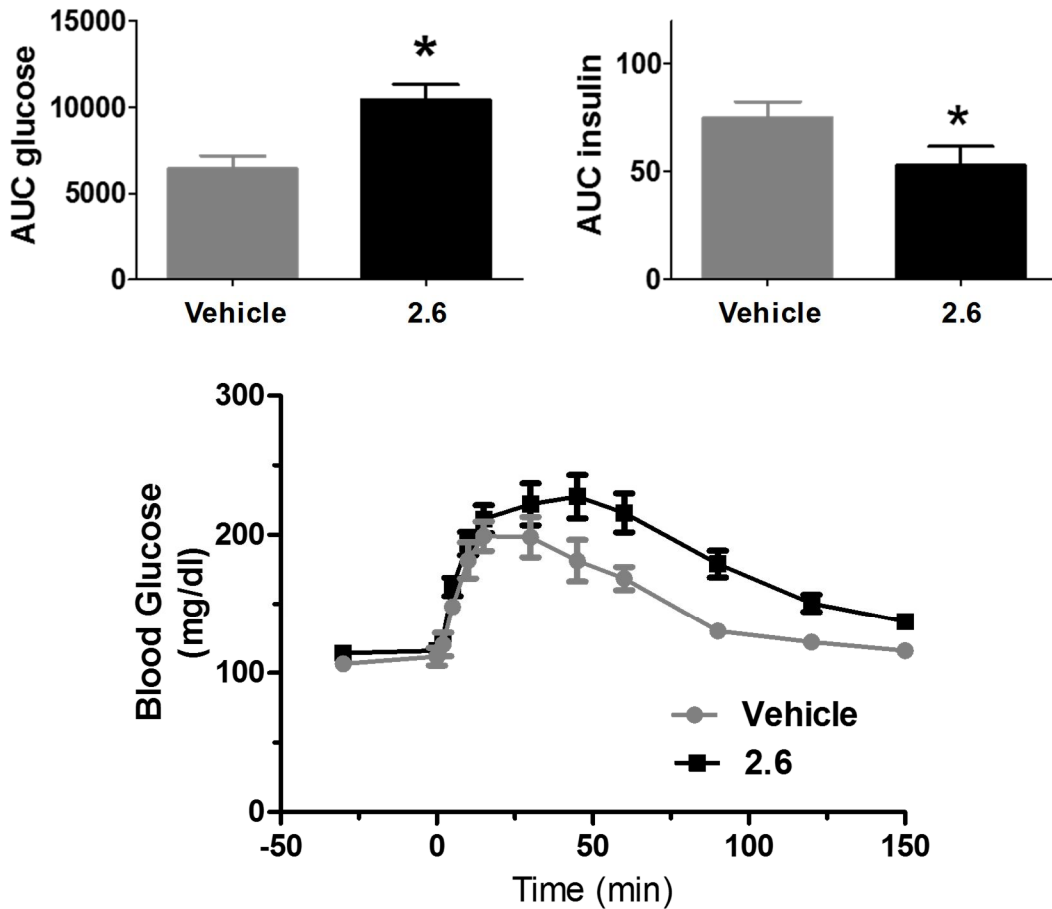


Figure 2.9: Effect of 2.6 on whole blood glucose and insulin levels in rats upon oral dosing at 10 mg/kg. Rats with carotid cannulae surgically implanted were randomized to receive 2.6 or vehicle 30 min prior to glucose dose (2 g/kg) given by gavage at time 0. Carotid blood samples were obtained at given intervals to assess whole blood glucose and insulin. Rats were crossed over to other treatment 7 days later and restudied. Area under the curve (AUC) was calculated for glucose and insulin excursion, and the mean values were compared by Student's t test: (*) $p < 0.05$. Glucose excursions were assessed by two-way ANOVA, $p < 0.0001$ for drug interaction, (*) Bonferroni post-test $p < 0.01$ at these time points. Surgery and OGTT experiments were conducted by the Vanderbilt University Medical Center Rat Metabolic Physiology Core.

Summary and future directions

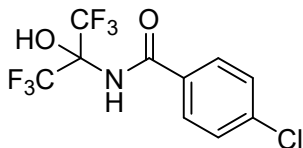
In summary, we discovered what we believed to be a novel GLP-1 agonist through an HTS campaign, which gave rise to a new series of this class of compounds. However, subsequent pharmacological studies lead to the reclassification of the compounds as GLP-1R antagonists. Two compounds, **2.6** (VU0650991) and **2.14** (VU0650973) were an improvement on the original hit compound, **2.4** (VU0138721) both providing a nearly 10-fold increase in potency. Further pharmacological studies determined both compounds to be non-competitive antagonist devoid of probe dependency with GLP-1 or EX-4. DMPK studies provided the first differentiation between these two lead compounds. Both possessed a good profile with low clearance; however, in *in vivo* DMPK studies **2.6** was both brain penetrant and orally bioavailable, where **2.14** was not. We examined the off-target effects of **2.6** in an ancillary pharmacology screen and only found 1 instance of significant binding out of 68 targets. Finding few liabilities, we then subjected **2.6** to an *in vivo* OGTT and found efficacy in both lowering insulin secretion as well as increasing blood glucose. In conclusion, we have developed the first known CNS-penetrant, orally-bioavailable small molecule GLP-1 antagonist with *in vivo* efficacy. We look forward to performing future studies with regards to the GLP-1 antagonist indications of chronic stress and CHI.

Experimental methods

General synthetic methods and instrumentation

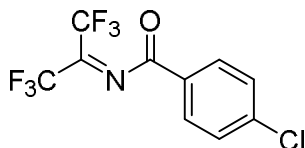
All reactions were carried out employing standard chemical techniques under inert atmosphere. Solvents used for extraction, washing, and chromatography were HPLC grade. Unless otherwise noted, all reagents were purchased from Sigma-Aldrich Chemical Co. and were used without further purification. Analytical thin layer chromatography was performed on 250 μm silica gel plates from Sorbent Technologies. Analytical HPLC was performed on an Agilent 1200 LCMS with UV detection at 215 nm and 254 nm along with ELSD detection and electrospray ionization, with all final compounds showing > 95% purity and a parent mass ion consistent with the desired structure. All NMR spectra were recorded on a 400 MHz Brüker AV-400 instrument. ^1H chemical shifts are reported as δ values in ppm relative to the residual solvent peak (MeOD = 3.31, CDCl_3 = 7.26, DMSO). Data are reported as follows: chemical shift, multiplicity (br = broad, s = singlet, d = doublet, t = triplet, q = quartet, quint = quintet, m = multiplet), coupling constant (Hz), and integration. ^{13}C chemical shifts are reported as δ values in ppm relative to the residual solvent peak (MeOD = 49.0, CDCl_3 = 77.16). Low resolution mass spectra were obtained on an Agilent 1200 LCMS with electrospray ionization. High resolution mass spectra were recorded on a Waters QToF-API-US plus Acquity system with electrospray ionization. Automated flash column chromatography was performed on a Teledyne ISCO Combiflash Rf system. Preparative purification of library compounds was performed

on a Gilson chromatograph using a Luna 5u C18 (2) 100A AXIA column (30 x 50 mm) using a water/acetonitrile gradient.

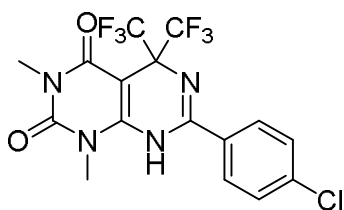


4-chloro-*N*-(1,1,1,3,3,3-hexafluoro-2-hydroxypropan-2-yl)benzamide (2.41a).

To an oven-dried three-necked round-bottom flask was added at room temperature 4-chlorobenzamide (311 mg, 2.0 mmol) and DCM (5 mL). To one neck of the flask was added a cold-finger with dry ice/isopropanol, the second neck was sealed with a septum, and the last neck was attached to a lecture bottle of hexafluoroacetone. The reaction was heated to 30 °C with stirring, at which point hexafluoroacetone was bubbled into the mixture until a vigorous reflux of the gas was observed. The resultant mixture was stirred 3 hours until reaction completion was confirmed by LC/MS. Upon completion, the reaction was purged with air to remove excess hexafluoroacetone, and concentrated *in vacuo* without heating to afford the desired product as a white solid (635 mg, 99%). ¹H NMR (400 MHz, CDCl₃) δ (ppm): 8.84 (br, 1H), 7.60 (d, *J* = 8.4 Hz, 2H), 7.39 (d, *J* = 8.4 Hz, 2H), 7.14 (s, 1H); ¹³C NMR (100.6 MHz, CDCl₃) δ (ppm): 171.99, 140.45, 130.24, 129.47, 128.63, 121.11 (q, ¹*J*_{C-F} = 288.9 Hz), 84.41 (sep, ²*J*_{C-F} = 33.0 Hz); LRMS (ES⁺) found for C₁₀H₆ClF₆NO₂ (M+H), 322.1.

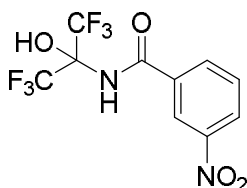


4-chloro-N-(perfluoropropan-2-ylidene)benzamide (2.42a). To a round-bottom flask was added at room temperature **2.41a** (635 mg, 1.97 mmol), which was dissolved in ether (10 mL). This was cooled with stirring to 0 °C before adding trifluoroacetic anhydride (282 μ L, 2.0 mmol) and pyridine (338 μ L, 4.2 mmol) dropwise simultaneously. The resultant mixture was slowly warmed to room temperature with stirring over 2 hours and reaction completion was verified by LC/MS. Upon completion, the reaction mixture was diluted with ether (20 mL), filtered to remove organic salts, and concentrated *in vacuo* without heating to afford the desired product as a colorless oil (580 mg, 97%). ^1H NMR (400 MHz, CDCl_3) δ (ppm): 7.70 (d, $J = 8.7$ Hz, 2H), 7.44 (d, $J = 8.7$ Hz, 2H); ^{13}C NMR (100.6 MHz, CDCl_3) δ (ppm): 171.65, 162.83 (d, $^2J_{\text{C-F}} = 36.8$ Hz), 140.27, 130.33, 129.43, 128.86, 121.11 (q, $^1J_{\text{C-F}} = 289.5$ Hz); LRMS (ES+) found for $\text{C}_{10}\text{H}_4\text{ClF}_6\text{NO}$ (M+1+MeOH), 336.0.



7-(4-chlorophenyl)-1,3-dimethyl-5,5-bis(trifluoromethyl)-5,8-dihydropyrimido[4,5-*d*]pyrimidine-2,4(1*H*,3*H*)-dione (2.6). To a vial was added at room temperature **2.42a** (580 mg, 1.91 mmol), 6-amino-1,3-dimethylpyrimidine-2,4(1*H*,3*H*)-dione (235 mg, 1.91 mmol), and triethylamine (39 μ L, 0.29 mmol), which was then dissolved in *N,N*-Dimethylformamide (2 mL). this mixture was heated to

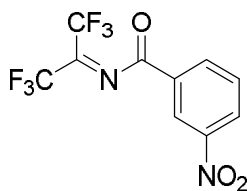
100 °C with stirring for 3 hours. Upon completion by LC/MS, the reaction mixture was diluted with 1:1 water/DCM (20 mL) and extracted three times with DCM (5 mL). The combined organic layers were washed twice with a 5% LiCl solution (10 mL), passed through a phase separator to dry, and concentrated *in vacuo*. The brown residue was purified by automated flash chromatography using 40-70% ethyl acetate in hexanes to elute. Desired product was afforded as a pale yellow solid (202 mg, 24%). ¹H NMR (400 MHz, CDCl₃) δ (ppm): 7.83 (d, *J* = 8.7 Hz, 2H), 7.54 (d, *J* = 8.7 Hz, 2H), 6.70 (s, 1H), 3.65 (s, 3H), 3.37 (s, 3H); ¹³C NMR (100.6 MHz, CDCl₃) δ (ppm): 159.60, 157.76, 153.32, 151.52, 140.55, 129.87, 129.80, 128.76, 122.51 (q, ¹*J*_{C-F} = 290.2 Hz), 80.96, 65.67-65.03 (m), 30.49, 28.41; HRMS (TOF, ES⁺) calc'd for C₁₆H₁₁ClF₆N₄O₂ (M+1), 440.0477; found, 440.0475.



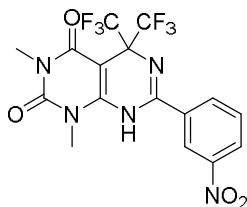
***N*-(1,1,1,3,3,3-hexafluoro-2-hydroxypropan-2-yl)-3-nitrobenzamide (2.41b).**

To an oven-dried three-necked round-bottom flask was added at room temperature 3-nitrobenzamide (332 mg, 2.0 mmol) and DCM (5 mL). To one neck of the flask was added a cold-finger with dry ice/isopropanol, the second neck was sealed with a septum, and the last neck was attached to a lecture bottle of hexafluoroacetone. The reaction was heated to 30 °C with stirring, at which point hexafluoroacetone was bubbled into the mixture until a vigorous reflux of the gas was observed. The resultant mixture was stirred 3 hours until reaction completion was confirmed by LC/MS. Upon completion, the reaction was purged with air to remove excess

hexafluoroacetone, and concentrated *in vacuo* without heating to afford the desired product as a white solid (658 mg, 99%). ¹H NMR (400 MHz, (CD₃)₂SO) δ (ppm) 9.93 (s, 1H), 9.34 (s, 1H), 8.63 (s, 1H), 8.44 (d, *J* = 8.2 Hz, 1H), 8.23 (d, *J* = 7.7 Hz, 1H), 7.80 (t, *J* = 8.0 Hz, 1H); ¹³C NMR (100.6 MHz, (CD₃)₂SO) δ (ppm): 166.74, 147.55, 134.99, 134.69, 130.13, 126.80, 123.09, 121.55 (q, ¹*J*_{C-F} = 289.7 Hz), 83.35 (q, ²*J*_{C-F} = 32.7 Hz); LRMS (ES+) found for C₁₀H₆F₆N₂O₄ (M+1), 332.1.



3-nitro-*N*-(perfluoropropan-2-ylidene)benzamide (2.42b). To a round-bottom flask was added at room temperature **2.41b** (622 mg, 1.98 mmol), which was dissolved in ether (10 mL). This was cooled with stirring to 0 °C before adding trifluoroacetic anhydride (282 μL, 2.0 mmol) and pyridine (338 μL, 4.2 mmol) dropwise simultaneously. The resultant mixture was slowly warmed to room temperature over 2 hours and reaction completion was verified by LC/MS. Upon completion, the reaction mixture was diluted with ether (20 mL), filtered to remove organic salts, and concentrated *in vacuo* without heating to afford the desired product as a colorless oil (610 mg, 98%). ¹H NMR (400 MHz, (CD₃)₂SO) δ (ppm) 8.60 (s, 1H), 8.43 (d, *J* = 8.3 Hz, 1H), 8.23 (d, *J* = 7.9 Hz, 1H), 7.79 (t, *J* = 8.0 Hz, 1H); ¹³C NMR (100.6 MHz, (CD₃)₂SO) δ (ppm): 166.40, 159.18 (d, ²*J*_{C-F} = 31.5 Hz), 147.52, 135.01, 134.65, 130.17, 126.79, 123.04, 121.56, (q, ¹*J*_{C-F} = 291.5 Hz); LRMS (ES+) found for C₁₀H₄F₆N₂O₃ (M+1+MeOH), 347.0.



1,3-dimethyl-7-(3-nitrophenyl)-5,5-bis(trifluoromethyl)-5,8-

dihydropyrimido[4,5-*d*]pyrimidine-2,4(1*H*,3*H*)-dione (2.14). To a vial was added

at room temperature **9c** (610 mg, 1.94 mmol), **10** (243 mg, 1.94 mmol), and

triethylamine (39 μ L, 0.29 mmol), which was then dissolved in *N,N*-

Dimethylformamide (2 mL). this mixture was heated to 100 $^{\circ}$ C with stirring for 3

hours. Upon completion by LC/MS, the reaction mixture was diluted with 1:1

water/ CH_2Cl_2 (20 mL) and extracted three times with CH_2Cl_2 (5 mL). The combined

organic layers were washed twice with a 5% LiCl solution (10 mL), passed through a

phase separator to dry, and concentrated *in vacuo*. The brown residue purified by

automated flash chromatography using 40-70% ethyl acetate in hexanes to elute.

Desired product was afforded as a pale-yellow solid (236 mg, 27%). ^1H NMR (400

MHz, CD_3OD) δ (ppm): 8.72 (t, $J=1.96$ 1H); 8.52-8.49 (m, 1H); 8.31-8.29 (m, 1H); 7.81

(t, $J = 8.04$, 1H); 3.62 (s, 3H); 3.33, (s, 3H); ^{13}C NMR (100.6 MHz, CD_3OD) δ (ppm) :

161.60, 161.52, 155.08, 153.01, 149.69, 135.59, 135.44, 131.38, 128.30, 124.58,

124.18 (q, $^1J_{\text{C-F}} = 291.7$ Hz) 81.63, 30.85, 28.70; HRMS (TOF, ES+) calc'd for

$\text{C}_{16}\text{H}_{11}\text{F}_6\text{N}_5\text{O}_4$ ($\text{M}+1$), 451.0715; found, 451.0716.

Sections of this chapter have been reprinted with permission from the following:

Discovery of a novel series of orally bioavailable and CNS penetrant Glucagon-like Peptide-1 receptor (GLP-1R) noncompetitive antagonists based on a 1,3-Disubstituted-7-aryl-5,5-bis(trifluoromethyl)-5,8-dihydropyrimido[4,5-*d*]pyrimidine-2,4(1*H*,3*H*)-dione Core. Kellie D. Nance, Emily L. Days, C. David Weaver, Anastasia Coldren, Tiffany D. Farmer, Hyekyung P. Cho, Colleen M. Niswender, Anna L. Blobaum, Kevin D. Niswender, and Craig W. Lindsley. *Journal of Medicinal Chemistry* **2017** 60 (4), 1611-1616. DOI: 10.1021/acs.jmedchem.6b01706. Copyright © 2017 American Chemical Society

CHAPTER 3

PROGRESS TOWARD THE TOTAL SYNTHESIS OF MELEARORIDE A

Introduction

Terrestrial and marine natural product discovery and medicinal uses

Terrestrial and marine flora and fauna have provided a plethora of novel and interesting organic molecules with the potential for medicinal uses, back to time immemorial^[158]. Complex mixtures of plant materials have been used as traditional medicines for millennia, the deconvoluted extracts of which can still be found in modern medicine: salicylic acid from willow tree bark^[159], and the opioids morphine, paramorphine, and codeine from *Papaver somniferum*,^[160] for example. Many of these molecules are produced as secondary metabolites and act as social signaling molecules within a given colony, communication molecules within symbiotic partnerships, and weapons against other biota that pose a threat^[161]; the latter of these provides a hypothesis as to why many of these molecules have antibiotic, antifungal, and cytotoxic effects. Study of these molecules can be traced back to the 18th century, when French nobleman Antoine Lavoisier wrote *Traité Élémentaire de Chimie*, explaining that elements are the building blocks from which all molecules are formed, and began applying this concept to the isolation of plant materials^[162]. In 1804, German pharmacist and chemist Friedrich Sertürner discovered morphine, the first plant alkaloid ever isolated, from the mixture known as opium latex^[163]. Later, chemist Charles Romley Alder Wright took morphine, which at the time in 1874 had

already developed a reputation of being addictive, and boiled it in acetic anhydride with the hopes of producing a less addictive form of the drug^[164]. The resultant compound, diamorphine, or heroin as it is better known today, became the first known natural product analog. Since then, plant and microbiotic natural products have been isolated and derivatized rapidly, and while natural product drug discovery was cast aside in favor of small molecule high-throughput screening in the late 20th and early 21st centuries, it has since experienced a significant renaissance^[165]. Through these efforts, many compounds or close derivatives have been discovered as useful therapeutics for common maladies (**Figure 3.1**)^[166-171].

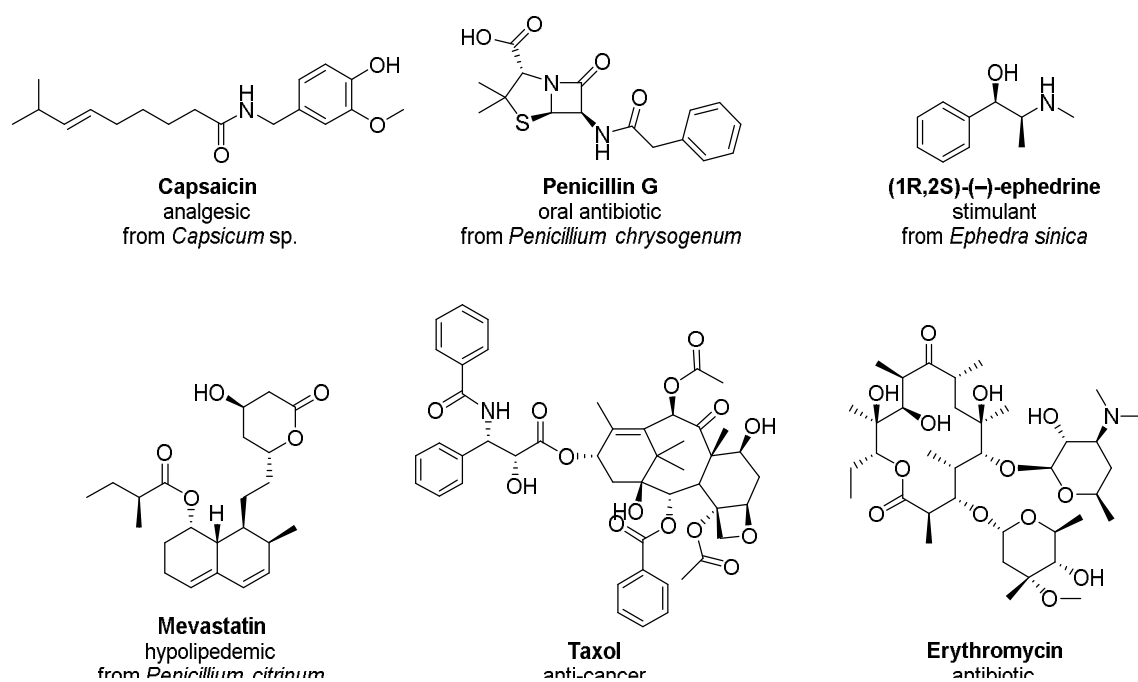


Figure 3.1: Structures, indications, and origins of well-known medicinal natural products

As many terrestrial sources of natural products have been exhausted over the past 200 years, efforts have turned to toward discovering new sources from the

ocean^[172]. Marine sponges, fungi, and animals have proven to be a vast source of new and often potent toxins that are efficacious against virulent terrestrial bacteria and fungi. One of the most well-known, bryotoxin 1, is a macrolide natural product isolated from the aquatic invertebrate *Bugula neritina* which has been studied clinically for its anti-cancer and antiviral properties^[173-175]. Another marine natural product, spongouridine from the Caribbean Sea sponge *Tethya crypta*^[176], gave rise to the anti-viral agent azidothymidine, a groundbreaking treatment for HIV/AIDs^[177]. The search for physiologically relevant marine natural products may prove more fruitful than that of their terrestrial counterparts, as a screen of marine samples looking for cytotoxicity, carried out by the National Cancer Institute, found a hit rate of approximately 1% versus 0.1% for terrestrial samples^[178]. Marine natural products have already provided, either directly or through derivatization, three FDA-approved drugs^[179], and with others in clinical trials, it is likely there will be more to come.

*Natural products from marine *Penicillium* sp.*

Two novel anti-fungal 13-membered macrolide natural products, designated PF1163A (**3.1**) and PF1163B (**3.2**) (Figure 3.2), were first isolated from a fungal broth by Nose and coworkers in 1999^[180]. Though these researchers taxonomically determined the fungus to be of the genus of *Penicillium*, they did not determine the exact species and instead designated it *Penicillium* sp. PF1163. Both compounds proved efficacious at inhibiting ergosterol biosynthesis, a known resistance pathway for azole-resistant *C. albicans* fungal infections^[181]. These products were isolated

again from the marine fungus *Penicillium meleagrinum* var. *viridiflavum* by Okabe and coworkers in 2016, along with other known PF1163 analogs PF1163D (**3.3**), PF1163H (**3.4**), and PF1163F (**3.5**), as well as two previously undiscovered macrolides, melearoride A (**3.6**) and melearoride B (**3.7**) (**Figure 3.2**)^[182]. These new

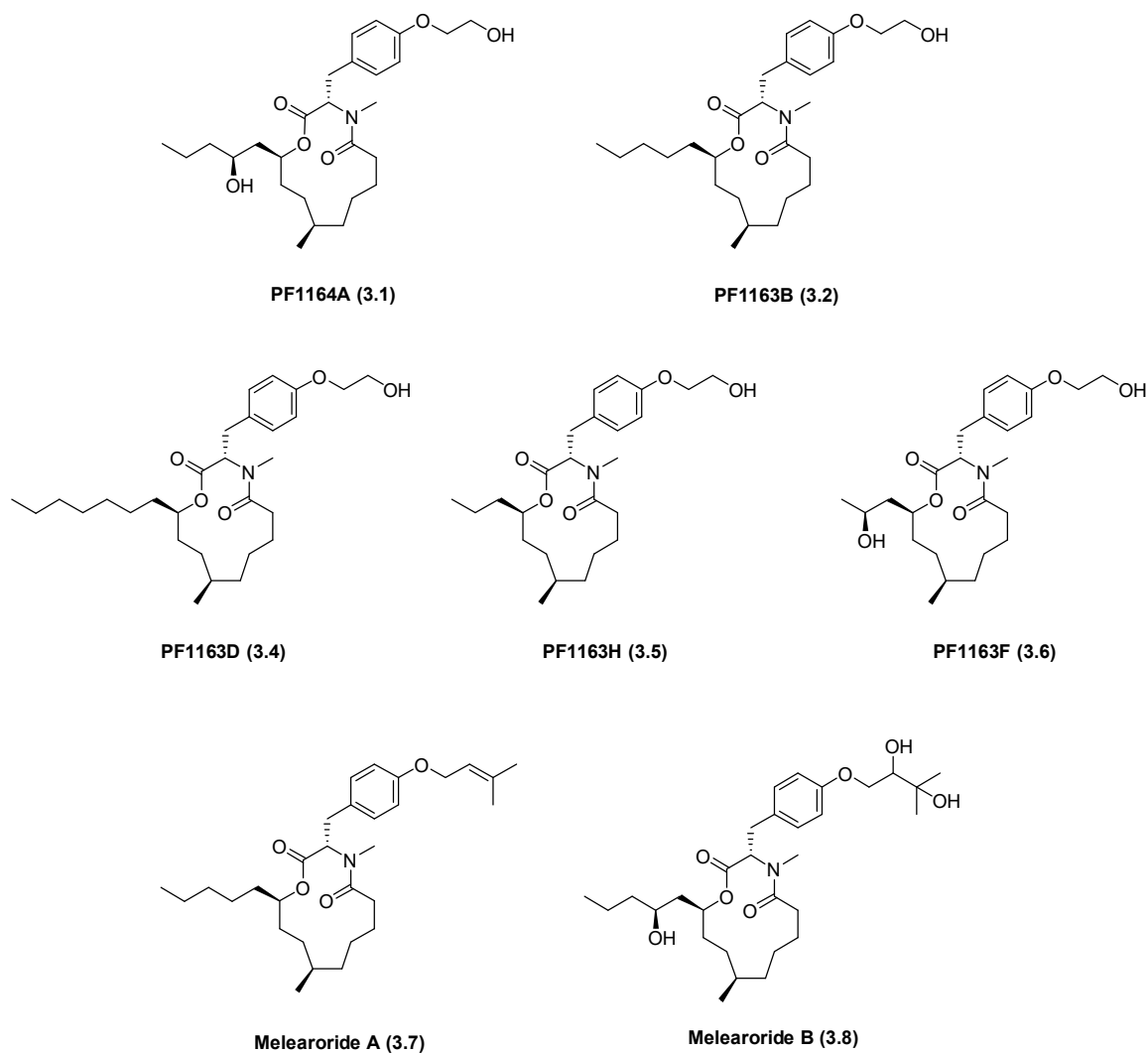


Figure 3.2: Structures of related marine macrolide natural products isolated from *Penicillium meleagrinum* var. *viridiflavum* by Okabe and coworkers in 2016

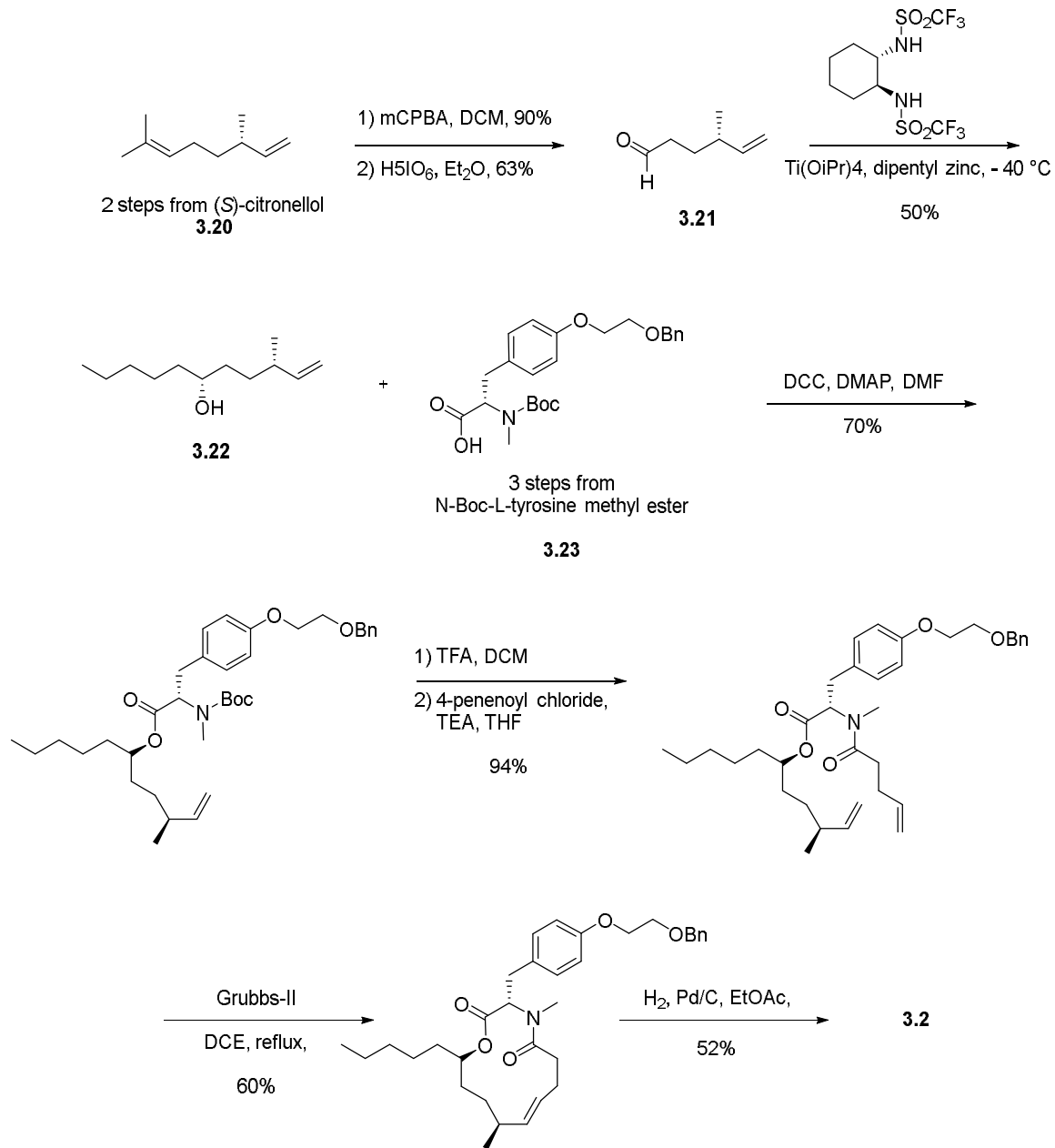
compounds, while possessing a similar core structure of L-tyrosine linked into a 13-membered macrocycle, were structurally distinct. All seven compounds were subjected to assay against azole-resistant *C. albicans* J2-36, and both **3.1** and **3.2** were similarly efficacious as before, with a minimum inhibitory concentration (MIC) of 1 µg/mL and 2 µg/mL respectively. Surprisingly, while both **3.6** and **3.7** displayed no activity against the fungus alone, they did show synergistic effects with azole-antifungal fluconazole; however, due to the small quantity of compound isolated, further mechanistic studies have not been performed. Deep-seated fungal infections pose a threat to many immunocompromised patients clinically^[183], and with the increase in azole-resistant strains, it is imperative to develop new anti-fungal agents. Therefore, we initiated the total synthesis of melearoride A, envisioning a modular synthesis that would allow for the quick production of analogs and terminating with enough material for screening against multiple fungal and bacterial targets.

Total syntheses of PF1163B

While no synthesis of melearoride A has been completed to this date, two groups have published total syntheses of PF1163B (**3.2**). This compound is structurally similar to melearoride A, with the only variation arising at the phenol headpiece. The first synthesis, performed by Tatsuta and coworkers in 1999^[184], used the logical disconnections of amide and ester linkages at the tyrosine moiety (**Scheme 3.1**). To link this amino acid macrocycle, a method was devised to arrive at alcohol

formation. These researchers began with commercially available (*R*)-citronellol, which underwent ozonolysis and Wittig olefination to arrive at ester **3.9**. This then underwent olefin reduction and alcohol oxidation to afford aldehyde **3.10**, which was subsequently homologated to provide aldehyde **3.11**. This compound was then subjected to diastereoselective Grignard conditions to provide **3.12** with 6:1 dr for the desired diastereomer and 72% yield. Protection of the resultant alcohol **3.13** was required to preserve yield during ozonolysis, and the protected alcohol was subjected to ozonolysis to provide aldehyde **3.14**. Wittig olefination and subsequent hydrogenation gave deprotected alcohol **3.15** in 69% yield. With alcohol in hand, they began attachment to tyrosine **3.16**, which was synthesized in 3 steps from Boc-L-tyrosine. Esterification via formation of mixed anhydride provided **3.17**, which was subjected to a one step Boc and *tert*-butyl ester deprotection then Bop-Cl-mediated amide synthesis to provide PF1163B in 6% yield, with the longest linear sequence being 15 steps. While many steps of this synthesis proceeded with moderate to good yields, it suffers from several redox steps, and is not amenable to quick analog synthesis.

In 2003, following the first synthesis of **3.2**, Bouazza and coworkers developed a shorter and more convergent synthesis with the key step reliant on successful ring-closing metathesis of the tyrosine macrocycle (**Scheme 3.2**)^[185]. In order to do this, these researchers divided the molecule into 3 synthons: chiral olefinic alcohol **3.22**, modified tyrosine **3.23**, and commercially available 4-pentenoyl chloride. To begin, (*S*)-citronellene was synthesized from commercially available (*S*)-citronellol in two steps, and the diene was subjected to epoxidation and oxidative cleavage to give



Scheme 3.2: Second total synthesis of related compound PF1163B described by Bouazza and coworker in 2003

aldehyde **3.21**. Diastereoselective addition of dipentylzinc to this aldehyde gave alcohol **3.22** in 50% yield with 98% ee. With the most difficult synthon in hand, the researchers proceeded with production of the tyrosine synthon and esterification of the two. Tyrosine **3.23** was produced in 3 steps from commercially available *N*-Boc-L-tyrosine methyl ester, and subsequent Steglich esterification of this with alcohol **3.22** provided **3.24** in 70% yield. Boc deprotection of this intermediate with subsequent acyl chloride-mediated amide formation provided the RCM-precursor **3.25** in 94% yield across two steps. Standard RCM conditions with Grubbs 2nd generation catalyst in refluxing DCE provided olefin **3.26** in 60% yield as a mixture of E/Z isomers, which were subjected to hydrogenation to arrive at final product PF1163B in 5.8% yield from the longest linear sequence of 10 steps. This synthesis, while shorter, more flexible, and more convergent than the first suffers slightly from a reliance on (*S*)-citronellol as a precursor, which may make analog synthesis slower. Taking lessons from both these syntheses, we envisioned a fully modular total synthesis of melearoride A that could allow for substitution of different amino acids, expansions and contractions of ring size, and modification of alkyl chain length.

Progress in the synthesis of Melearoride A

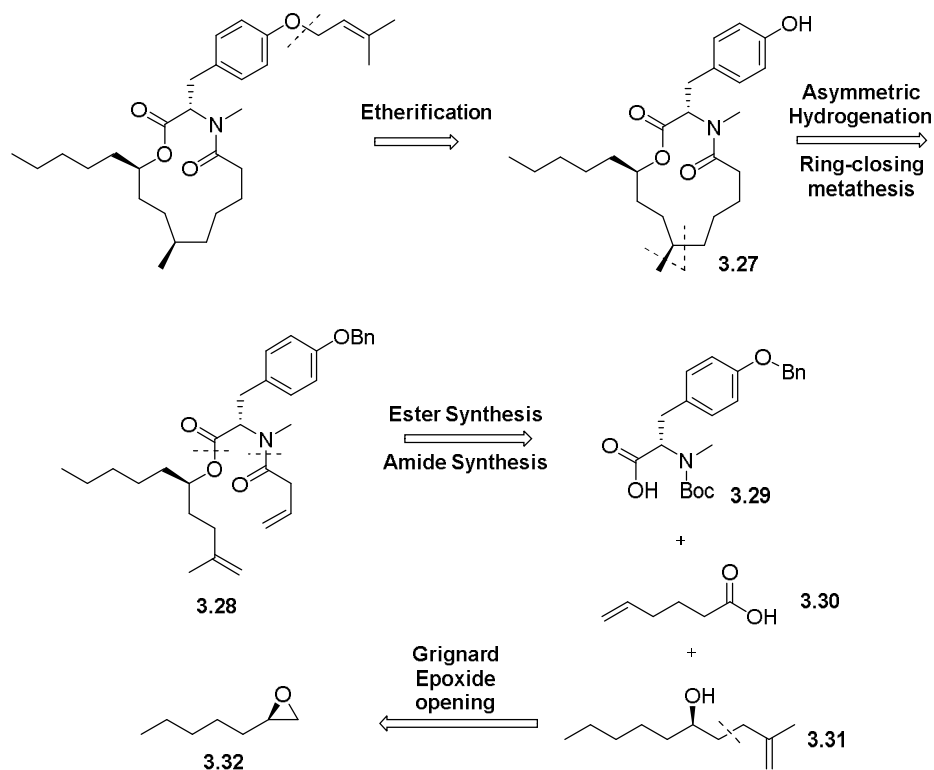
Retrosynthetic analysis of Melearoride A

In studying the prior syntheses of related macrolide PF1163B, we believed incorporating RCM into our synthetic strategy would provide the flexibility we desired for rapid analog synthesis (**Scheme 3.3**). We decided to incorporate this into our retrosynthetic analysis, however, we knew the dimethyl allyl phenol headpiece would not survive the necessary reduction following RCM, and would need to be installed last. We envisioned incorporating this functionality with an aryl etherification. Deprotection of a benzyl-protected phenol could be carried out in concert with hydrogenation of the metathesis product. We believed an asymmetric hydrogenation would be useful for setting the stereochemistry of the chiral methyl found in compound **3.27**. Cleavage of the macrocycle alpha to this methyl provided intermediate **3.28**, which could be derived from sequential amide and ester formations. From this we derived our 3 major synthons: commercially available *N*-methyl-*O*-benzyl-*L*-tyrosine **3.29**, commercially available 5-hexenoic acid **3.30**. And

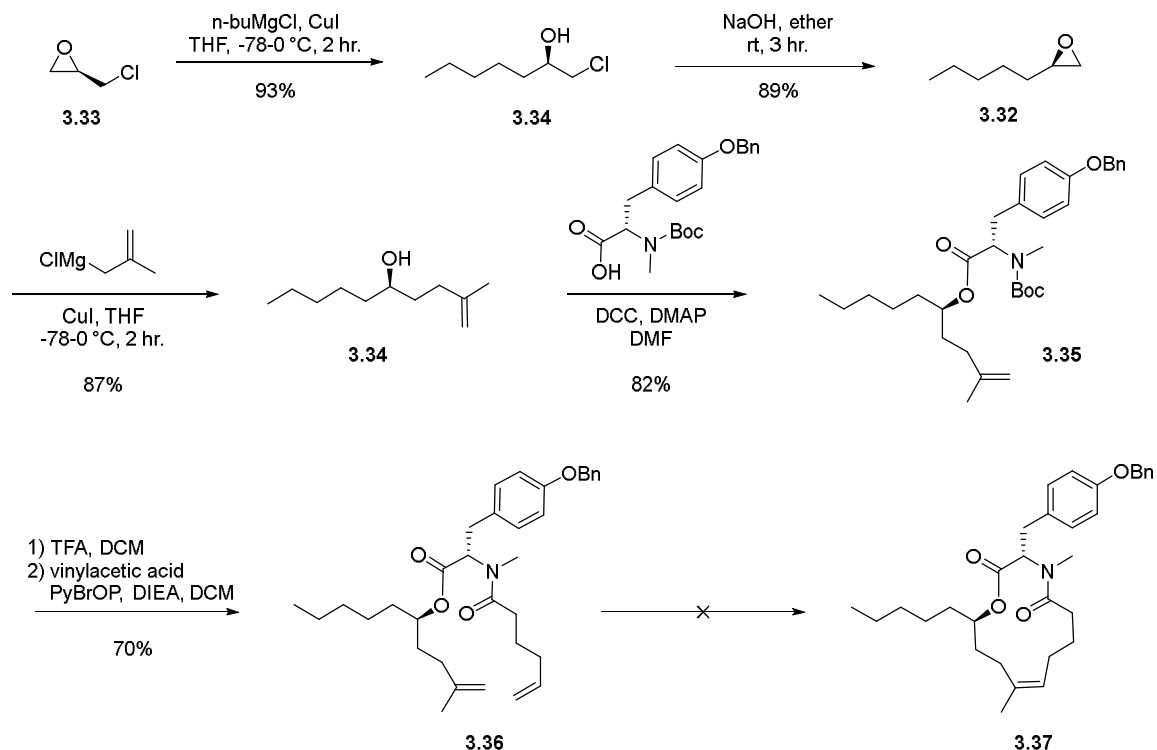
chiral alcohol **3.31**, which we believed could be derived from the Grignard-mediated epoxide opening of **3.32**.

First attempt at the synthesis of Melearoride A

With retrosynthetic analysis in hand, we set about our enacting our plans (**Scheme 3.4**). Ring opening of (*R*)-epichlorohydrin with *n*-butylmagnesium chloride in the presence of catalytic copper (I) iodide gave chlorohydrin **3.34** in excellent yield. This was subjected to basic epoxide closure conditions to arrive at the desired (*R*)-epoxyheptane. A second ring opening of this epoxide with 2-methylallylmagnesium chloride gave our first synthon, alcohol **3.34** in 87% yield. Combination of this with our second synthon **3.29** gave intermediate **3.35** in 82% yield. From there, Boc-



Scheme 3.3: Retrosynthetic analysis of melearoride A, using RCM to create macrocyclic linkage and asymmetric hydrogenation to set chiral methyl stereocenter.



Scheme 3.4: Synthetic route to melearoride A, using RCM to create macrocyclic linkage and asymmetric hydrogenation to set chiral methyl stereocenter.

deprotection and subsequent PyBrOP-mediated amide formation provided RCM-precursor **3.36** in 70% yield across two steps. We were excited to see the end so near, however, were disappointed that we were unable to effect closure of the macrolide as we had hoped. To troubleshoot this reaction, we examined four catalysts known to be useful for RCM, and investigated their efficacy with and without titanium isopropoxide as an additive, often necessary for chelation-prone starting materials. Unfortunately, we were unable to observe anything more than 13% conversion to product by LC/MS analysis of the reaction mixtures (**Table 3.1**). We hypothesized that the closure of this 13-member macrocycle, already a difficult size, was precluded by the incorporation of a di-substituted olefin at one coupling partner. At this result,

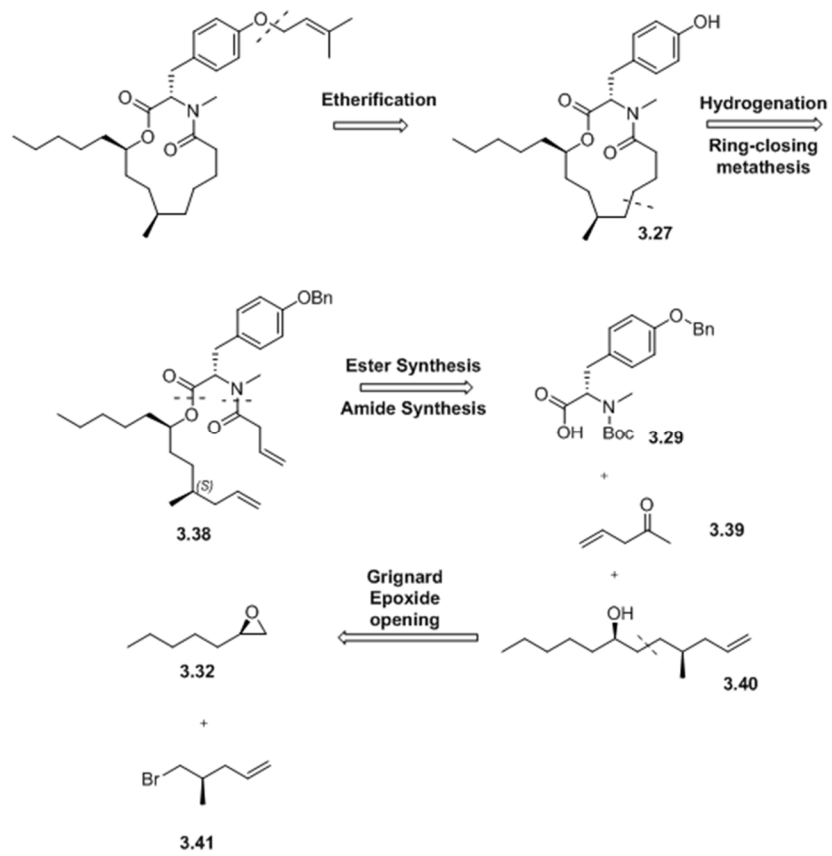
we revised our synthesis so that the RCM step involved 2 mono-substituted olefins instead.

Table 3.1: Catalysts and results of attempted ring-closing metathesis of **3.6**, Reactions were performed in refluxing DCM at a concentration of 5 mM. Reaction completion was determined by LC/MS analysis.

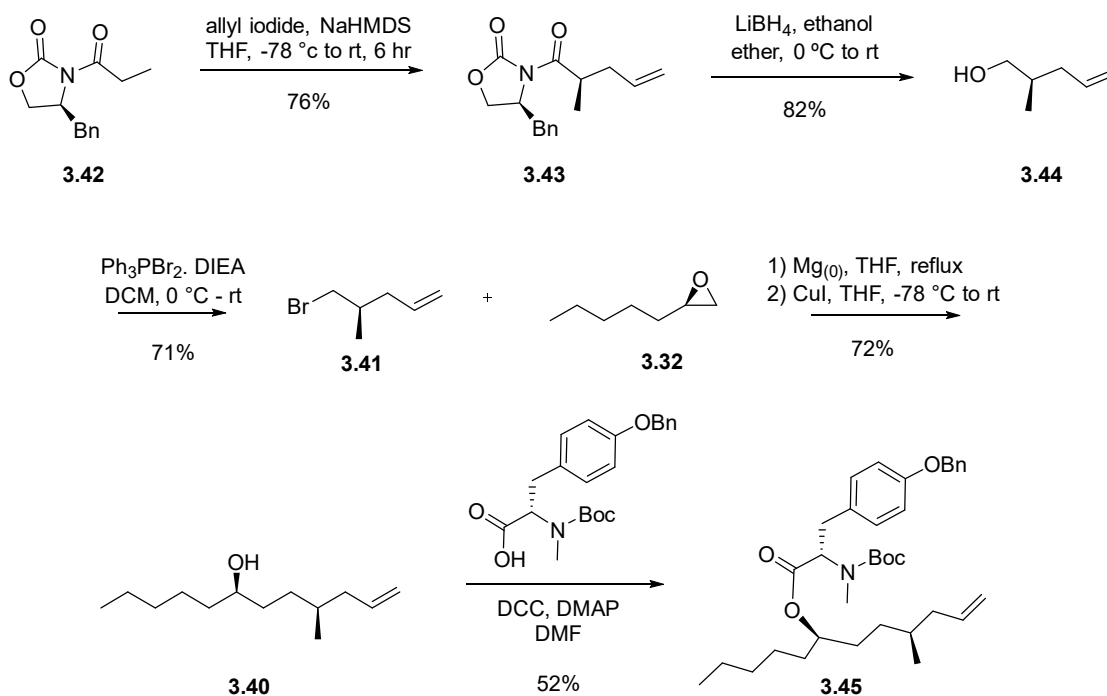
Catalyst (20 mol%)	10% Ti(iPrO)₄	Result
Grubbs 1 st Generation	-	N.R.
	+	N.R.
Grubbs 2 nd Generation	-	10% conversion
	+	13% conversion
Hoveyda-Grubbs 2 nd Generation	-	N.R.
	+	N.R.
Schrock's Catalyst	-	N.R.
	+	N.R.

Progress toward the second attempt at synthesis of Melearoride A

After the failure of our first synthetic route, we quickly developed a new route which would involve metathesis at a different position of the macrocycle (**Scheme 3.5**). By shifting this position two carbons over, we found we could install the chiral methyl in the first step, setting all stereocenters early into the synthesis (**Scheme 3.6**). To do this, we devised a method to arrive at Grignard precursor **3.41** using Evan's oxazolidinone alkylation^[186] and Appel bromination conditions. Treating



Scheme 3.5: Second retrosynthetic analysis of melearoride A, shifting bonds from RCM precursor to create macrocyclic linkage.

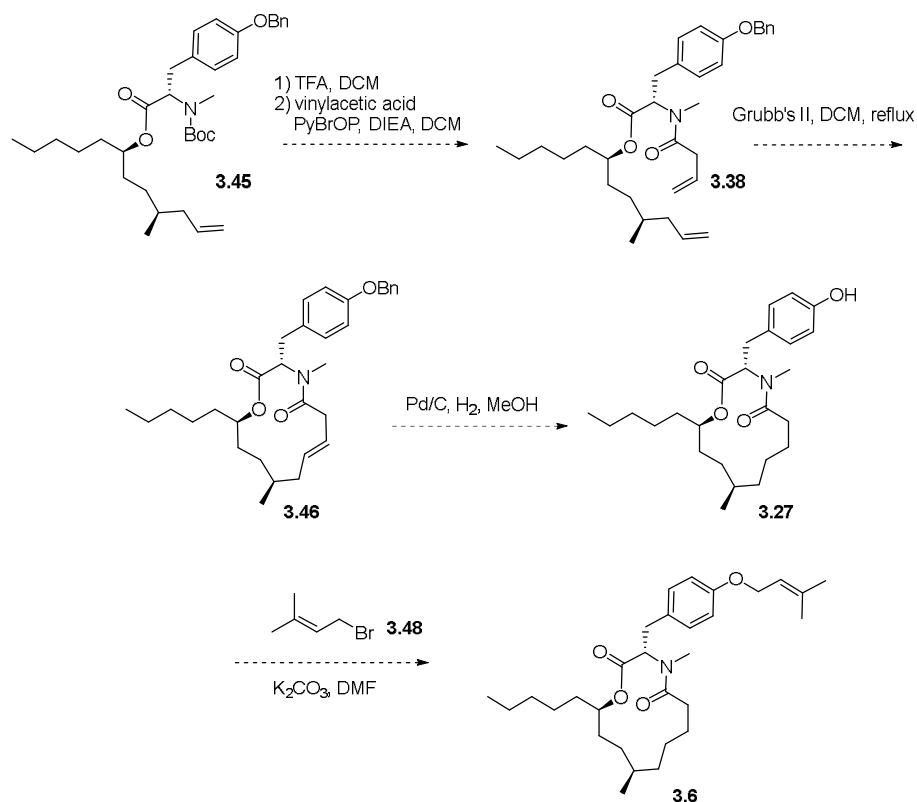


Scheme 3.6: Progress in the synthesis of melearide A up to intermediate **3.45**

oxazolidinone **3.42** with allyl iodide after deprotonation with NaHMDS at $-78\text{ }^\circ\text{C}$ provided **3.43** in 76% yield with $>20:1$ dr. Subsequent reduction to remove chiral auxiliary then gave chiral alcohol **3.44** in 82% yield. Appel bromination of this alcohol with triphenylphosphine dibromide at $0\text{ }^\circ\text{C}$ afforded bromide **3.41** in good yields. This reagent proved necessary to use rather than the standard conditions of triphenylphosphine with tetrabromomethane due to the inseparability of the bromide product from the bromoform byproduct. Next, the Grignard reagent formed by from this bromide was used to open epoxide **3.32**, affording alcohol **3.40** in 72% yield. Steglich esterification of this alcohol with tyrosine **3.29** provided intermediate **3.45** in moderate yield. This reaction will be optimized in the future, as the DCC

rearrangement byproduct was observed in nearly 1:1 ratio with product; an issue we hope to prevent with stoichiometric rather than catalytic DMAP addition.

Though we have been unable to complete the synthesis to this date, we hope to conclude it in the coming weeks. We believe we may do this quickly due to our



Scheme 3.7: Proposed completion of mearoride A synthesis from completed intermediate **3.45**

previous success up to the RCM in our first synthetic route and literature precedence (**Scheme 3.7**). We envision accomplishing this through the following route (Scheme). Boc-deprotection and subsequent PyBrOP-mediated amide formation of intermediate **3.45** will afford RCM precursor **3.46**. Due to the small amount of product found with Grubb's II previously, we hope to employ this catalyst to give **3.46**, which may then be hydrogenated to give phenol **3.27**. Aryl etherification will

provide the first total synthesis of melearoride A with the longest linear sequence being 10 steps.

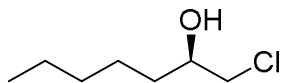
Summary and future directions

In conclusion, we have described progress toward the first total synthesis of melearoride A using a modular approach that may allow for rapid analog synthesis in the future. We envision completing this synthesis in the coming weeks, at which point we will further probe the biological activity of this compound. We would like to examine the synthetic material for any antibacterial, anti-fungal, or anti-cancer activity it may have. We would also like to confirm its activity against azole-resistant *C. albicans*, examining efficacy in tandem with the synthetic intermediates to determine which structures are necessary for activity. Hopefully, these efforts will prove fruitful, and lead to a better understanding of the biological activity of this compound and others like it.

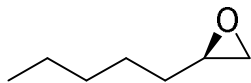
Experimental Methods

General

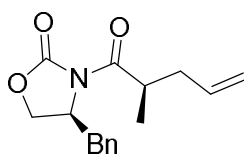
All reagents and solvents were commercial grade and purified prior to use when necessary. Thin layer chromatography (TLC) was performed on glass-backed silica gel. Visualization was accomplished with UV light and/or the use of iodine, KMnO_4 , or Seebach's solution followed by heat gun development. Chromatography on silica gel was performed using Teledyne ISCO pre-packed silica gel columns. ^1H and ^{13}C NMR spectra were recorded on Bruker DRX-400 (400 MHz) or Bruker AV-600 (600 MHz) instrument. Chemical shifts are reported in ppm relative to residual solvent peaks as an internal standard at the following chemical shifts (^1H and ^{13}C respectively): 7.26 and 77.0 ppm for CDCl_3 . Data are reported as follows: chemical shift, multiplicity (s = singlet, d = doublet, t = triplet, q = quartet, dd = doublet of doublets, br = broad, m = multiplet), coupling constant (Hz), integration. Optical rotations were measured on a JASCO P-2000 digital polarimeter. Concentration in g/100 ml and solvent are given in parentheses and the reported value is an average of $n=3$ independent measurements. Low resolution mass spectra (LCMS) were obtained on an Agilent 1200 LCMS with electrospray ionization.



(R)-1-chloroheptan-2-ol (3.34). To an oven-dried round bottom flask was added CuI (484 mg, 5.4 mmol), THF (54 mL) and (*R*)-epichlorohydrin (5 g, 54.0 mmol). This mixture was cooled to -78 °C before adding *n*-butylmagnesium chloride (9.5 g, 40.5 mL, 81.1 mmol) dropwise as a 2 M solution in THF. The resultant mixture was stirred 1 hour at -78 °C before warming to 0 °C and stirring for 2 hours. Reaction progression was monitored by TLC with Seebach staining to visualize. Upon completion, the reaction was quenched with aqueous NH₄Cl (250 mL) and 6 N HCl (25 mL) and stirred until a black film appeared between phases and both phases were clear. After this, the phases were separated, and the organic phase was washed 2x with aqueous saturated sodium thiosulfate (30 mL) and 1x with brine (30 mL), dried, and concentrated before purification by flash chromatography using 0-10% EtOAc in hexanes to elute. Pure fractions were pooled and concentrated in vacuo to afford product as a colorless liquid (7.5 g, 93% yield). ¹H NMR (400 MHz, CDCl₃) δ ppm): 3.78 (br, 1H), 3.61 (dd, *J* = 3.3, 11.1 Hz, 1H), 3.46 (dd, *J* = 7.1, 11.1 Hz, 1H), 2.34-2.29 (m, 1H), 1.56-1.40 (m, 3H), 1.38-1.22 (m, 5H), 0.88 (t, *J* = 6.7, 3H); ¹³C NMR (100.6 MHz, CDCl₃) δ (ppm): 51.9, 46.5, 32.2, 31.3, 25.3, 22.3, 13.6; Specific rotation $[\alpha]_D^{20} = -2.3^\circ$ (c = 1.0, MeOH).

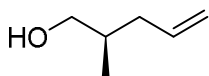


(R)-2-pentylloxirane (3.45). To a solution of **3.34** (5 g, 33.2 mmol) in THF (72 mL) was added NaOH (6.6 g, 166.0 mmol) as a finely ground powder. Reaction progression was monitored by TLC with Seebach staining to visualize. Upon completion, the reaction was poured into ice water (200 mL) and quickly extracted 3x with diethyl ether (50 mL). The organic phases were combined, dried over sodium sulfate, and concentrated. Purification was carried out by simple distillation (bp = 36 °C, 10 mm/Hg) to afford product as a colorless liquid (3.36 g, 89% yield). ¹H NMR (400 MHz, CDCl₃) δ ppm): 2.85-2.81 (m, 1H), 2.67 (t, *J* = 4.5 Hz, 1H), 2.39 (dd, *J* = 2.7, 5.0 Hz, 1H), 1.49-1.33 (m, 4H), 1.31-1.20 (m, 4H), 0.84 (t, *J* = 7.0 Hz, 3H); ¹³C NMR (100.6 MHz, CDCl₃) δ (ppm): 52.2, 47.0, 32.3, 31.5, 25.5, 22.5, 13.8; Specific rotation $[\alpha]_{D}^{20} = 11.9^{\circ}$ (*c* = 1.0, CHCl₃).



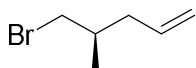
(S)-4-benzyl-3-((R)-2-methylpent-4-enoyl)oxazolidin-2-one (3.43). To an oven-dried round-bottom flask was added (*S*)-4-benzyl-3-propionyloxazolidin-2-one (22 g, 94.3 mmol, Combi-Blocks) and THF (267 mL). This solution was cooled to -78 °C before adding sodium bis(trimethylsilyl)amide (99 mL as 1M solution in THF, 99 mmol) and stirring at -78 °C for 2 hours. Allyl iodide (12.9 mL, 141.5 mmol) was then added and the resultant mixture was stirred an additional 4 hours at -78 °C. Reaction completion was verified by LC/MS at this point. Upon completion, the reaction was

quenched at -78 °C with aqueous saturated ammonium chloride and warmed slowly to room temperature. The organic phase was then separated, and the aqueous phase extracted 3x with diethyl ether (100 mL). The combined organic phases were dried and concentrated before purifying by flash chromatography using 0-30% EtOAc in hexanes to elute. Pure fractions were pooled and concentrated *in vacuo* to afford product as a colorless oil (19.6 g, 76% yield). ¹H NMR (400 MHz, CDCl₃) δ ppm): 7.34-7.20 (m, 5H), 5.87-5.77 (m, 1H), 5.12-5.04 (m, 2H), 4.70-4.64 (m, 1H), 4.19-4.12 (m, 2H), 3.86 (sex, *J* = 6.8 Hz, 1H), 3.27 (dd, *J* = 3.2, 13.5 Hz, 1H), 2.70 (dd, *J* = 9.8, 13.3 Hz, 1H), 2.56-2.49 (m, 1H), 2.27-2.20 (m, 1H), 1.18 (d, *J* = 6.8 Hz, 3H); ¹³C NMR (100.6 MHz, CDCl₃) δ (ppm): 176.4, 153.0, 135.3, 135.2, 129.3, 128.8, 127.2, 117.1, 65.9, 55.3, 38.0, 37.9, 37.1, 16.3; Specific rotation $[\alpha]_D^{20} = -39.4^\circ$ (*c* = 1.0, CHCl₃).

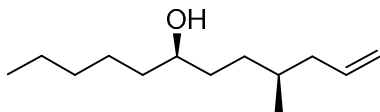


(R)-2-methylpent-4-en-1-ol (3.44). To a stirred solution of **3.43** (19.6 g, 71.7 mmol) in diethyl ether (250 mL) cooled to 0 °C was added ethanol (6.3 mL, 107.6 mmol) and lithium borohydride (53.8 mL, 107.6 mmol) as a 2 M solution in THF. The resultant mixture was slowly warmed to room temperature and stirred for 12 hours. Reaction completion was verified by LC/MS. Upon completion, the reaction was quenched with the slow addition of 1 N NaOH (400 mL) and stirred until both organic and aqueous layers were free of particulates. These phases were separated, and the aqueous phase was extracted 3x with diethyl ether (100 mL). The combined organic phases were dried and concentrated before purifying by flash chromatography using 0-40% EtOAc in hexanes to elute. Pure fractions were pooled and concentrated *in vacuo* to afford

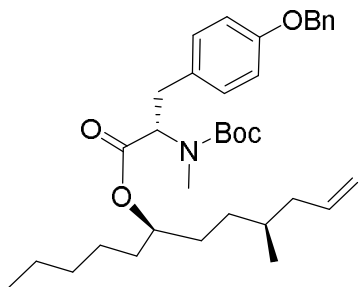
product as a colorless liquid (6.9 g, 83 % yield). ^1H NMR (400 MHz, CDCl_3) δ ppm): 5.80-5.70 (m, 1H), 5.02-4.94 (m, 2H), 3.46-3.35 (m, 2H), 2.49 (br, 1H), 2.17-2.10 (m, 1H), 1.90-1.83 (m, 1H), 1.73-1.61 (m, 1H), 0.87 (d, $J = 6.8$, 3 H); ^{13}C NMR (100.6 MHz, CDCl_3) δ (ppm): 136.9, 115.8, 67.5, 37.7, 35.4, 16.2; Specific rotation $[\alpha]_D^{20} = +3.9^\circ$ ($c = 1.0$, CHCl_3).



(R)-5-bromo-4-methylpent-1-ene (3.41). To a stirred solution of **3.44** (2.5 g, 21.7 mmol) in DCM at 0 °C was added triphenylphosphine dibromide (18.3 g, 43.4 mmol) and DIEA (7.6 mL, 43.4 mmol). This mixture was stirred at 0 °C for 1 hour before warming to room temperature. Reaction progression was monitored by TLC with KMnO_4 staining to visualize. Upon consumption of starting material, the reaction was concentrated *in vacuo*, and triturated with diethyl ether to precipitate triphenylphosphine oxide byproduct. This mixture was cooled to -20 °C for 12 hours before filtering to remove precipitate. The supernatant was washed 2x with 1N HCl and concentrated before purification by distillation (bp = 57 °C, 250 mm/Hg). Product was afforded as a clear liquid (2.53 g, 71% yield). ^1H NMR (400 MHz, CDCl_3) δ ppm): 5.79-5.69 (m, 1H), 5.10-5.04 (m, 2H), 3.41-3.31 (m, 2H), 2.24-2.17 (m, 1H), 2.07-2.00 (m, 1H), 1.93-1.85 (m, 1H), 1.02 (d, $J = 6.6$ Hz, 3H); ^{13}C NMR (100.6 MHz, CDCl_3) δ (ppm): 135.7, 116.9, 40.5, 39.0, 34.9, 18.5; Specific rotation $[\alpha]_D^{20} = -13.2^\circ$ ($c = 1.0$, CHCl_3).



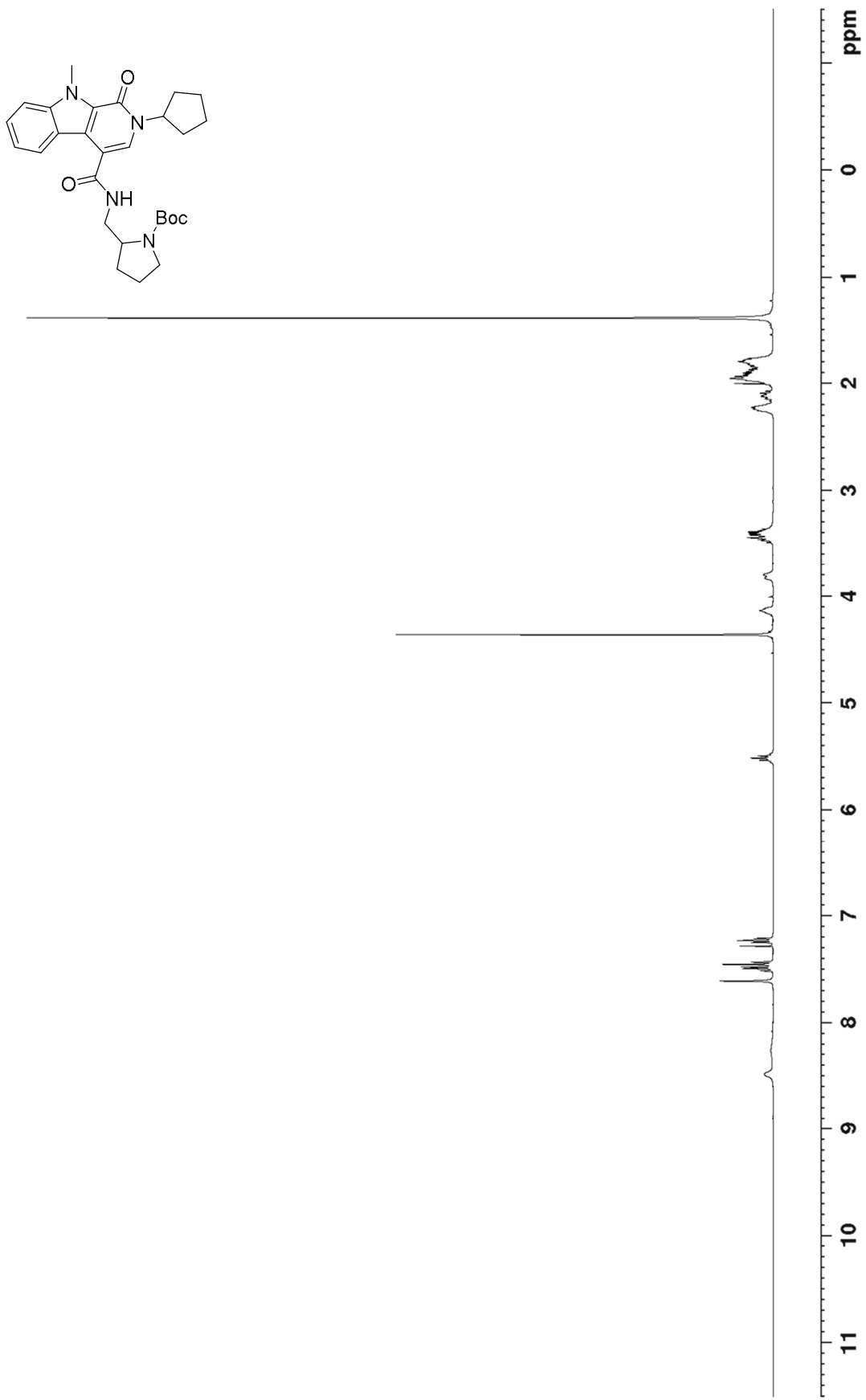
(6R,9S)-9-methyldodec-11-en-6-ol (3.40). To an oven-dried round bottom flask was added magnesium (204 mg, 8.4 mmol), 1 crystal of iodine, and THF (20 mL). **3.41** (1.28 g, 7.9 mmol) was then added as solution in THF (5 mL). The resultant mixture was refluxed until consumption of magnesium was halted. This solution was then added to a second oven-dried round bottom flask containing CuI (200 mg, 1.1 mmol) and THF (20 mL) at -78 °C and stirred 20 minutes before adding **3.32** (600 mg, 5.3 mmol) as a solution in THF (5 mL). This mixture was stirred an additional hour at -78 °C before warming to 0 °C. Reaction progression was monitored by TLC with Seebach staining to visualize. Upon completion, the reaction was quenched with aqueous NH₄Cl (100 mL) and 6 N HCl (10 mL) and stirred until a black film appeared between phases and both phases were clear. After this, the phases were separated, and the organic phase was washed 2x with aqueous saturated sodium thiosulfate (30 mL) and 1x with brine (30 ml), dried, and concentrated before purification by flash chromatography using 15% acetone in hexanes to elute. Pure fractions were pooled and concentrated *in vacuo* to afford product as a colorless liquid (750 mg, 72% yield). ¹H NMR (400 MHz, CDCl₃) δ ppm): 5.83-5.72 (m, 1H), 5.01-4.97 (m, 2H), 3.59-3.53 (m, 1H), 2.10-2.04 (m, 1H), 1.94-1.87 (m, 1H), 1.54-1.21 (m, 14H), 0.91-0.87 (m, 6H). ¹³C NMR (100.6 MHz, CDCl₃) δ (ppm): 137.5, 115.6, 72.2, 41.4, 37.5, 34.9, 32.8, 32.3, 31.9, 25.3, 22.6, 19.4, 14.0; Specific rotation $[\alpha]_D^{20} = -13.2^\circ$ (c = 1.0, CHCl₃).

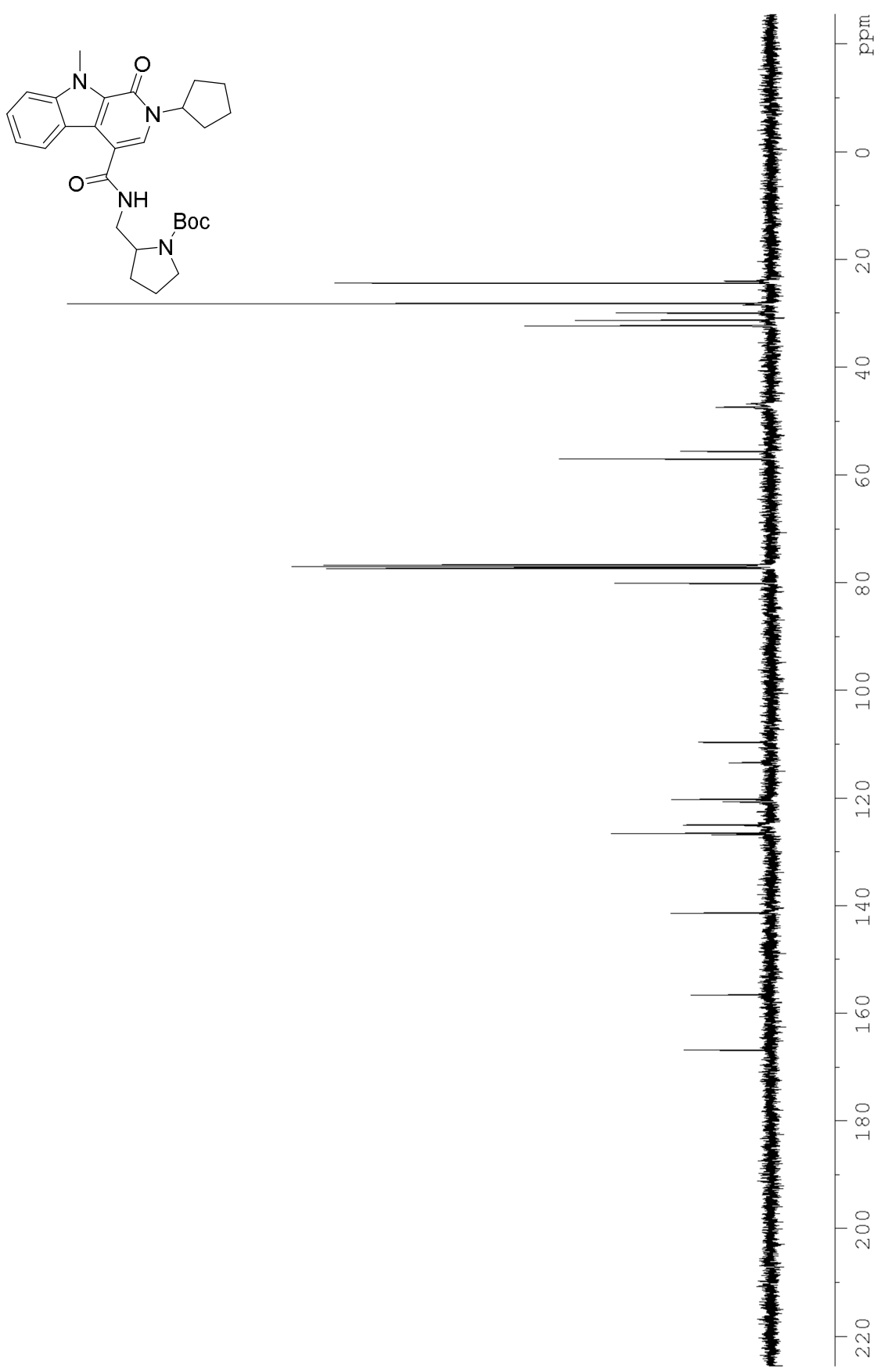


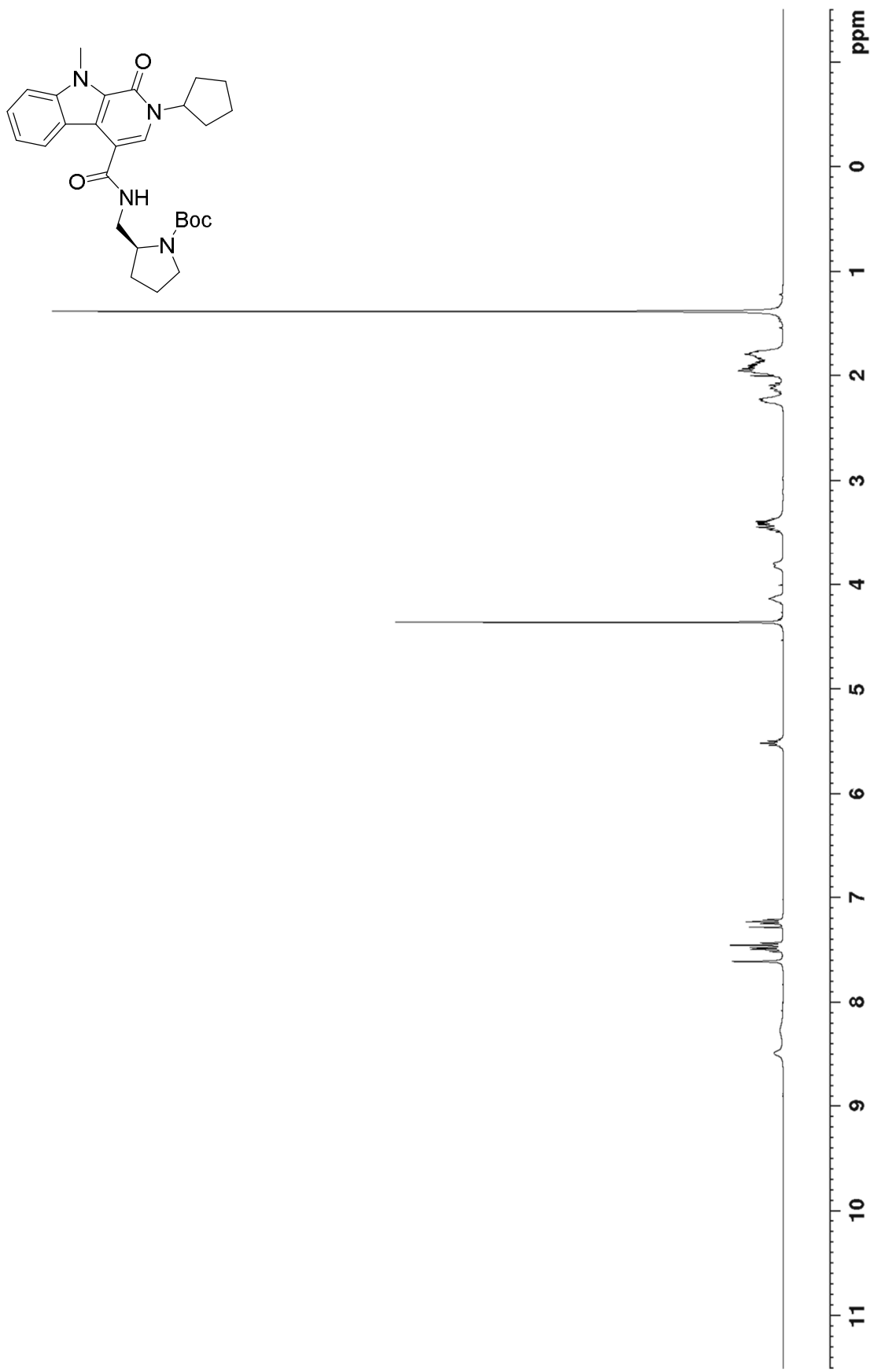
(6*R*,9*S*)-9-methyldodec-11-en-6-yl-(*S*)-3-(4-(benzyloxy)phenyl)-2-((*tert*-butoxycarbonyl)(methyl)amino)propanoate (3.45). To a solution of *N*-Boc-*O*-benzyl-L-tyrosine (350 mg, 0.91 mmol) in DMF (1.3 mL) at 0 °C was added *N,N'*-dicyclohexylcarbodiimide (281 mg, 1.36 mmol), 4-dimethylaminopyridine (22 mg, 0.18 mmol), and **3.40**. This mixture was stirred 30 minutes at 0 °C before warming to room temperature and stirring an additional 3 hours. Reaction progression was monitored by LC/MS. Upon consumption of starting material, the reaction mixture was filtered to remove urea by-product and concentrated. The residue was purified by flash chromatography using 100% DCM to elute. Pure fractions were pooled and concentrated to afford product as a colorless, viscous oil (270 mg, 52% yield). ¹H NMR (400 MHz, CDCl₃) δ (ppm): 7.42-7.28 (m, 5H), 7.16-7.09 (m, 2H), 6.91-6.89 (m, 1H), 5.82-5.71 (m, 1H), 5.01 (s, 3H), 4.98 (s, 1H), 4.91-4.89 (m, 1H), 3.28-3.20 (m, 1H), 3.00-2.88 (m, 1H), 2.79:2.74 (s, 3H, N-CH₃ rotamers), 2.10-2.02 (m, 1H), 1.93-1.89 (m, 1H), 1.60-1.13 (m, 21H), 0.90-0.88 (m, 6H); ¹³C NMR (100.6 MHz, CDCl₃) δ (ppm): 171.1*, 170.8*, 157.5*, 157.4*, 155.6, 155.1, 137.4, 137.2, 137.1, 129.8, 128.5, 127.8, 127.3, 115.8, 115.7, 115.6, 114.8, 114.7, 79.9*, 79.6*, 75.6*, 75.3*, 71.9, 69.9, 60.78, 59.4, 41.1, 33.8, 32.6, 31.6, 31.5, 31.4, 28.2, 28.1, 24.8, 22.4, 19.3, 13.9; Specific rotation $[\alpha]_D^{20} = -24.2^\circ$ (c = 1.0, CHCl₃). *designates rotamers

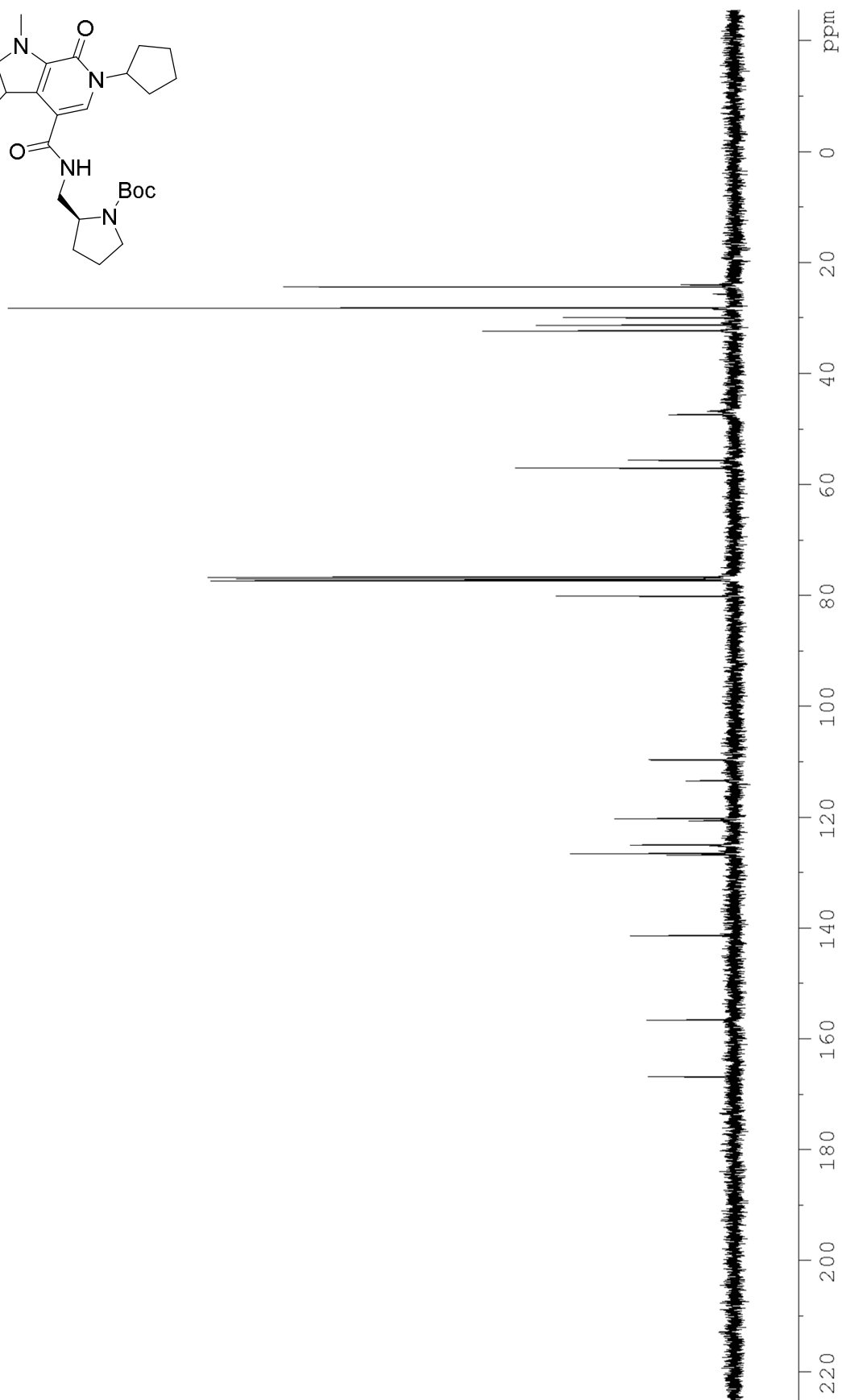
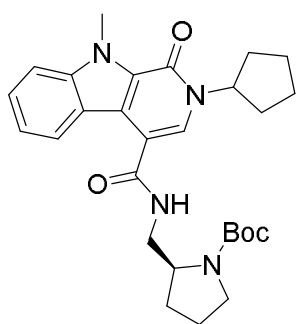
Appendix A

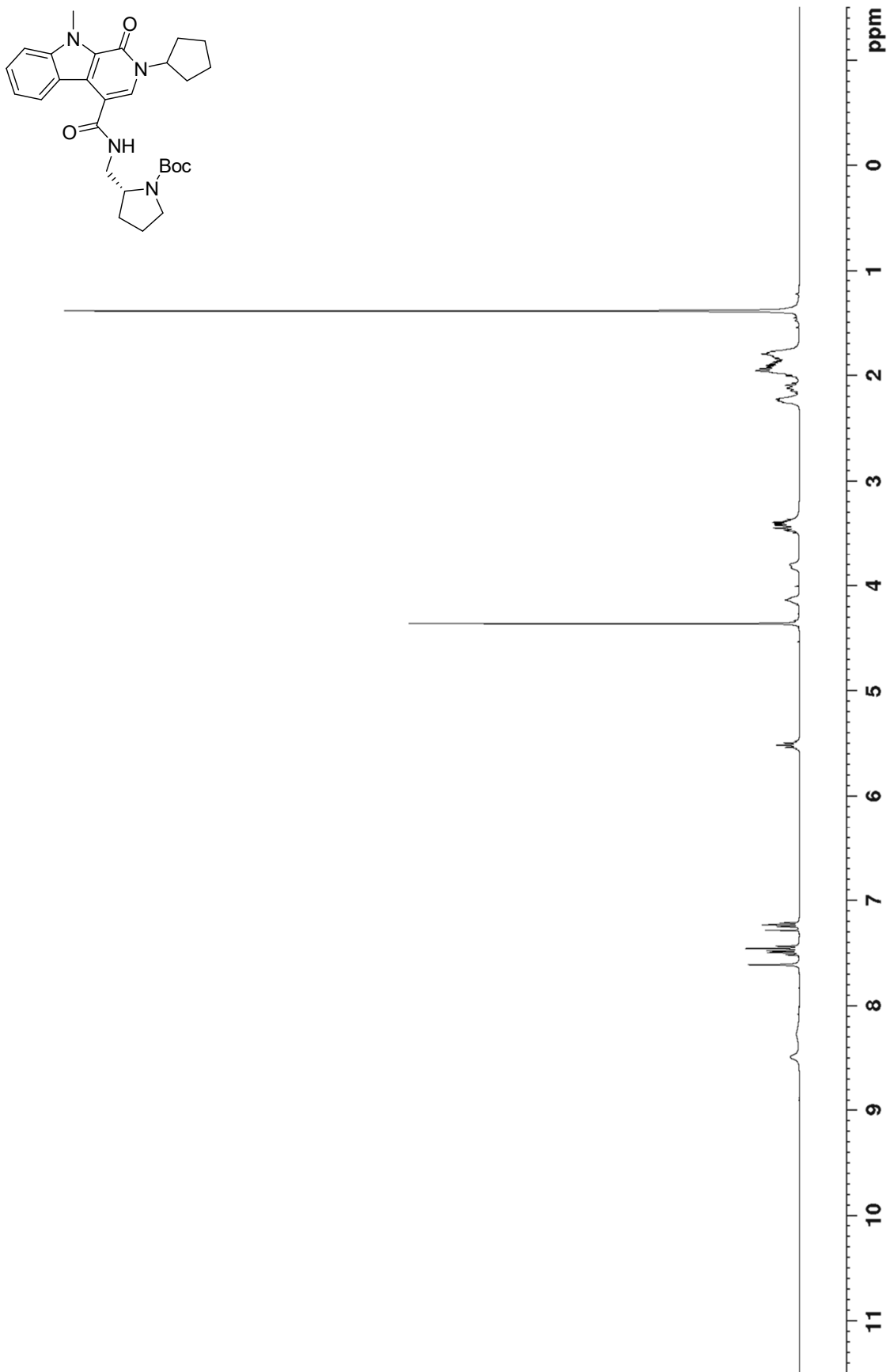
Relevant spectra for chapter 1

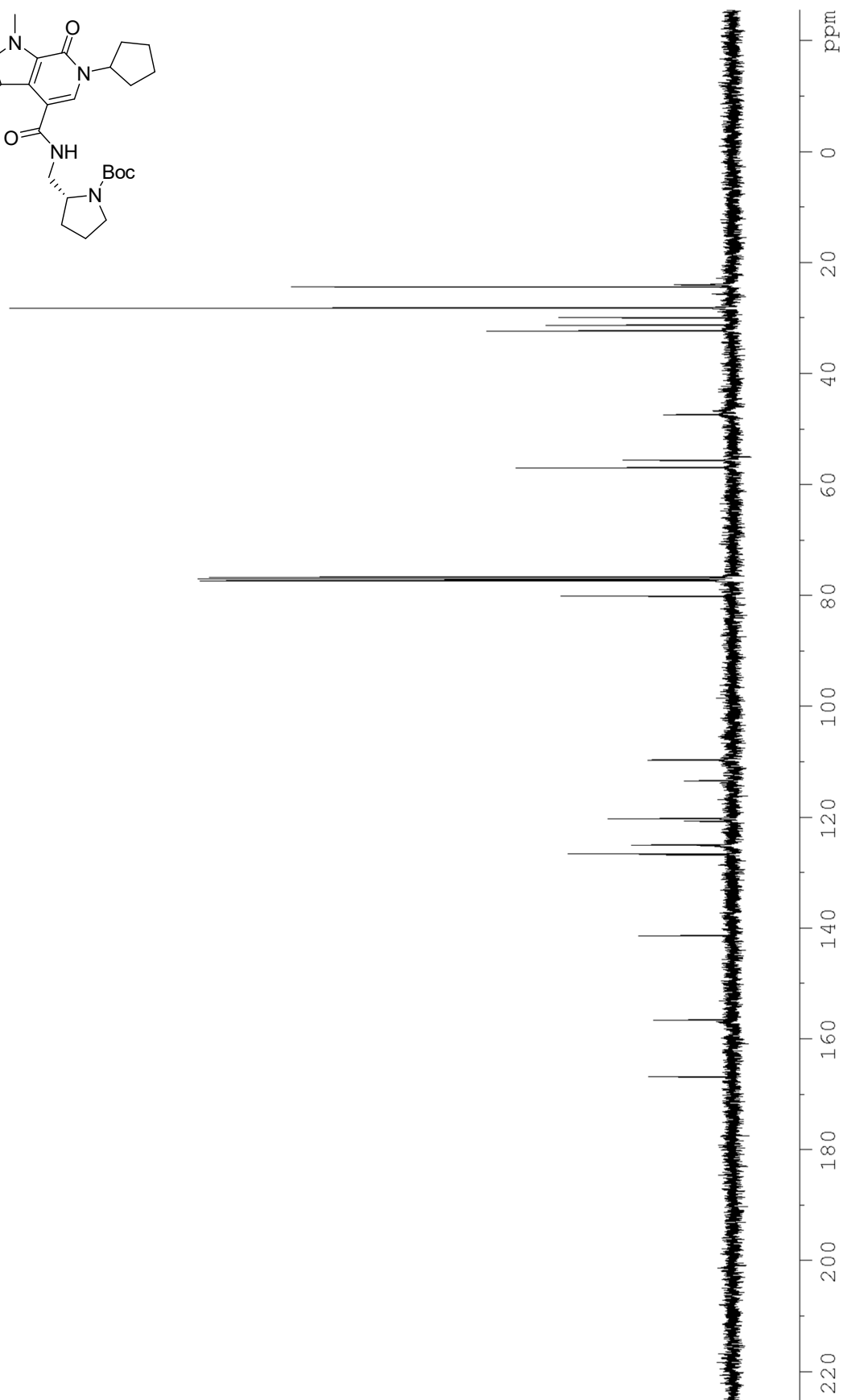
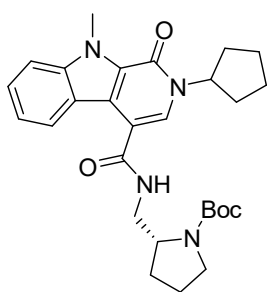


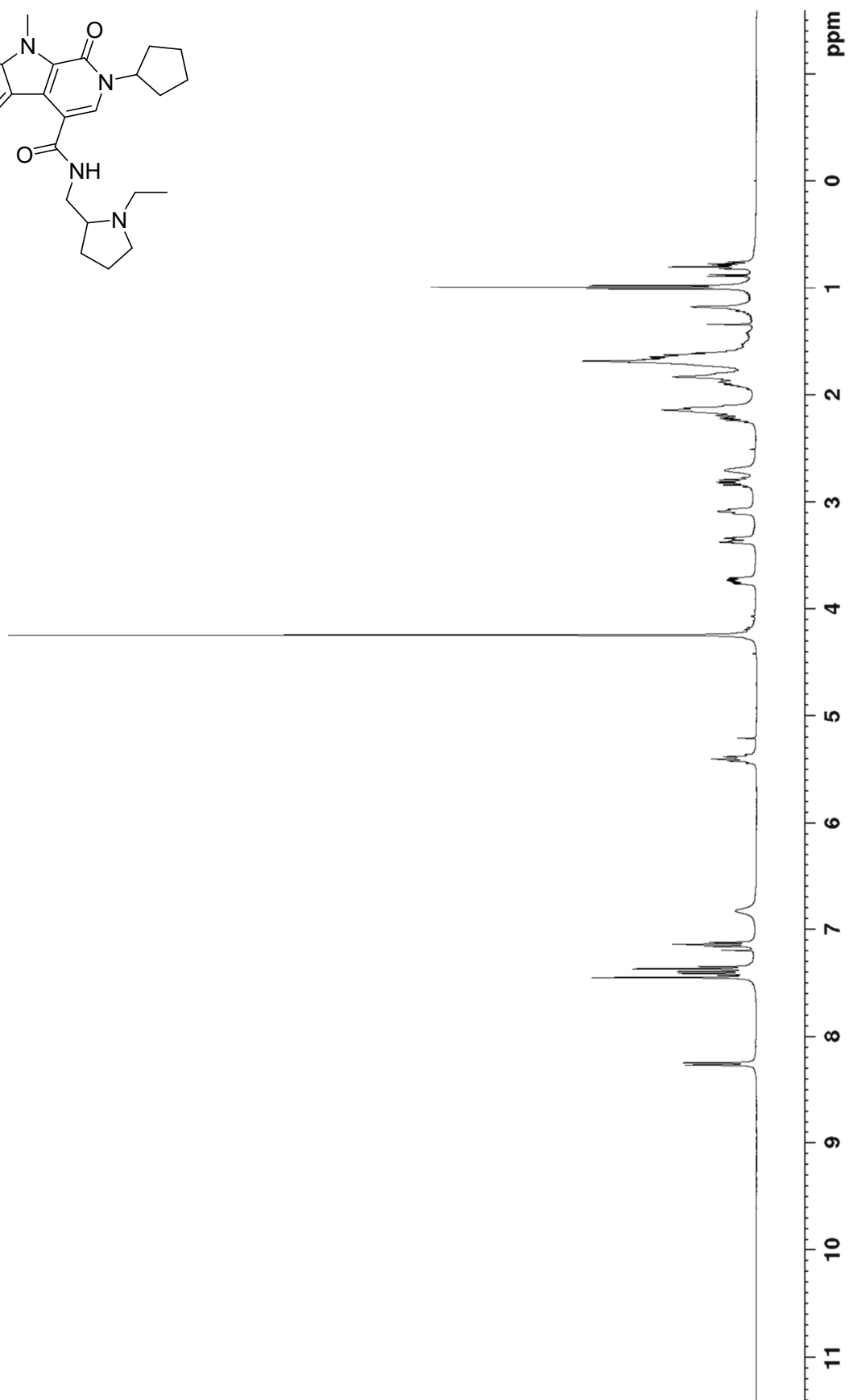
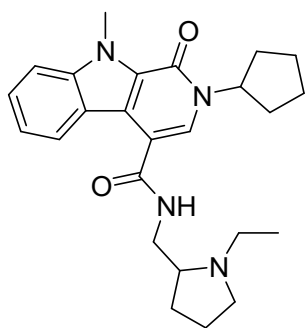


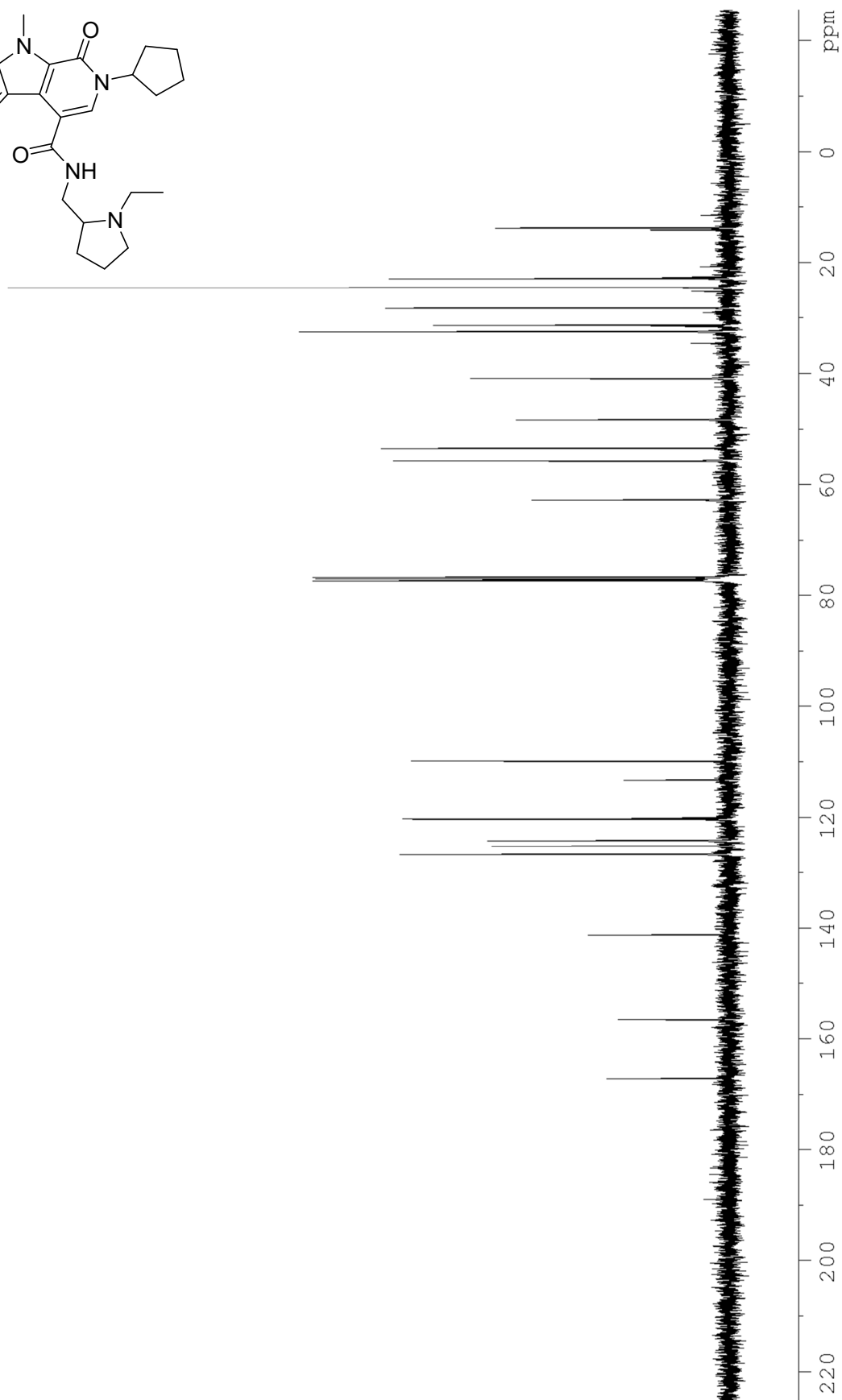
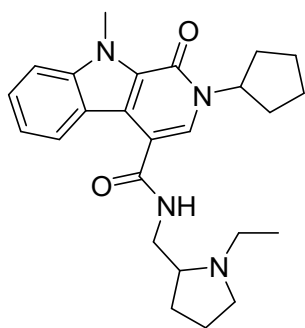


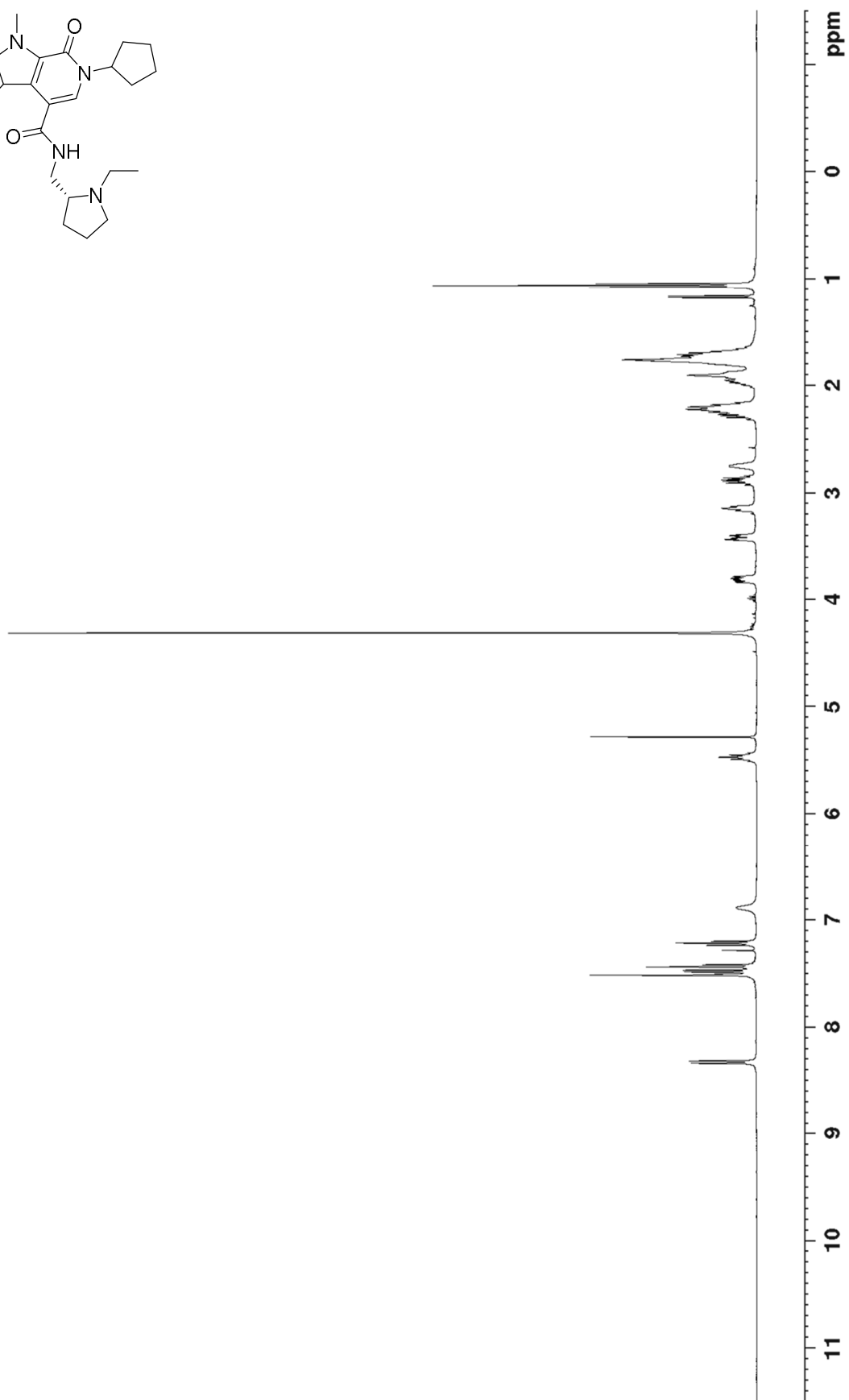
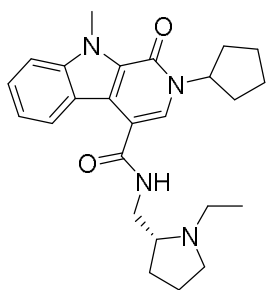


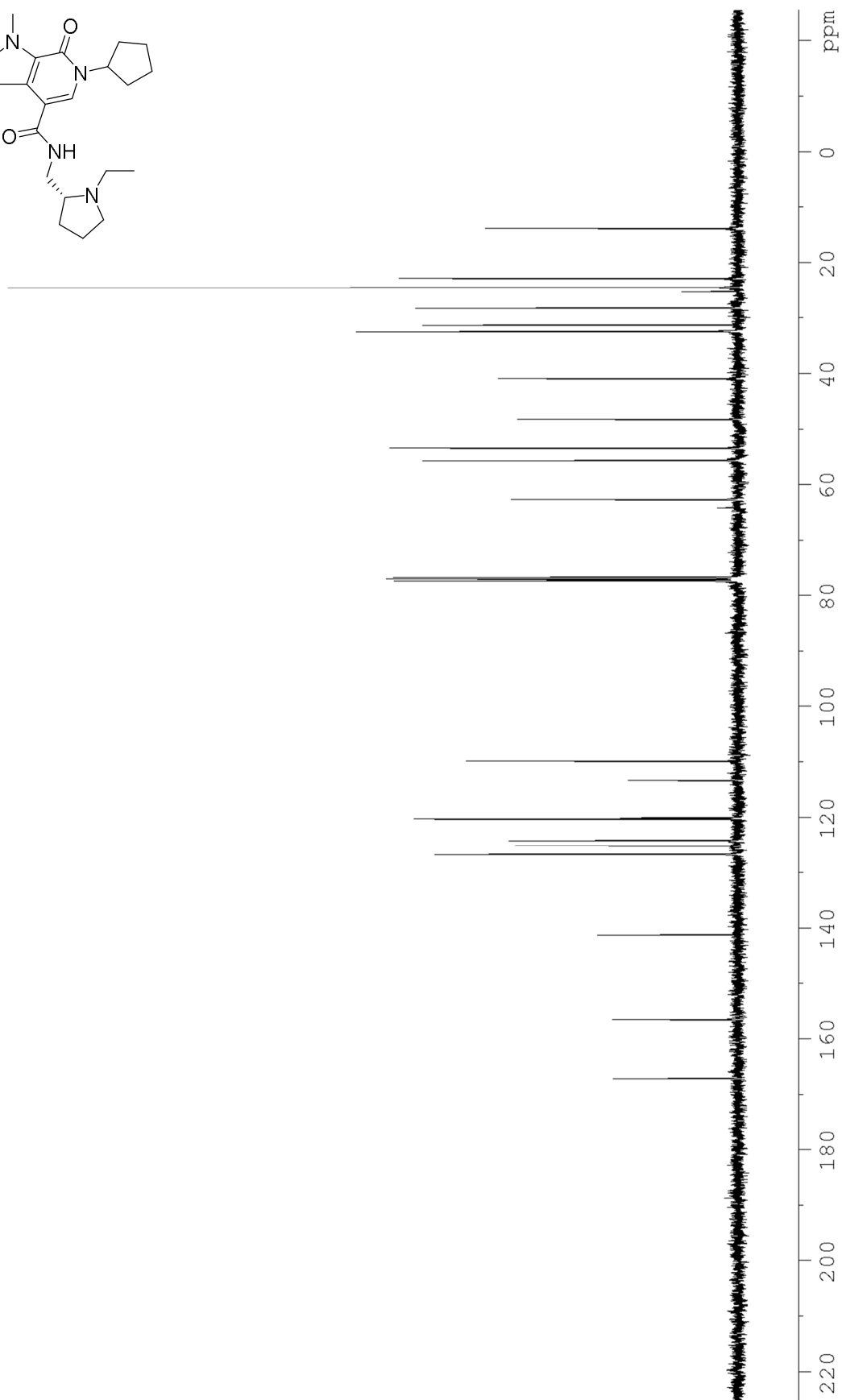
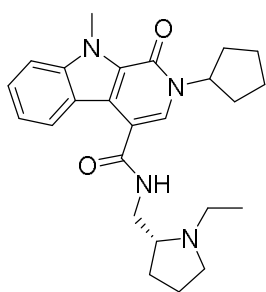


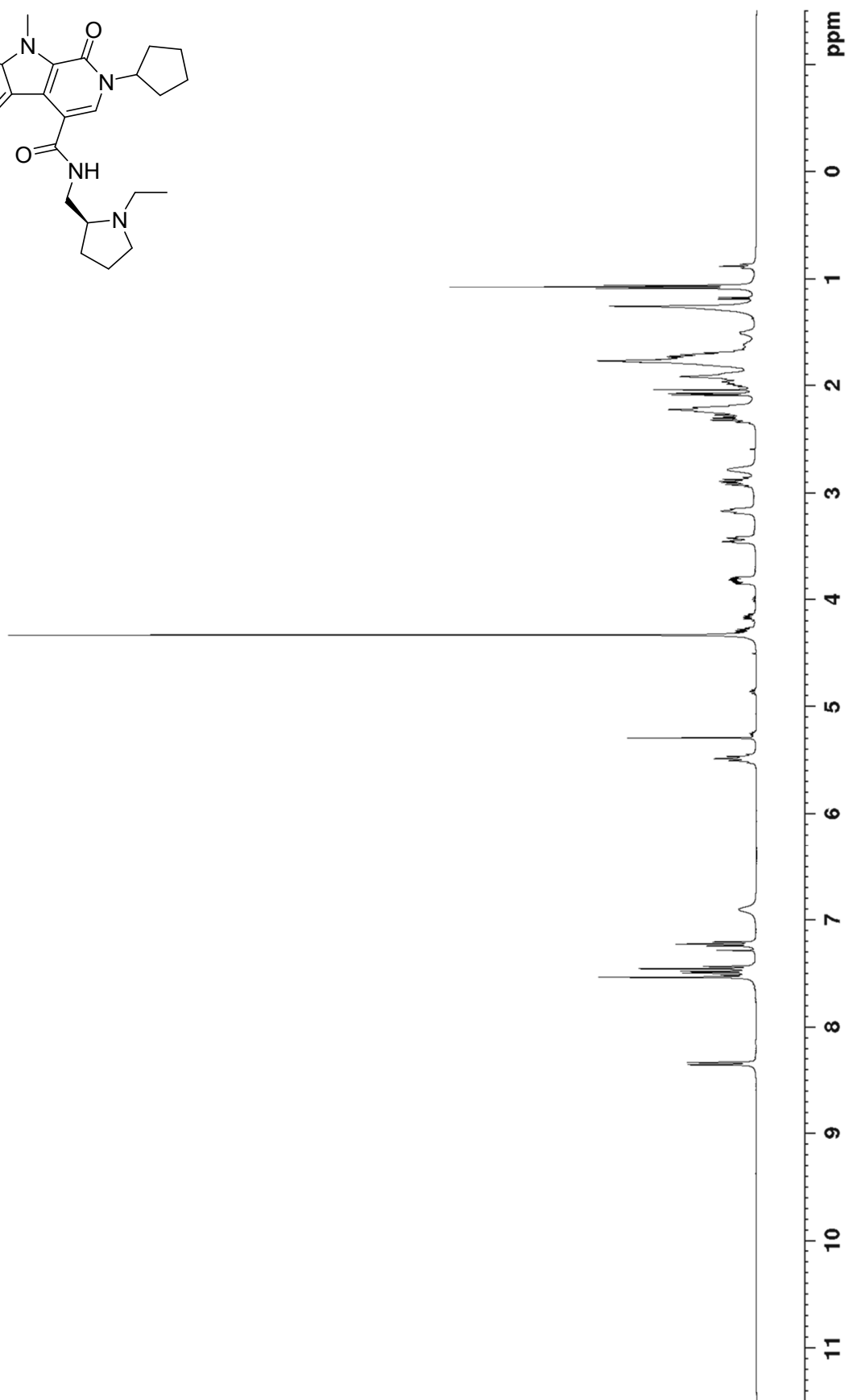
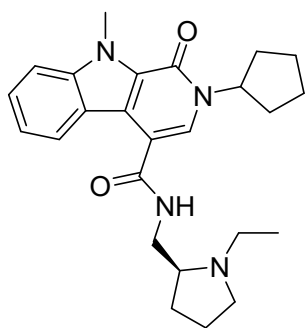


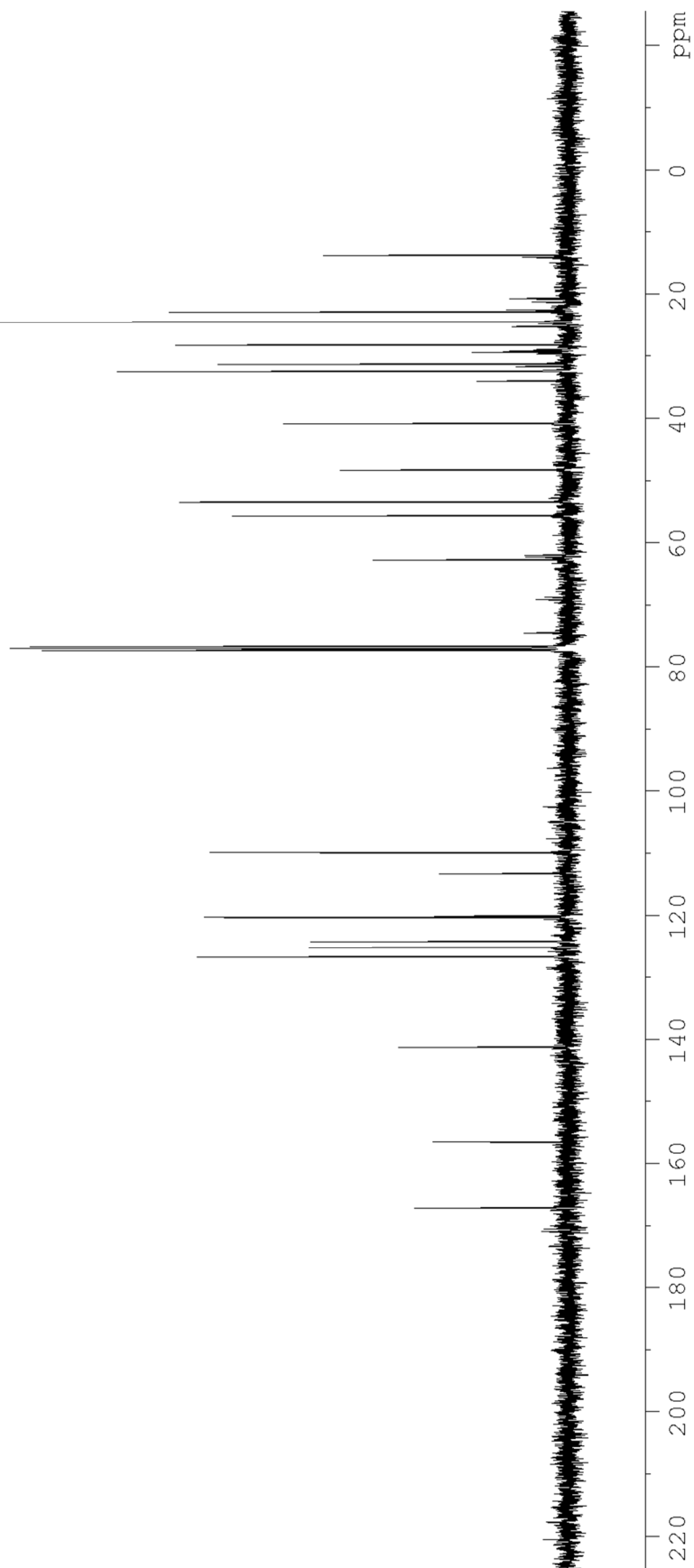
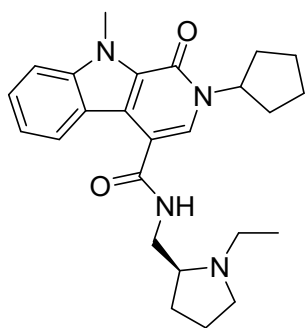


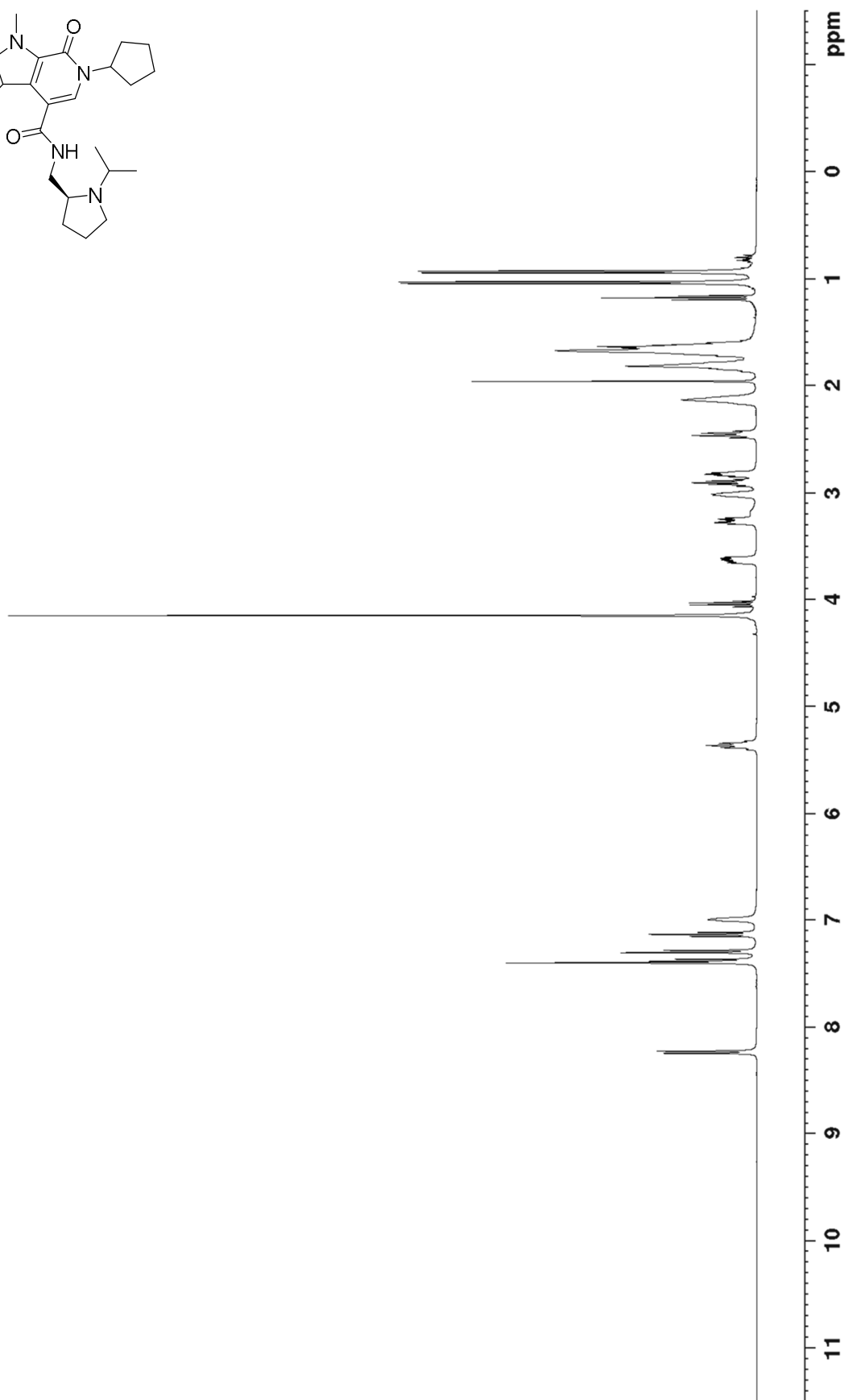
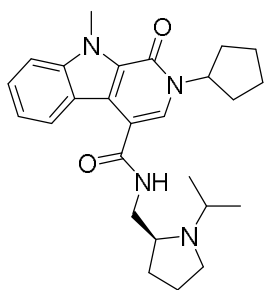


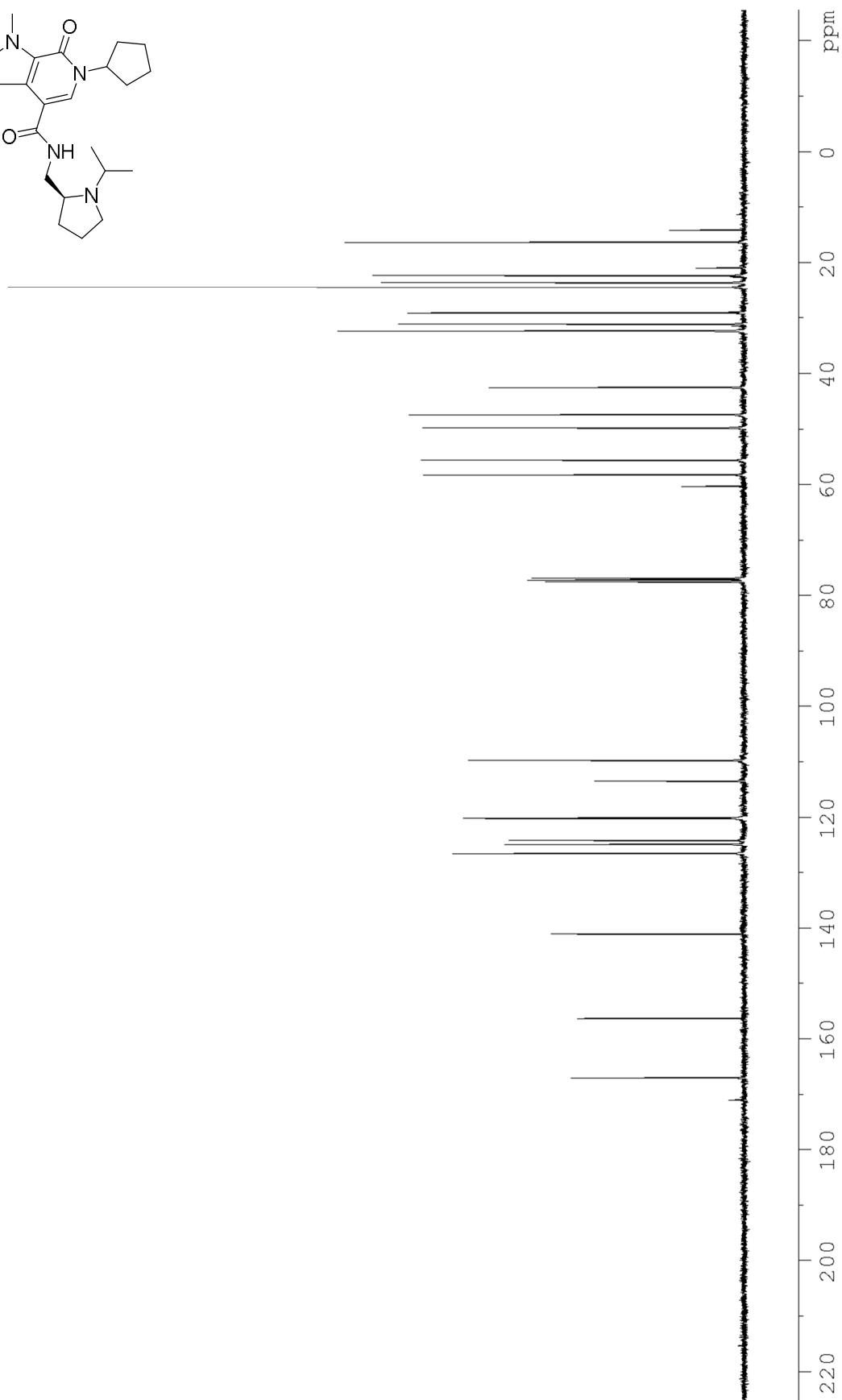
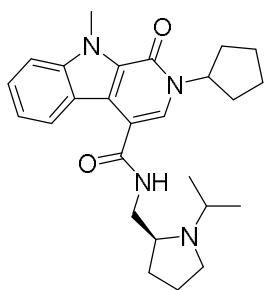


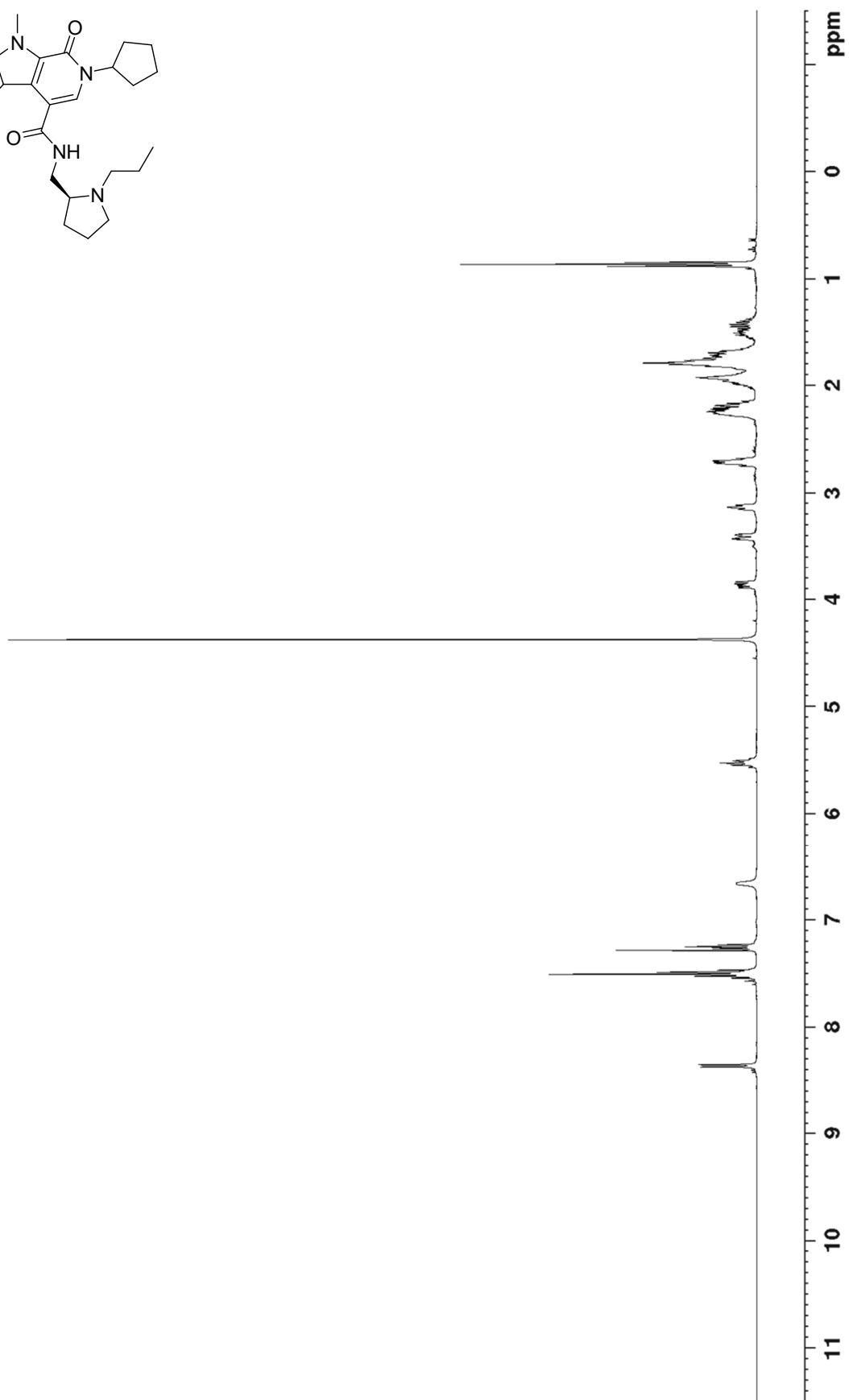
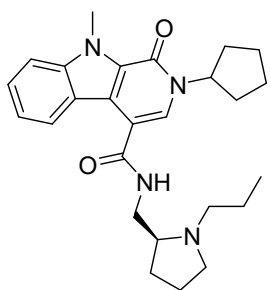


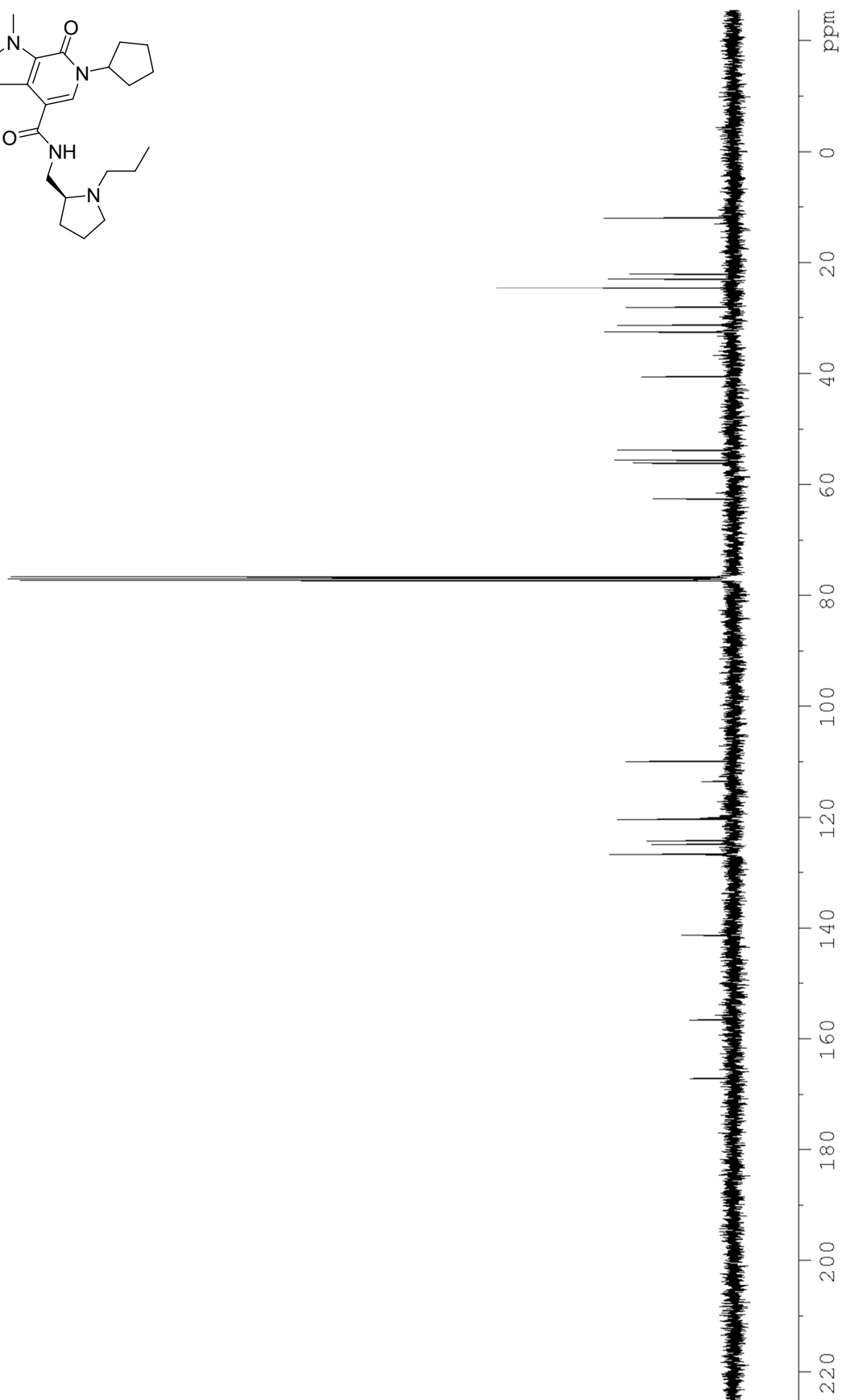
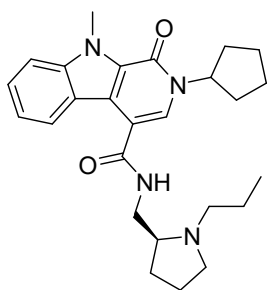


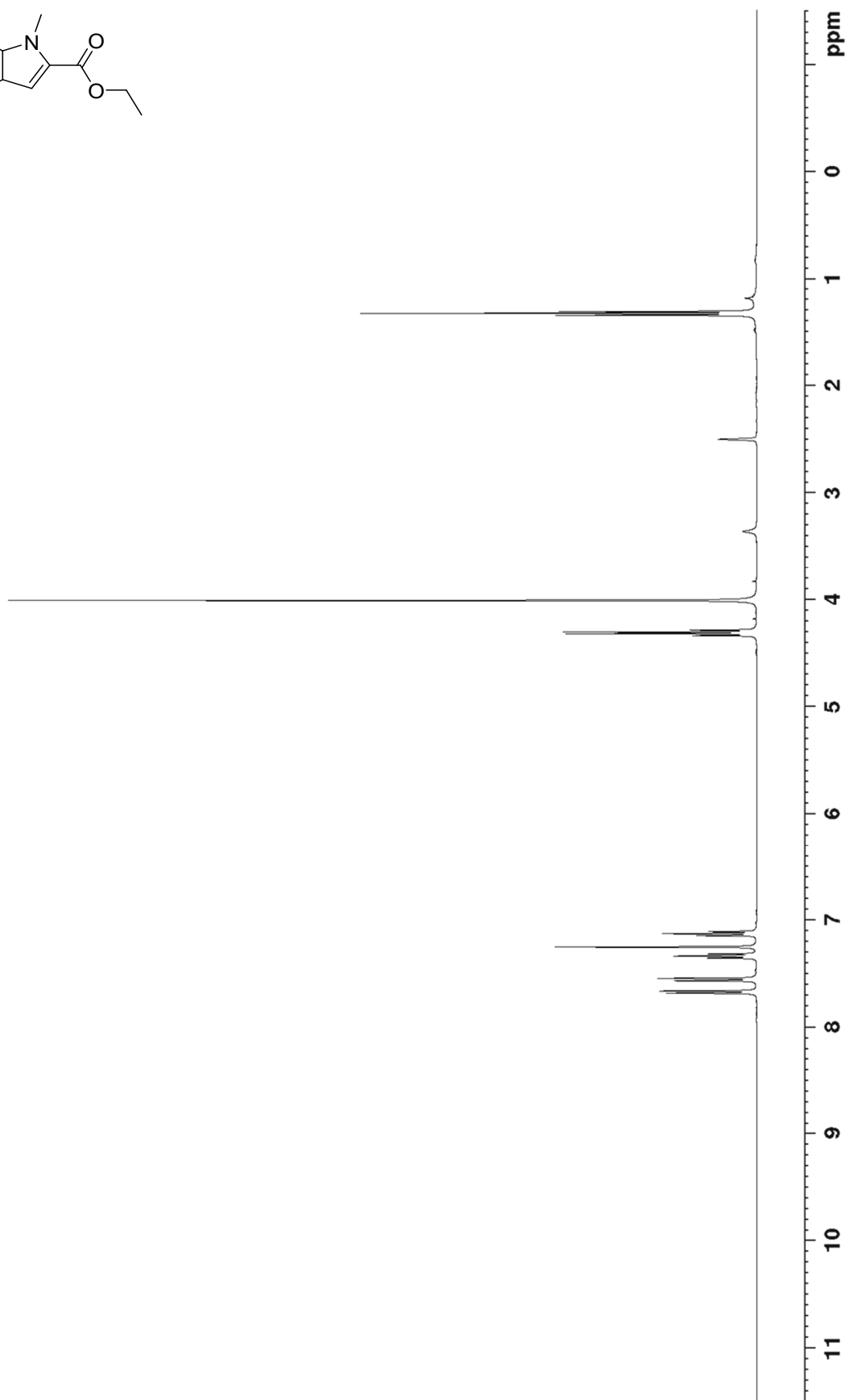
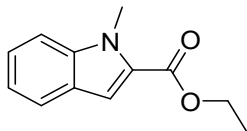


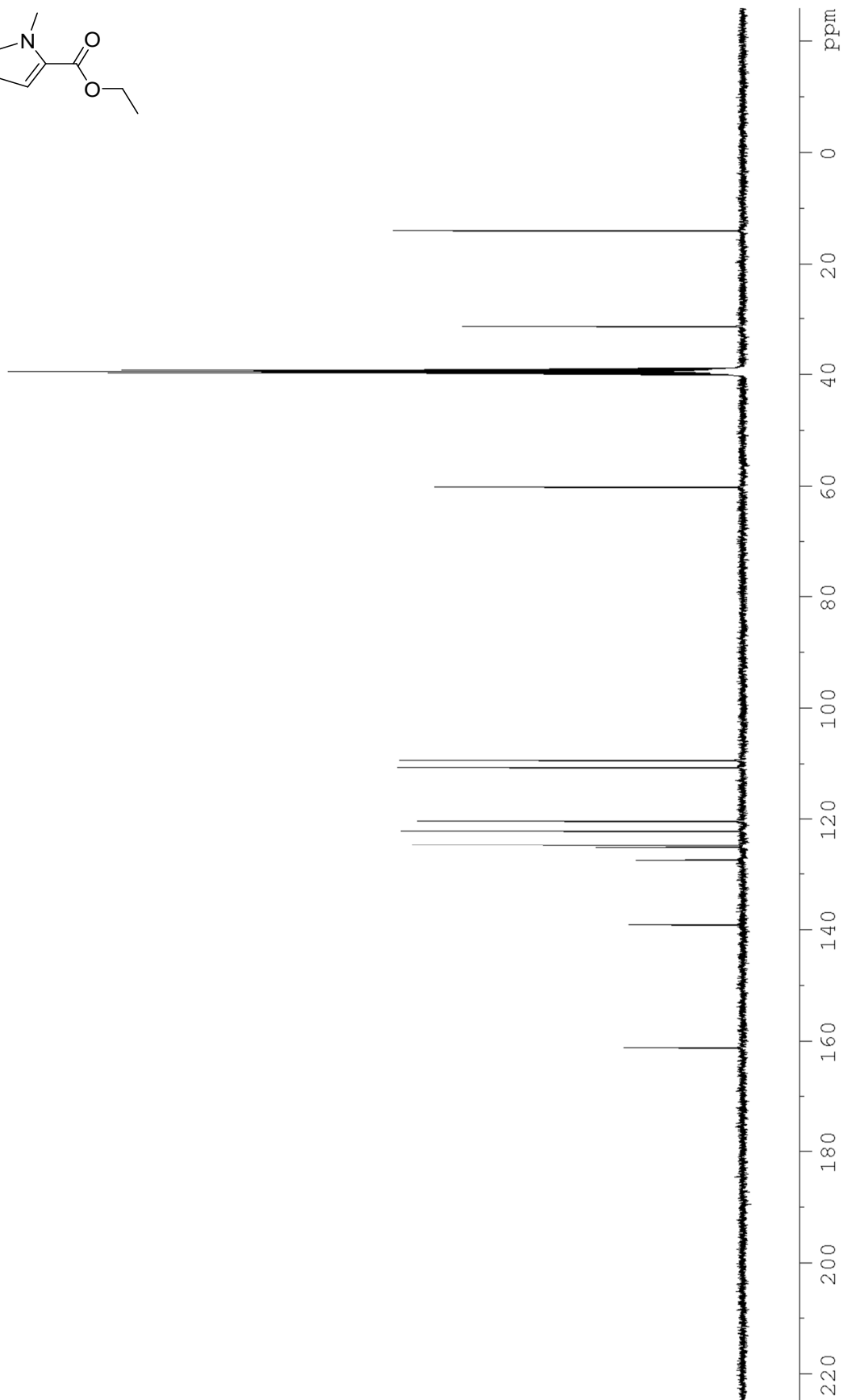
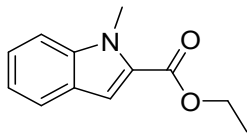


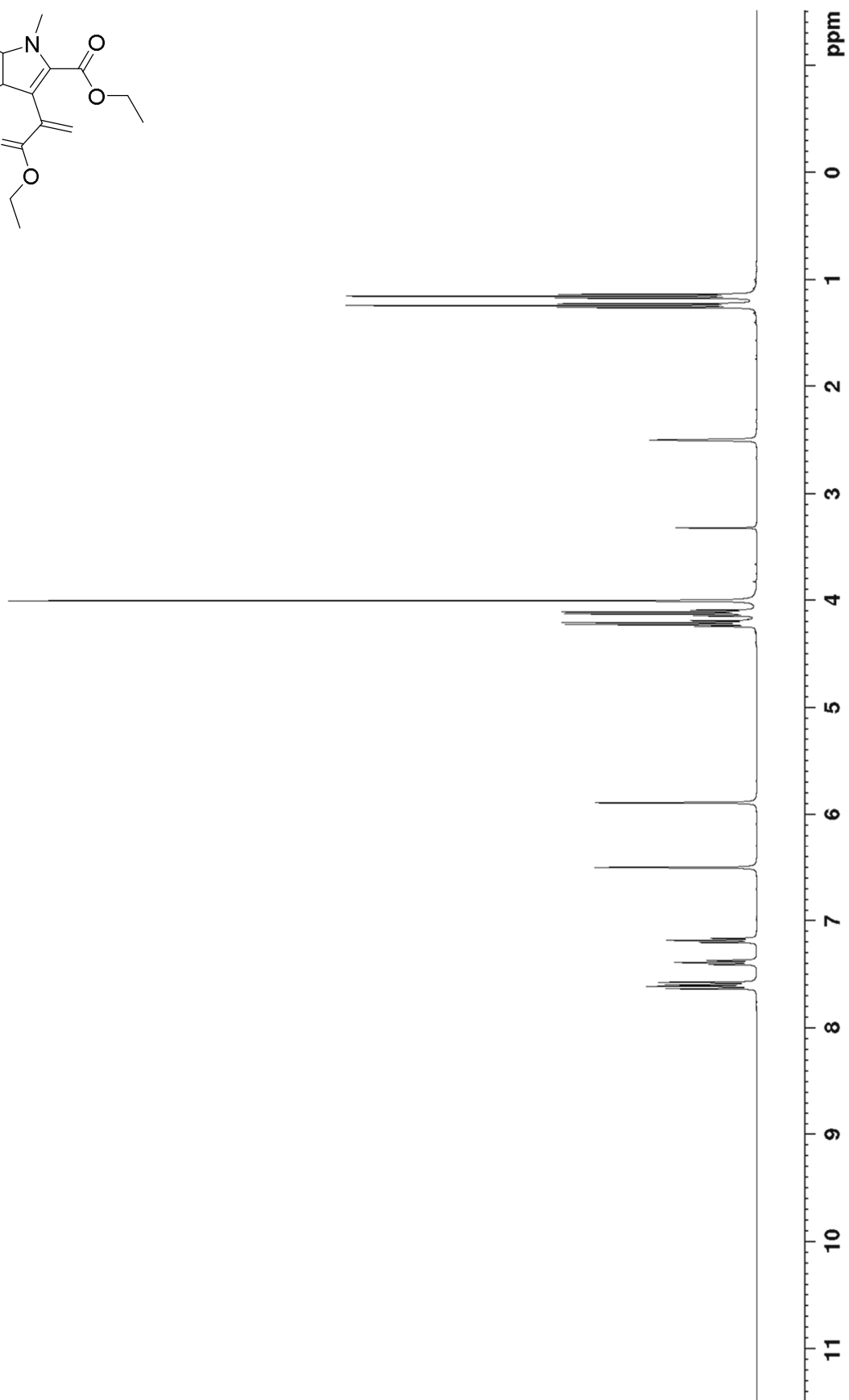
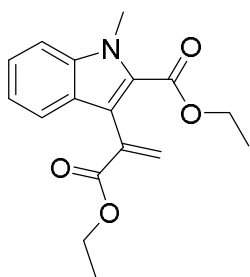


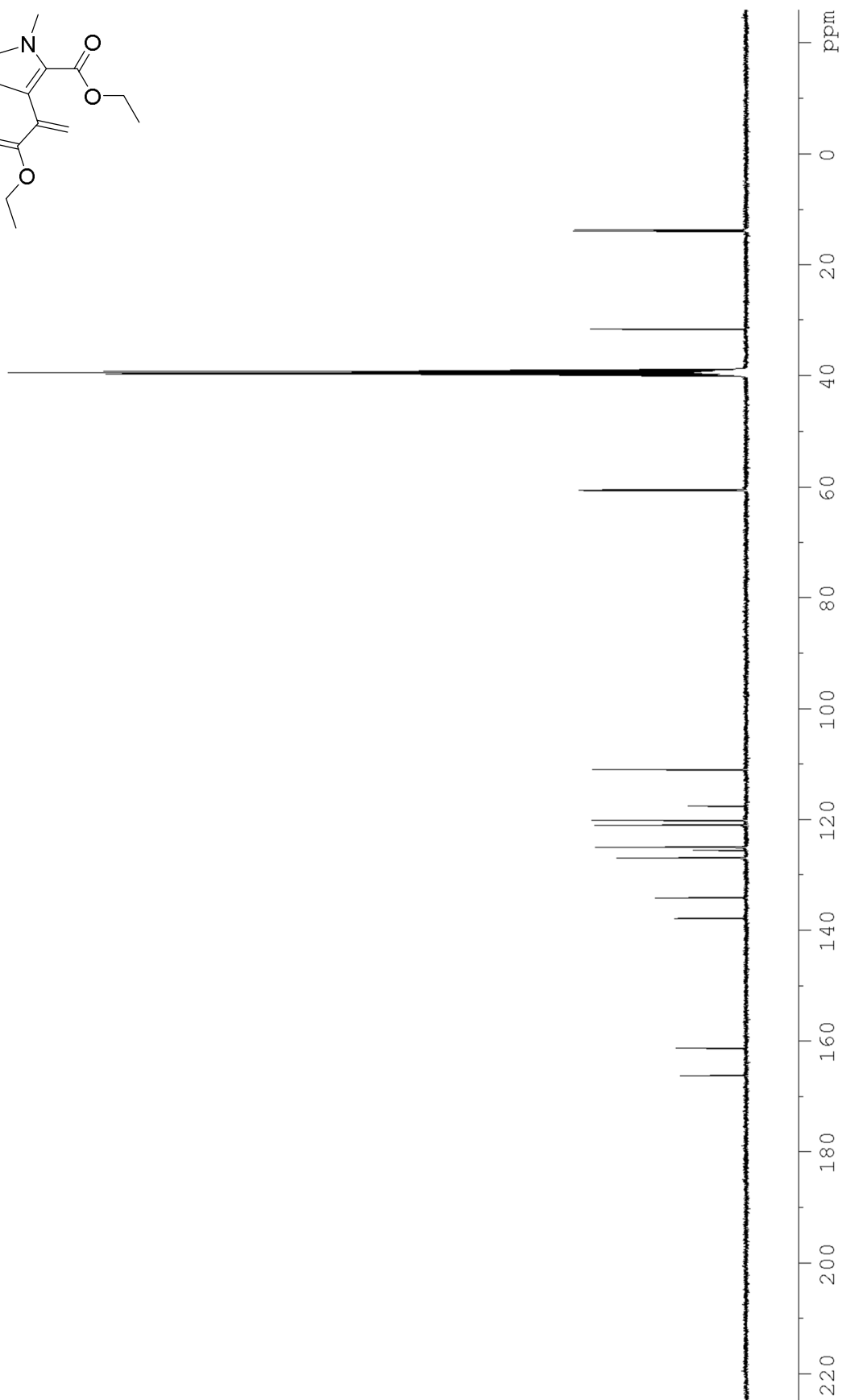
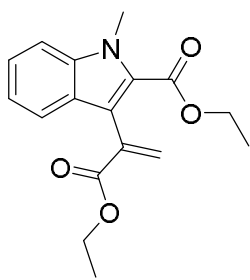


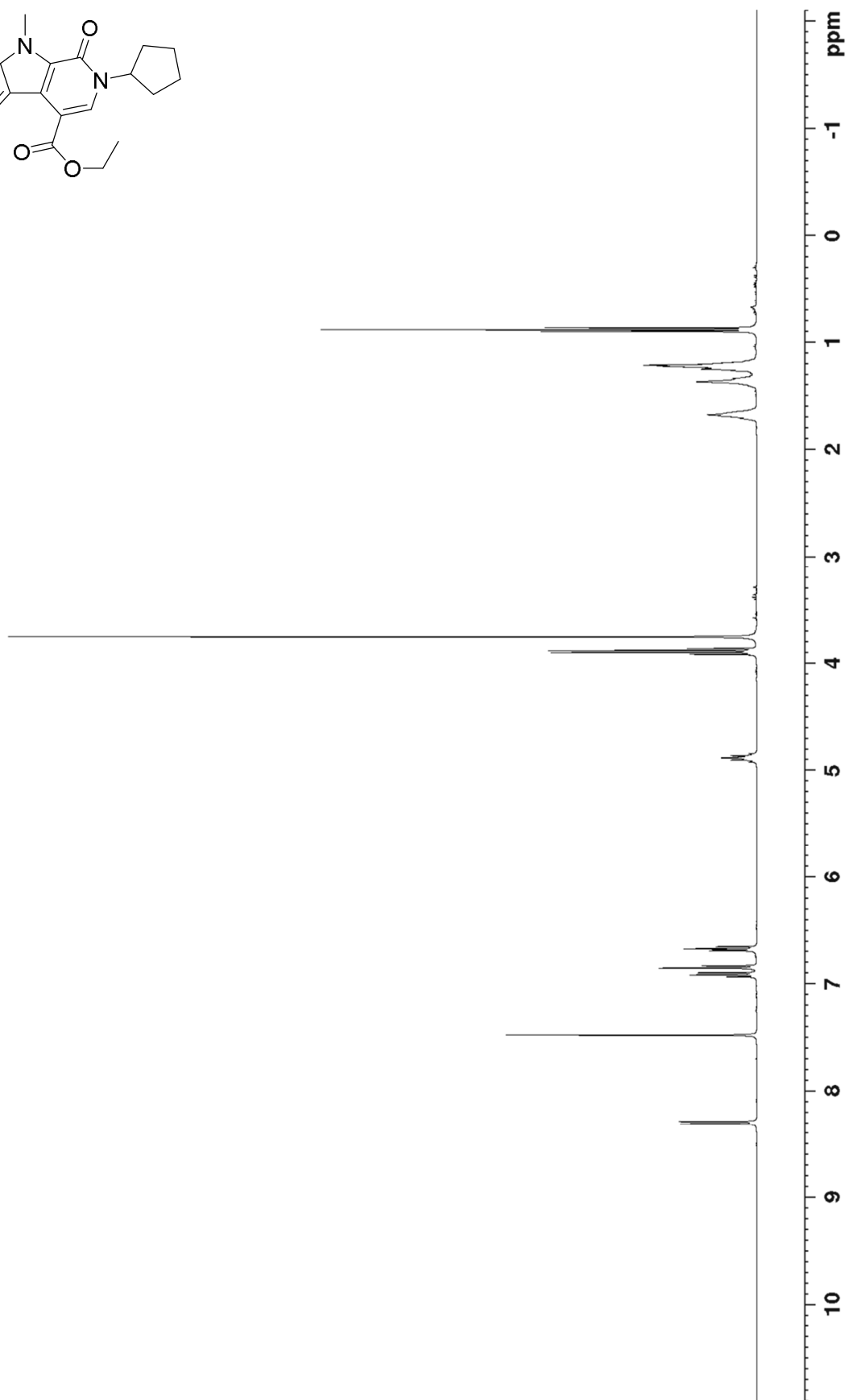
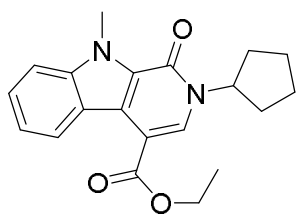


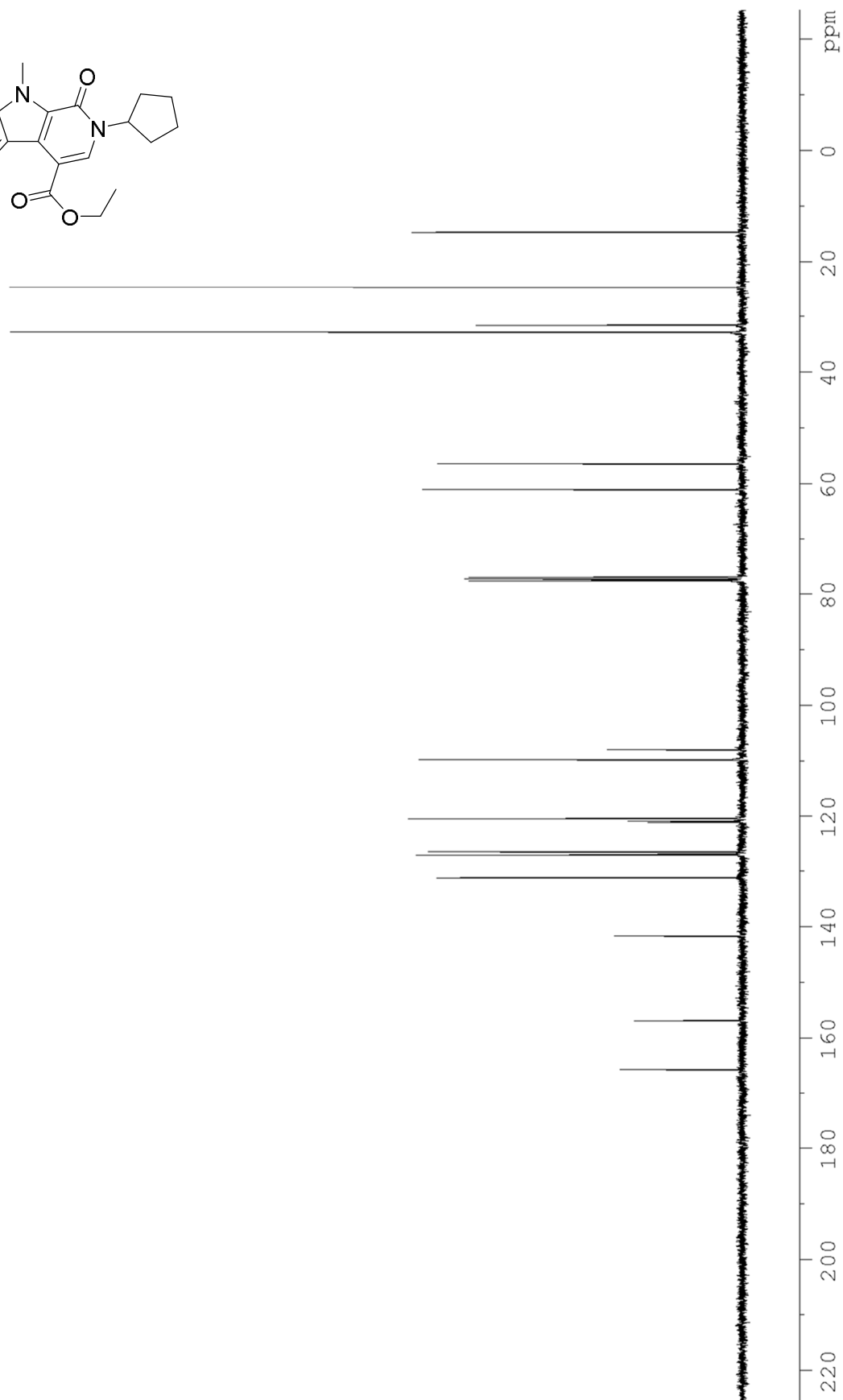
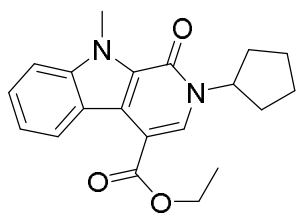


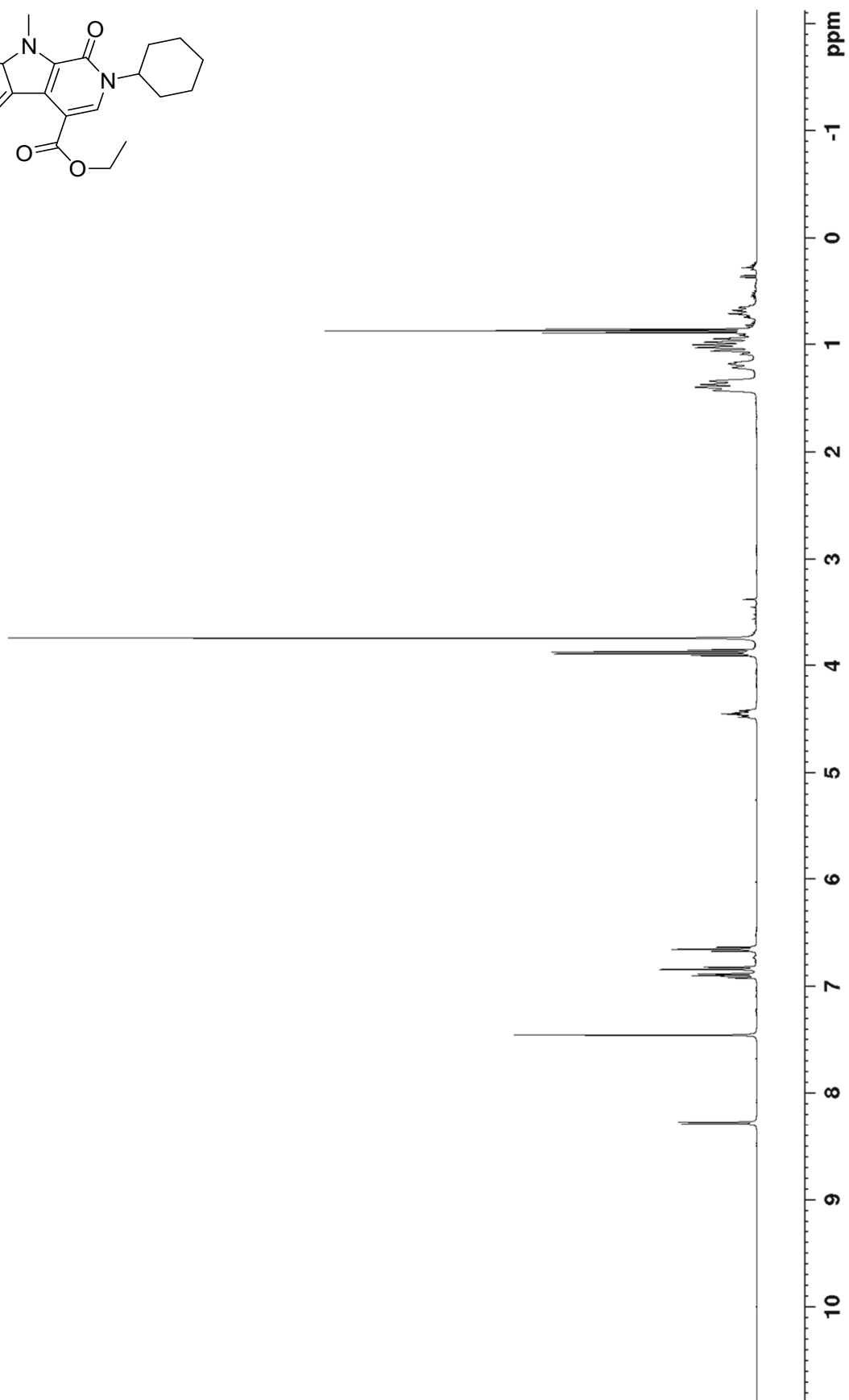
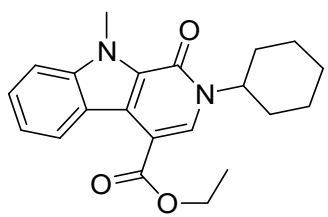


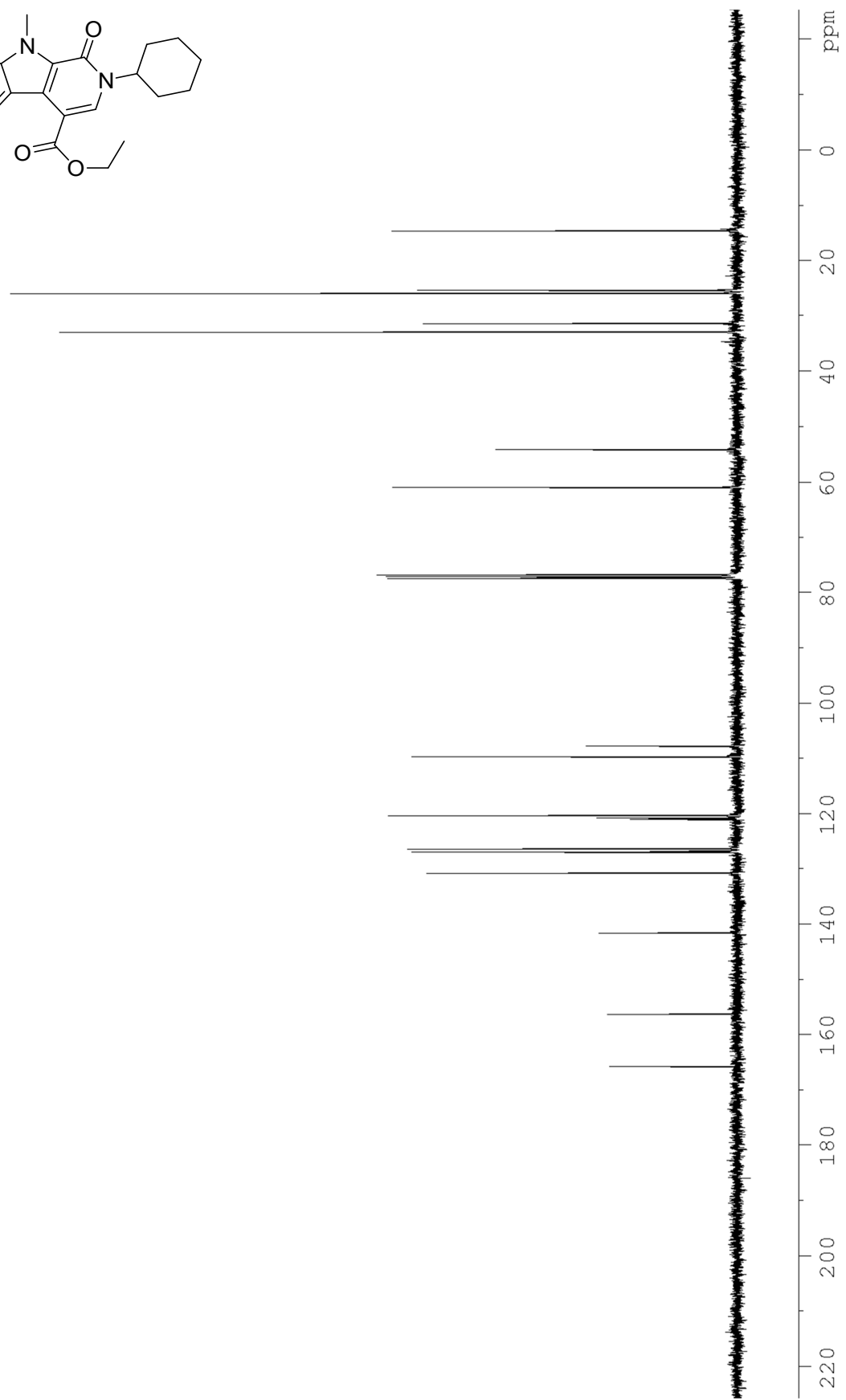
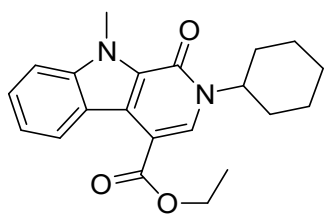


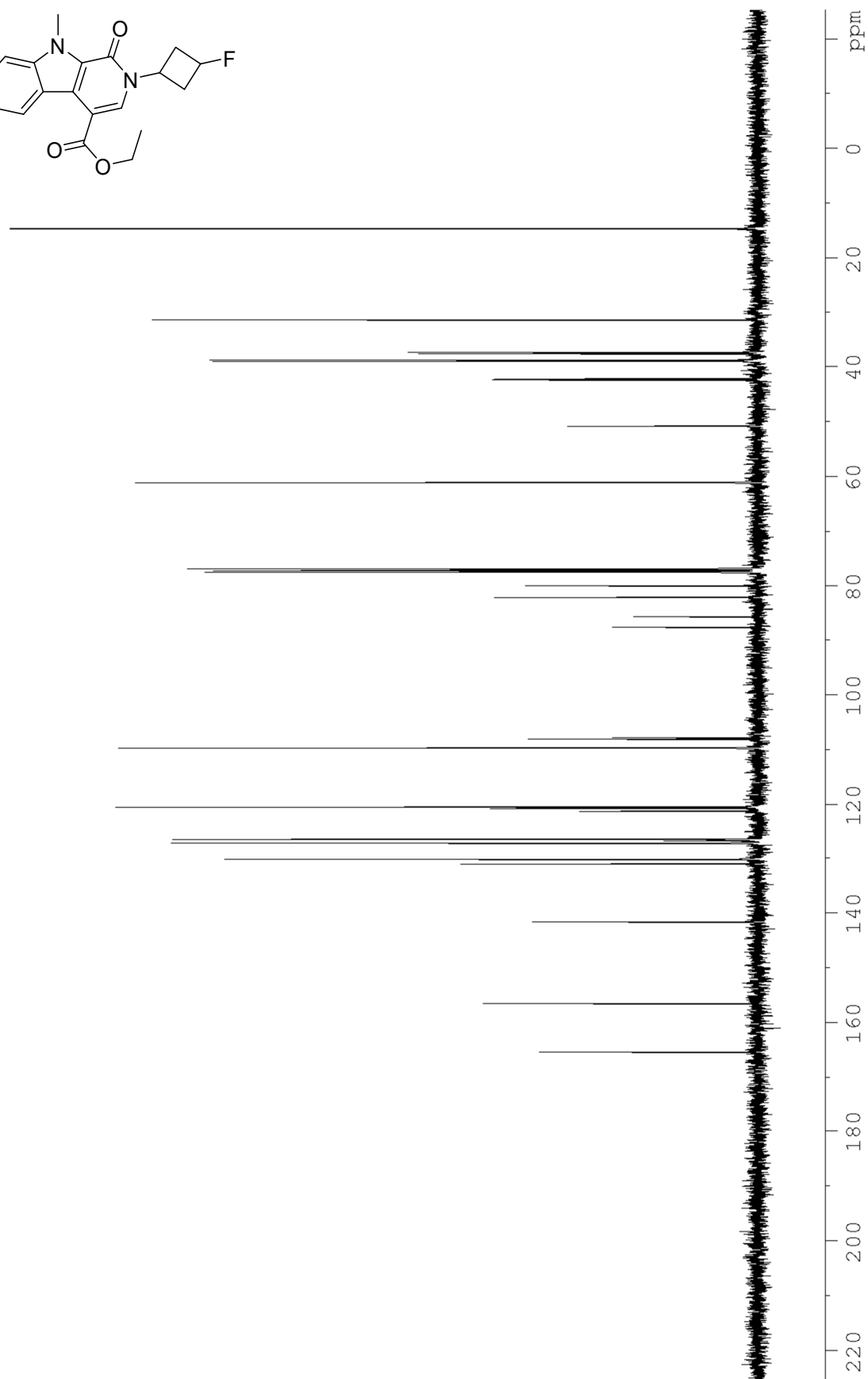
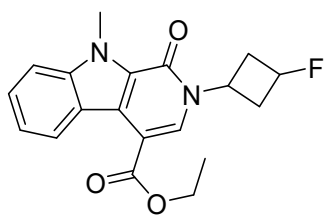


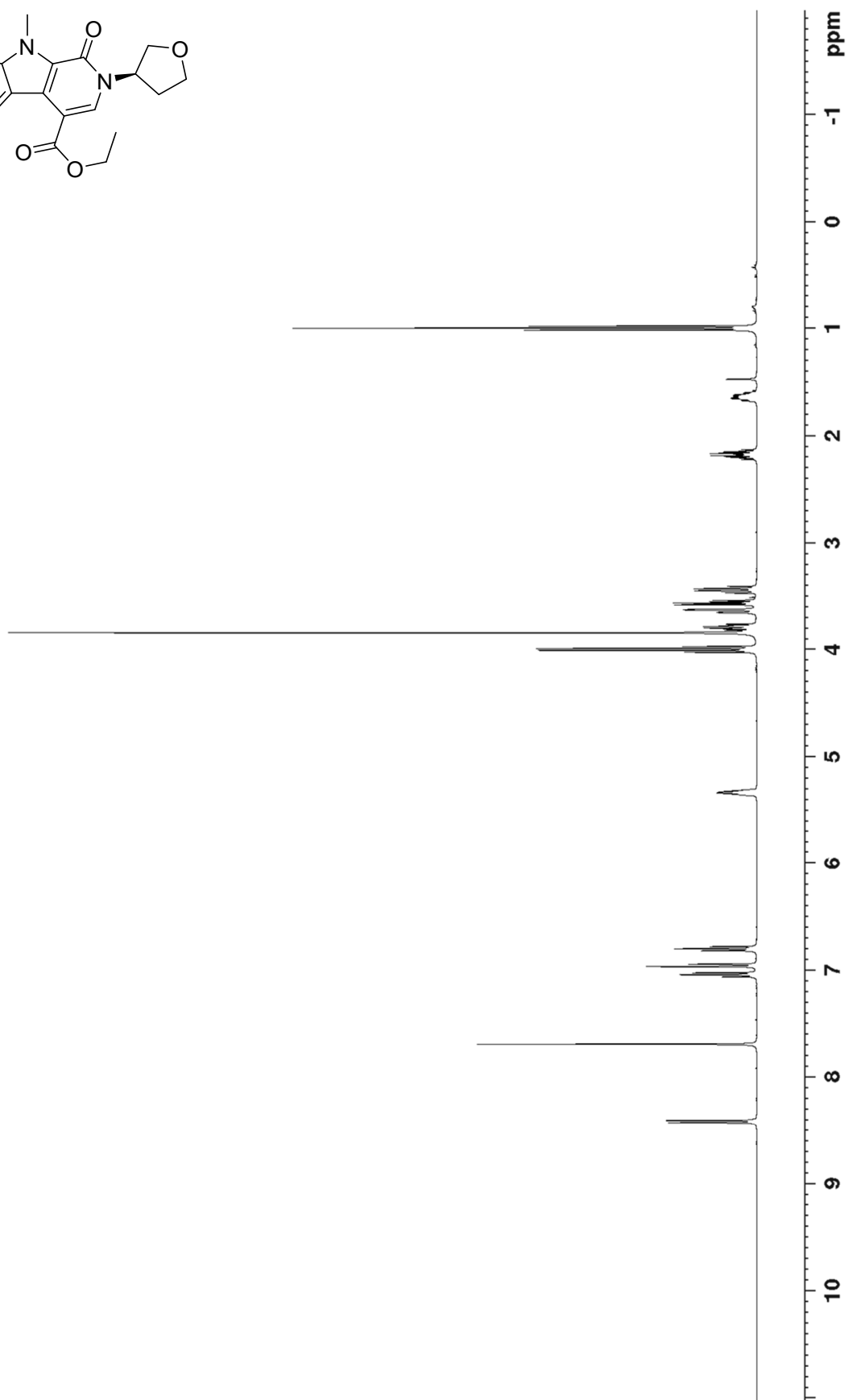
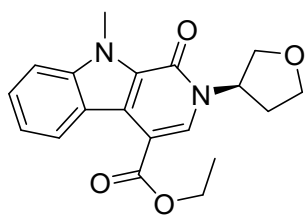


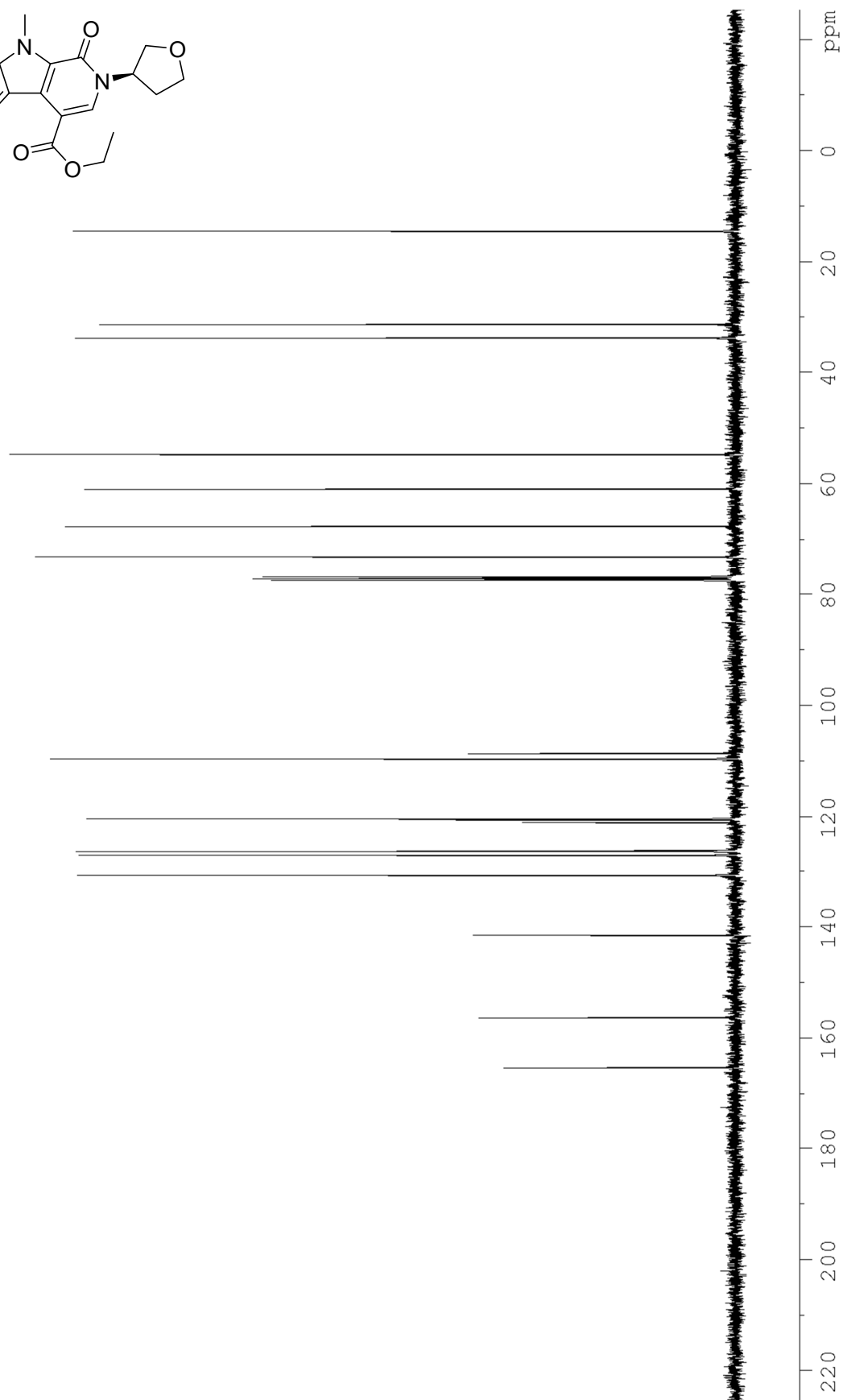
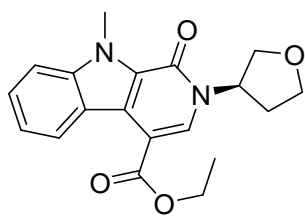


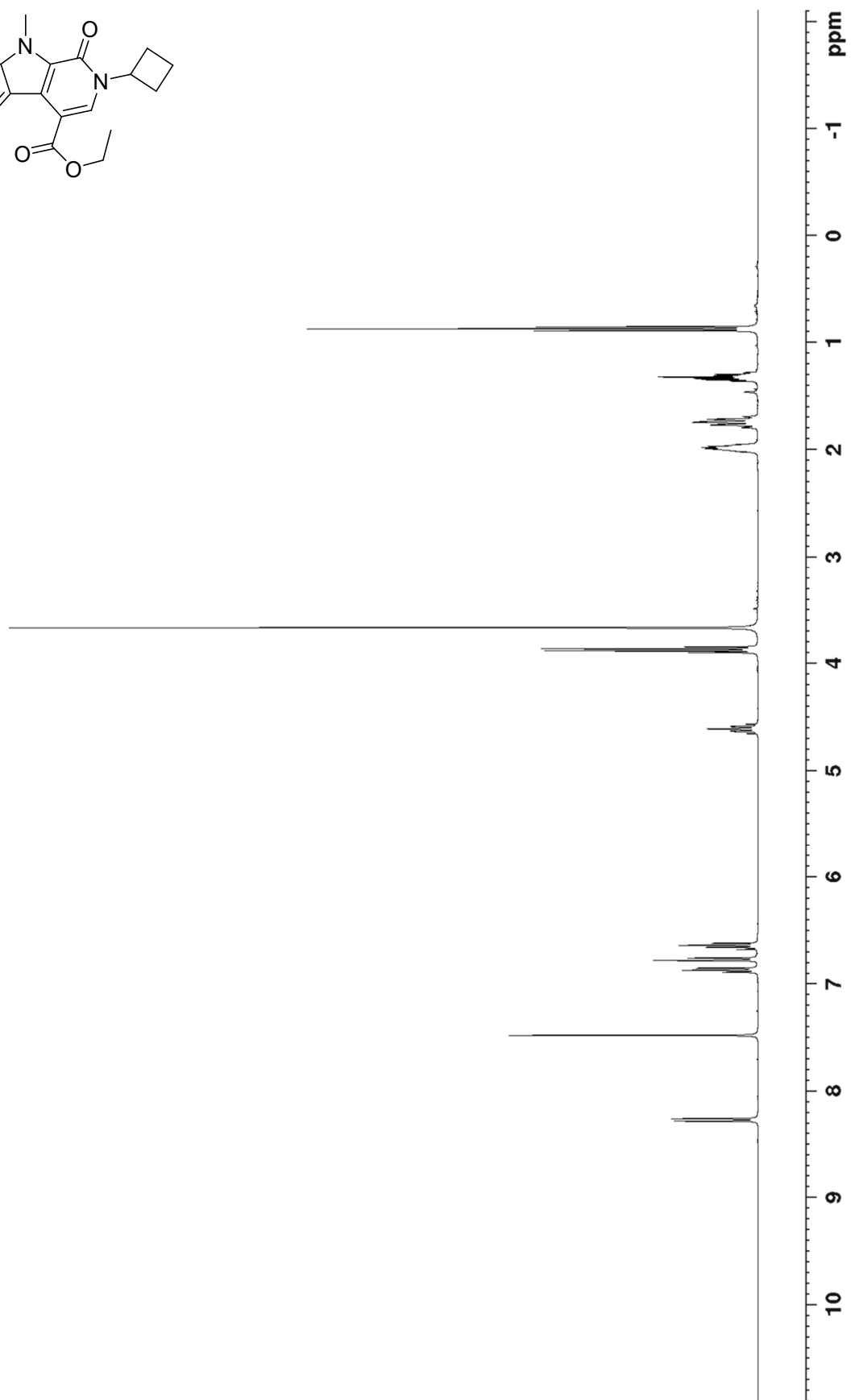
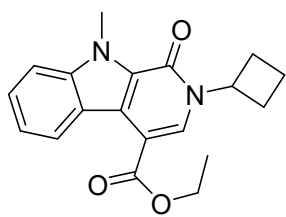


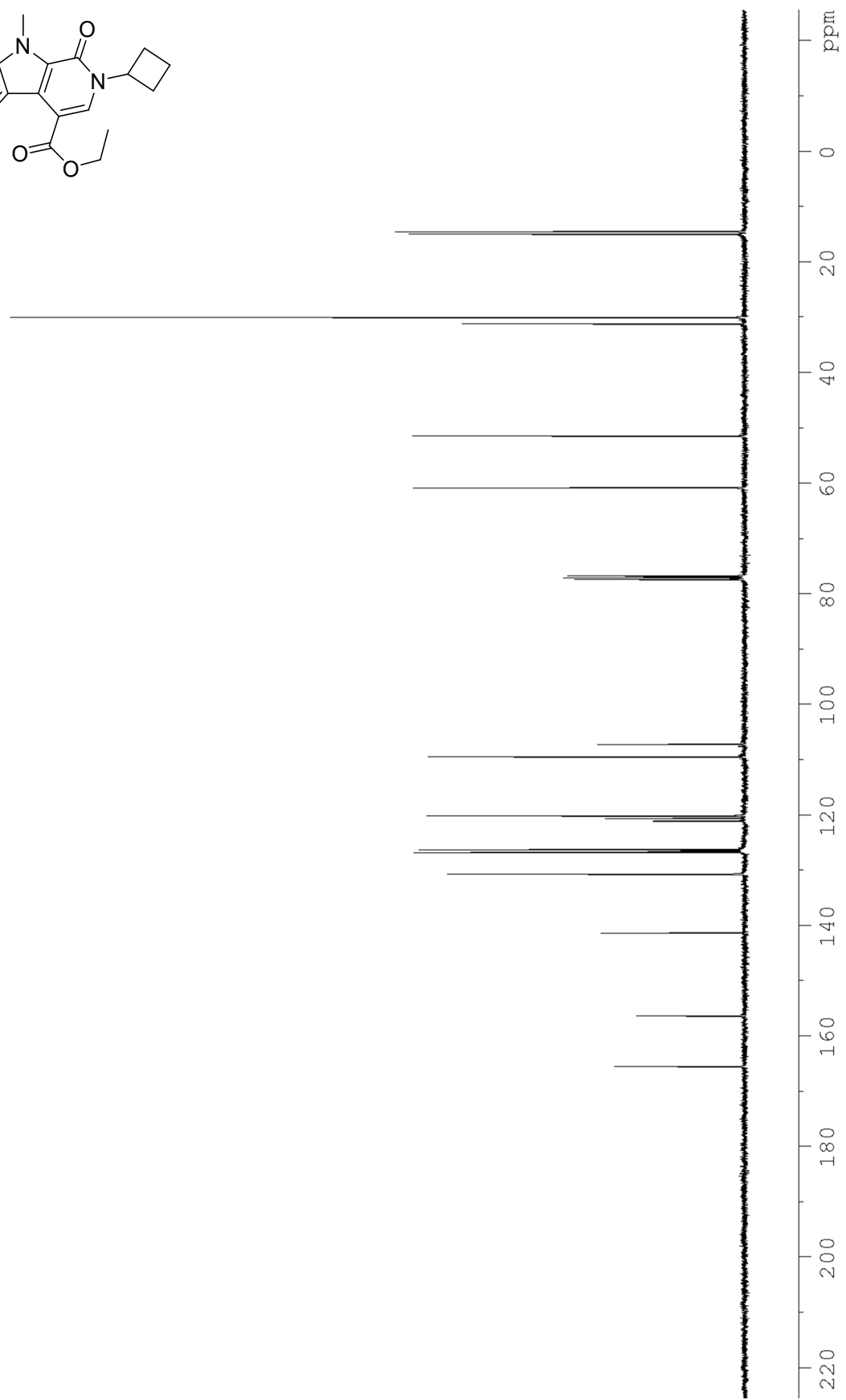
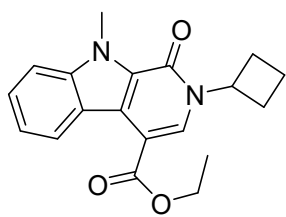


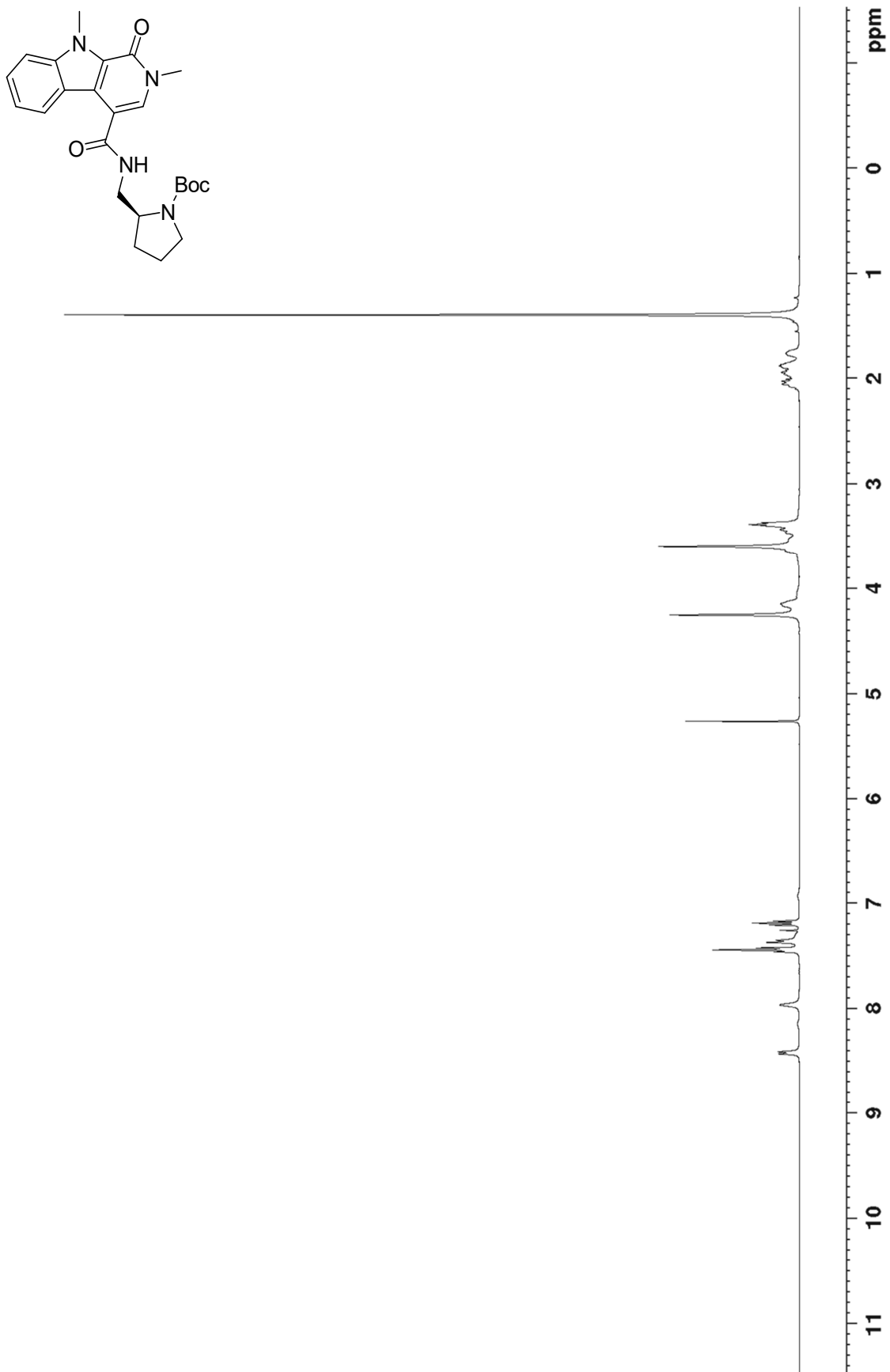


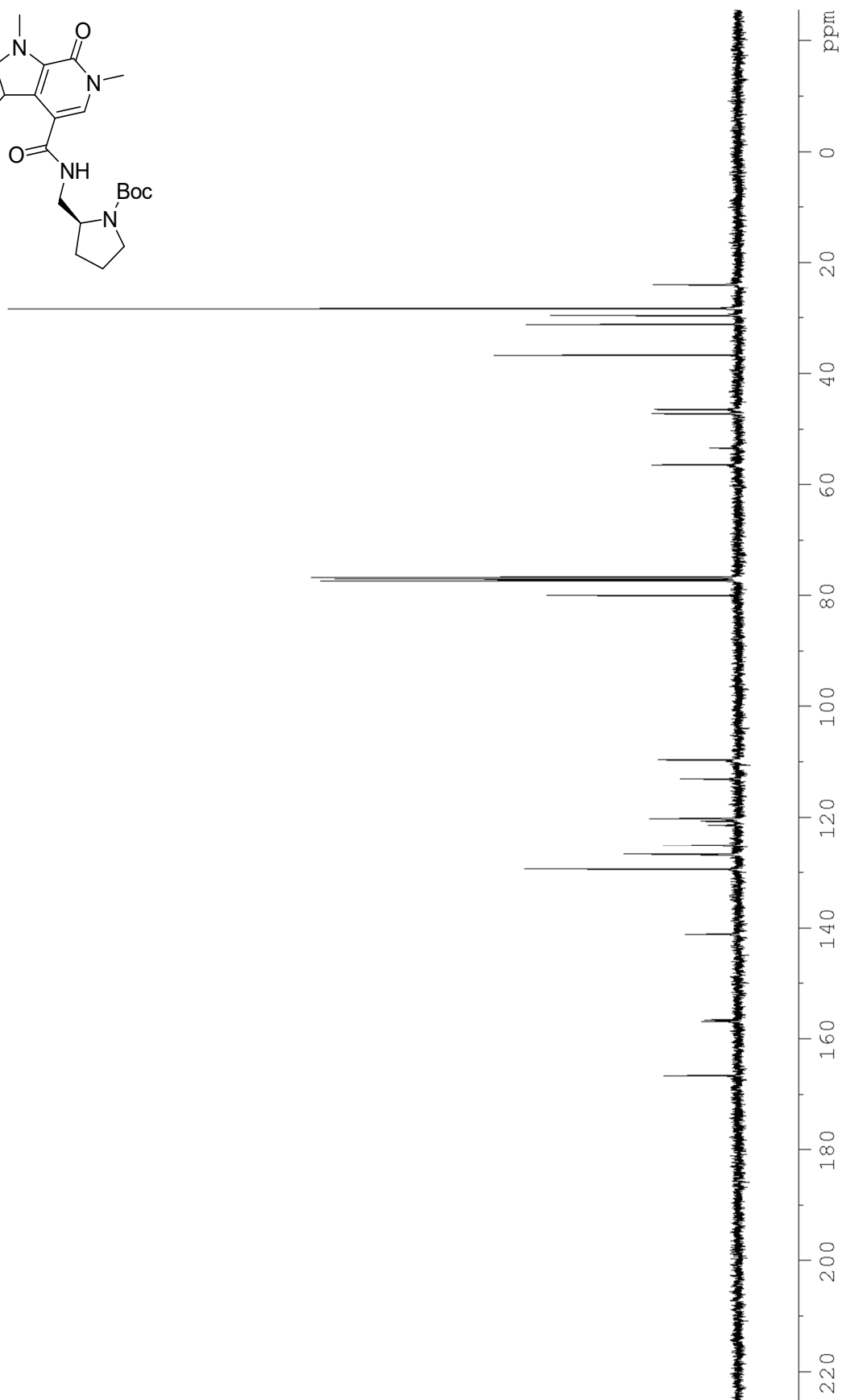
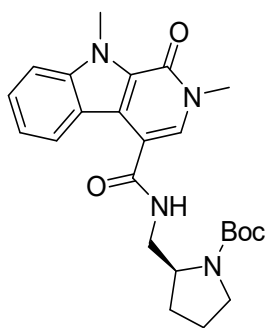


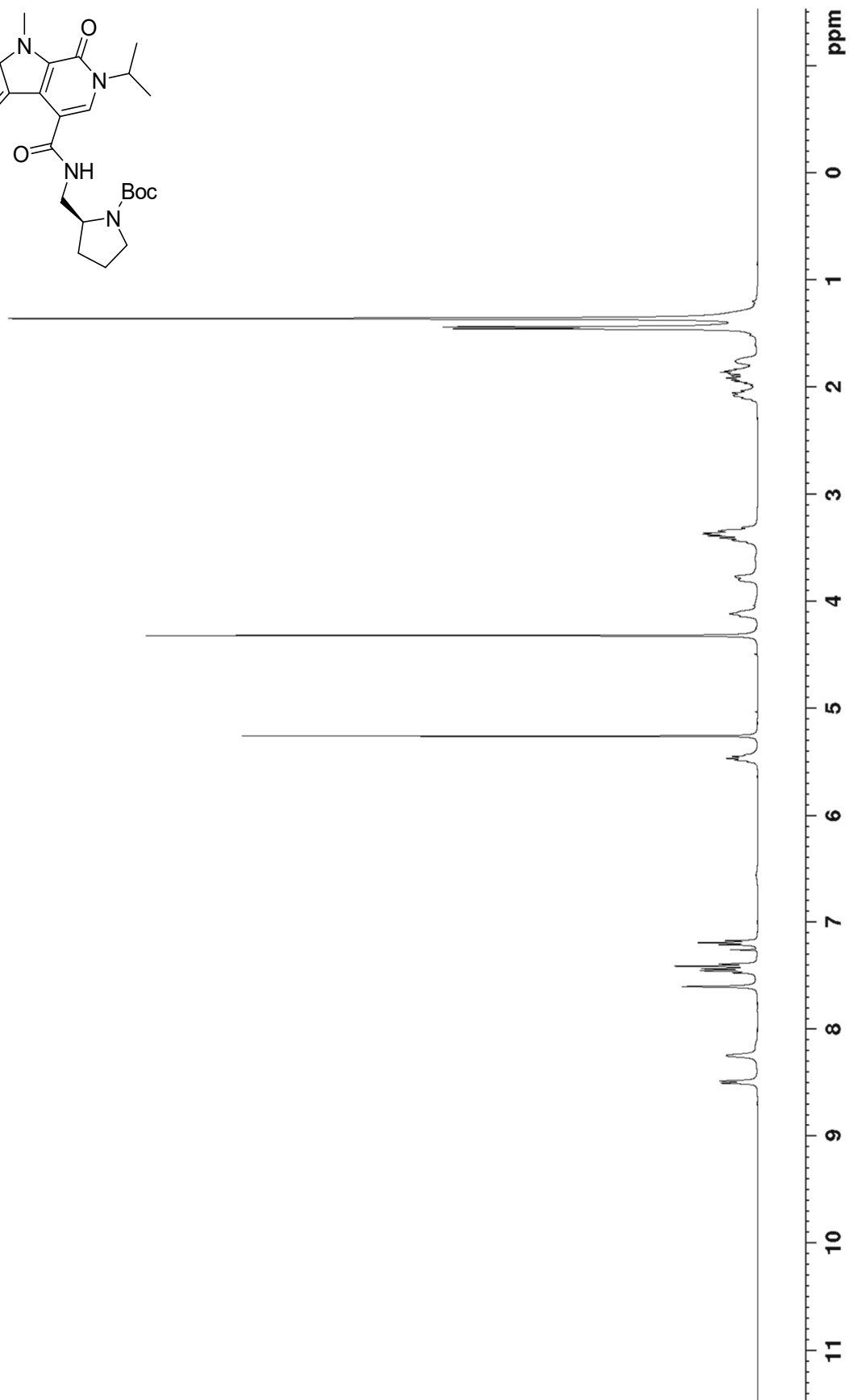
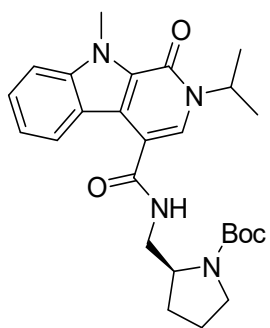


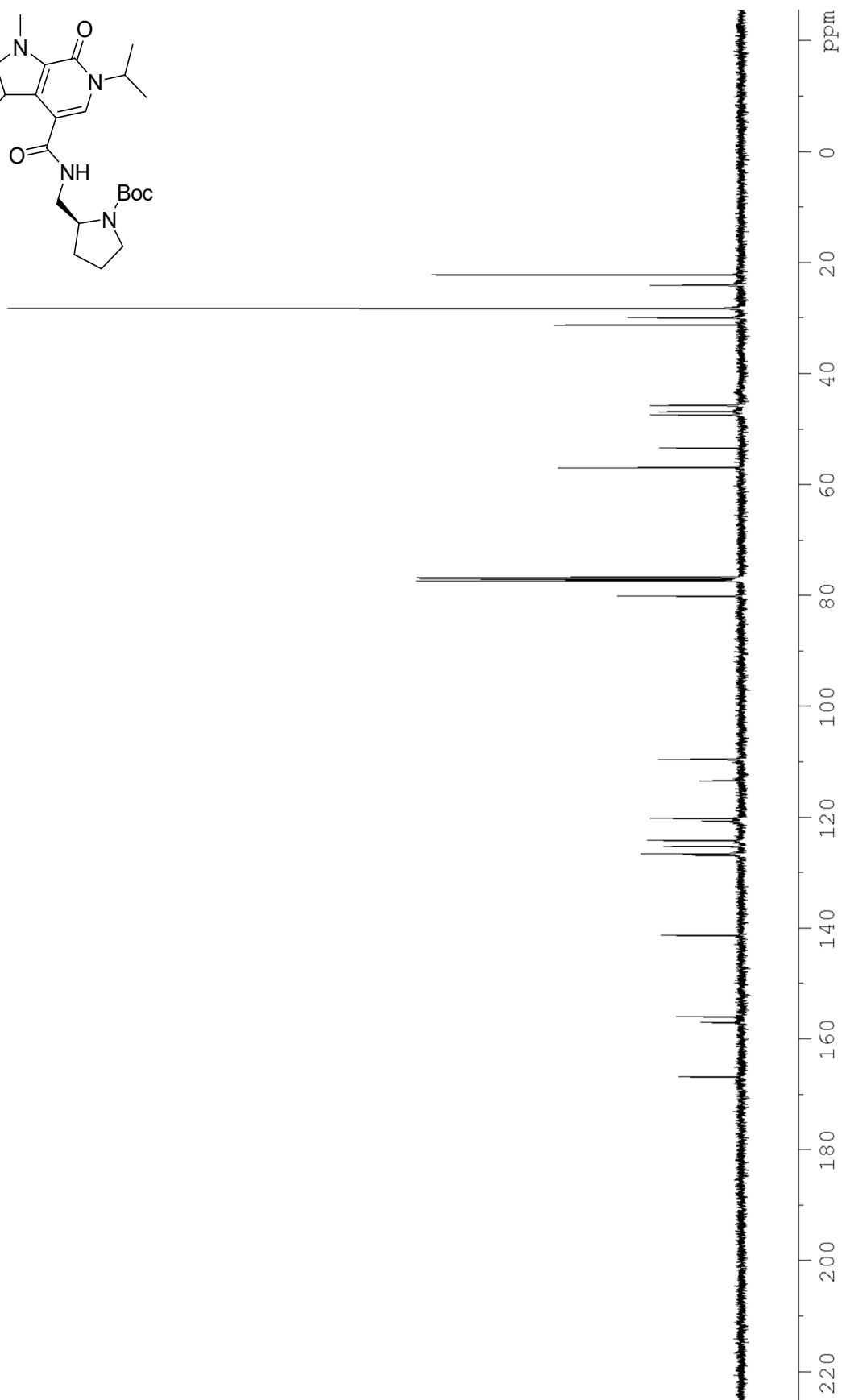
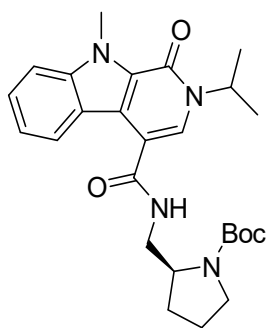


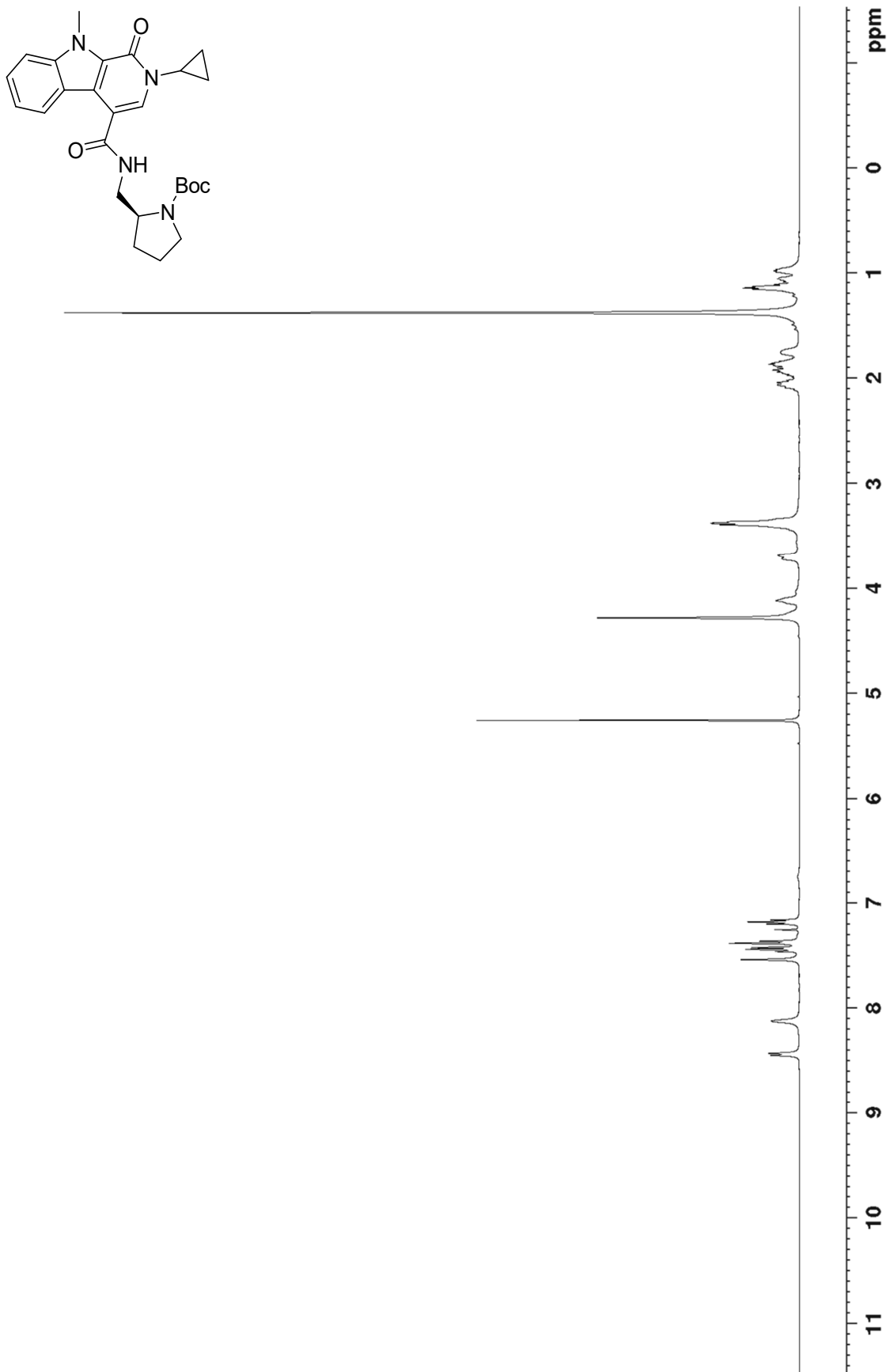


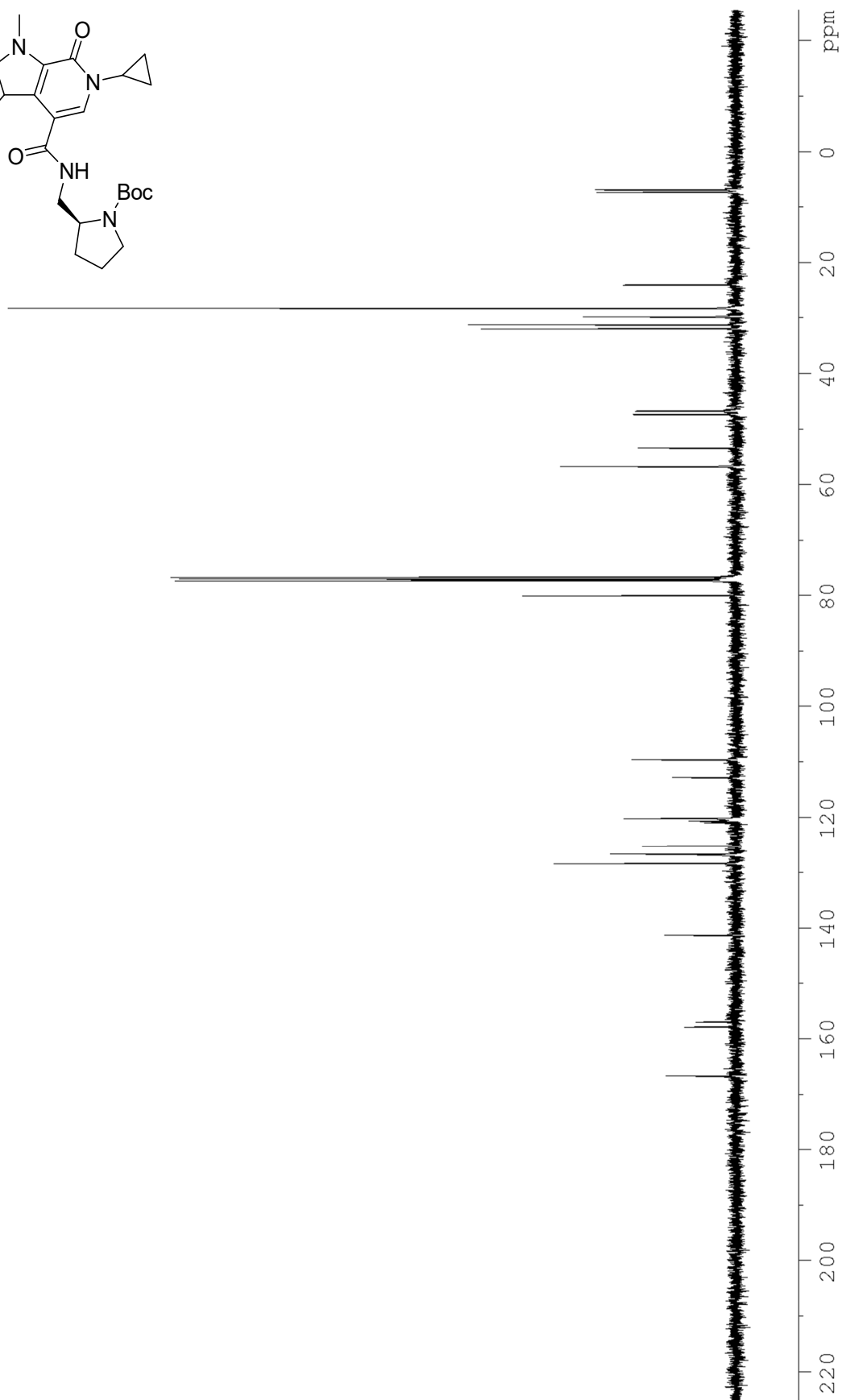
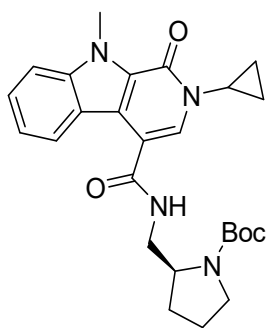


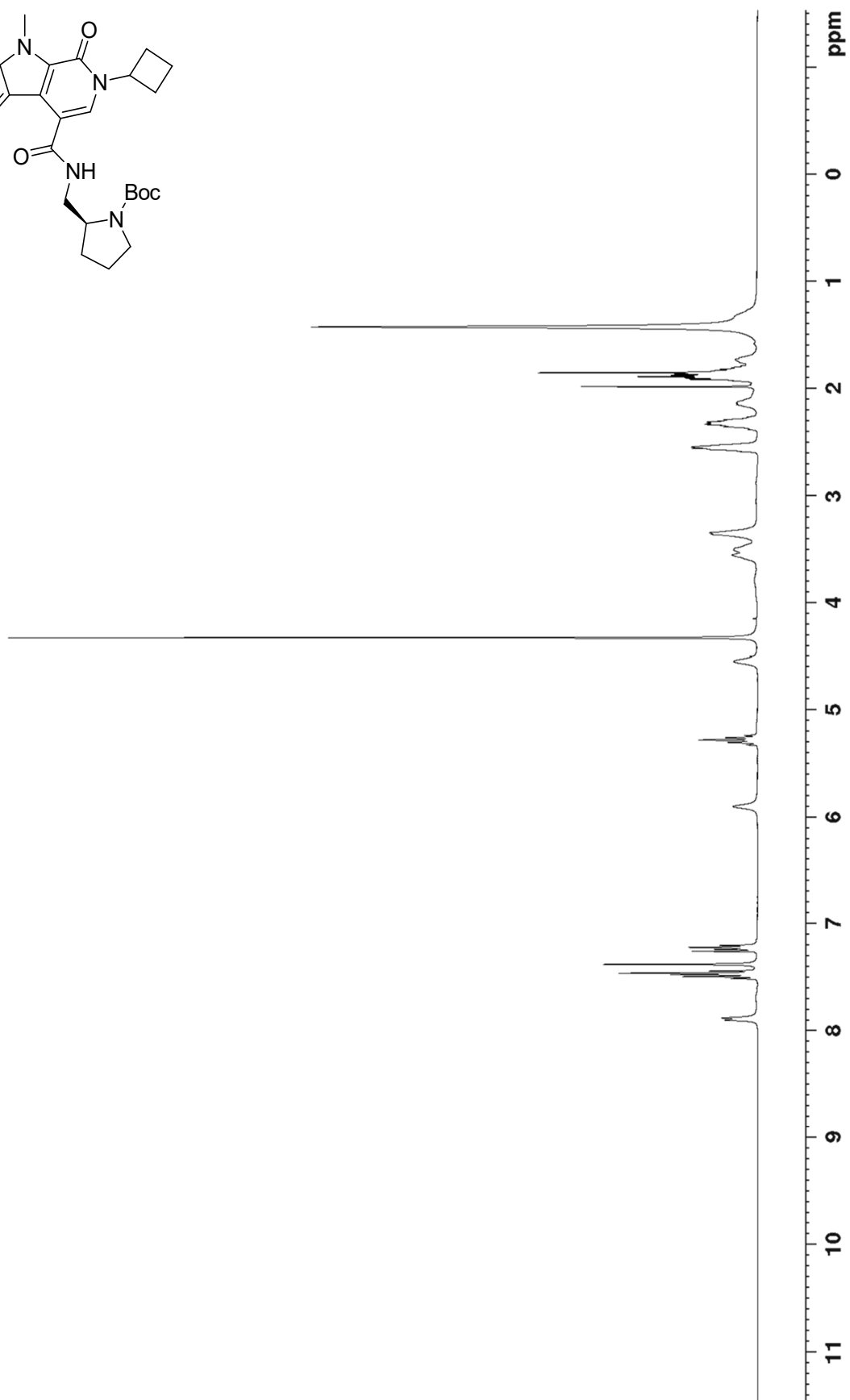
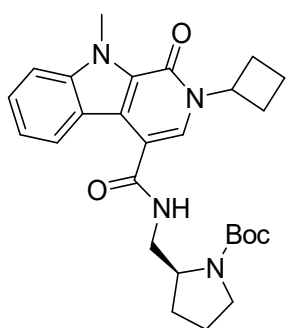


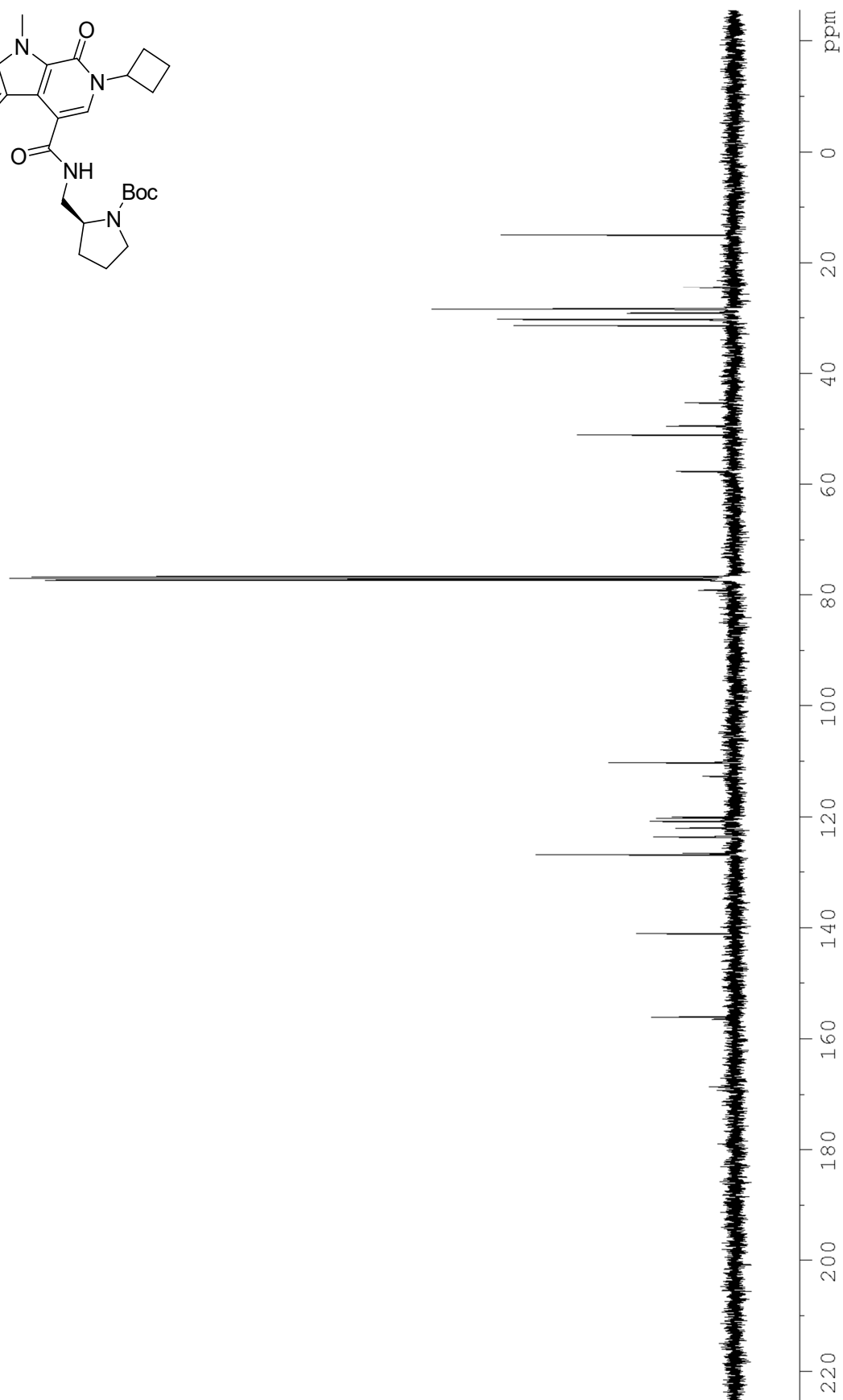
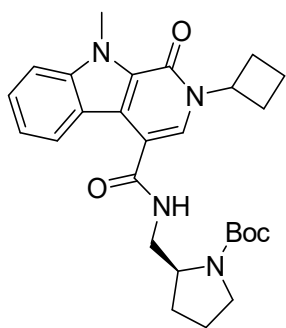


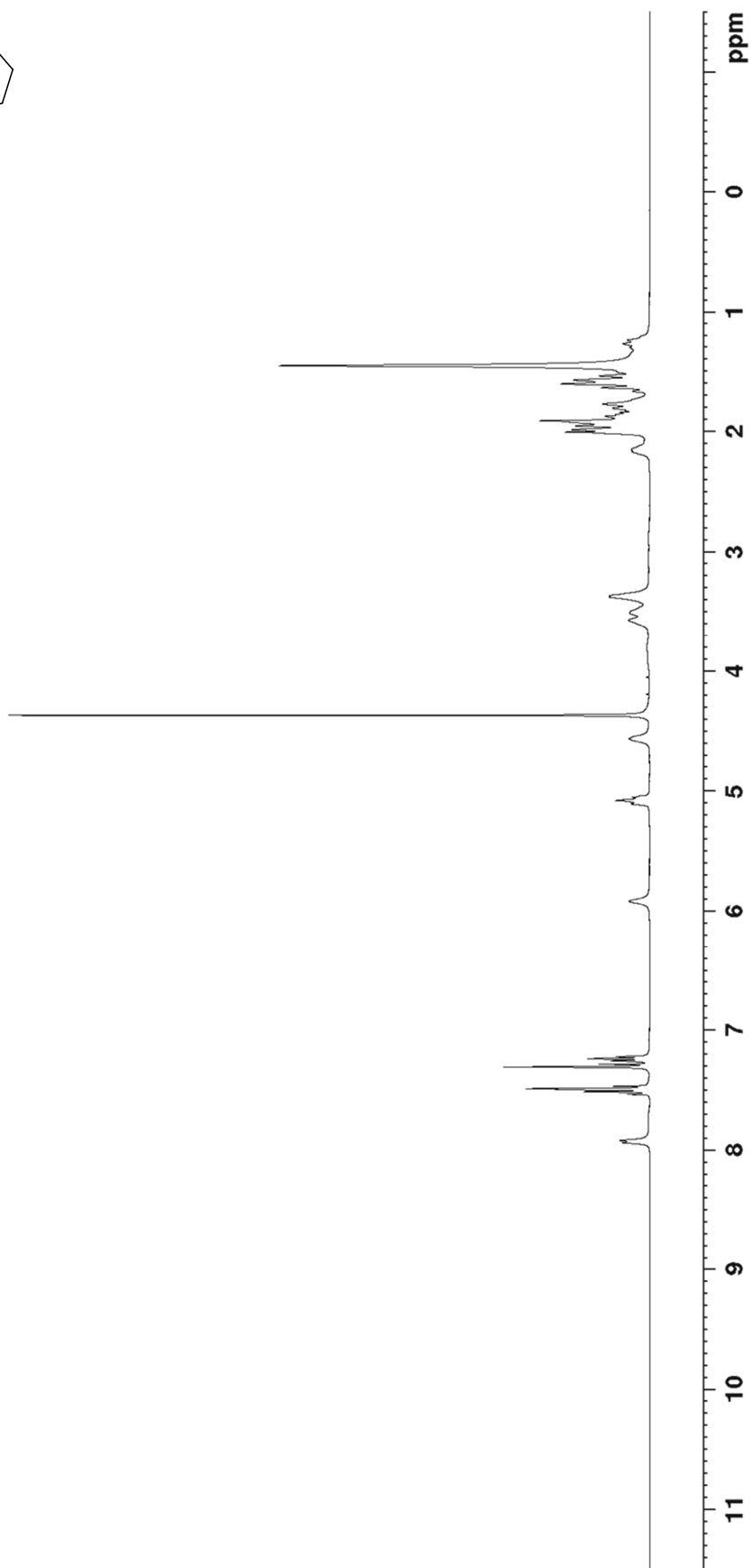
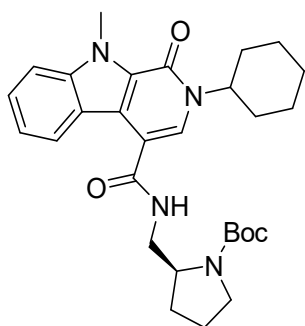


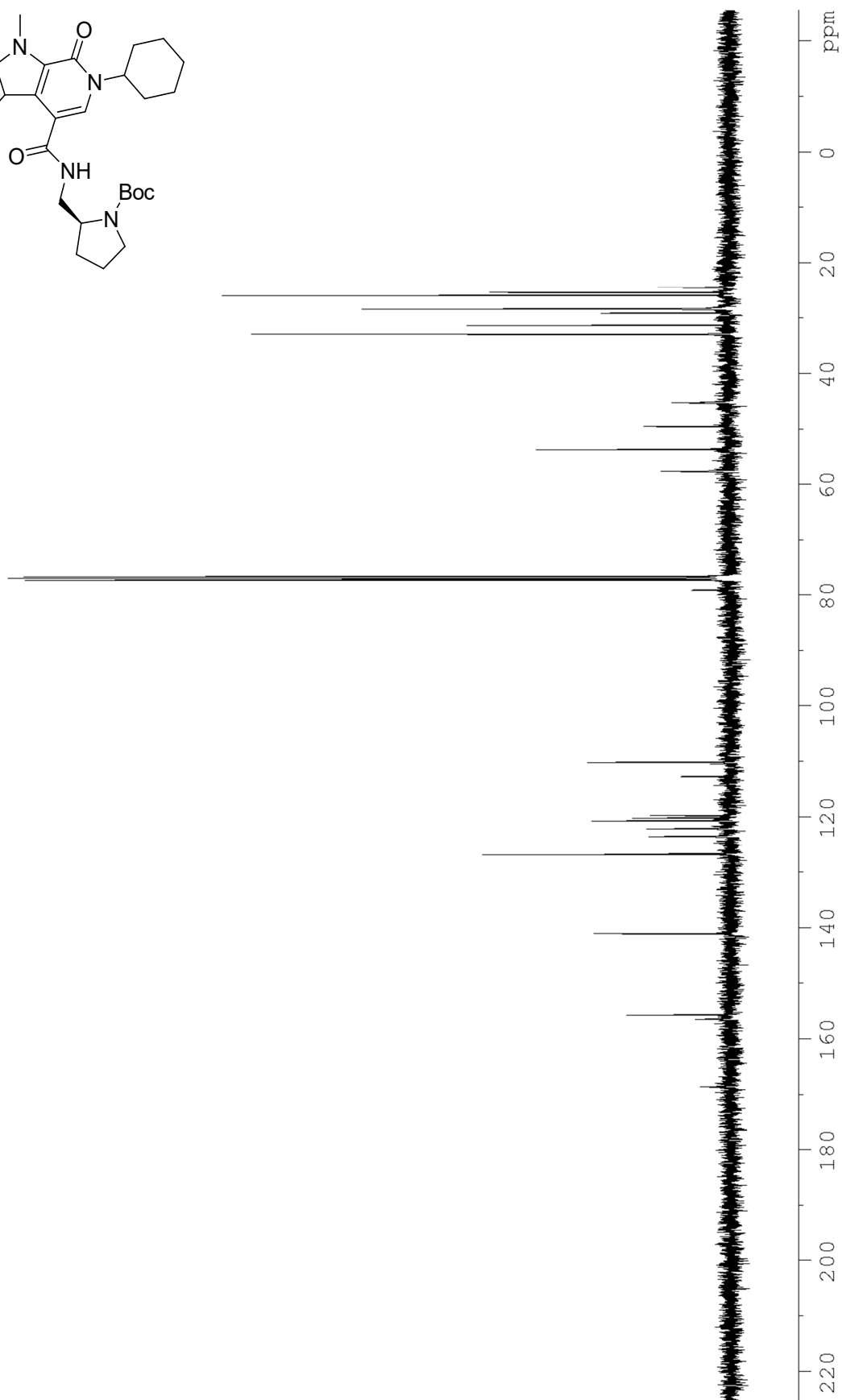
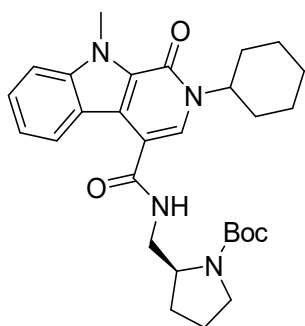


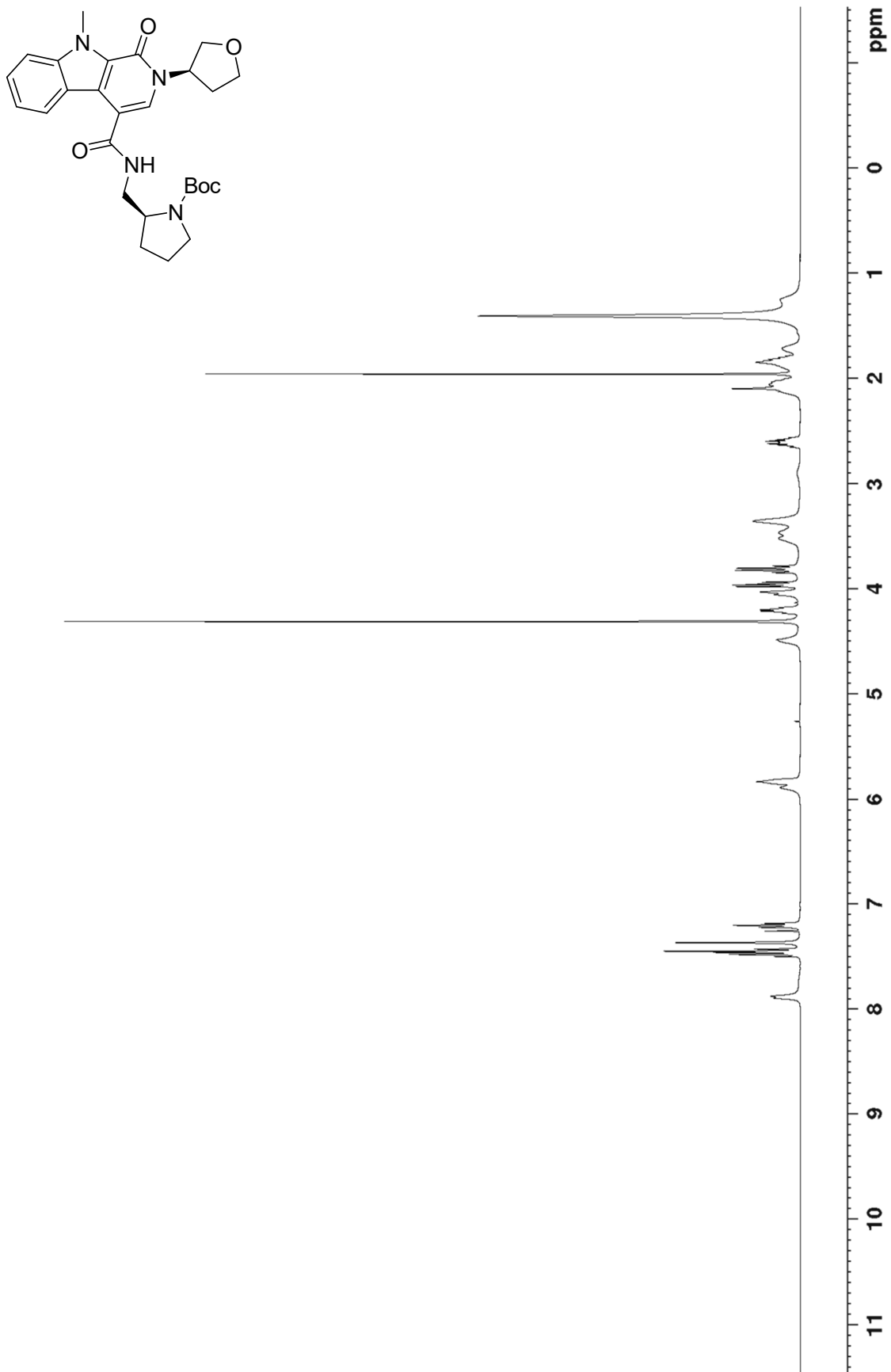


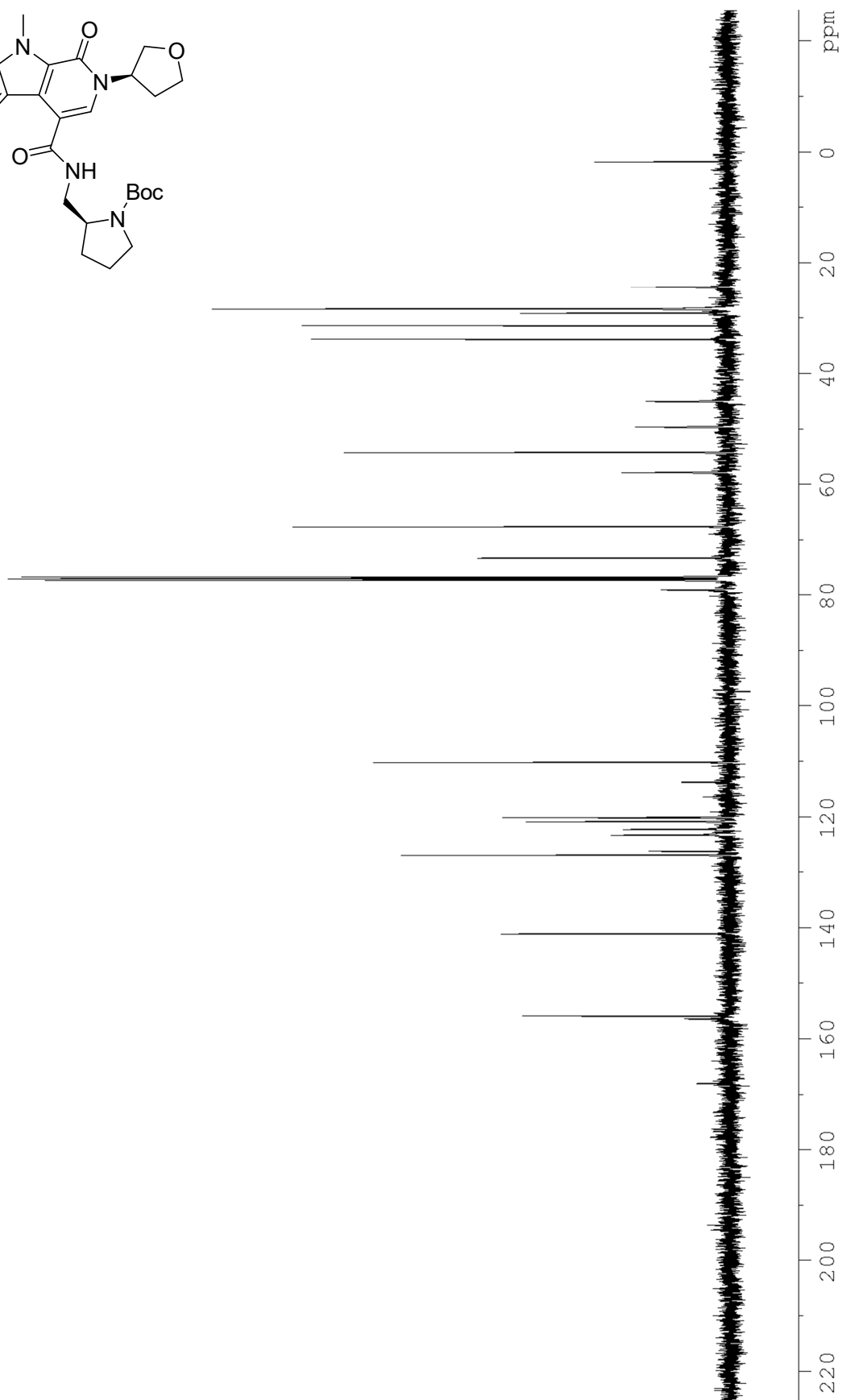
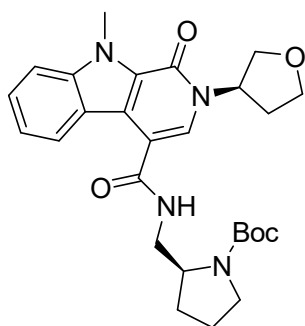


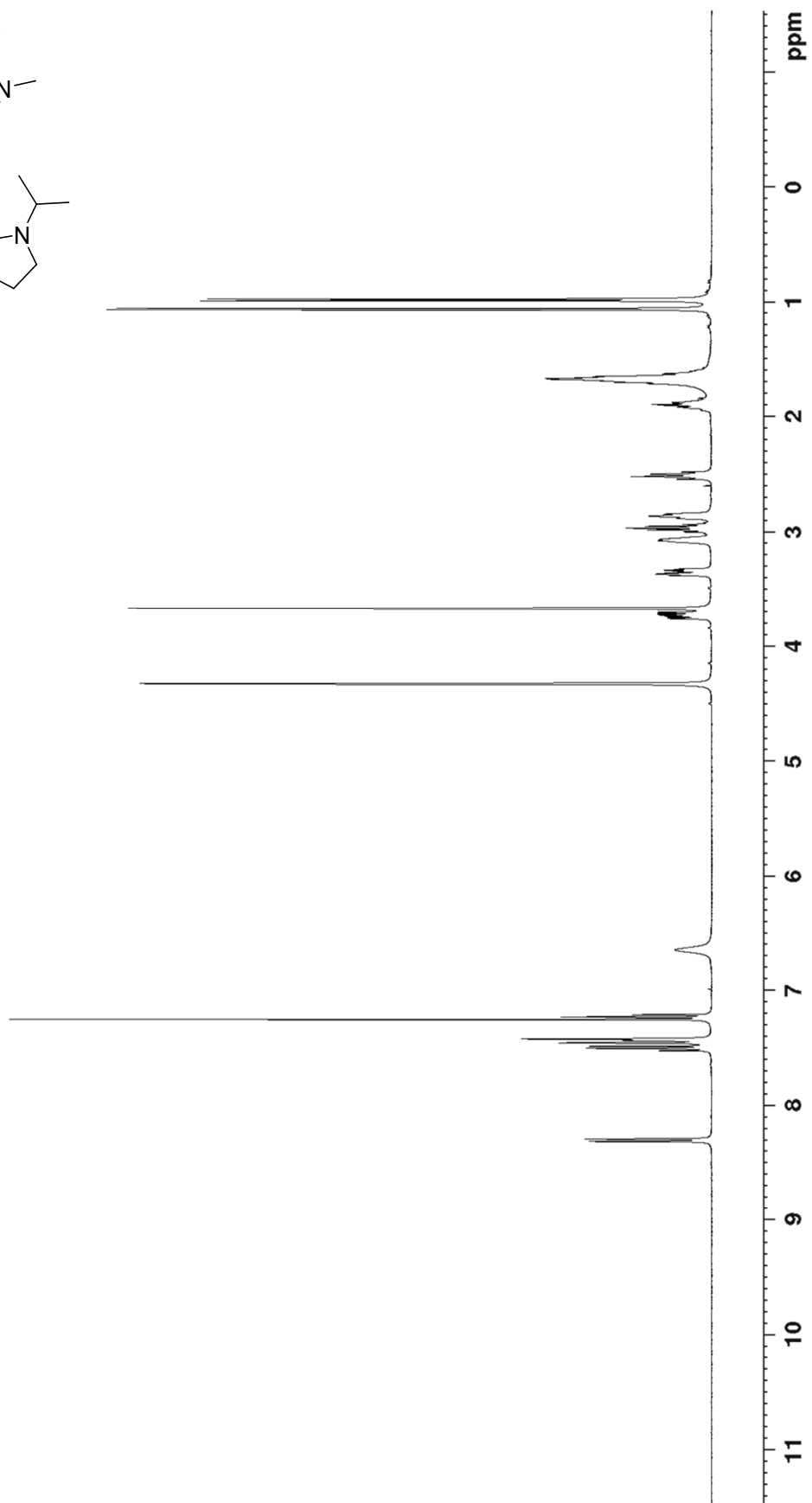
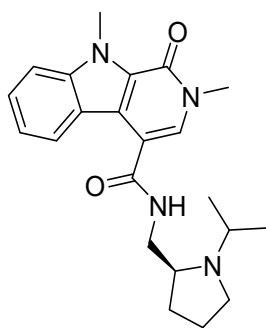


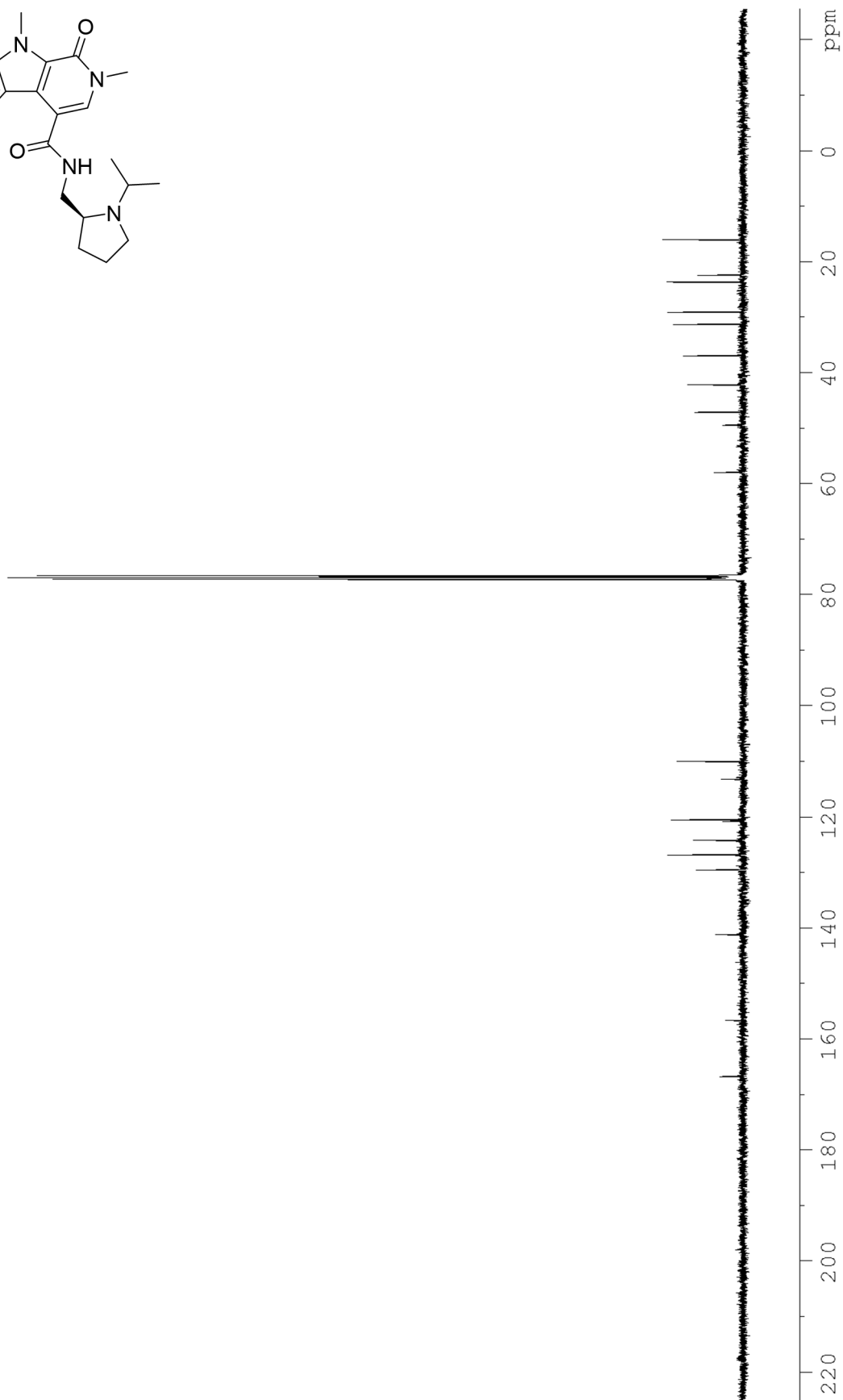
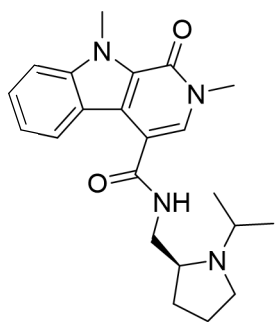


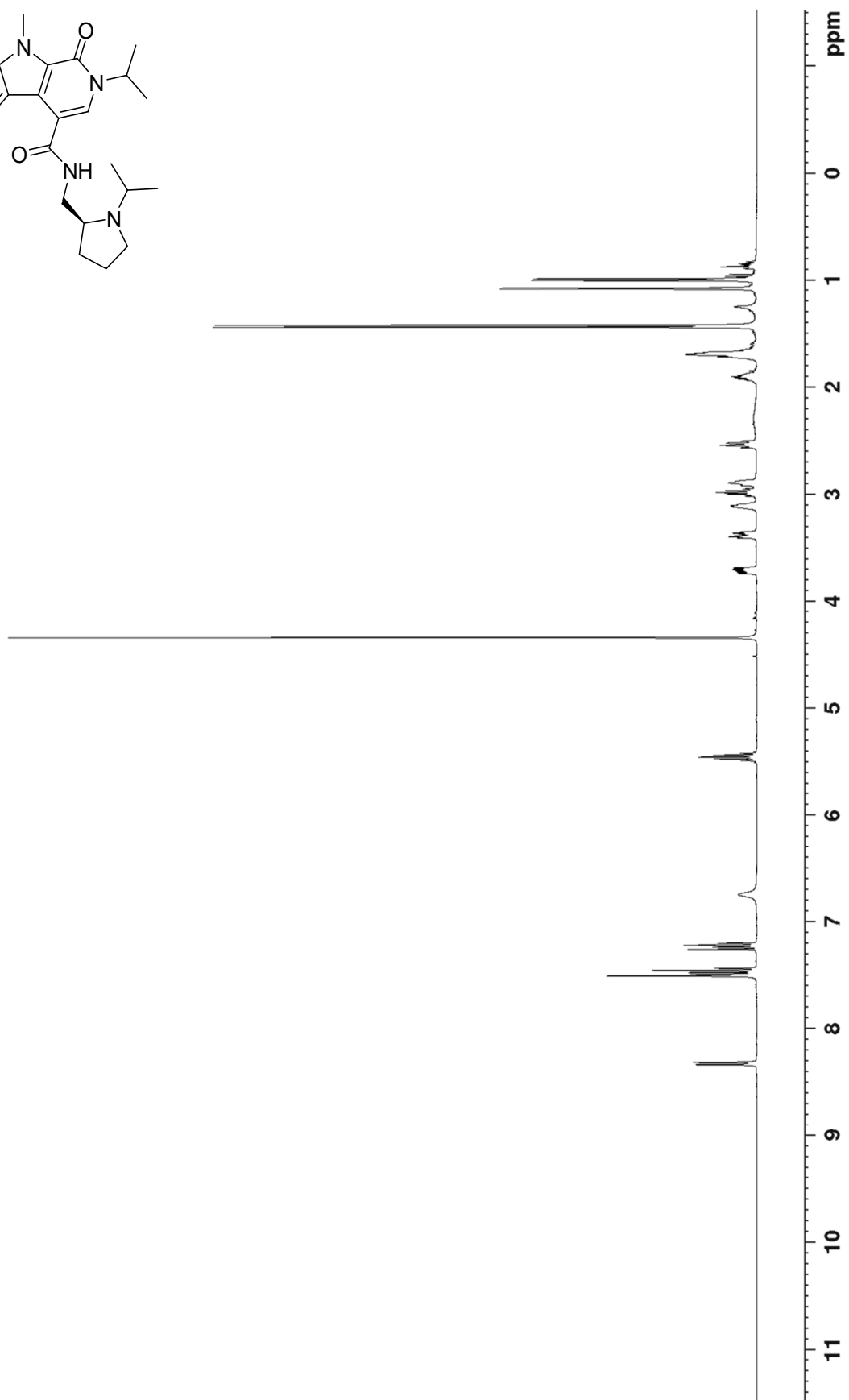
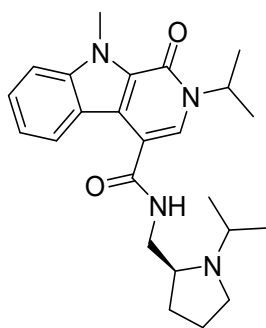


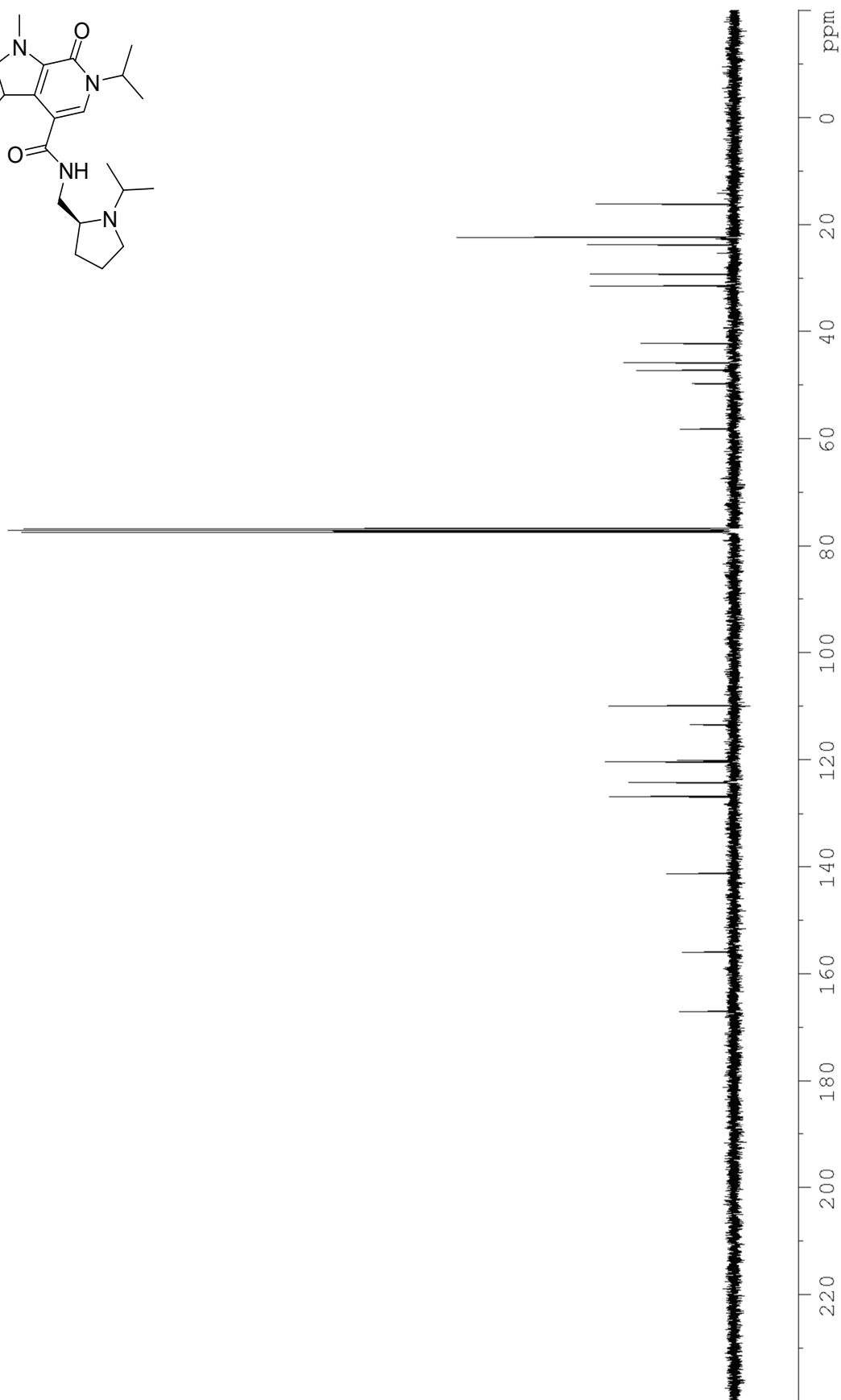
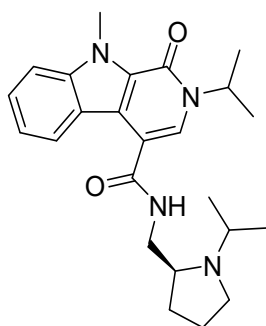


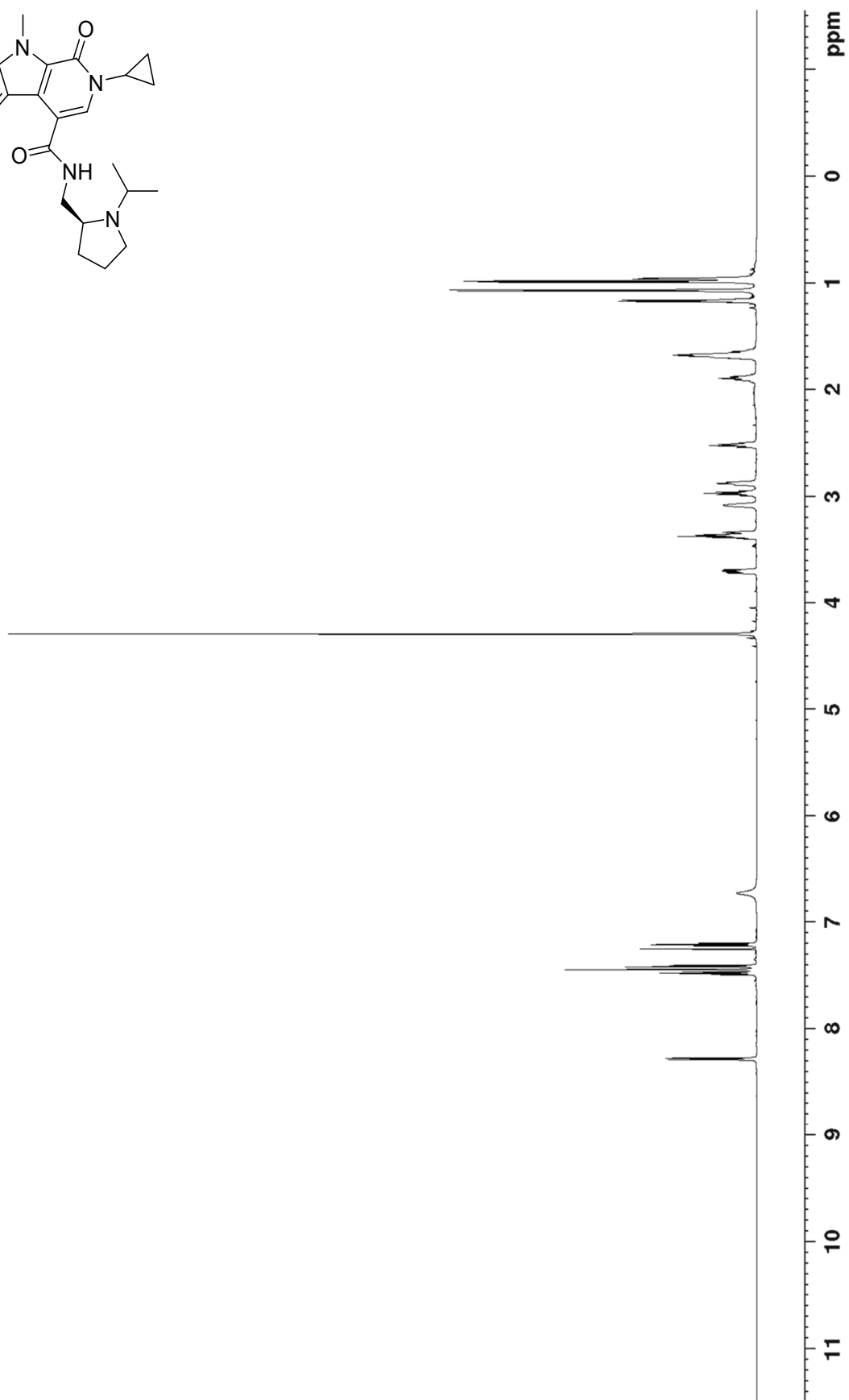
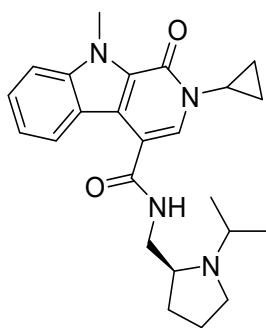


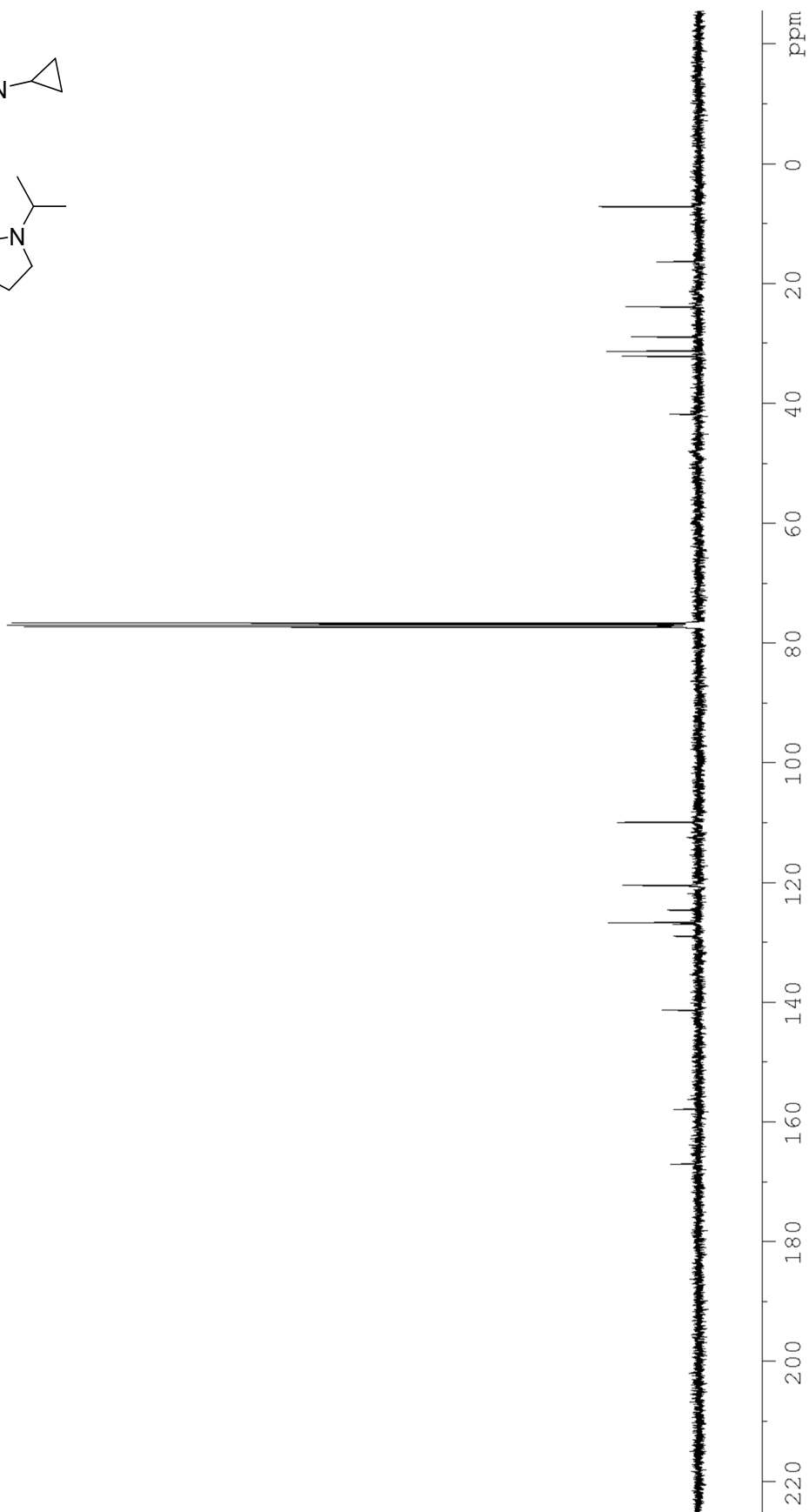
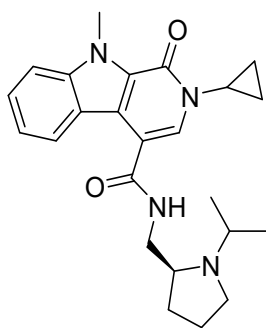


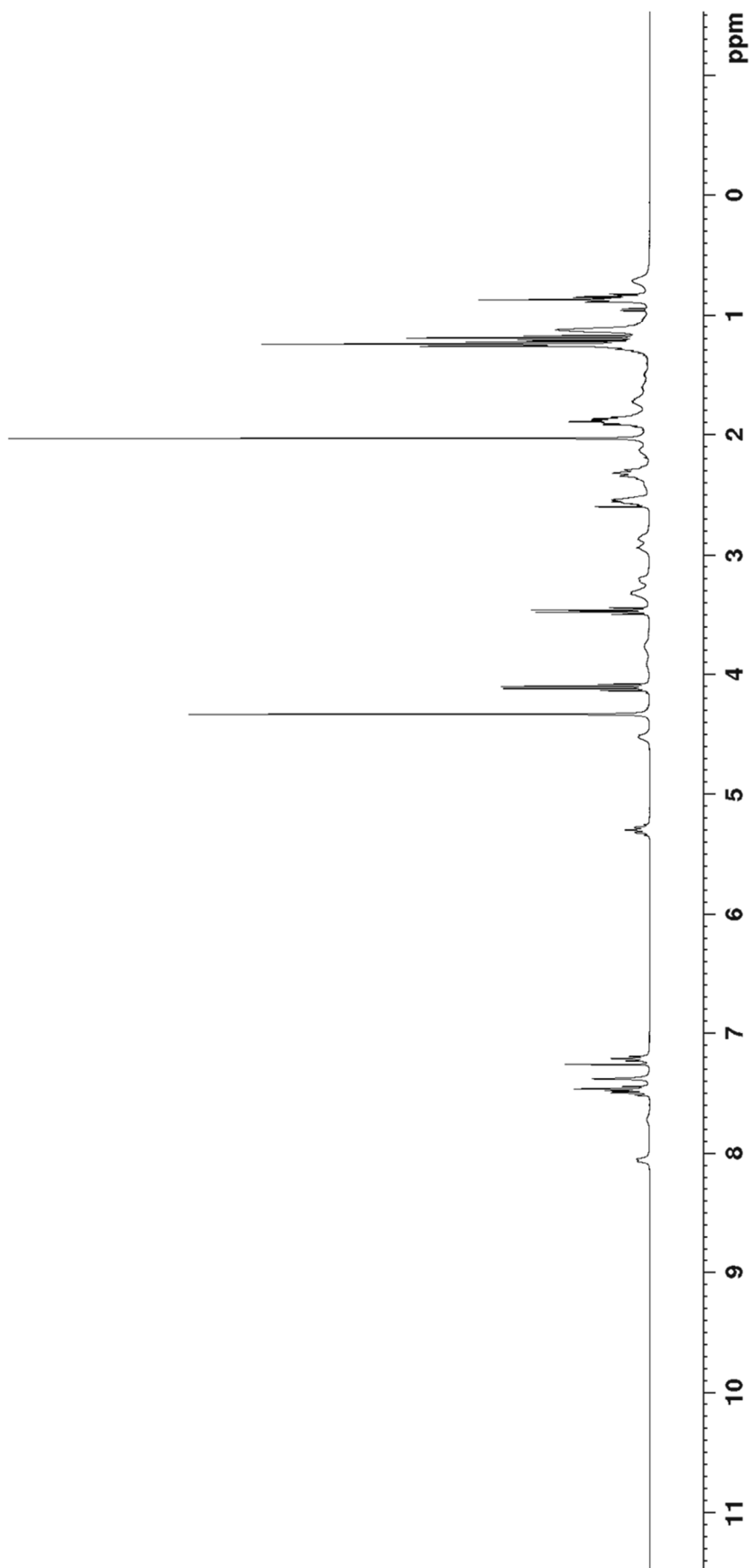
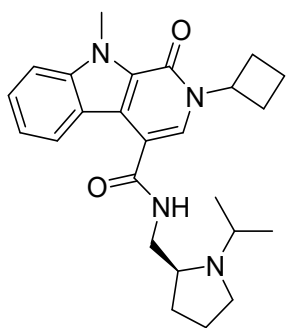


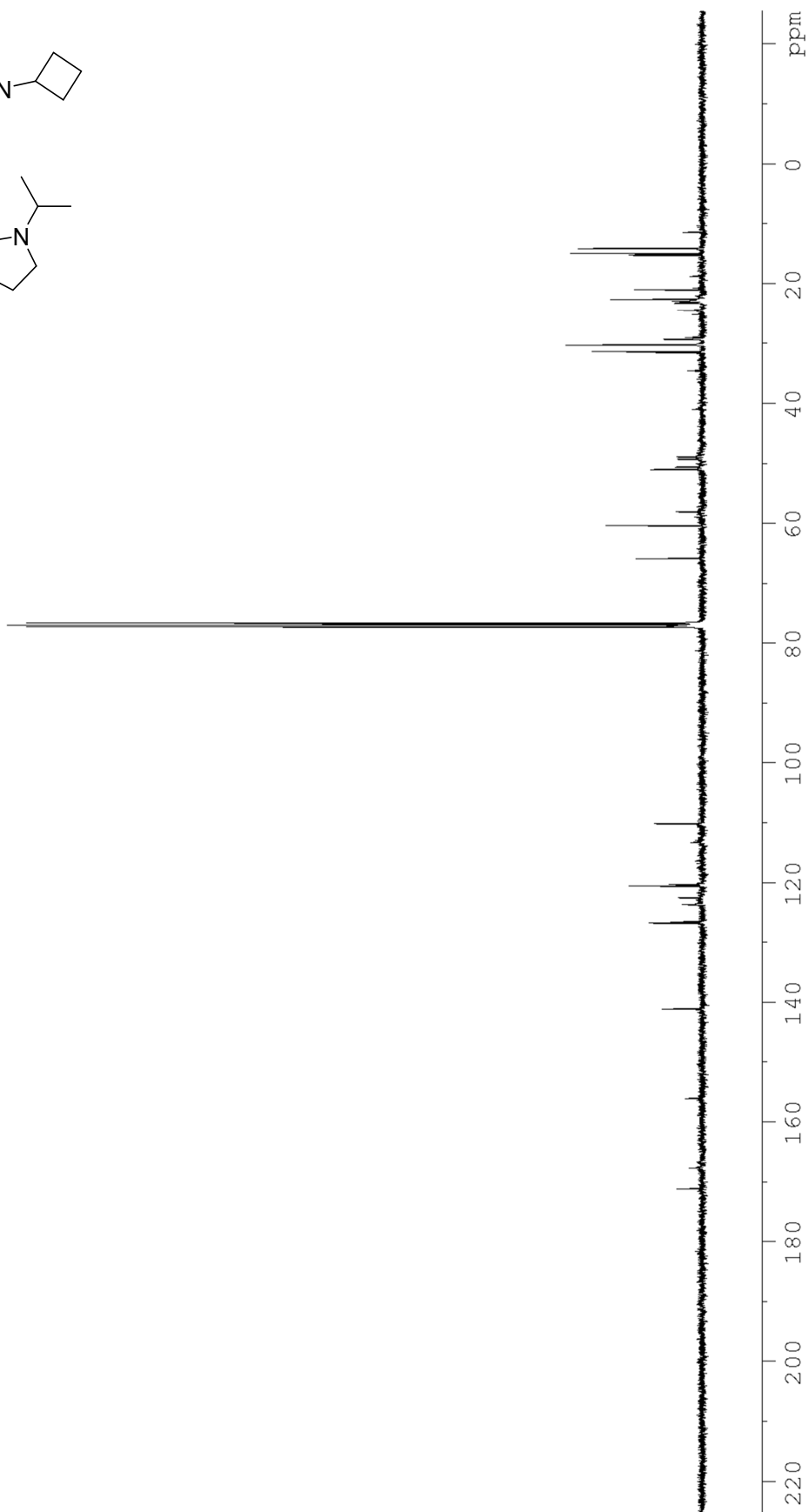
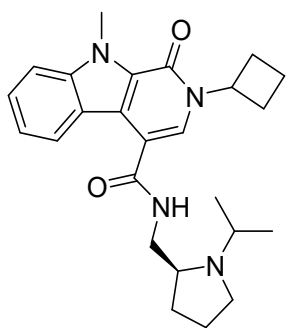


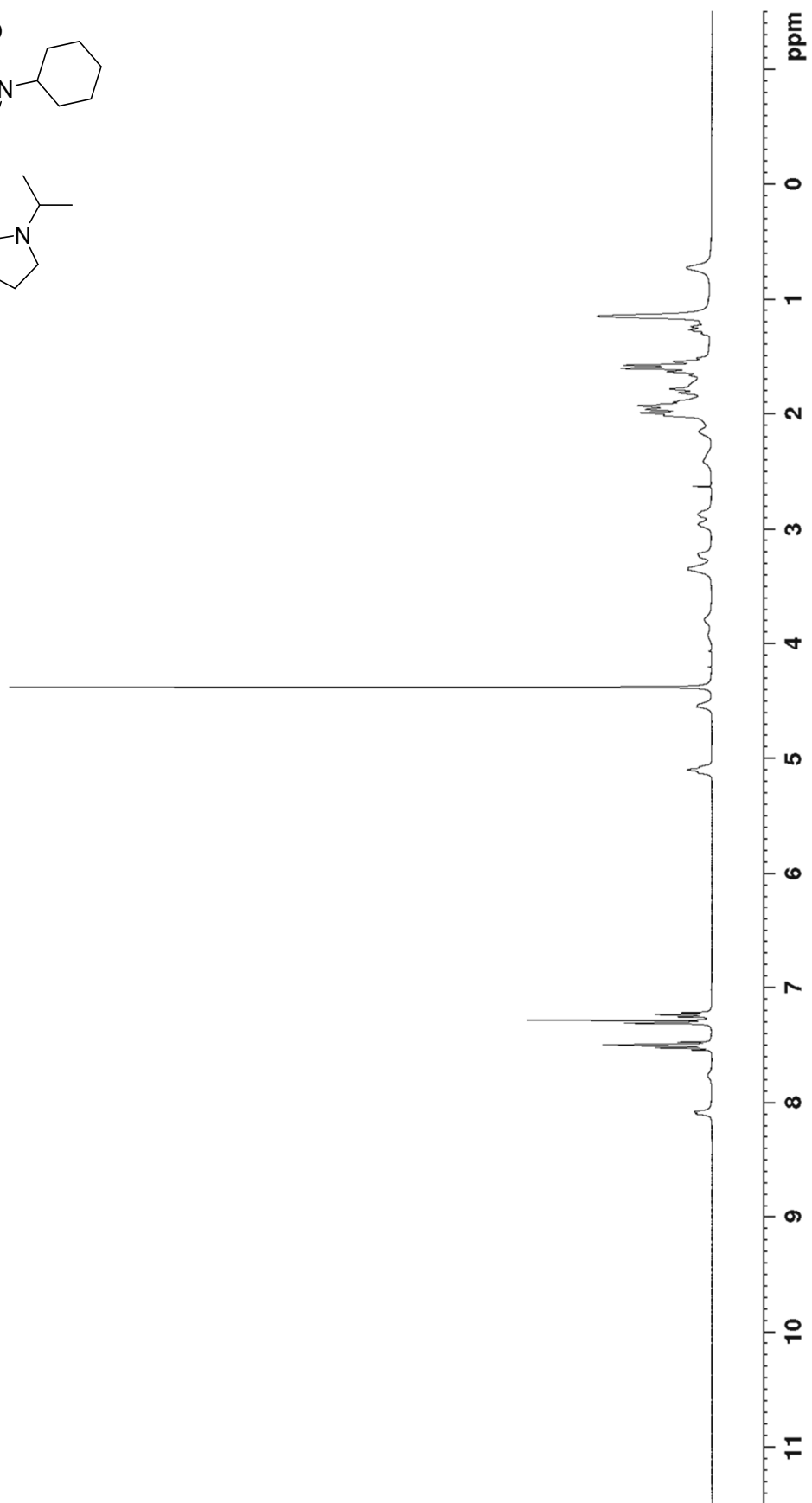
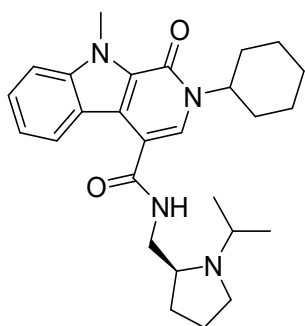


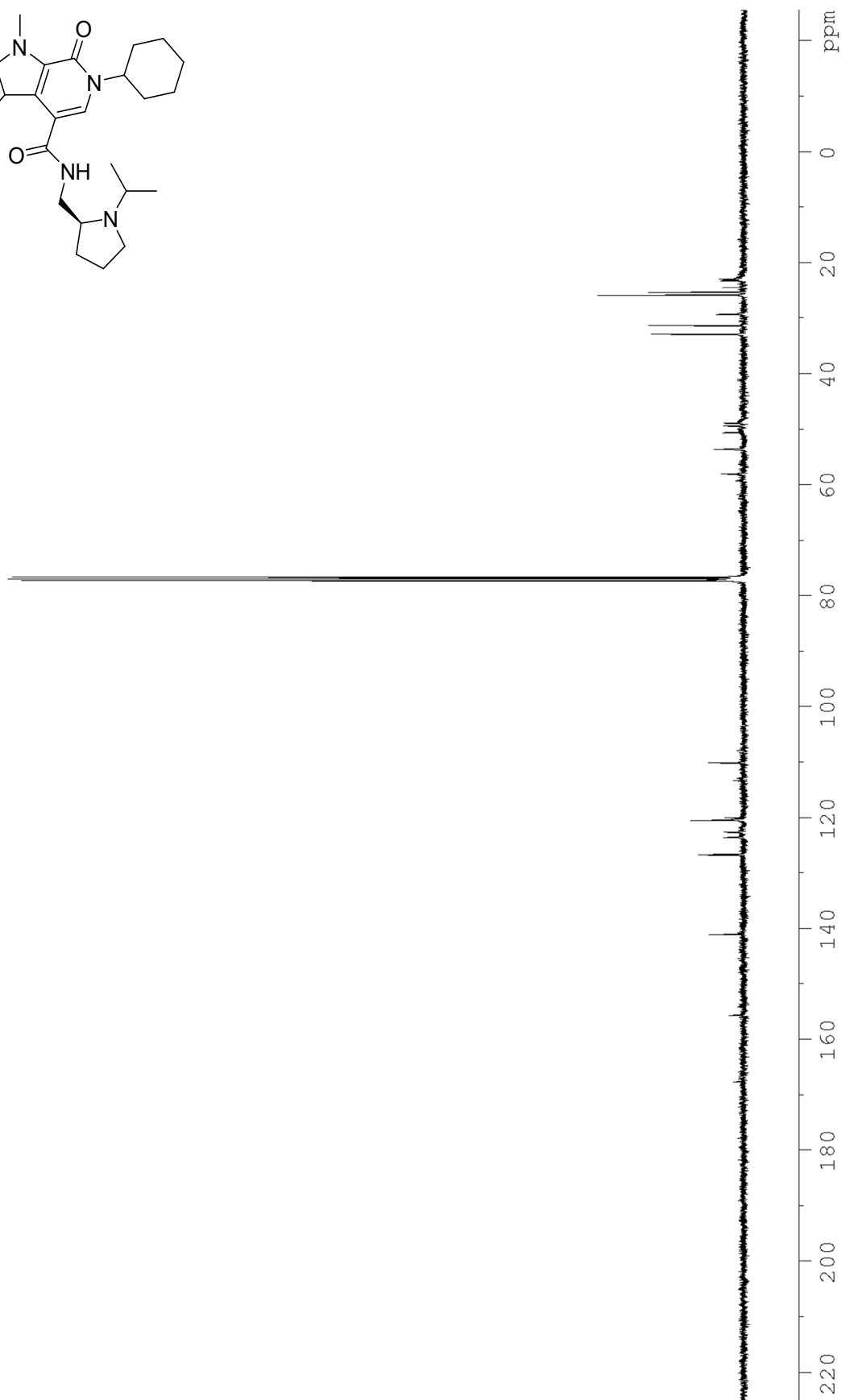
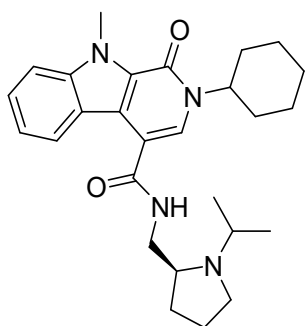






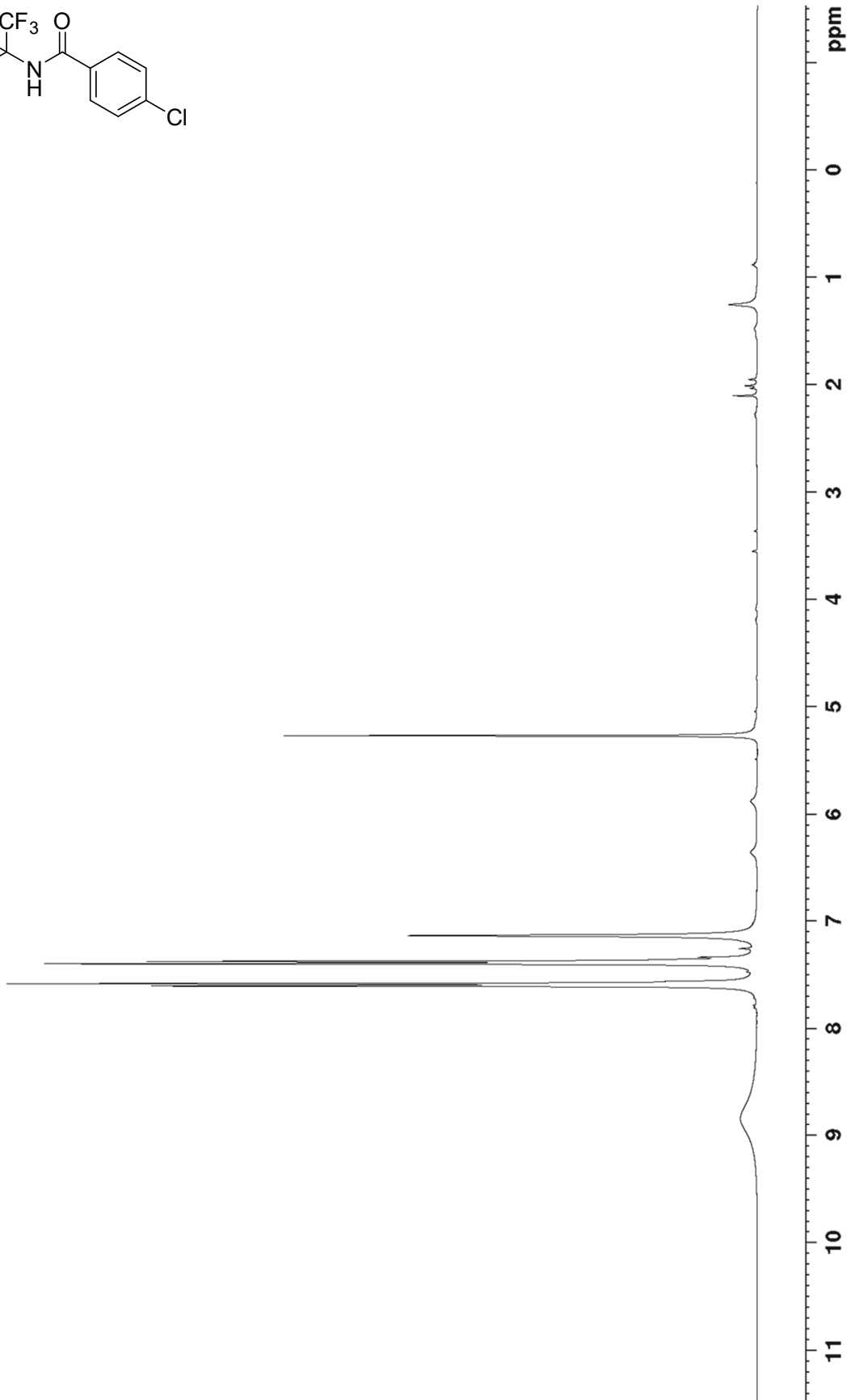
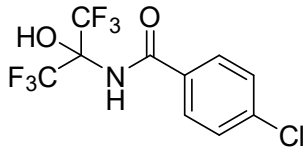


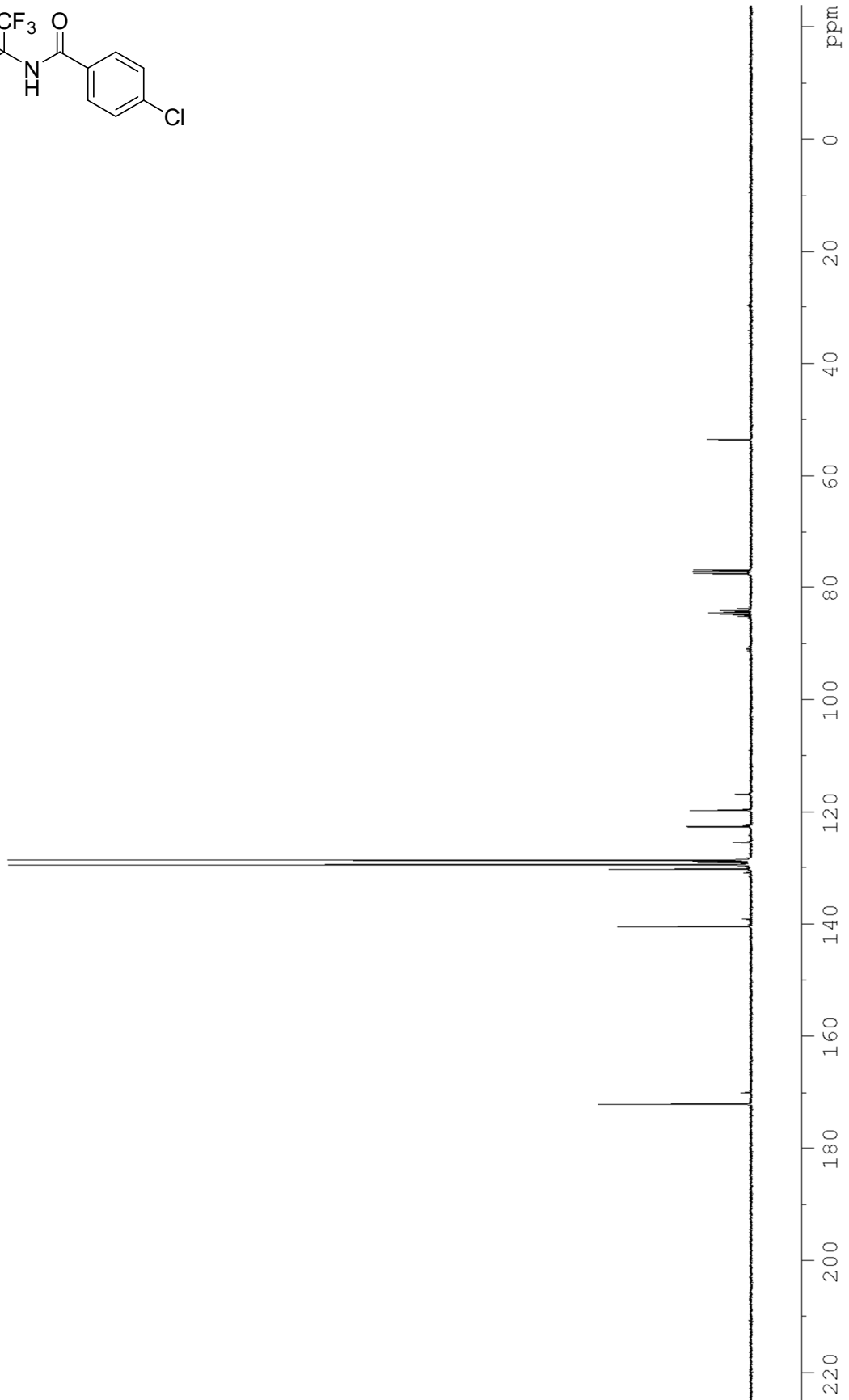
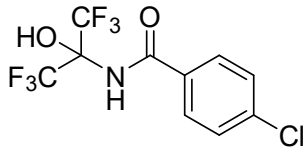


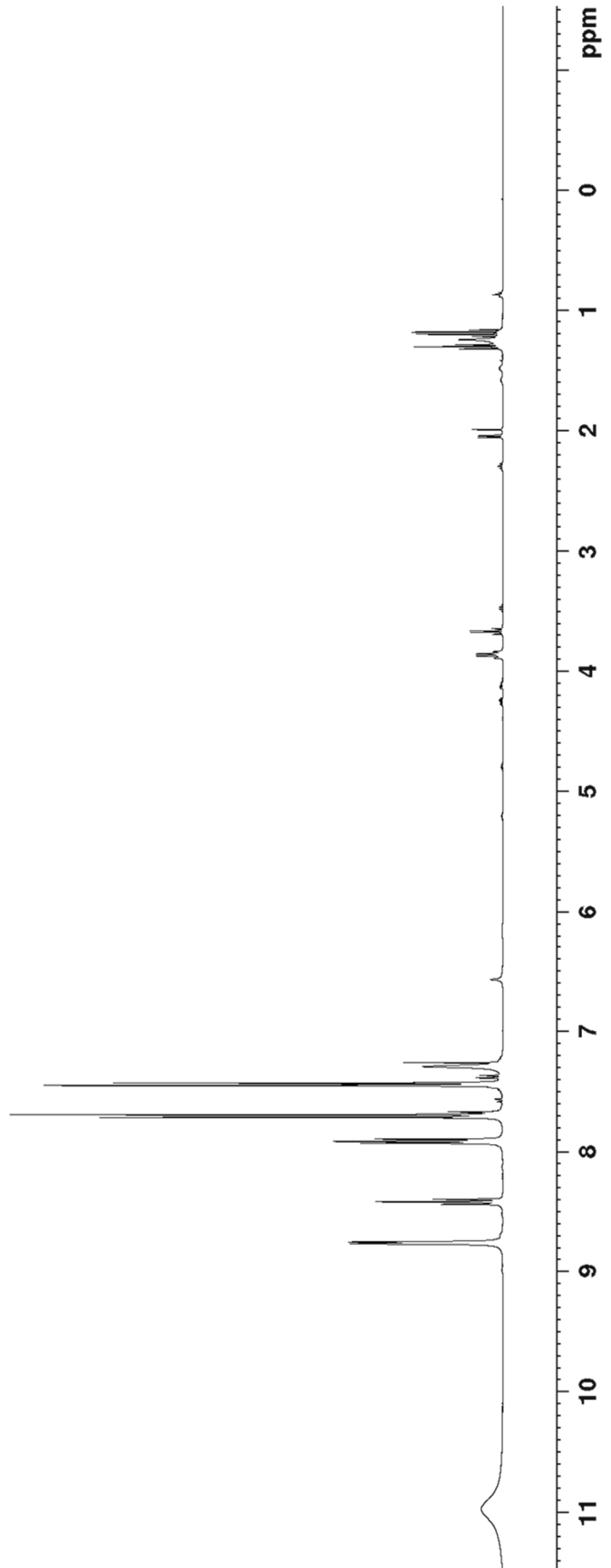
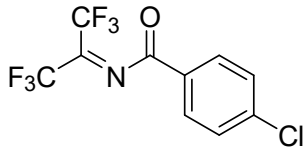


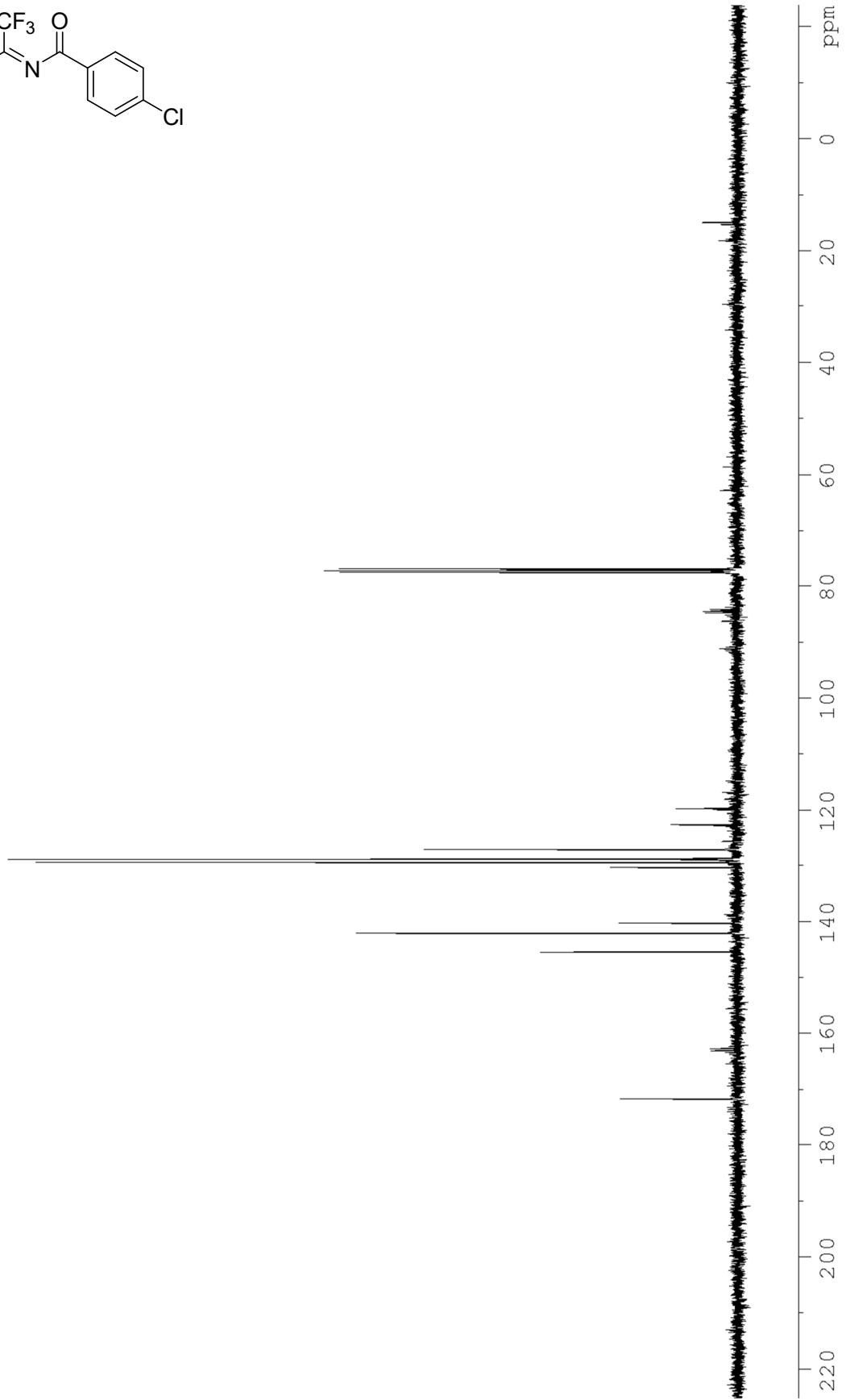
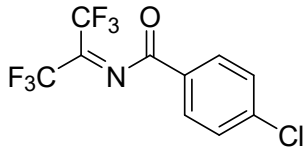
Appendix B

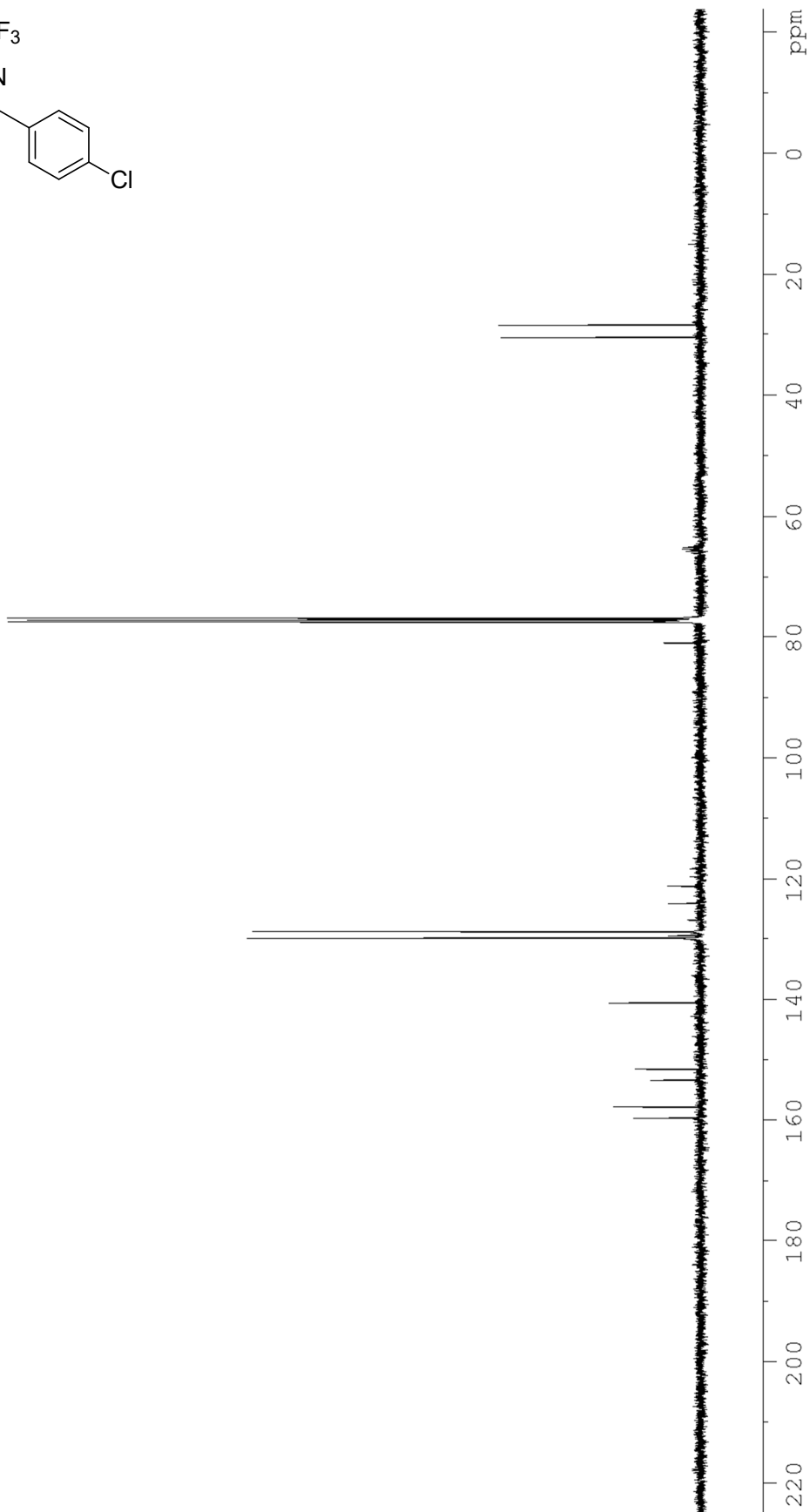
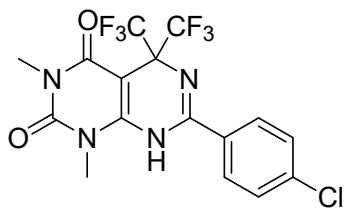
Relevant spectra for chapter 2

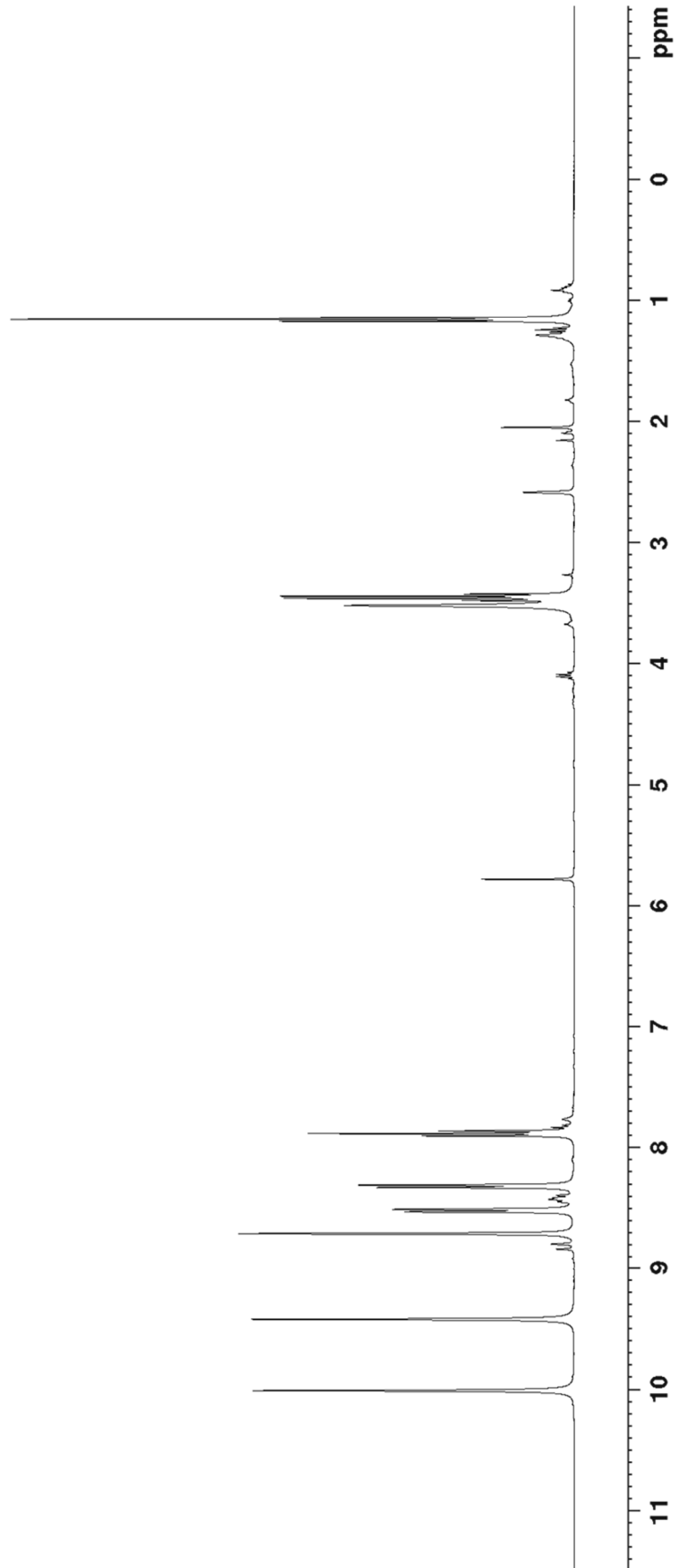
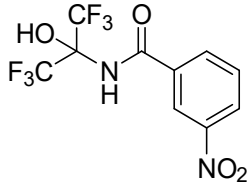


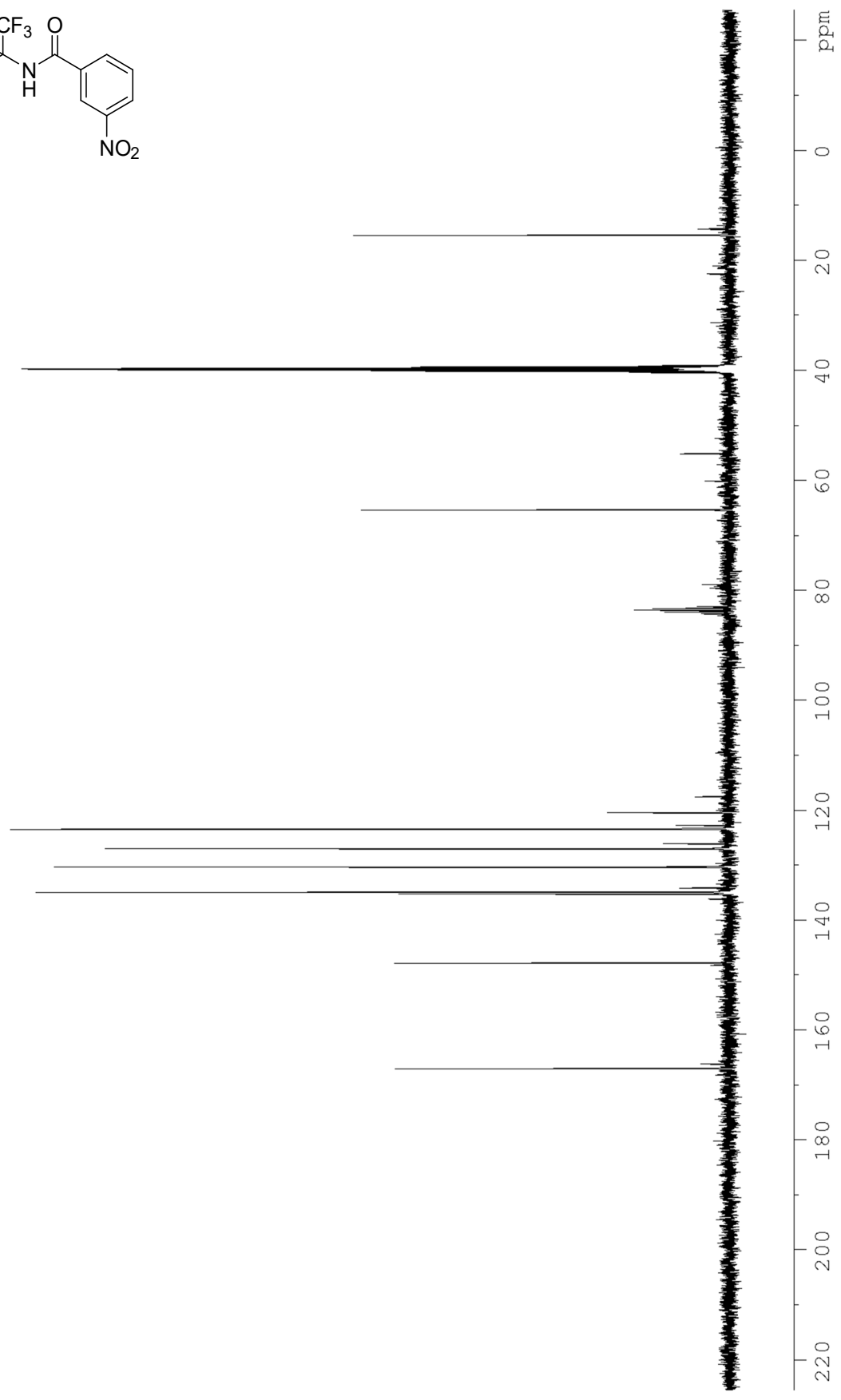
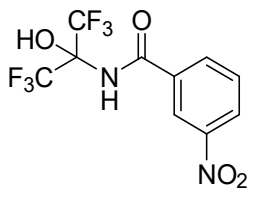


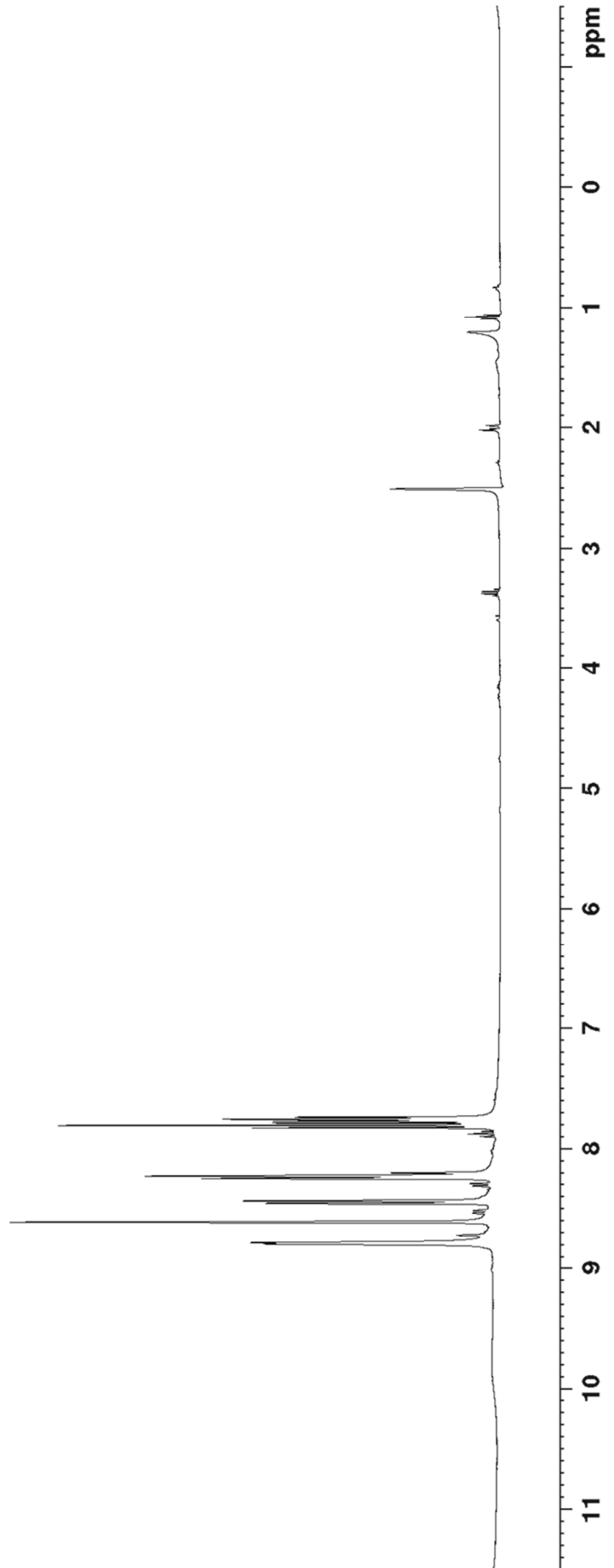
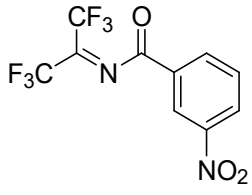


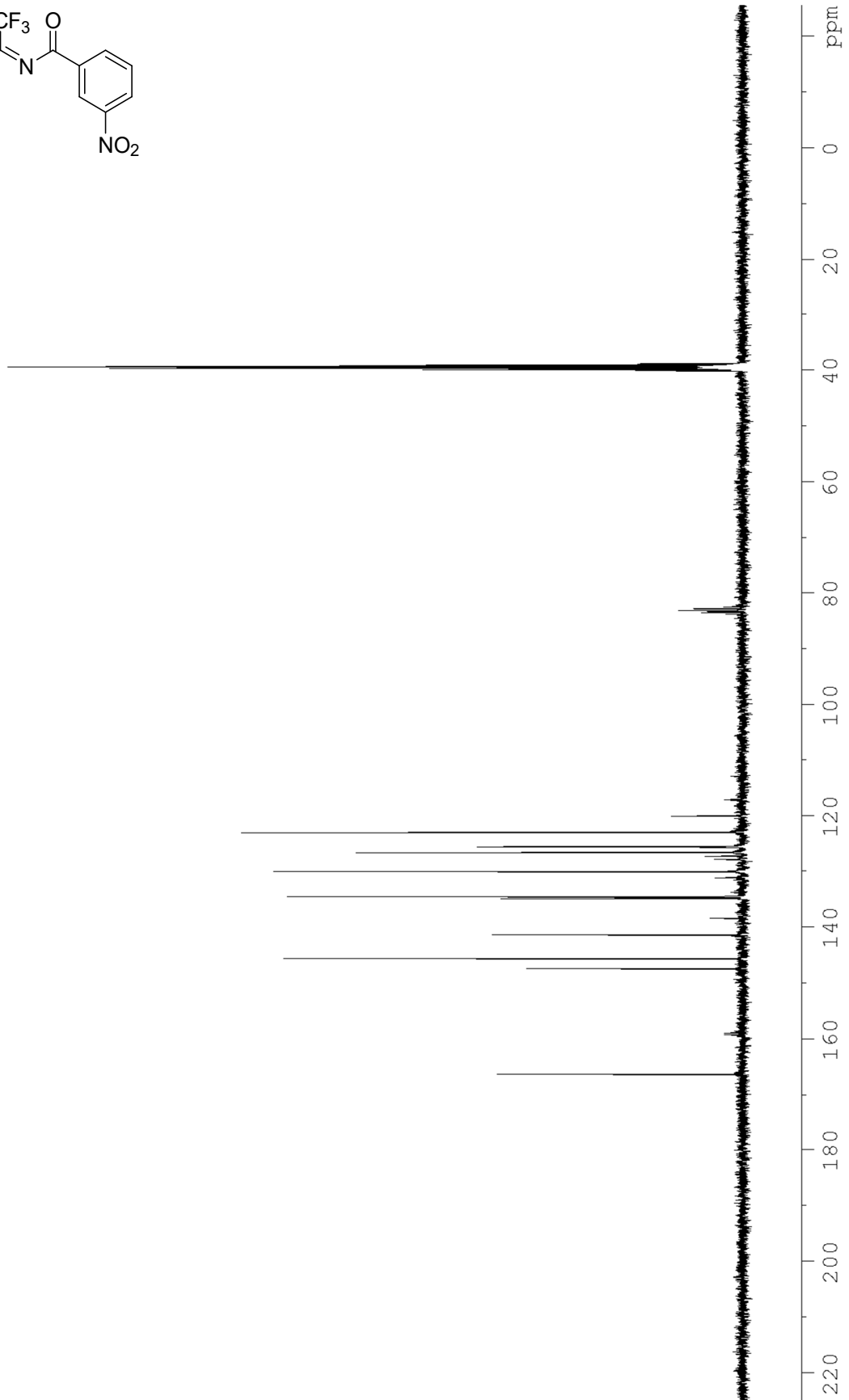
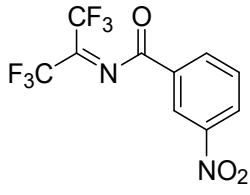


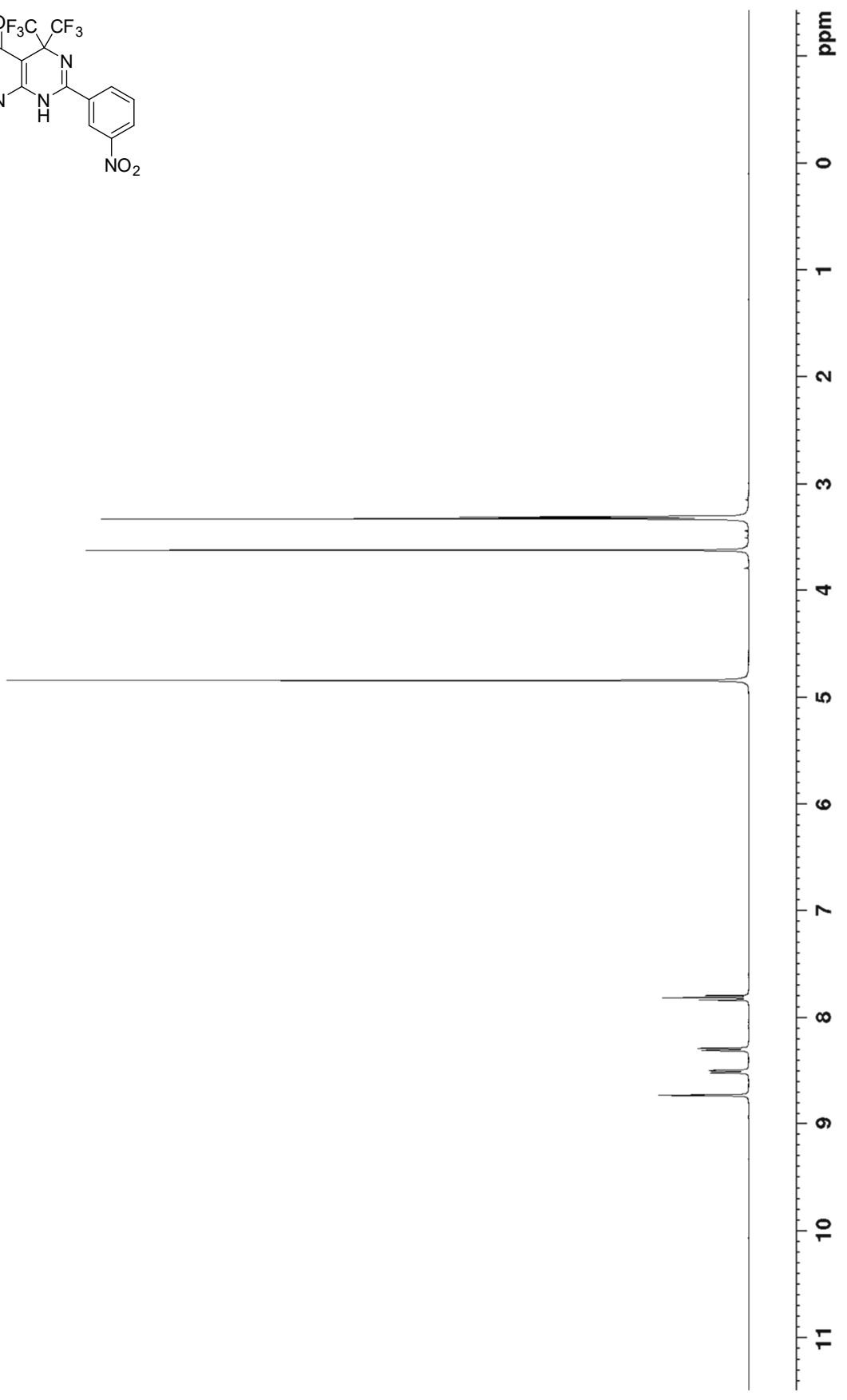
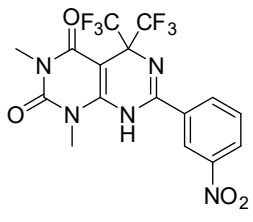


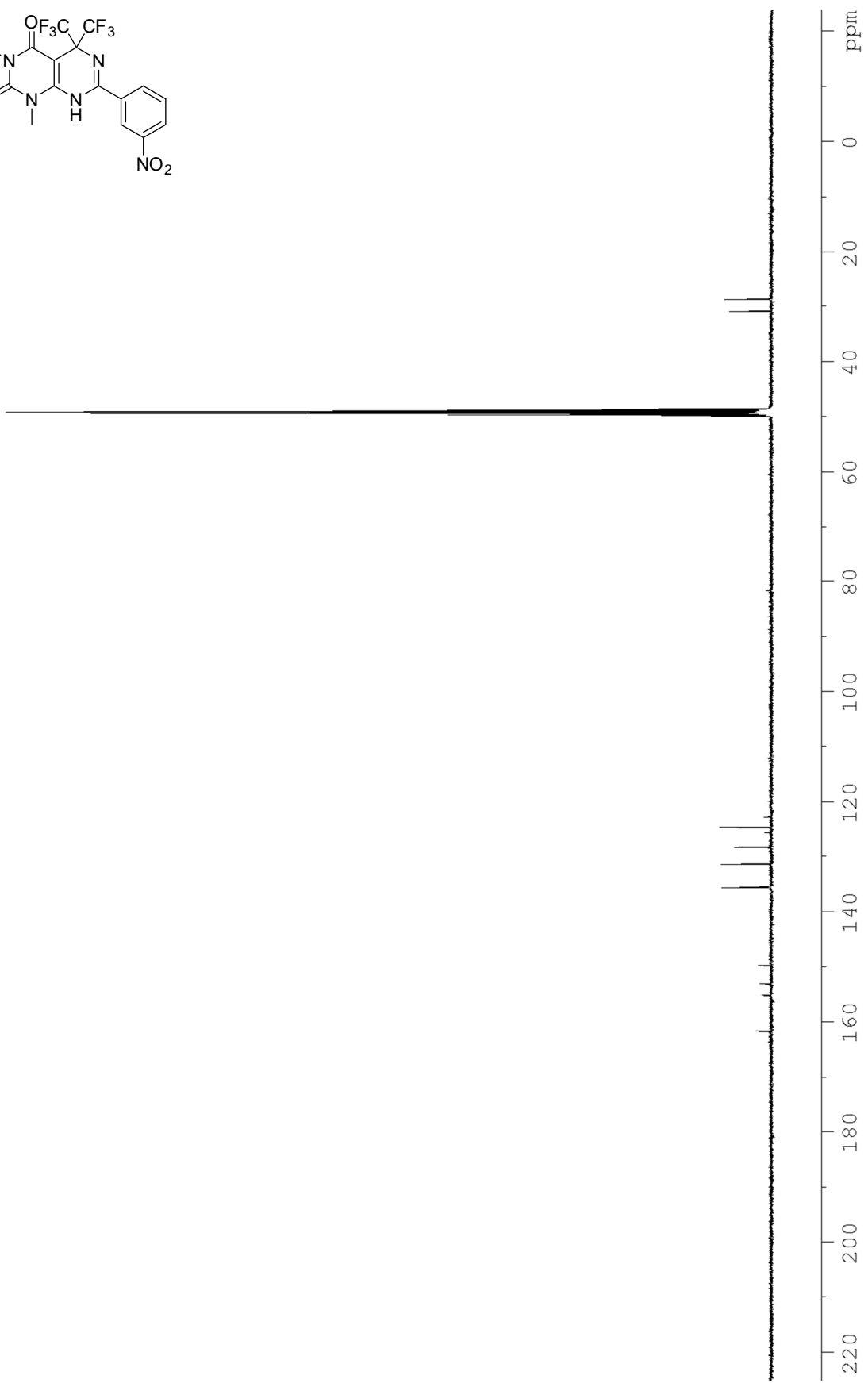
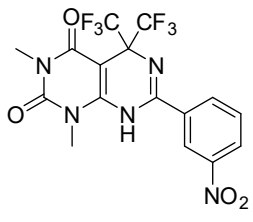






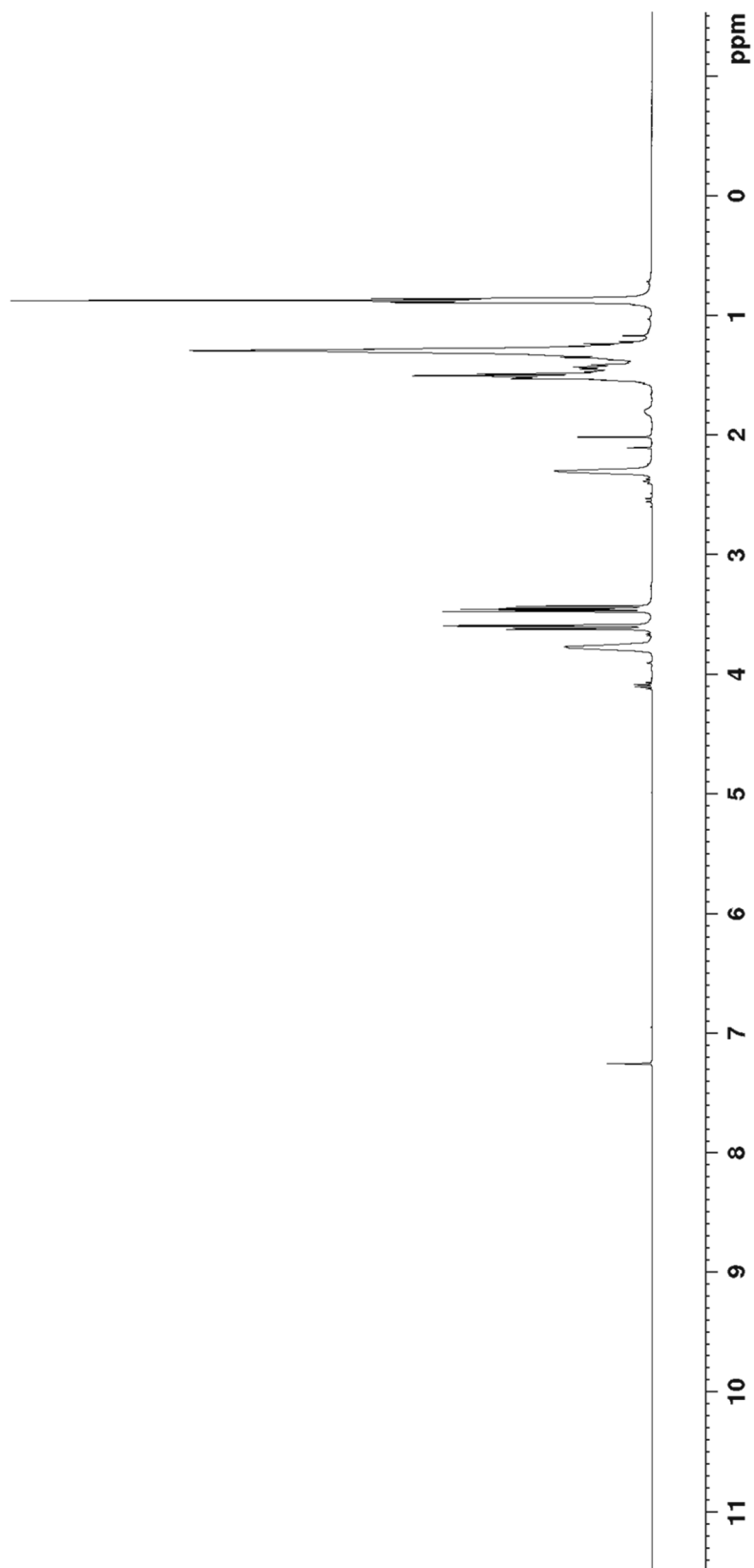
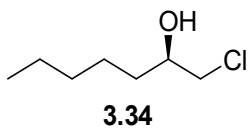


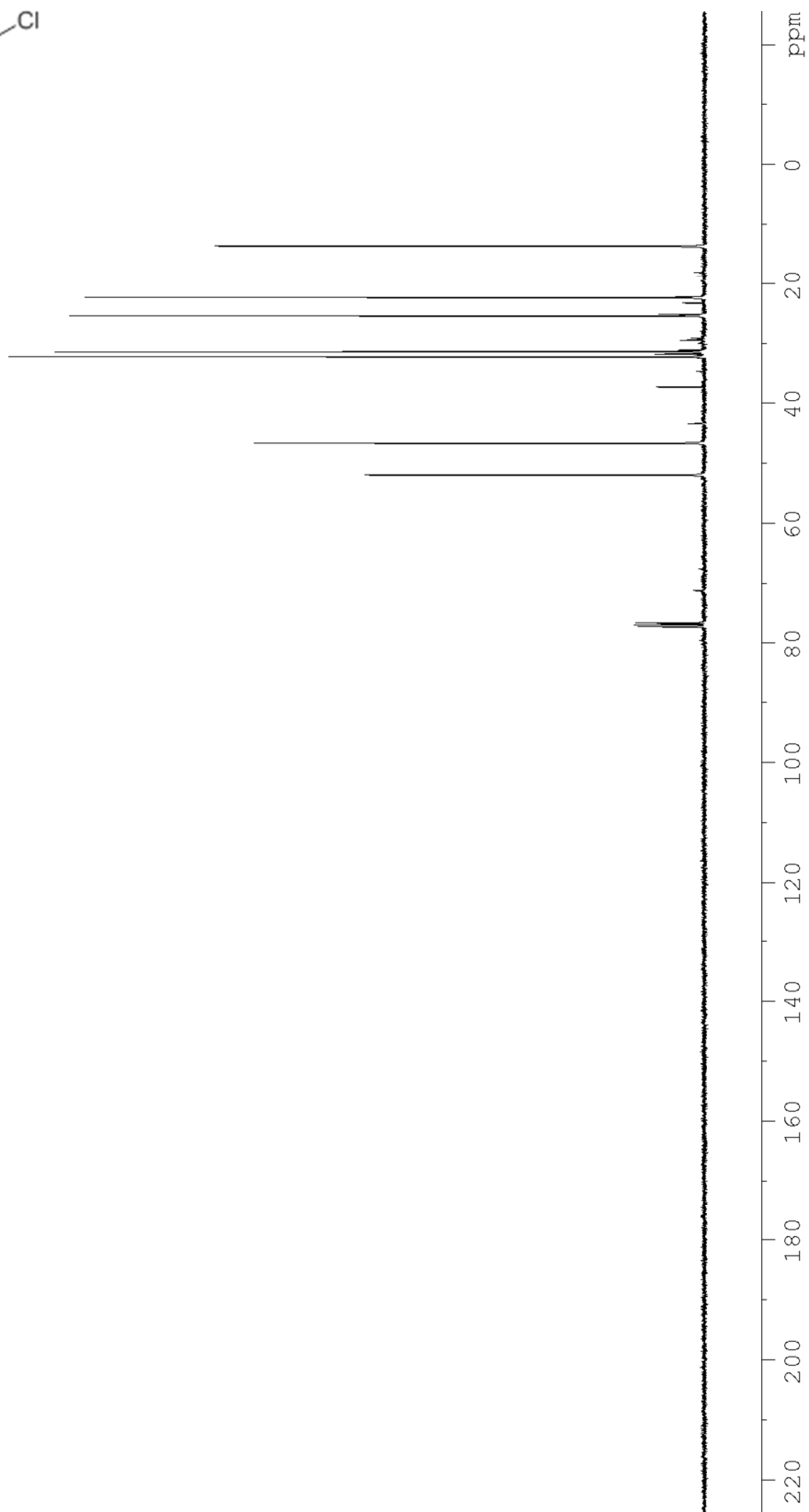
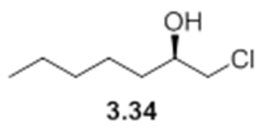


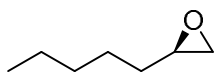


Appendix C

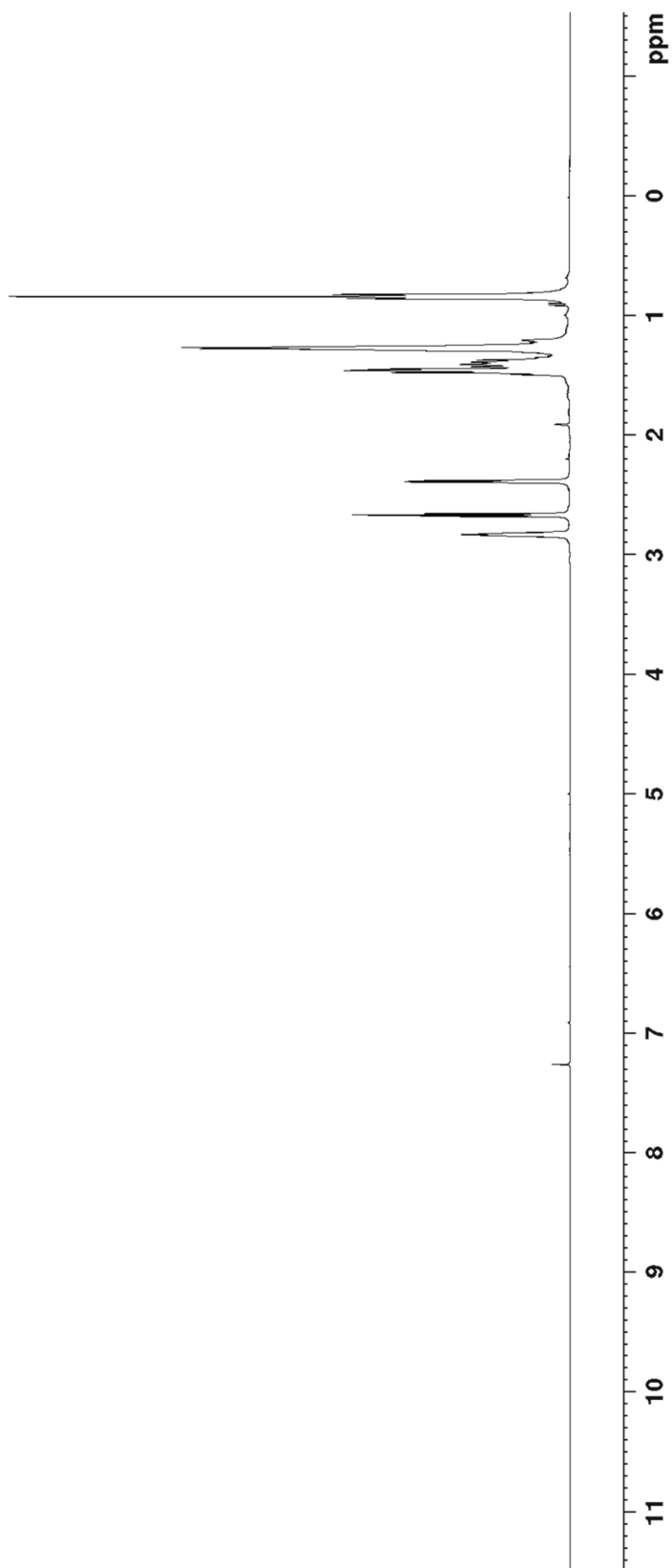
Relevant spectra for chapter 3

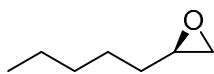




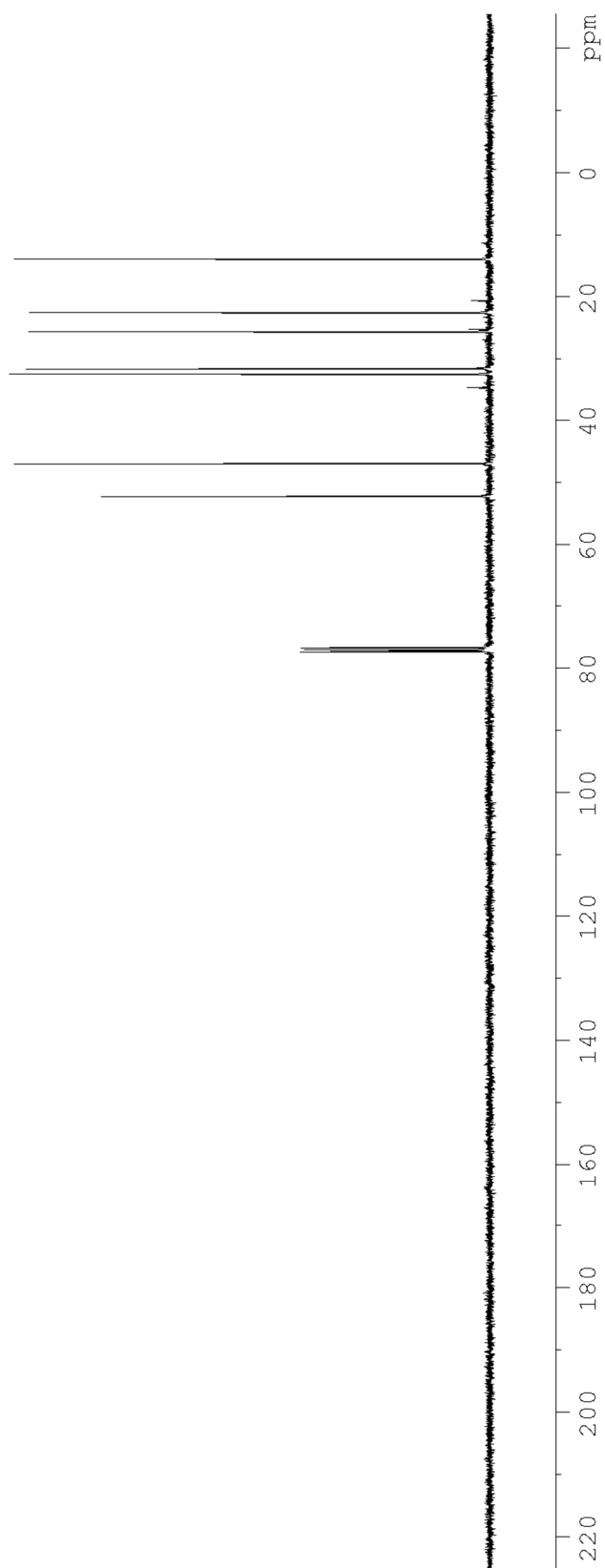


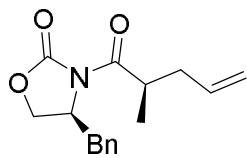
3.35



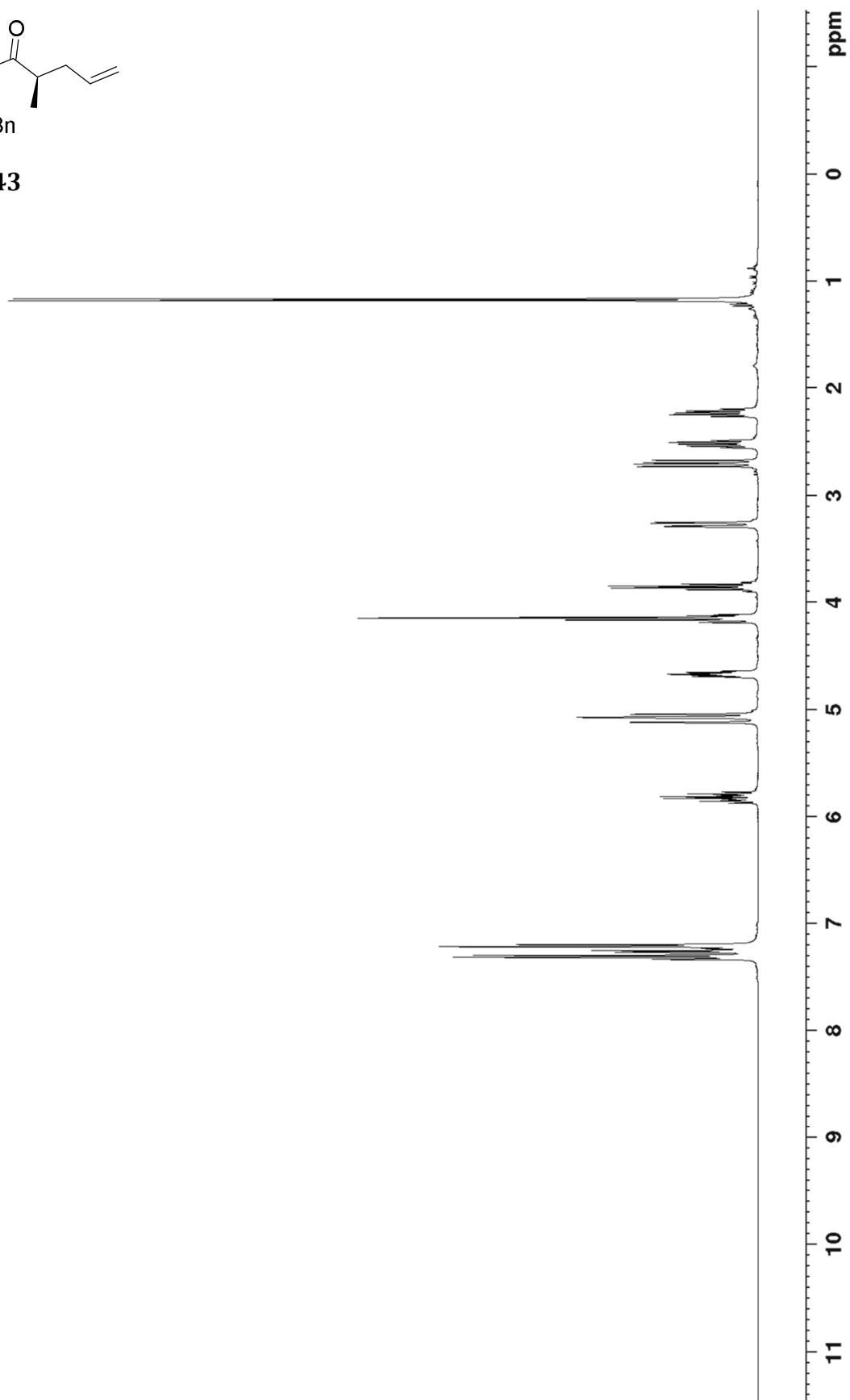


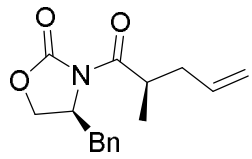
3.35



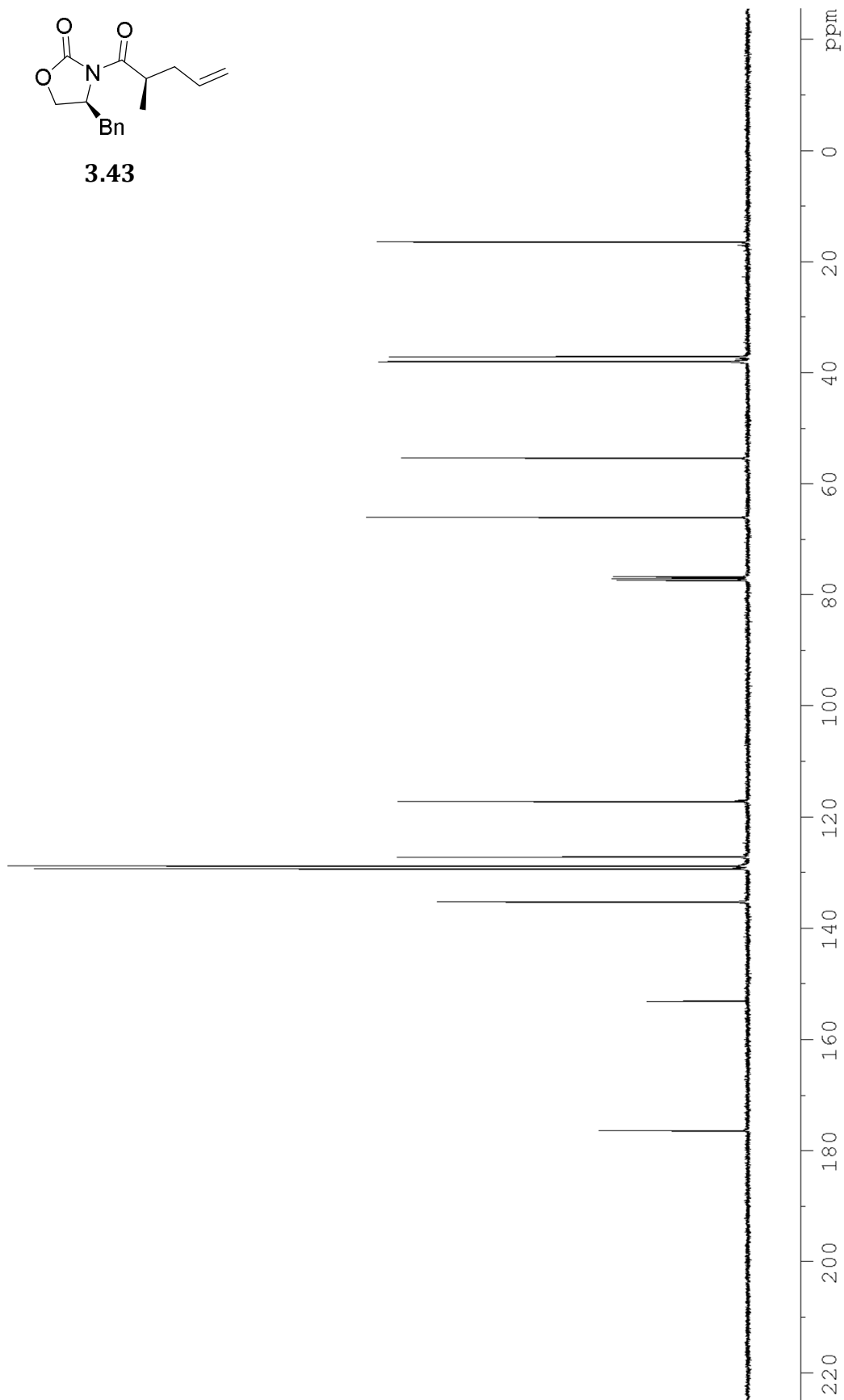


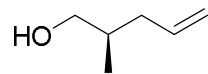
3.43



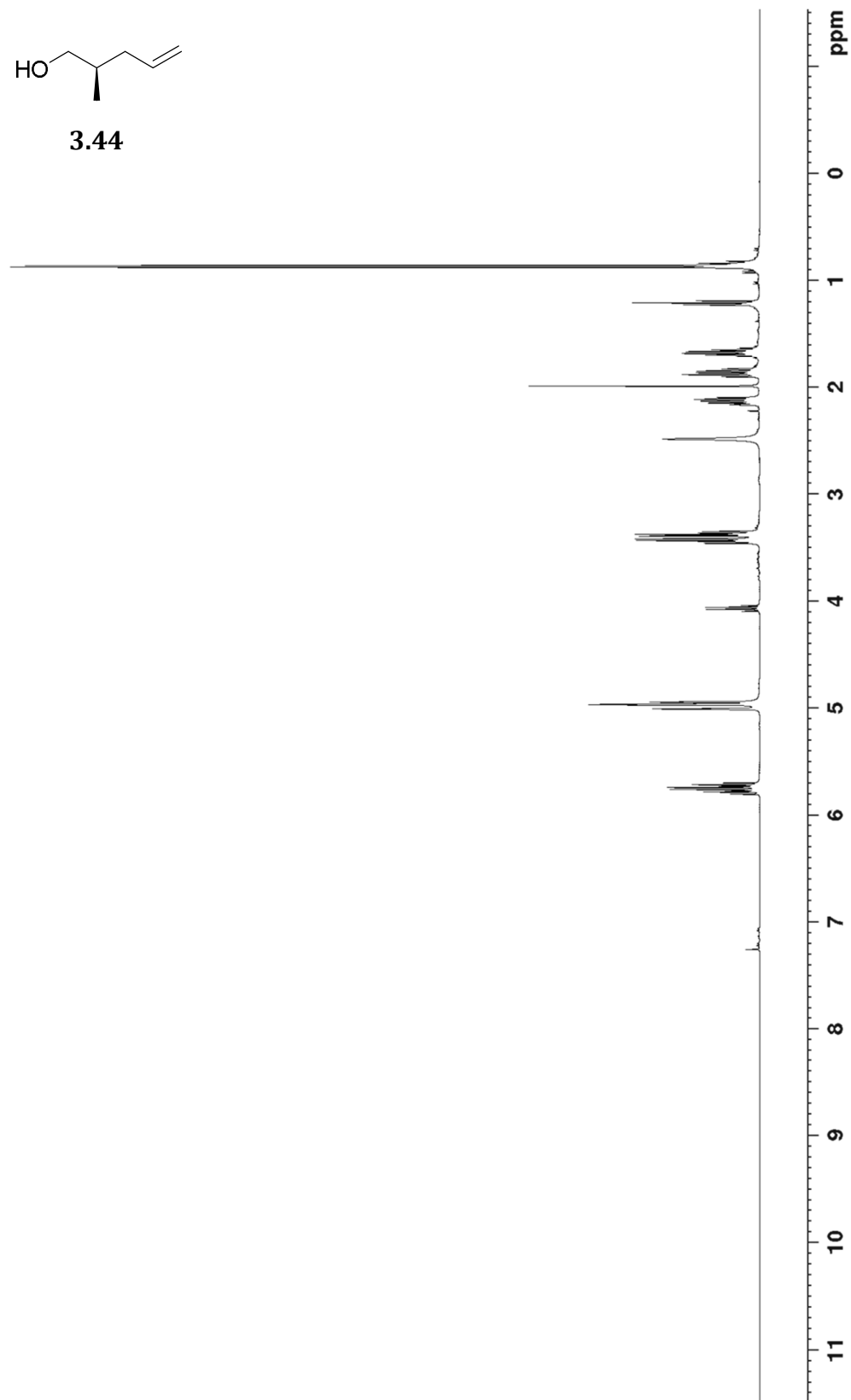


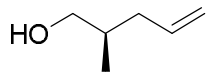
3.43



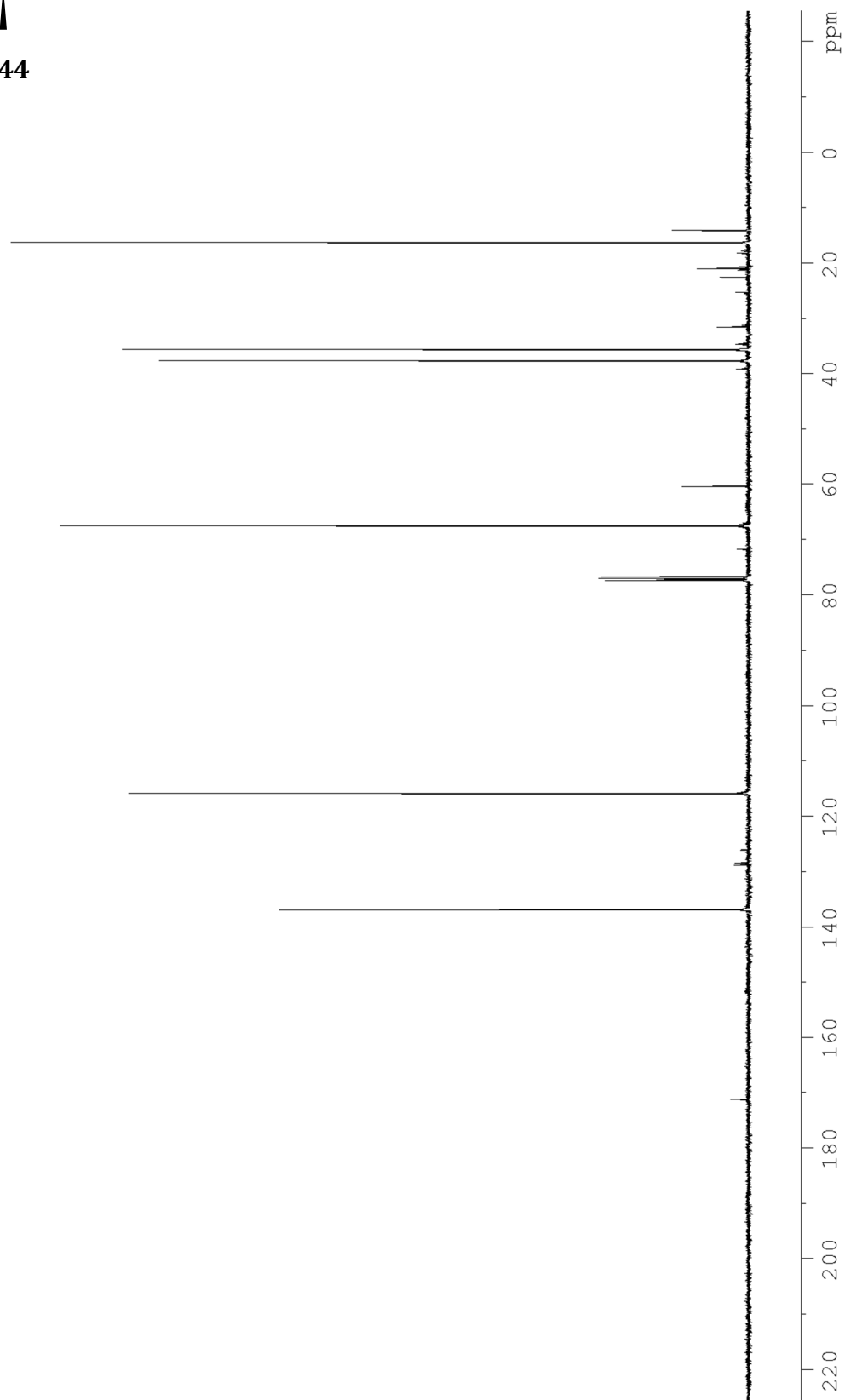


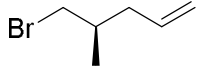
3.44



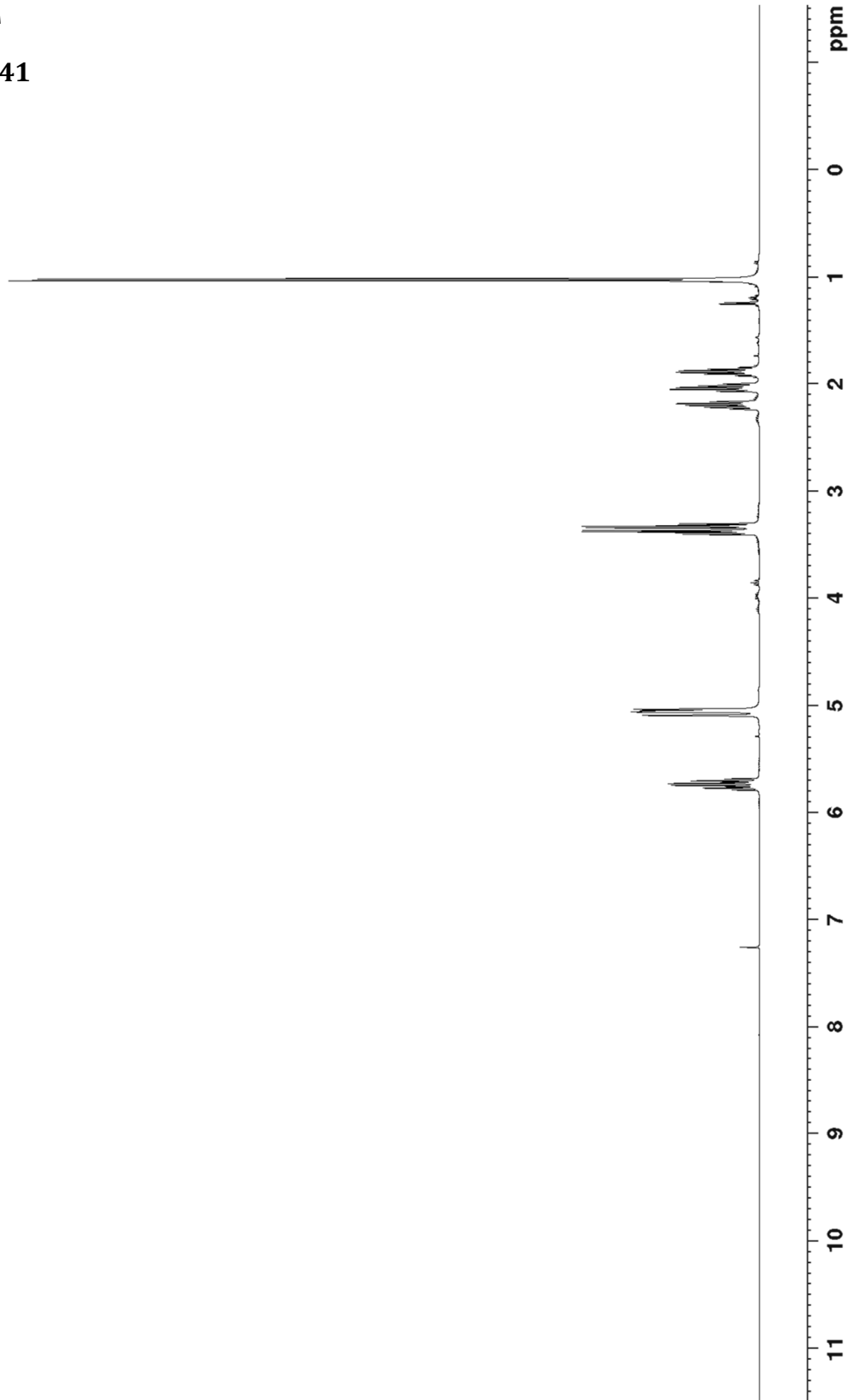


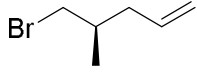
3.44



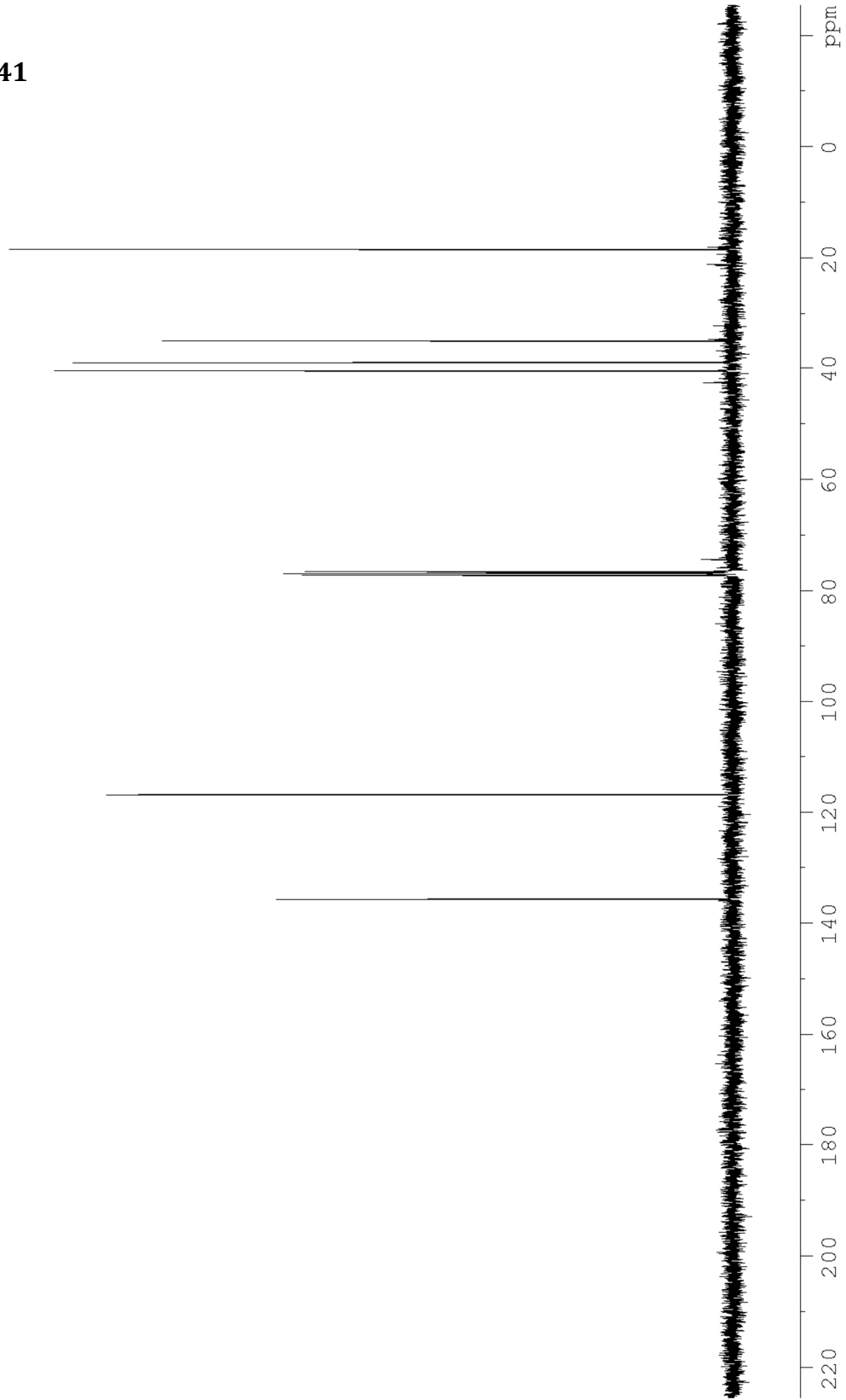


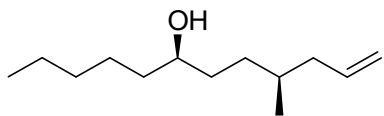
3.41



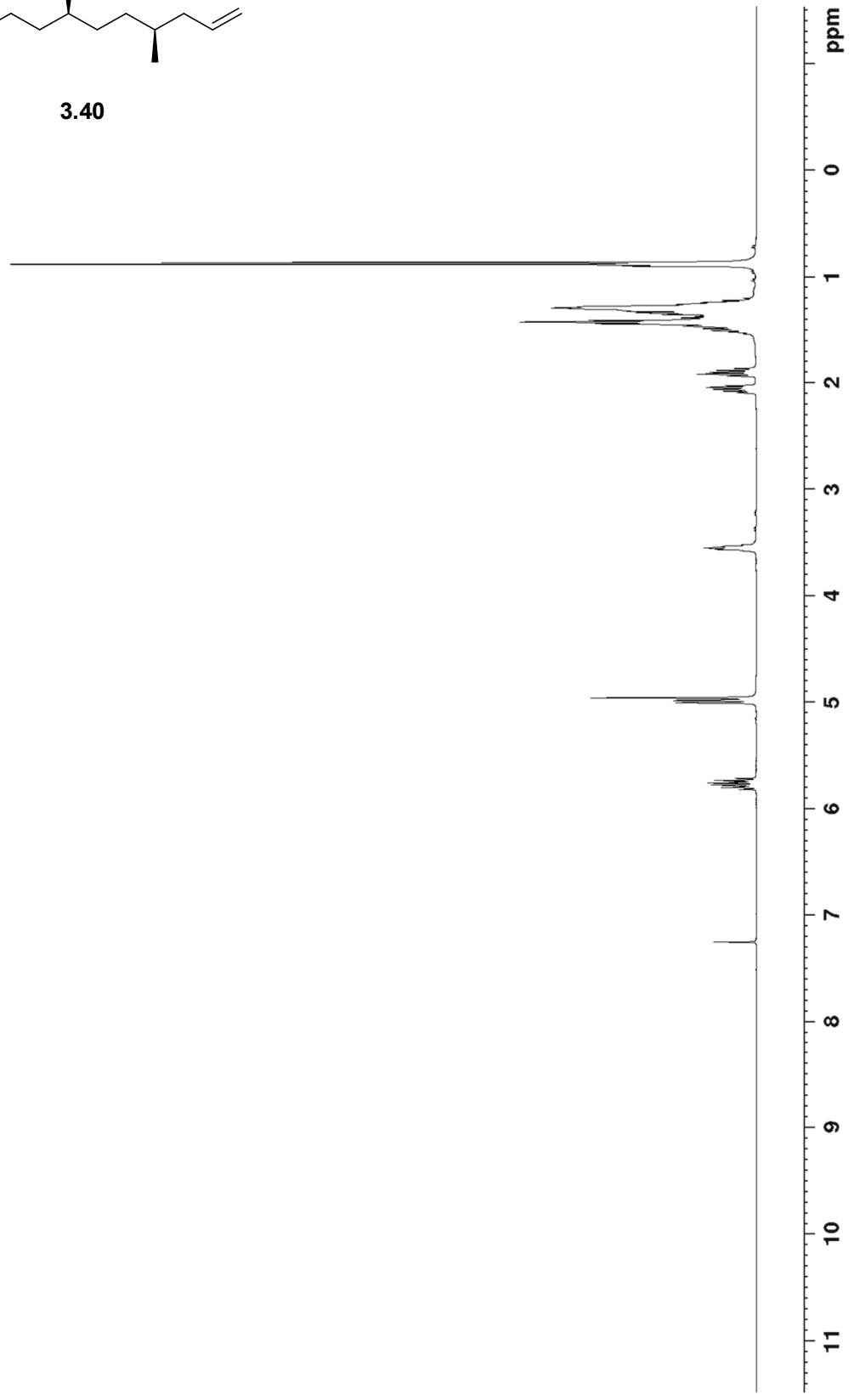


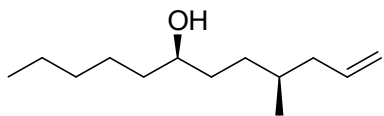
3.41



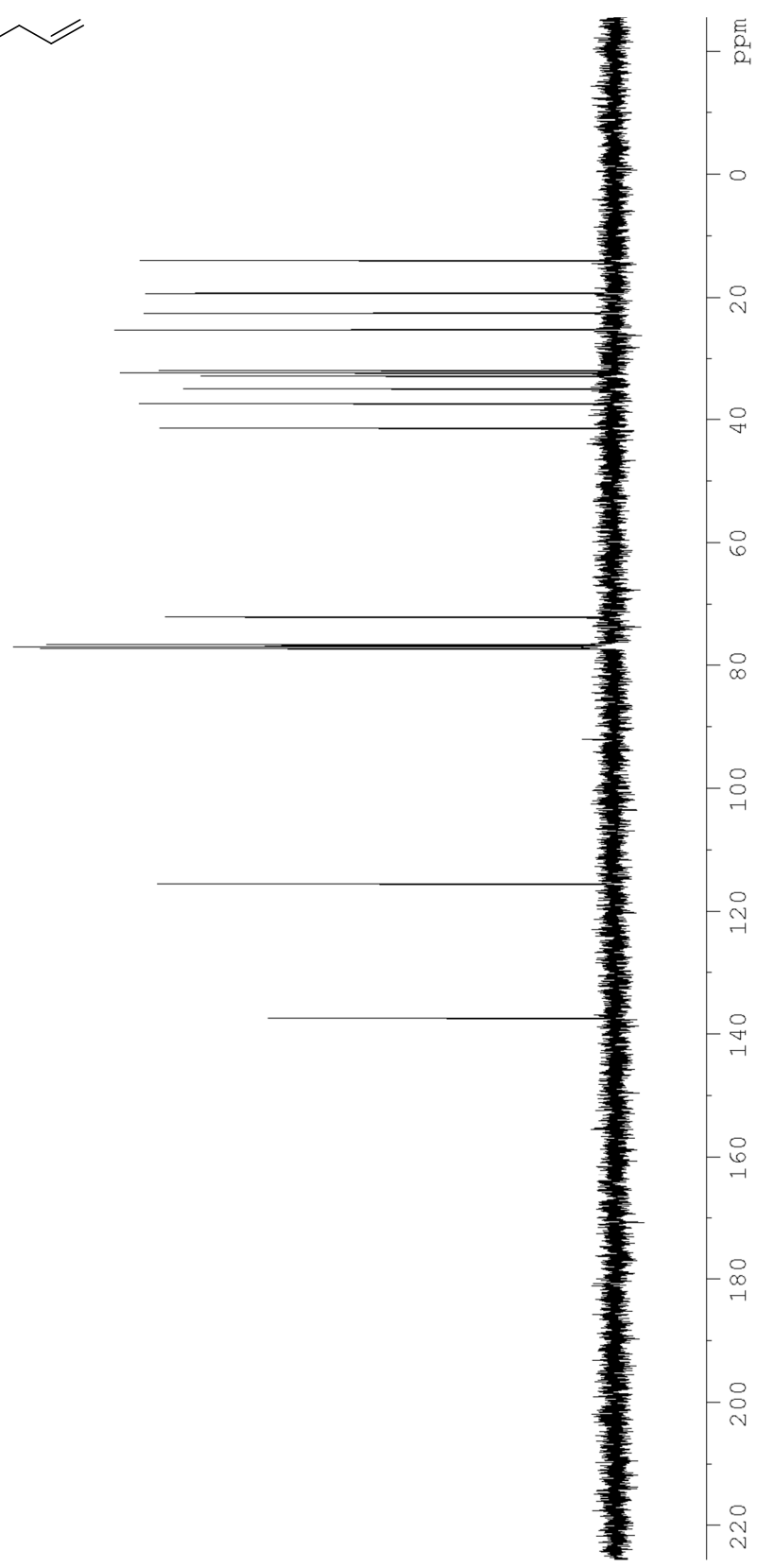


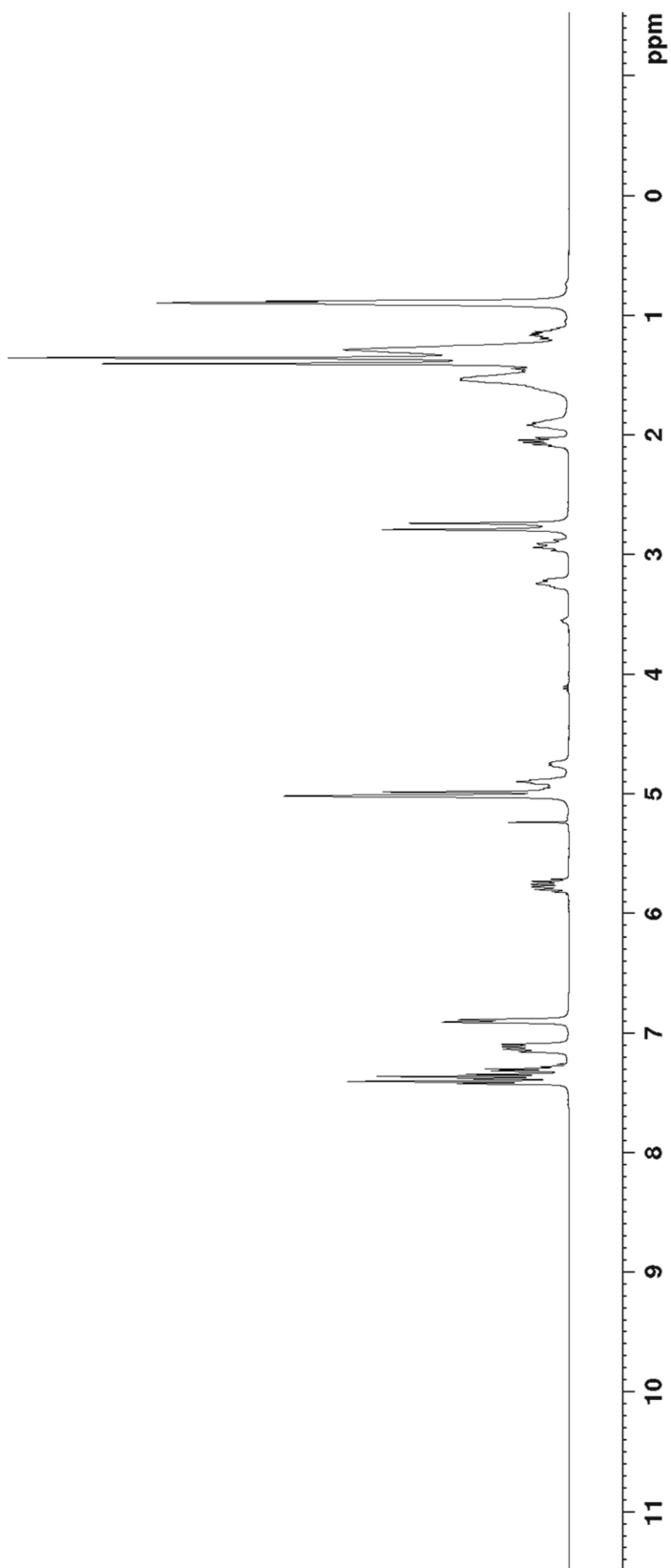
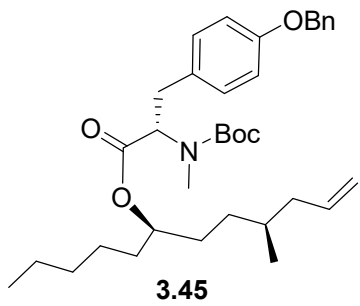
3.40

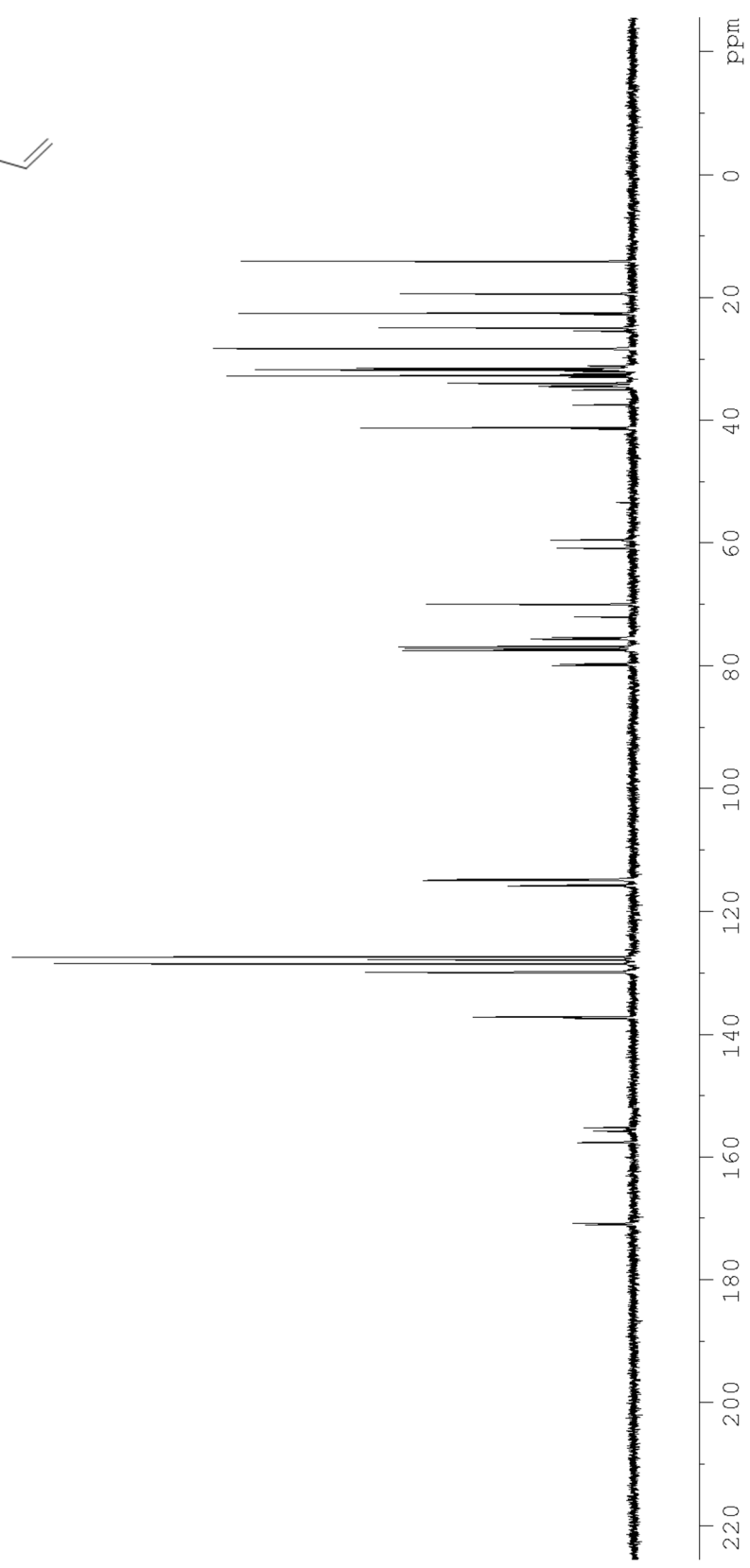
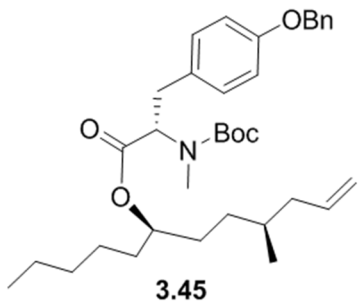




3.40







REFERENCES

- 1) Dillon, J.S.; Tanizawa, Y.; Wheeler, M.B.; Leng, X.H.; Ligon, B.B.; Rabin, D. U.; Yoo-Warren, H.; Permutt, M.A.; Boyd, A., *Endocrinology* **1993**, 133, 1907-1910
- 2) Trapp, S.; Richards, J. E. *Current Opinion in Pharmacology* **2013**, 13 (6), 964-969.
- 3) Mojsov, S.; Heinrich, G.; Wilson, I. B.; Ravazzola, M.; Orci, L.; Habener, J. F. *The Journal of Biological Chemistry* **1986**, 216 (25), 1180-1189.
- 4) Patzelt, C.; Schiltz, E., *Proceedings of the National Academy of Sciences of the United States of America*, **1984**, 81 (16), 5007-5011.
- 5) Leung, P. S.; In *The Gastrointestinal System: Gastrointestinal, Nutritional and Hepatobiliary Physiology*; Springer Netherlands: Dordrecht, **2014**.
- 6) Macdonald, P. E.; El-Kholy, W.; Riedel, M. J.; Salapatek, A. M. F.; Light, P. E.; Wheeler, M. B. *Diabetes* **2002**, 51 (Supplement 3).
- 7) Rickels, M. R.; Mueller, R.; Markmann, J. F.; Naji, A. *The Journal of Clinical Endocrinology & Metabolism* **2009**, 94 (1), 181-189.
- 8) Holst, J. J.; Orskov, C. *Diabetes* **2004**, 53 (Supplement 3).
- 9) Li, Y.; Hansotia, T.; Yusta, B.; Ris, F.; Halban, P. A.; Drucker, D. J. *Journal of Biological Chemistry* **2002**, 278 (1), 471-478.
- 10) Skogar, S.; Jacobsson, H.; Holst, J.; Naoslund, E.; Gryback, P.; Hellstrallm, P. *Gastroenterology* **1998**, 114.
- 11) Flint, A.; Raben, A.; Astrup, A.; Holst, J. J. *Journal of Clinical Investigation* **1998**, 101 (3), 515-520.
- 12) Gutzwiller, J. P.; Goke, B.; Drewe, J.; Hildebrand, P.; Ketterer, S.; Handschin, D.; Winterhalder, R.; Conen, D.; Beglinger, C. *Gut* **1999**, 14 (1), 81-86.
- 13) Schjoldager, B. T. G.; Mortensen, P. E.; Christiansen, J.; Ørskov, C.; Holst, J. J. *Digestive Diseases and Sciences* **1989**, 34 (5), 703-708.
- 14) Deacon, C. F. *Hormone and Metabolic Research* **2004**, 36 (11/12), 761-765.
- 15) Hui, H.; Farilla, L.; Merkel, P.; Perfetti, R. *European Journal of Endocrinology* **2002**, 146, 863-869.
- 16) Donnelly, D. *British Journal of Pharmacology* **2012**, 166 (1), 27-41.
- 17) Brubaker, P. L.; Drucker, D. J. *Receptors and Channels* **2002**, 8, 179-188.
- 18) Tornehave, D.; Kristensen, P.; Ramer, J.; Knudsen, L. B.; Heller, R. S. *Journal of Histochemistry & Cytochemistry* **2008**, 56 (9), 841-851.

- 19) Cork, S. C.; Richards, J. E.; Holt, M. K.; Gribble, F. M.; Reimann, F.; Trapp, S. *Molecular Metabolism* **2015**, 4 (10), 718–731.
- 20) Skov, J. *Reviews in Endocrine and Metabolic Disorders* **2014**, 15 (3), 197–207.
- 21) Richards, P.; Parker, H. E.; Adriaenssens, A. E.; Hodgson, J. M.; Cork, S. C.; Trapp, S.; Gribble, F. M.; Reimann, F. *Diabetes* **2013**, 63 (4), 1224–1233.
- 22) Broide, E.; Bloch, O.; Ben-Yehudah, G.; Cantrell, D.; Shirin, H.; Rapoport, M. J. *Journal of Histochemistry & Cytochemistry* **2013**, 61 (9), 649–658.
- 23) Willard, F. S.; Sloop, K. W. *Experimental Diabetes Research* **2012**, 2012, 1–12.
- 24) Yang, H.; Levine, M. A.; Schwindinger, W.; Bernier, M. *Endocrinology* **1999**, 140 (3), 1132–1140.
- 25) Koole, C.; Pabreja, K.; Savage, E. E.; Wootten, D.; Furness, S. G.; Miller, L. J.; Christopoulos, A.; Sexton, P. M. *Biochemical Society Transactions* **2013**, 41(1), 172–179.
- 26) Purves, D.; Augustine, G. J.; Fitzpatrick, D.; Hall, W. C.; LaMantia, A.-S.; White, L. E. In *Neuroscience*; Sinauer Associates, Inc.: Sunderland, Massachusetts., **2012**.
- 27) Dumaz, N.; Marais, R. *FEBS Journal* **2005**, 272 (14), 3491–3504.
- 28) Meloni, A. R.; Deyoung, M. B.; Lowe, C.; Parkes, D. G. *Diabetes, Obesity and Metabolism* **2012**, 15 (1), 15–27.
- 29) Widmann, C.; Dolci, W.; Thorens, B. *Molecular Endocrinology* **1997**, 11 (8), 1094–1102.
- 30) Claing, A. *Progress in Neurobiology* **2002**, 66 (2), 61–79.
- 31) Roed, S. N.; Nahr, A. C.; Wismann, P.; Iversen, H.; Brauner-Osborne, H.; Knudsen, S. M.; Waldhoer, M. *Journal of Biological Chemistry* **2014**, 290 (2), 1233–1243.
- 32) Sonoda, N.; Imamura, T.; Yoshizaki, T.; Babendure, J. L.; Lu, J.-C.; Olefsky, J. M. *Proceedings of the National Academy of Sciences* **2008**, 105 (18), 6614–6619.
- 33) Drucker, D. J. *Endocrinology* **2001**, 142 (2), 521–527.
- 34) Marathe, C. S.; Rayner, C. K.; Jones, K. L.; Horowitz, M. *Experimental Diabetes Research* **2011**, 2011, 1–10.
- 35) Li, J.; Zheng, J.; Wang, S.; Lau, H. K.; Fathi, A.; Wang, Q. *Frontiers in Physiology*, **2017**, 8.
- 36) Zietek, T.; Rath, E. *Frontiers in Immunology* **2016**, 7.
- 37) Merck Sharp & Dohme Corp. Natriuretic Effect of GLP-1 in Healthy Non Obese Subjects <https://clinicaltrials.gov/ct2/show/NCT02130778>

- 38) Filippatos, T. D.; Elisaf, M. S. *World Journal of Diabetes* **2013**, *4* (5), 190–201.
- 39) Lockie, S. H. *Journal of Neuroendocrinology* **2013**, *25* (7), 597–604.
- 40) Trapp, S.; Cork, S. C. *American Journal of Physiology - Regulatory, Integrative and Comparative Physiology* **2015**, *309* (8).
- 41) Kastin, A. J.; Akerstrom, V.; Pan, W. *Journal of Molecular Neuroscience* **2002**, *18* (1-2), 07–13.
- 42) Busek, P. *Frontiers in Bioscience* **2008**, *13* (13), 2319.
- 43) Burcelin, R.; Dolci, W.; Thorens, B. *Diabetes* **2000**, *49* (10), 1635–1642.
- 44) Baggio, L. L.; Drucker, D. J. *Journal of Clinical Investigation* **2014**, *124* (10), 4223–4226.
- 45) Shah, M.; Vella, A. *Reviews in Endocrine and Metabolic Disorders* **2014**, *15* (3), 181–187.
- 46) Fonseca, F. R. D.; Navarro, M.; Alvarez, E.; Roncero, I.; Chowen, J. A.; Maestre, O.; Gomez, R.; Munoz, R. A. M.; Eng, J.; Blazquez, E. *Metabolism* **2000**, *49* (6), 709–717.
- 47) Kappe, C.; Tracy, L. M.; Patrone, C.; Iverfeldt, K.; Sjöholm, A. *Journal of Neuroinflammation* **2012**, *9* (1).
- 48) Roh, E.; Song, D. K.; Kim, M.-S. *Experimental & Molecular Medicine* **2016**, *48* (3).
- 49) Hölscher, C. *CNS Drugs* **2012**, *26* (10), 871–882.
- 50) Mossello, E.; Ballini, E.; Boncinelli, M.; Monami, M.; Lonetto, G.; Mello, A. M.; Tarantini, F.; Baldasseroni, S.; Mannucci, E.; Marchionni, N. A. *Experimental Diabetes Research* **2011**, *2011*, 1–6.
- 51) Stayte, S.; Vissel, B. *Brain* **2017**, *140* (5), 1177–1179.
- 52) Kazakos, K. *Diabetes Research and Clinical Practice* **2011**, *93*.
- 53) Baggio, L. L.; Drucker, D. J. *Gastroenterology* **2007**, *132* (6), 2131–2157.
- 54) Kim, W.; Egan, J. M. *Pharmacological Reviews* **2008**, *60* (4), 470–512.
- 55) Nauck, M.; Ebert, R.; Creutzfeldt, W.; Stöckmann, F. *Diabetologia* **1986**, *29* (1), 46–52.
- 56) Holst, J. J. *Diabetes, Obesity and Metabolism* **2008**, *10*, 14–21.
- 57) Holst, J. J.; Knop, F. K.; Vilsboll, T.; Krarup, T.; Madsbad, S. *Diabetes Care* **2011**, *34* (Supplement 2).
- 58) Seghieri, M.; Rebelos, E.; Gastaldelli, A.; Astiarraga, B. D.; Casolaro, A.; Barsotti, E.; Pocai, A.; Nauck, M.; Muscelli, E.; Ferrannini, E. *Diabetologia* **2012**, *56*(1), 156–161.

- 59) Larsen, J.; Hylleberg, B.; Ng, K.; Damsbo, P. *Diabetes Care* **2001**, *24* (8), 1416–1421.
- 60) Eng, J.; Kleinmann, W. A.; Singh, L.; Singh, G.; Raufman, J. P. *Journal of Biological Chemistry* **1992**, *267* (11), 7402–7405.
- 61) Egido, E. M.; Silvestre, R. A.; Marco, J.; Hernández, R. *Hormone and Metabolic Research* **2004**, *36* (9), 595–600.
- 62) Parkes, D.; Jodka, C.; Smith, P.; Nayak, S.; Rinehart, L.; Gingerich, R.; Chen, K.; Young, A. *Drug Development Research* **2001**, *53* (4), 260–267.
- 63) Davidson, M. B.; Bate, G.; Kirkpatrick, P. *Nature Reviews Drug Discovery* **2005**, *4*(9), 713–714.
- 64) Bond, A. *Proceedings (Baylor University Medical Center)* **2006**, *19* (3), 281–284.
- 65) Ballav, C.; Gough, S. *Prescriber* **2012**, *23* (1-2), 30–33.
- 66) University College of London, Trial of Exenatide for Parkinson's Disease <https://clinicaltrials.gov/ct2/show/NCT01971242>
- 67) Talbot, K. *Neurodegenerative Disease Management* **2014**, *4* (1), 31–40.
- 68) Neumiller, J. J.; Campbell, R. K. *Annals of Pharmacotherapy* **2009**, *43* (9), 1433–1444.
- 69) FDA Approves Novo-Nordisk's Diabetes Drug Victoza <https://www.drugs.com/newdrugs/fda-approves-novo-nordisk-s-diabetes-victoza-1965.html>.
- 70) Pi-Sunyer, X.; Astrup, A.; Fujioka, K.; Greenway, F.; Halpern, A.; Krempf, M.; Lau, D. C.; Roux, C. W. L.; Ortiz, R. V.; Jensen, C. B.; Wilding, J. P. *New England Journal of Medicine* **2015**, *373* (1), 11–22.
- 71) Fonseca, V. A.; Alvarado-Ruiz, R.; Raccach, D.; Boka, G.; Miossec, P.; Gerich, J. E. *Diabetes Care* **2012**, *35* (6), 1225–1231.
- 72) Rosenstock, J.; Reusch, J.; Bush, M.; Yang, F.; Stewart, M. *Diabetes Care* **2009**, *32* (10), 1880–1886.
- 73) Thompson, A. M.; Trujillo, J. M. *Annals of Pharmacotherapy* **2015**, *49* (3), 351–359.
- 74) Tamargo, I. A.; Bader, M.; Li, Y.; Yu, S.-J.; Wang, Y.; Talbot, K.; Dimarchi, R. D.; Pick, C. G.; Greig, N. H. *Experimental Neurology* **2017**, *288*, 176–186.
- 75) Moran, B. M.; Mckillop, A. M.; O'Harte, F. P. M. *Current Opinion in Pharmacology* **2016**, *31*, 57–62.
- 76) Gao, H.; Zhao, Q.; Song, Z.; Yang, Z.; Wu, Y.; Tang, S.; Alahdal, M.; Zhang, Y.; Jin, L. *The FASEB Journal* **2017**, *31* (8), 3527–3539.

- 77) Frias, J. P.; Bastyr, E. J.; Vignati, L.; Tschop, M. H.; Schmitt, C.; Owen, K.; Christensen, R. H.; Dimarchi, R. D. *Cell Metabolism*, **2017**, *26* (2).
- 78) Prasad-Reddy, L.; Isaacs, D. *Drugs in Context* **2015**, *4*, 1–19.
- 79) Wilke, T.; Mueller, S.; Groth, A.; Berg, B.; Fuchs, A.; Sikirica, M.; Logie, J.; Martin, A.; Maywald, U. *Diabetes Therapy* **2015**, *7* (1), 105–124.
- 80) Unger, J. R.; Parkin, C. G. *Diabetes Therapy* **2011**, *2* (1), 29–39.
- 81) Singh, S. *JAMA Internal Medicine* **2013**, *173* (19), 1843.
- 82) Butler, P. C.; Dry, S.; Elashoff, R. *Diabetes Care* **2010**, *33* (2), 453–455.
- 83) Thornberry, N.; Weber, A. *Current Topics in Medicinal Chemistry* **2007**, *7* (6), 557–568.
- 84) Thornberry, N. A.; Gallwitz, B. *Best Practice and Research Clinical Endocrinology and Metabolism* **2009**, *23* (4), 479–486.
- 85) Ahrén, B. *Expert Opinion on Investigational Drugs* **2006**, *15* (4), 431–442.
- 86) Augeri, D. J.; Robl, J. A.; Betebenner, D. A.; Magnin, D. R.; Khanna, A.; Robertson, J. G.; Wang, A.; Simpkins, L. M.; Taunk, P.; Huang, Q.; Han, S.-P.; Abboa-Offei, B.; Cap, M.; Xin, L.; Tao, L.; Tozzo, E.; Welzel, G. E.; Egan, D. M.; Marcinkeviciene, J.; Chang, S. Y.; Biller, S. A.; Kirby, M. S.; Parker, R. A.; Hamann, L. G. *Journal of Medicinal Chemistry* **2005**, *48* (15), 5025–5037.
- 87) Deacon, C. F.; Holst, J. J. *Expert Opinion on Investigational Drugs* **2009**, *19* (1), 133–140.
- 88) Feng, J.; Zhang, Z.; Wallace, M. B.; Stafford, J. A.; Kaldor, S. W.; Kassel, D. B.; Navre, M.; Shi, L.; Skene, R. J.; Asakawa, T.; Takeuchi, K.; Xu, R.; Webb, D. R.; Gwaltney, S. L. *Journal of Medicinal Chemistry* **2007**, *50* (10), 2297–2300.
- 89) Brunton, S. *International Journal of Clinical Practice* **2014**, *68* (5), 557–567.
- 90) Devries, J. H.; Rosenstock, J. *Diabetes Care* **2017**, *40* (2), 161–163.
- 91) Godinho, R.; Mega, C.; Teixeira-De-Lemos, E.; Carvalho, E. A.; Teixeira, F.; Fernandes, R.; Reis, F. *Journal of Diabetes Research* **2015**, *2015*, 1–28.
- 92) Flor, P. J.; Acher, F. C. *Biochemical Pharmacology* **2012**, *84* (4), 414–424.
- 93) Kruse, A. C.; Ring, A. M.; Manglik, A.; Hu, J.; Hu, K.; Eitel, K.; Häbner, H.; Pardon, E.; Valant, C.; Sexton, P. M.; Christopoulos, A.; Felder, C. C.; Gmeiner, P.; Steyaert, J.; Weis, W. I.; Garcia, K. C.; Wess, J. Å.; Kobilka, B. K. *Nature* **2013**, *504* (7478), 101–106.
- 94) Odagaki, Y. *Frontiers in Clinical Drug Research – Central Nervous System* **2013**, *1*(41), 3–43.

- 95) Shannon, H.; Bymaster, E.; Calligaro, D.; Delapp, N.; Mitch, C.; Warc, J.; Olesen, P.; Sheardown, M.; Swedberg, M.; Sauerberg, P. *European Neuropsychopharmacology* **1995**, *5* (3), 254.
- 96) Mirza, N. R.; Peters, D.; Sparks, R. G. *CNS Drug Reviews* **2006**, *9* (2), 159–186.
- 97) Bodick, N.; Offen, W.; Rasmussen, K.; Paul, S. *Neurobiology of Aging* **1996**, *17*(4).
- 98) Filippatos, T. D.; Panagiotopoulou, T. V.; Elisaf, M. S. *The Review of Diabetic Studies* **2014**, *11* (3-4), 202–230.
- 99) Conn, P. J.; Christopoulos, A.; Lindsley, C. W. *Nature Reviews Drug Discovery* **2009**, *8* (1), 41–54.
- 100) May, L. T.; Leach, K.; Sexton, P. M.; Christopoulos, A. *Annual Review of Pharmacology and Toxicology* **2007**, *47* (1), 1–51.
- 101) Gentry, P. R.; Sexton, P. M.; Christopoulos, A. *Journal of Biological Chemistry* **2015**, *290* (32), 19478–19488.
- 102) Urwyler, S. *Pharmacological Reviews* **2011**, *63* (1), 59–126.
- 103) Conn, P. J.; Lindsley, C. W.; Meiler, J.; Niswender, C. M. *Nature Reviews Drug Discovery* **2014**, *13* (9), 692–708.
- 104) Christopoulos, A.; Mitchelson, F. *Journal of Pharmacy and Pharmacology* **1997**, *49*(8), 781–786.
- 105) Liu, J.; Nussinov, R. *PLOS Computational Biology* **2016**, *12* (6).
- 106) Klotz, U. *Progress in Clinical Biochemistry and Medicine Essential and Non-Essential Metals Metabolites with Antibiotic Activity Pharmacology of Benzodiazepines Interferon Gamma Research* **1984**, 117–167.
- 107) Bartholini, G. *Medicinal Chemistry Advances* **1981**, 345–353.
- 108) Wenthur, C. J.; Gentry, P. R.; Mathews, T. P.; Lindsley, C. W. *Annual Review of Pharmacology and Toxicology* **2014**, *54* (1), 165–184.
- 109) Langmead, C. J. *Journal of Biomolecular Screening* **2007**, *12* (5), 668–676.
- 110) Willard, F. S.; Bueno, A. B.; Sloop, K. W. *Experimental Diabetes Research* **2012**, *2012*, 1–9.
- 111) Knudsen, L. B.; Kiel, D.; Teng, M.; Behrens, C.; Bhumralkar, D.; Kodra, J. Ā. T.; Holst, J. J.; Jeppesen, C. B.; Johnson, M. D.; Jong, J. C. D.; Jorgensen, A. S.; Kercher, T.; Kostrowicki, J.; Madsen, P.; Olesen, P. H.; Petersen, J. S.; Poulsen, F.; Sidelmann, U. G.; Sturis, J.; Truesdale, L.; May, J.; Lau, J. *Proceedings of the National Academy of Sciences* **2007**, *104* (3), 937–942.

- 112) Wootten, D.; Savage, E. E.; Willard, F. S.; Bueno, A. B.; Sloop, K. W.; Christopoulos, A.; Sexton, P. M. *Molecular Pharmacology* **2013**, *83* (4), 822–834.
- 113) Wootten, D.; Simms, J.; Koole, C.; Woodman, O. L.; Summers, R. J.; Christopoulos, A.; Sexton, P. M. *Journal of Pharmacology and Experimental Therapeutics* **2010**, *336* (2), 540–550.
- 114) Baell, J. B. *Journal of Natural Products* **2016**, *79* (3), 616–628.
- 115) Rein, C.; Piwnica, D.; Giordanetto, F.; Rognan, D.; de Graaf, C. *ChemMedChem* **2011**, *6* (12), 2159–2169. Morris, L. C.; Days, E. L.; Turney, M.; Mi, D.; Lindsley, C. W.; Weaver, C. D.; Niswender, K. D. *Journal of Biomolecular Screening* **2014**, *19* (6), 847–858.
- 116) Morris, L. C.; Nance, K. D.; Gentry, P. R.; Days, E. L.; Weaver, C. D.; Niswender, C. M.; Thompson, A. D.; Jones, C. K.; Locuson, C. W.; Morrison, R. D.; Daniels, J. S.; Niswender, K. D.; Lindsley, C. W. *Journal of Medicinal Chemistry* **2014**, *57* (23), 10192–10197.
- 117) Tseng, C.; Zhang, X.; Wolfe, M. M. *American Journal of Physiology - Endocrinology and Metabolism* **1999**, *276* (6), 1049–1054.
- 118) Knudsen, L. B.; Prodal, L. *European Journal of Pharmacology* **1996**, *318* (2-3), 429–435.
- 119) Schirra, J.; Junck, M.; Kraft, G.; Schmidt, H.; Wank, U.; Leicht, P.; Katschinski, M.; Goke, B. *Gastroenterology* **1998**, *114*.
- 120) *Regulatory Peptides* **1995**, *57* (2), 201.
- 121) Li, N.; Lu, J.; Willars, G. B. *PLoS ONE* **2012**, *7* (10).
- 122) Tomas, E.; Stanojevic, V.; Habener, J. *Hormone and Metabolic Research* **2010**, *42* (09), 657–662.
- 123) Meier, J. J. *AJP: Endocrinology and Metabolism* **2006**, *290* (6).
- 124) Ban, K.; Kim, K.-H.; Cho, C.-K.; SauvÃ©, M.; Diamandis, E. P.; Backx, P. H.; Drucker, D. J.; Husain, M. *Endocrinology* **2010**, *151* (4), 1520–1531.
- 125) Göke, R.; Fehmann, H. C.; Linn, T.; Schmidt, H.; Krause, M.; Eng, J.; Göke, B. *Journal of Biological Chemistry* **1993**, *168*, 19650–19655.
- 126) Thorens, B.; Porret, A.; Buhler, L.; Deng, S.-P.; Morel, P.; Widmann, C. *Diabetes* **1993**, *42* (11), 1678–1682.
- 127) Schirra, J.; Sturm, K.; Leicht, P.; Arnold, R.; Goke, B.; Katschinski, M. *Journal of Clinical Investigation* **1998**, *101* (7), 1421–1430.
- 128) Meeran, K.; Oâ€™Shea, D.; Edwards, C. M. B.; Turton, M. D.; Heath, M. M.; Gunn, I.; Abusnana, S.; Rossi, M.; Small, C. J.; Goldstone, A. P.; Taylor, G. M.; Sunter, D.;

- Steere, J.; Choi, S. J.; Ghatei, M. A.; Bloom, S. R. *Endocrinology* **1999**, *140* (1), 244–250.
- 129) Arnoux, J.-B.; Verkarre, V.; Saint-Martin, C. Æ.; Montravers, F. Æ.; Brassier, A. Æ.; Valayannopoulos, V.; Brunelle, F.; Fournet, J.-C.; Robert, J.-J.; Aigrain, Y.; Bellanné-Chantelot, C.; Lonlay, P. D. *Orphanet Journal of Rare Diseases* **2011**, *6*(1), 63.
- 130) Gillespie, R. S.; Ponder, S. Congenital Hyperinsulinism Clinical Presentation <http://emedicine.medscape.com/article/923538-clinical#b1>
- 131) Arnoux, J.B.; Lonlay, P. D.; Ribeiro, M.-J.; Hussain, K.; Blankenstein, O.; Mohnike, K.; Valayannopoulos, V.; Robert, J.-J.; Rahier, J.; Sempoux, C.; Bellanné-Chantelot, C.; Verkarre, V.; Aigrain, Y.; Jaubert, F.; Brunelle, F.; Nihoul-Fékété, C. *Early Human Development* **2010**, *86* (5), 287–294.
- 132) Yorifuji, T. *Annals of Pediatric Endocrinology & Metabolism* **2014**, *19* (2), 57.
- 133) James, C.; Kapoor, R. R.; Ismail, D.; Hussain, K. *Journal of Medical Genetics* **2009**, *46*(5), 289–299.
- 134) Mazor-Aronovitch, K.; Gillis, D.; Lobel, D.; Hirsch, H. J.; Pinhas-Hamiel, O.; Modan-Moses, D.; Glaser, B.; Landau, H. *European Journal of Endocrinology* **2007**, *157*(4), 491–497.
- 135) Pinney, S. E.; Macmullen, C.; Becker, S.; Lin, Y.-W.; Hanna, C.; Thornton, P.; Ganguly, A.; Shyng, S.-L.; Stanley, C. A. *Journal of Clinical Investigation* **2008**, *118* (8), 2877–2886.
- 136) Thorton, P. S.; Alter, C. A. *The Journal of Pediatrics* **1993**, *123* (4), 637–643.
- 137) Mohnike, K.; Blankenstein, O.; Pfuetzner, A.; Pötzsch, S.; Schober, E.; Steiner, S.; Hardy, O.; Grimberg, A.; Waarde, W. V. *Hormone Research* **2008**, *70* (1), 59–64.
- 138) Huang, T.; Kelly, A.; Becker, S. A.; Cohen, M. S.; Stanley, C. A. *Archives of Disease in Childhood - Fetal and Neonatal Edition* **2013**, *98* (4).
- 139) Shilyansky, J.; Fisher, S.; Cutz, E.; Perlman, K.; Filler, R. M. *Journal of Pediatric Surgery* **1997**, *32* (2), 342–346.
- 140) León, D. D. D.; Li, C.; Delson, M. I.; Matschinsky, F. M.; Stanley, C. A.; Stoffers, D. A. *Journal of Biological Chemistry* **2008**, *283* (38), 25786–25793.
- 141) Calabria, A. C.; Li, C.; Gallagher, P. R.; Stanley, C. A.; Leon, D. D. D. *Diabetes* **2012**, *61*(10), 2585–2591.
- 142) Lin, J. *Current Drug Metabolism* **2009**, *10* (7), 661–691.
- 143) Park, C. L.; Folkman, S. *Review of General Psychology* **1997**, *1* (2), 115–144.
- 144) Chandola, T. *Bmj* **2006**, *332* (7540), 521–525.

- 145) Jansen, A. S. P.; Nguyen, X. V.; Karpitskiy, V.; Mettenleiter, T. C.; Loewy, A. *D. Science* **1995**, *270* (5236), 644–646.
- 146) Dickerson, S. S.; Kemeny, M. E. *Psychological Bulletin* **2004**, *130* (3), 355–391.
- 147) Chiba, S.; Numakawa, T.; Ninomiya, M.; Richards, M. C.; Wakabayashi, C.; Kunugi, H. *Progress in Neuro-Psychopharmacology and Biological Psychiatry* **2012**, *39* (1), 112–119.
- 148) Moller, C.; Sommer, W.; Thorsell, A.; Rimondini, R.; Heilig, M. *Progress in Neuro-Psychopharmacology and Biological Psychiatry* **2002**, *26* (1), 119–122.
- 149) Gil-Lozano, M.; PPérez-Tilve Diego; Alvarez-Crespo, M.; Martis, A.; Fernandez, A. M.; Catalina, P. A. F.; Gonzalez-Matias, L. C.; Mallo, F. *Endocrinology* **2010**, *151* (6), 2629–2640.
- 150) Holt, M. K.; Trapp, S. *Cogent Biology* **2016**, *2* (1).
- 151) Kinzig, K. P.; D'alessio, D. A.; Herman, J. P.; Sakai, R. R.; Vahl, T. P.; Figueiredo, H. F.; Murphy, E. K.; Seeley, R. J.; Figueredo, H. F. *The Journal of neuroscience: the official journal of the Society for Neuroscience* **2003**, *23* (15), 6163–6170.
- 152) Ghosal, S.; Packard, A. E.; Mahbod, P.; Mcklveen, J. M.; Seeley, R. J.; Myers, B.; Ulrich-Lai, Y.; Smith, E. P.; D'alessio, D. A.; Herman, J. P. *The Journal of Neuroscience* **2016**, *37* (1), 184–193.
- 153) Tibaduiza, E. C.; Chen, C.; Beinborn, M. *The Journal of biological chemistry* **2001**, *276*(41), 37787–37793.
- 154) Taniguchi, H.; Yomota, E.; Kume, E.; Shikano, T.; Endo, T.; Nagasaki, M. *Japanese journal of pharmacology* **1997**, *73* (2), 105–112.
- 155) Truesdale, L. K.; Bychowski, R. A.; Gonzalez, J.; Kuki, A.; Rajapakse, R. J.; Teng, M.; Kiel, D.; Dhanoa, D. S.; Hong, Y.; Chou, T. S.; Ling, A. L.; Johnson, M. D.; Gregor, V. E. Non-Peptide Antagonists Of GLP-1 Receptor And Methods Of Use.
- 156) Gronberg, A.; Sol, E. R.; Danielsson, A.; Colca, J. R.; Bergsten, P. *Diabetes* **2000**, A251.
- 157) Nance, K. D.; Days, E. L.; Weaver, C. D.; Coldren, A.; Farmer, T. D.; Cho, H. P.; Niswender, C. M.; Blobaum, A. L.; Niswender, K. D.; Lindsley, C. W. *Journal of Medicinal Chemistry* **2017**, *60* (4), 1611–1616.
- 158) Dias, D. A.; Urban, S.; Roessner, U. *Metabolites* **2012**, *2* (4), 303–336.
- 159) Raskin, I. *Annual Review of Plant Physiology and Plant Molecular Biology* **1992**, *43* (1), 439–463.
- 160) Brownstein, M. J. *Proceedings of the National Academy of Sciences of the United States of America* **1993**, *90* (12), 5391–5393.
- 161) Guerrini, A. *Eighteenth-Century Studies* **1996**, *29* (3), 339–340.

- 162) Krishnamurti, C.; Rao, S. *Indian Journal of Anaesthesia* **2016**, *60* (11), 861.
- 163) Sneader, W. *The Lancet* **1998**, *352* (9141), 1697–1699.
- 164) Molinski, T. *Organic Letters* **2014**, *16* (15), 3849–3855.
- 165) Fusco, B. M.; Giacobuzzo, M. *Drugs* **1997**, *53* (6), 909–914.
- 166) Ligon, B. *Seminars in Pediatric Infectious Diseases* **2004**, *15* (1), 52–57.
- 167) Astrup, A.; Breum, L.; Toubro, S. A. *Obesity Research* **1995**, *3* (S4).
- 168) Endo, A. *Proceedings of the Japan Academy, Series B* **2010**, *86* (5), 484–493.
- 169) Wall, M. E.; Wani, M. C. *Cancer research* **1995**, *55* (4), 753–760.
- 170) Lewis, K. *Nature Reviews Drug Discovery* **2013**, *12* (5), 371–387.
- 171) Blunt, J. W.; Copp, B. R.; Keyzers, R. A.; Munro, M. H. G.; Prinsep, M. A. R. *Nat. Prod. Rep.* **2016**, *33* (3), 382–431.
- 172) Pettit, G. R.; Herald, C. L.; Doubek, D. L.; Herald, D. L.; Arnold, E.; Clardy, J. *Journal of the American Chemical Society* **1982**, *104* (24), 6846–6848.
- 173) Kollar, P.; Rajchard, J.; Balounova, Z.; Pazourek, J. A. *Pharmaceutical Biology* **2013**, *52* (2), 237–242.
- 174) Gutierrez, C.; Serrano-Villar, S.; Madrid-Elena, N.; Martan, M. E.; Barbas, C.; Ruiparez, J.; Muaoz, E.; Castor, T.; Moreno, S.; Perez-Elas, M. J.; Muaoz-Fernandez, M. A. *Aids* **2016**, *30* (9), 1385–1392.
- 175) Zonder, J. A.; Shields, A. F.; Zalupski, M.; Chaplen, R.; Heilbrun, L. K.; Arlauskas, P.; Philip, P. A. *Clinical cancer research : an official journal of the American Association for Cancer Research* **2001**, *7* (1), 38–42.
- 176) Sagar, S.; Kaur, M.; Minneman, K. P. *Marine Drugs* **2010**, *8* (10), 2619–2638.
- 177) Broder, S. *Antiviral Research* **2010**, *85* (1), 1–18.
- 178) Molinski, T. F.; Dalisay, D. S.; Lievens, S. L.; Saludes, J. P. *Nature Reviews Drug Discovery* **2008**, *8* (1), 69–85.
- 179) Malve, H. *Journal of Pharmacy and Bioallied Sciences* **2016**, *8* (2), 83.
- 180) Nose, H.; Fushimi, H.; Seki, A.; Sasaki, T.; Watabe, H.; Hoshiko, S. *The Journal of Antibiotics* **2002**, *55* (11), 969–974.
- 181) Sasaki, T.; Nose, H.; Hosoya, A.; Yoshida, S.; Kawaguchi, M.; Watanabe, T.; Usui, T.; Ohtsuka, Y.; Shomura, T.; Takano, S.; Tatsuta, K. *The Journal of Antibiotics* **2000**, *53* (1), 38–44.
- 182) Okabe, M.; Sugita, T.; Kinoshita, K.; Koyama, K. *Journal of Natural Products* **2016**, *79* (4), 1208–1212.

- 183) Richardson, M.; Lass-Flarl, C. *Clinical Microbiology and Infection* **2008**, *14*, 5–24.
- 184) Tatsuta, K.; Takano, S.; Ikeda, Y.; Nakano, S.; Miyazaki, S. *The Journal of Antibiotics* **1999**, *52* (12), 1146–1151.
- 185) Bouazza, F.; Renoux, B.; Bachmann, C.; Gesson, J.-P. *Organic Letters* **2003**, *5*(22), 4049–4052.
- 186) Meiries, S.; Bartoli, A.; Decostanzi, M. A.; Parrain, J.-L.; Commeiras, L. *Organic & Biomolecular Chemistry* **2013**, *11*(29), 4882.